Technical Report

TR-12-12

Assessment of the evolution of the redox conditions in SFR 1

Lara Duro, Mireia Grivé, Cristina Domènech,
Gabriela Roman-Ross, Jordi Bruno

Amphos[21]

December 2012

Svensk Kärnbränslehantering AB
Swedish Nuclear Fuel
and Waste Management Co

Box 250, SE-101 24 Stockholm
Phone +46 8 459 84 00

ISSN 1404-0344
SKB TR-12-12
ID 1346539

Assessment of the evolution of the redox conditions in SFR 1

Lara Duro, Mireia Grivé, Cristina Domènech,
Gabriela Roman-Ross, Jordi Bruno

Amphos[21]

December 2012

Abstract

The evaluation of the redox conditions in the intermediate and low level waste repository is of high relevance in performance assessment. The SFR 1 repository contains heterogeneous types of wastes, of different activity levels and containing very different materials, both in the waste itself and used as immobilisation matrices and packaging. The level of complexity also applies to the different reactivity of the materials, so that the assessment of the uncertainties in the study of how the redox conditions evolve must consider different processes, materials and parameters.

In this report an assessment of the evolution of the redox conditions in the SFR 1 is presented. The approach followed is based on the evaluation of the evolution of the redox conditions and the reducing capacity in 12 individual waste package types, selected as being representative of most of the different type of waste package types present or planned to be deposited in the SFR 1. The model has considered different geochemical processes of redox relevance in the system. The assessment of the redox evolution of the different vaults of the repository has considered a combination of the modelled individual waste package types.

According to the results obtained from the modelling presented in this report, the corrosion of the steel-based material present in the repository keeps the system under reducing conditions for long time periods. In the initial step after the repository closure, the microbially mediated oxidation of organic matter rapidly causes the depletion of oxygen in the system. If the role of organic matter is neglected, and only steel corrosion is considered, the initial oxygen is exhausted in less than 1 year after repository closure. The system is afterwards kept under reducing conditions, and hydrogen is generated due to the anoxic corrosion of steel. The simulations have considered both the presence and the absence of microbial activity. The times for exhaustion of the steel contained in the vaults vary from 5,000 years in the BLA to more than 60,000 years in the BMA and the Silo, depending on the amount and the surface area of steel. After the complete corrosion of steel, the system still keeps a high reducing capacity, due to the magnetite formed as steel corrosion product.

The redox potential in the vaults is calculated to evolve from oxidising at very short times, due the initial oxygen content, to very reducing at times shorter than 5 years after repository closure. The redox potential imposed by the anoxic corrosion of steel and hydrogen production is on the order of –0.75 V at pH 12.5. In case of assuming that the system responds to the Fe(III)/Magnetite system, and considering the uncertainty in the pH due to the degradation of the concrete barriers, the redox potential would be in the range –0.7 to –0.01V.

A Monte-Carlo probabilistic analysis on the rate of corrosion of steel shows that the reducing capacity of the system provided by magnetite is not exhausted at the end of the assessment period, even assuming the highest corrosion rates for steel.

Simulations assuming presence of oxic water due to glacial melting, intruding the system 60,000 years after repository closure, indicate that magnetite is progressively oxidised, forming Fe(III) oxides. The time at which magnetite is completely oxidised varies depending on the amount of steel initially present in the waste package.

The vault having the lowest capacity to buffer an oxidant intrusion is BLA, mainly due to the absence of concrete barriers, which results in more neutral pH values than those imposed by the cementitious materials present in the other vaults. In any case, under non-disturbed conditions, the reducing capacity of the BLA vault is not exhausted under the times considered in this study.

Contents

1 Background and objective 7

2 The SFR 1 system 9
2.1 Redox evolution in the previous safety assessment SAR-08 9
2.2 SFR 1 components 10
2.2.1 The Silo 10
2.2.2 The BMA vault 12
2.2.3 The 1 BTF and 2 BTF vaults 14
2.2.4 The BLA vault 16

3 Redox processes of relevance in the SFR 1 system 19
3.1 Metal corrosion 19
3.2 Degradation of organic matter 24
3.2.1 Degradation of cellulose 24
3.2.2 Degradation of bitumen 26
3.3 Brief summary 27

4 General approach to the model 29
4.1 Methodology of the assessment 30

5 Conceptual model and numerical implementation 31
5.1 Calculation code and thermodynamic database used 33
5.2 Groundwater composition 34
5.3 Steel corrosion 34
5.3.1 Conceptual model 34
5.3.2 Numerical parameterisation 35
5.4 Degradation of organic matter 35
5.4.1 Conceptual model 35
5.4.2 Bitumen, “generic organic matter” and acetate degradation 36
5.4.3 Cellulose degradation 36
5.4.4 Biomass behaviour 37
5.4.5 Numerical parameterization 38
5.5 Calculation strategy 40
5.6 Assessment of the ReDucing Capacity (RDC) 41

6 Results of the modelling of individual waste package types 43
6.1 Very short-term results (up to 30 days) 43
6.1.1 Waste package types containing only steel as reducing material 43
6.1.2 Waste package types containing steel and generic organic matter as reducing material 45
6.1.3 Waste package types containing steel and bitumen as reducing material 48
6.1.4 Waste package types containing cellulose 49
6.1.5 Brief summary of the very short-term results 52
6.2 Short term results (up to 5 years) 54
6.2.1 Waste package types containing only steel as reducing material 54
6.2.2 Waste package types containing steel and generic organic matter as reducing materials 55
6.2.3 Waste package types containing bitumen 55
6.2.4 Waste package types containing cellulose 55
6.2.5 Brief summary of the short-term results 58

6.3 Long term results (up to 100,000 years) 60
6.3.1 Waste package types containing only steel as reducing material 63
6.3.2 Waste package types containing steel and generic organic matter as reducing materials 64
6.3.3 Waste package types containing bitumen 66
6.3.4 Waste package types containing cellulose 67
6.3.5 Brief summary of the long-term results 69
6.4 Calculation of reducing capacity 72
6.4.1 Results of the different waste package types 72
6.4.2 RDC of the vaults 78

7 Sensitivity analyses 81
7.1 Uncertainty on the steel corrosion rate 81
7.2 Glacial event scenario 83

8 Assessment of the redox potential and its influence on the radionuclide behaviour 87

9 Radionuclide behaviour 91
9.1 Neptunium 92
9.2 Plutonium 95
9.3 Selenium 98
9.4 Technetium 100

10 Discussion and Conclusions 103

References 107

Appendix 1 Waste package types cross references 113
Appendix 2 Preliminary calculations: initial oxygen consumption by fast corroding metals 115
Appendix 3 Redox considerations in similar repository systems 119
Appendix 4 Algorithm of cellulose degradation implemented in PHREEQC 127
Appendix 5 Results for all cases 131
Appendix 6 Visualisation of the results 197
Appendix 7 Glossary 203

1 Background and objective

The SFR 1 repository at Forsmark in Sweden is used for the final disposal of low- and intermediate-level radioactive waste (L/ILW) produced by the Swedish nuclear power programme, industry, medicine and research. Waste disposed in SFR 1 belongs to the short-lived waste category according to the IAEA definition. This means that there is a limitation of long-lived α-activity of an average overall of 400 Bq/g per waste package, allowing a maximum per individual waste package of 4,000 Bq/g.

Different types of waste packages are present in the repository, prepared to receive different type of materials depending on their physical forms and activity levels. The repository is composed on different vaults:

- Silo – for intermediate-level, solidified waste.
- BMA – for intermediate-level, mostly solidified waste.
- 1 BTF and 2 BTF – for dewatered and relatively low-level ion exchange resins.
- BLA – for low-level solid waste such as trash and scrap.

Some wastes are conditioned in cement; some others in bitumen and some of them are not conditioned. The repository contains large amounts of cementitious materials, also metals, either in the form of containers or as scrap in the wastes, as well as organic materials, bitumen, and some sand and bentonite.

The SFR 1 repository has several particularities that make it a unique environment from the perspective of redox evolution.

The repository system is currently placed in a shallow subsurface area of Forsmark under the Baltic Sea. It contains a sizeable amount of metals, particularly iron; a relative large amount of organic materials, including bitumen and the overall system is buffered by the presence of substantial amounts of cement.

The reference evolution for the repository and its environs (SKB 2008b) describes two important changes of the external conditions of the repository that can affect its performance:

- Shoreline displacement is expected to occur so that the shoreline will lie above SFR 1 in about one thousand years.
- Climatic evolution: advances of ice sheet may induce great changes in groundwater flow conditions. Periods of up-coning of deep groundwater can be followed by periods of glacial meltwater seeping down into the rock. This melting water can contain oxygen in high concentrations.

In the previous SAR-08 safety assessment report, reducing conditions were assumed in the repository. Inflowing groundwaters were assumed to be reducing due to the presence of bacterial activity in surface and to the fast consumption of oxygen after the repository closure. Inside the repository, the presence of steel and iron was considered to buffer any intrusion of oxidants through corrosion. It was also estimated that total corrosion of the iron materials present in the repository would occur for more than 10,000 years, so that the prevalence of reducing conditions was ensured until 20,000 years. After this period, it was assumed that following the Weichselian cycles, a glaciation event would occur and permafrost could develop. In SAR-08 it was considered that glacial meltwater could reach repository depths and cause the infiltration of oxygenated water. Different processes, such as microbial activity at the surface and dissolution of minerals containing Fe(II) were considered to consume oxygen and oxidants in the infiltrating groundwaters, although in the long-term safety assessment it was stated that the possibility of oxygenated waters infiltrating could not be excluded, so that reducing conditions could not be granted for the total time frame of the assessment.

In the present work we have performed a description of the SFR 1 system as a whole and of the individual vaults in particular, with specific descriptions of the main system components of the SFR 1 that can affect and may be affected by redox reactions. The qualification and quantification of the processes governing redox evolution of the system and their relative importance for the different parts of the repository is included.

The repository has been divided into its different vaults and the various materials contained in the vaults have been considered. The effect of organic materials, metals and bituminized wastes under hyperalkaline conditions for those systems where the presence of concrete materials prevails is discussed. The potential presence of microbial activity and the main parts of the system where this process may play a role on the redox evolution of the system is also taken into consideration.

The SFR 1 system is compared with other systems where intermediate and low level wastes are (or are planned to be) conditioned with similar materials. The open scientific literature and specific reports devoted to assess redox evolution in similar systems has been reviewed to bring additional evidence on the main processes acting in the different parts of the system and how the redox processes have been tackled in different safety assessments.

The objective of the work presented here is to develop a methodology that allows SKB to provide a robust answer to SSM concerning the expected evolution of the redox state of SFR 1. To this aim, the redox processes most likely to occur in the system are presented and discussed, a conceptual model for the evolution of the redox state of the repository is proposed and a simplified numerical model that allows the quantification of these redox processes is developed. The time frame for the assessment must span over 100,000 years after the repository closure.

The structure of the report is as follows:

- Chapter 2 gives a brief presentation of the SFR 1 system and how its redox evolution has been discussed in previous assessments.
- Chapter 3 discusses the main redox processes of relevance in the SFR 1 system and provides some scoping calculations to center the discussion of the conceptual and numerical model that follows.
- Chapter 4 presents the general approach and the methodology followed to model the system.
- Chapter 5 presents the conceptual and numerical model set up for the system.
- Chapter 6 discusses the results of the modelling.
- Chapter 7 presents the results of two sensitivity analyses.
- Chapter 8 assess the redox potential and its influence on the radionuclide behaviour
- Chapter 9 presents a discussion on the behaviour of the radionuclides Np, Pu, Se and Tc.
- And finally, Chapter 10 includes a discussion on the results and a set of conclusions.

In order to make the report more readable, some relevant information has been included in the Appendices:

- Appendix 1 presents a cross-reference table with a list of the SFR 1 waste package types and the tables of the report where they are listed.
- Appendix 2 presents preliminary calculations on the initial oxygen consumption by fast corroding metals in the repository.
- Appendix 3 presents other repository systems with common features to the SFR 1, focused on how the redox problem has been tackled with in their respective Performance and Safety assessments.
- Appendix4 contains a discussion on the numerical model of cellulose degradation.
- Appendix 5 contains the presentation of the numerical results for all waste package types.
- Appendix 6 contains a 3D visualisation of the results.
- Appendix 7 contains a glossary.

2 The SFR 1 system

2.1 Redox evolution in the previous safety assessment SAR-08

The description of the redox evolution of the repository in SAR-08 is mainly based on the corrosion of the metals present. The most detailed model accounting for the redox evolution of SFR 1 is that aimed at quantifying the generation of gases in the repository due to the various corrosion processes and in particular the anaerobic corrosion of the iron components (Moreno et al. 2001).

In the SAR-08 document (SKB 2008b) three different time frames are defined for the description of the evolution of the repository:

- The first 1,000 years after repository closure (until 3,000 years AD).
- The period from 3,000 to 20,000 years AD.
- The period from 20,000 to 100,000 years AD.

According to the SAR-08 description, during the first 1,000 years after repository closure, the oxygen remaining after operation will be consumed by different corrosion processes; mainly the degradation of organic matter and the aerobic corrosion of aluminium, zinc and steel. Assuming that the corrosion of aluminium and zinc is faster than that of steel, O_2 will be mainly consumed by their corrosion. It is foreseen that from then on, the repository will be kept under reducing conditions for long-term.

In the period from 3,000 to 20,000 years AD, reducing conditions are assumed to prevail in all barriers and in all repository parts. Groundwater that can enter the repository system will be also reducing, due to different microbially mediated processes and oxygen will have been consumed in the first 1,000 years after closure, so that the presence of a high amount of material prone to be oxidised will ensure the prevalence of reducing conditions.

According to the models in SAR-08, it will take 10,000 years for all iron-based material to corrode anerobically. This means, that the reducing capacity of the system, defined as its capacity to buffer an oxidant intrusion, will be enough as to counteract an extremely unlikely intrusion of oxidants occurring during 10,000 years.

During the last period covered by the SAR-08, from 20,000 to 100,000 years AD, glaciation effects were assumed to occur. A permafrost domain can develop, without ice-sheet, and also glacial domains may exist, where the soil surfaces will be covered by ice-sheets. During the permafrost and its melting period, oxygen-rich waters may infiltrate. The redox conditions of the groundwater reaching the repository are, nevertheless, expected to be reducing due to the buffering processes of mineral alteration and microbial processes that will occur before water enters the repository domain. These assumptions have been challenged in the recent SR-Site assessment, as the biosphere is assumed to be quite dormant during the permafrost and glaciation periods and the much larger hydrological gradient that may cause the fast intrusion of melt waters.

Therefore, the assessment of the redox conditions of the groundwater from permafrost and ice-sheet melting when reaching the repository level will help in the understanding on the capacity of the system to remain under reducing conditions.

2.2 SFR 1 components

The SFR 1 system consists of several vaults containing different type of wastes conditioned in different way. This section provides a short description of the repository. For more detailed information the reader is referred to the different documents in the SKB bibliography dealing with the SFR 1 system.

2.2.1 The Silo

The Silo contains most of the activity in SFR 1 and consequently it is the vault with the most effective barriers. The waste packages are located in the different vertical cement-walled shafts. The existing spaces between the waste packages are backfilled with concrete. The external walls of the Silo are made of reinforced concrete 0.8 m thick. A backfill of bentonite is placed between the Silo walls and the surrounding rock. The bottom of the Silo is made of concrete (1 m thick) placed on a layer of a bentonite/sand mixture. The same concrete thickness will be used for the lid of the Silo, but in this case, it will be covered with a layer of sand and a mixture of sand/bentonite of 1.5 m thickness.

A simplified sketch from the Silo is shown in Figure 2-1.

The wastes placed in the Silo are mainly ionic exchange resins, filter aids, scrap metals and some sludge (Table 2-1). The amount of organic material is kept to a minimum.

All the wastes placed in the Silo are conditioned, either in concrete or in bitumen matrices. Different types of waste packages are used: concrete moulds, steel moulds and steel drums. There are (or will be) 11 types of waste packages in the Silo. The resulting combinations between waste package materials and conditioning matrices, as well as the conditioned wastes, are shown in Table 2-1.

A detailed description of each type of waste package is given in Almkivst and Gordon (2007). It is important to notice that concrete moulds contain some amount of steel for reinforcement, so that steel is present in all containers of the Silo as shown in Table 2-2.

It is also interesting to point out that the bituminised wastes are located in the central shafts of the Silo, as shown in Figure 2-2.

Figure 2-1. *Picture showing a sketch of the Silo.*

Table 2-1. Description of the different waste types deposited in the Silo of the SFR 1 repository. Data from Almkvist and Gordon (2007).

Waste type	Packaging	Treatment and Conditioning	Waste	Number of packages*	Surface area (m^2) #	Volume (m^3)
O.02	1.73 m^3 concrete moulds	Concrete matrix	Ion-exchange resins and inert filter aid	2,342	11.8/1(waste)[&]	Waste: 0.85 Void: 0.17[&]
R.02	1.73 m^3 concrete moulds	Concrete matrix	Ion-exchange resins and inert filter aid	371	12.8	Waste: 0.85 Void: 0.15
R.16	1.73 m^3 steel moulds	Concrete matrix	Ion-exchange resins and inert filter aid	3,437	17/3(waste)[&]	Waste: 1.615 Void: 0.323[&]
B.06	Standard 200-litre stainless steel drum	Bitumen matrix	Ion-exchange resins	1,840	4.1[&]	Waste: 0.2 Void: 0.03
B.04	Standard 200-litre stainless steel drum	Cement matrix	Ion-exchange resins	1,000	5.1	Waste: 0.19 Void: 0.02
F.18	1.73 m^3 steel moulds	Bitumen matrix	Ion-exchange resins	992	10[&]	Waste: 1.53 Void: 0.17
S.11	1.73 m^3 steel moulds	Cement matrix	Ion-exchange resins and sludges	60	17/3(waste)	Waste: 1.615 Void: 0.085
S.04	Standard 200-litre stainless steel drum	Cement matrix	Ion-exchange resins	221	5.1	Waste: 0.2 Void: 0.01
S.24	1.73 m^3 concrete moulds	Concrete matrix	Scrap metal	134	10/5.8(waste)	Waste: 0.95 Void: 0.05
C.02	1.73 m^3 concrete moulds	Concrete matrix	Ion-exchange resins and inert filter aid	1,460	10/ 1(waste)	Waste: 0.85 Void: 0.15
C.24/O.24	1.73 m^3 concrete moulds	Concrete matrix	Scrap metals	194	10/0.9(waste)	Waste: 0.99 Void: 0.01

* Number of packages Year 2050. # Total packaging surface (except when indicated). [&] from Zazzi (2011).

Table 2-2. Content of ion exchange resins, cement, concrete, steel, Al, bitumen, cellulose and other organics in the waste package types deposited in the Silo. Data from Almkvist and Gordon (2007).

Waste type	Ion exchange resin (kg)	Cement (kg)	Concrete (kg)	Steel (kg)	Aluminium (kg)	Bitumen (kg)	Cellulose (kg)	Other organics (kg)
O.02	130	1,540	–	29	–	–	–	10
R.02	130	1,340	–	290[&]	–	–	–	10
R.16	250	2,100	–	425	–	–	–	–
B.06	50	–	–	23+17*	–	150	–	–
B.04	33	302	–	40	–	–	–	–
F.18	600	–	–	550[&]	–	960	–	–
S.11	667	1,820	–	425	–	–	3	–
S.04	65	238	–	67	–	–	–	–
S.24	–	–	1,905	374	3.8	–	–	–
C.02	130	1,540	–	29	–	–	–	10
C.24/O.24	–	–	1,905	698	–	–	35	24

* C-Steel. [&] from Zazzi (2011).

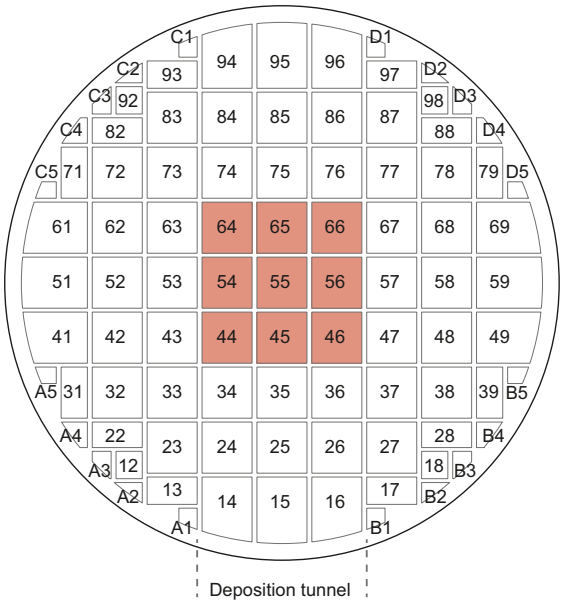

Figure 2-2. *Cross section of the Silo, indicating the location of the bituminised wastes in the central shafts (Zazzi 2011).*

2.2.2 The BMA vault

The BMA is a rock vault for intermediate-level waste, containing less than 20% of the total activity in SFR 1. The bottom of the vault, made of cast reinforced concrete, is grounded on a base of shot rock leveled with gravel. The walls and floor structures are also made of cast reinforced concrete and are lined with shotcrete. The vault is 160 m long and 19.5 m wide.

After the compartments are filled with waste a concrete lid is put in place and concrete is poured. The concrete structure in the vault is divided into 15 compartments with concrete walls in between. According to the plans, there is a 2 m wide space that will be filled with sand between the concrete structure and the rock wall.

A sketch from the vault is shown in Figure 2-3.

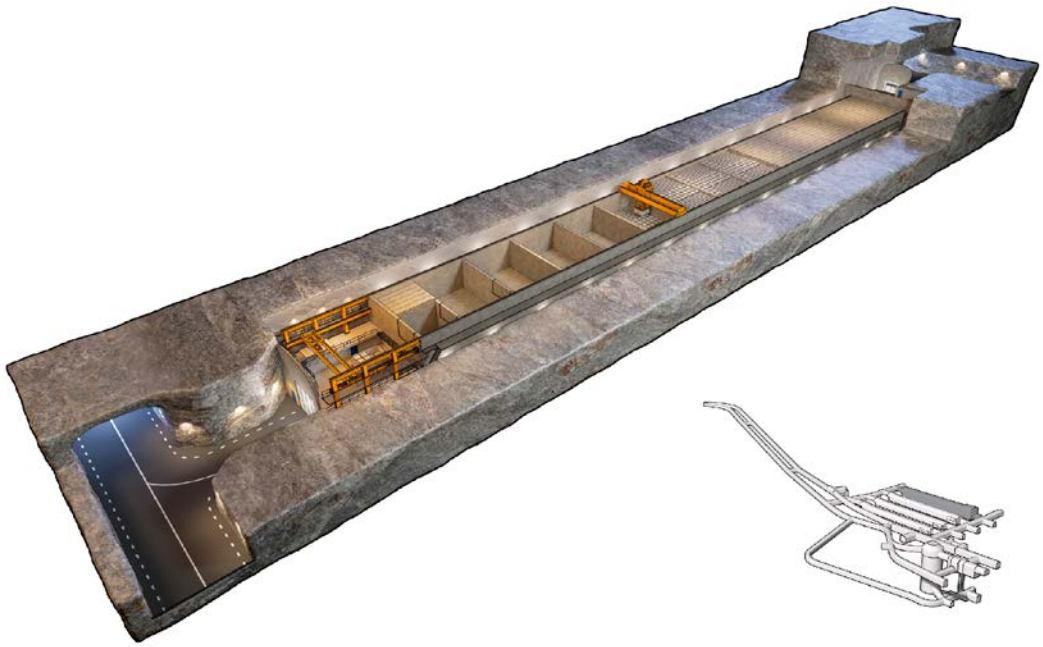

Figure 2-3. *Picture showing the BMA vault.*

The wastes in BMA are mainly ion-exchange resins, scrap and refuse metals, with some packages containing evaporate concentrates, sludges and slurries from oxidation tests (Table 2-3). Most types of wastes are conditioned in concrete, although 2 types of steel drums contain ionic exchange resins conditioned in bitumen. In fact, the amount of bitumen in the BMA vault is estimated to be higher than in the Silo. As in all vaults of the repository, steel is present everywhere (Table 2-4). Organic matter and cellulose contents are higher than in the Silo.

Table 2-3. Description of the different waste types deposited in the BMA vault of the SFR 1 repository. Data from Almkvist and Gordon (2007).

Waste type	Packaging	Treatment and Conditioning	Waste	Number of packages*	Surface area (m^2)#	Volume (m^3)
B.05	Standard 200-litre stainless steel drum	Bitumen matrix	Ion-exchange resins	4,188	3.8[&]	Waste: 0.2 Void: 0.03
F.05	Standard 200-litre stainless steel drum	Bitumen matrix	Ion-exchange resins	1,712	3.5[&]	Waste: 0.195 Void: 0.02
F.15	1.73 m^3 steel moulds	Concrete matrix	Ion-exchange resins	11	17/3(waste)	Waste: 1.53 Void: 0.17
F.17	1.73 m^3 steel moulds	Bitumen matrix	Ion-exchange resins	1,605	10[&]	Waste: 1.615 Void: 0.085
F.23	1.73 m^3 concrete/ steel moulds	Concrete matrix	Scrap metal and refuse	469	20/7.6(waste)[&]	Waste: 1.615 Void: 0.085
O.01	1.73 m^3 concrete moulds	Concrete matrix	Ion-exchange resins and inert filter aid	675	12.8	Waste: 0.85 Void: 0.15
C.01	1.73 m^3 concrete moulds	Concrete matrix	Ion-exchange resins and inert filter aid	68	12.8	Waste: 0.85 Void: 0.15
O.23	1.73 m^3 concrete moulds	Concrete matrix	Scrap metal and refuse	640	13.6/ 5.3(waste)[&]	Waste: 1.728[&] Void: 0.19[&]
C.23	1.73 m^3 concrete moulds	Concrete matrix	Scrap metal and refuse	202	11.8/5.7(waste)	Waste: 0.95 Void: 0.05
R.01	1.73 m^3 concrete moulds	Concrete matrix	Ion-exchange resins and inert filter aid	1,686	11.8/ 1.0(waste)[&]	Waste: 0.85 Void: 0.17[&]
R.10	1.73 m^3 concrete moulds	Concrete matrix	Sludges	146	12.8	Waste: 0.90 Void: 0.10
R.15	1.73 m^3 steel moulds	Concrete matrix	Ion-exchange resins and inert filter aid	163	17/ 3(waste)[&]	Waste: 1.728[&] Void: 0.323[&]
R.23	1.73 m^3 concrete/ steel moulds	Concrete matrix	Scrap metal and refuse	608	10	Waste: 1.615 Void: 0.085
R.29	1.73 m^3 concrete moulds	Concrete matrix	Evaporator concentrate	960	7.9	Waste: 1.53 Void: 0.17
S.09	Standard 200-litre stainless steel drum	Cement matrix	Sludges	1,080	5.1	Waste: 0.2 Void: 0.01
S.23	1.73 m^3 concrete moulds	Concrete matrix	Scrap metal and refuse	440	10/5.8(waste)	Waste: 0.95 Void: 0.05
F99:1	1.73 m^3 steel moulds	Cement matrix	Steel drums with a rest slurry from oxidation tests	2	10	Waste: 1.615 Void: 0.085

* Number of packages Year 2050. # Total packaging surface (except when indicated). [&] from Zazzi (2011).

Table 2-4. Content of ion exchange resins, cement, concrete, steel, Al, bitumen, cellulose and other organics in the waste package types deposited in the BMA vault. Data from Almkvist and Gordon (2007).

Waste type	Ion exchange resin (kg)	Cement (kg)	Concrete (kg)	Steel (kg)	Aluminium (kg)	Bitumen (kg)	Cellulose (kg)	Other organics (kg)
B.05	50	–	–	39.25****	–	150	4.3****	–
F.05	130	–	–	41.6****	–	95	–	–
F.15	375	805	–	425	–		–	–
F.17	650	–	–	550****	–	820	–	–
F.23	–	–	1,356****	612****	5****	–	150****	450****
O.01	130	1,540	1,340	300	–	–	–	10
C.01	130	1,540	1,340	300	–	–	–	10
O.23	–	–	1,905****	392****	3.5	–	30	66.5
C.23	–	–	1,905	386	3.5	–	30	66.5
R.01	130	–	2,740****	290****	–	–	–	10
R.10	–	1,120	1,340	300	–	–	–	10
R.15	250	–	2,100****	425****	–	–	–	–
R.23	–	–	1,365**/1,905***	750**/300***	4**/1***	–	44**/11***	100**/25***
R.29	–	–	1,600	160	–	–	–	–
S.09	–	280	–	76	–	–	–	–
S.23	–	–	1,905	380	3.8	–	29	–
F99:1	–	–	–	625	–	–	–	35

* C-Steel. ** steel mould. *** concrete mould. **** from Zazzi (2011).

2.2.3 The 1 BTF and 2 BTF vaults

These are two rock vaults for concrete tanks. The BTF vaults contain very low activity material. The floor of the vaults is made of concrete, and the rock walls and roofs are lined with shotcrete. The waste containers are grouted with concrete. The vaults are 160 m long and 15 m wide.

A sketch of the vaults is shown in Figure 2-4.

The waste in BTF is de-watered low-level ion exchange resin in concrete tanks as well as some ashes originated from the residue left after incineration of low level waste as textiles, plastics and wood. There are also "odd wastes" mainly consisting on old steam separators from Forsmark. The different types of waste package of 1 BTF and 2 BTF are shown in Table 2-5 to Table 2-8.

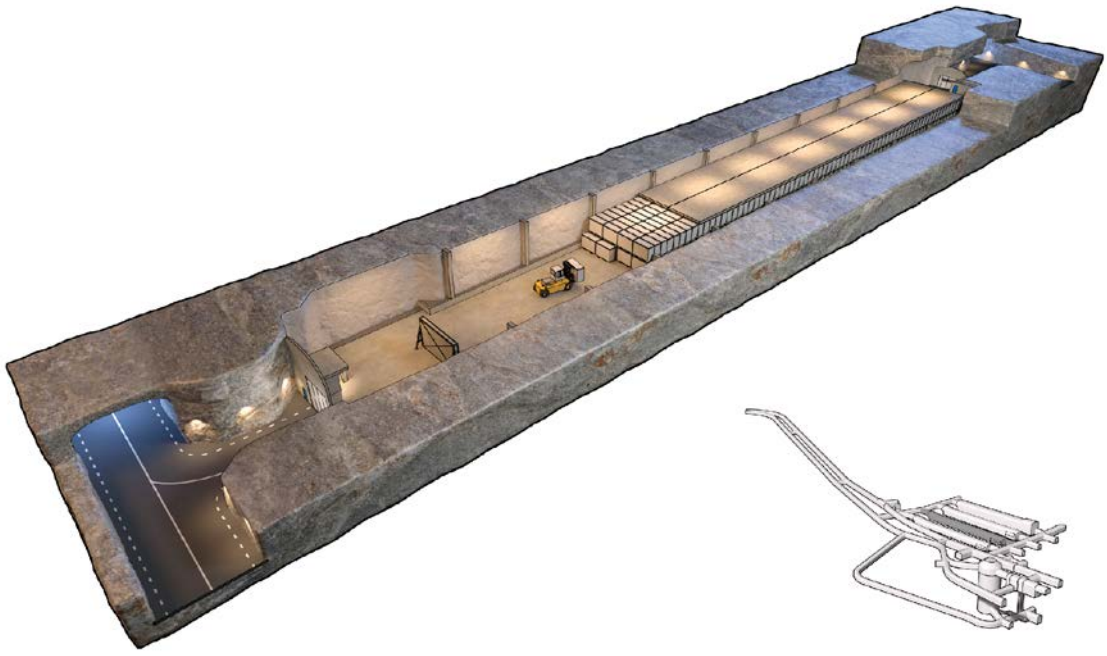

Figure 2-4. *Picture showing the BTF vaults.*

Table 2-5. Description of the different waste types deposited in the 1 BTF vault of the SFR 1 repository. Data from Almkvist and Gordon (2007).

Waste type	Packaging	Treatment and Conditioning	Waste	Number of packages*	Surface (m^2)**	Volume (m^3)
B.07	Concrete tank	–	De-watered ion-exchange resins	29	40***	Waste: 2.2 Void: 3.8
O.07	Concrete tank	–	De-watered ion-exchange resins	159	40	Waste: 2.2 Void: 3.8
S.13	Standard 200-litre stainless steel drum	–	Ashes	5,130	7.1***	Waste: 0.107 Void: 0.042
O.99:1	40 Concrete moulds	–	Ion-exchange resins	20	38	Waste: 3.37 Void: 0.18
R.01	1.73 m^3 concrete moulds	Concrete matrix	Ion-exchange resins and inert filter aid	91	11.8/ 1.0(waste)***	Waste: 0.85 Void: 0.15
R.10	1.73 m^3 concrete moulds	Concrete matrix	Sludges	4	12.8	Waste: 0.90 Void: 0.10
R.99:1	Reactor tank lid	–	Low level waste	1	150	Not specified
R.23	1.73 m^3 concrete/ steel moulds	Concrete matrix	Scrap metal and refuse	21	10	Waste: 1.615 Void: 0.085
O.01	1.73 m^3 concrete moulds	Concrete matrix	Ion-exchange resins and inert filter aid	28	12.8	Waste: 0.85 Void: 0.15

*Number of packages Year 2050. **Total packaging surface (except when indicated). *** from Zazzi (2011).

Table 2-6. Content of ion exchange resins, cement, concrete, stainless steel, Al, bitumen, cellulose and other organics in the waste package types deposited in the 1 BTF vault. Data from Almkvist and Gordon (2007).

Waste type	Ion exchange resin (kg)	Cement (kg)	Concrete (kg)	Steel (kg)	Aluminium (kg)	Bitumen (kg)	Cellulose (kg)	Other organics (kg)
B.07	1,400	–	10,300	647	–	–	–	116***
O.07	1,000	–	10,300	647	–	–	–	66
S.13	–	–	240	30*	6.5	–	–	–
O.99:1	130	–	–	1,220	–	–	8.3	–
R.01	130	1,400	1,340	300	–	–	–	10
R.10	–	1,120	1,340	300	–	–	–	10
R.99:1	–	–	–	65,000	–	–	–	–
R.23	–	–	1,365***/1,905**	750***/300**	4&/1**		44***/11**	100***/25**
O.01	130	1,540	1,340	300	–	–	–	10

* C-Steel and steel mould. ** concrete mould. *** from Zazzi (2011).

Table 2-7. Description of the different waste types deposited in the 2 BTF vaults of the SFR 1 repository. Data from Almkvist and Gordon (2007).

Waste type	Packaging	Treatment and Conditioning	Waste	Number of packages*	Surface (m^2) **	Volume (m^3)
B.07	Concrete tank	–	De-watered ion-exchange resins	194	40***	Waste: 2.2 Void: 3.8
O.07	Concrete tank	–	De-watered ion-exchange resins	577	40	Waste: 2.2 Void: 3.8
S.13	Standard 200-litre stainless steel drum	–	Ashes	474	7.1***	Waste: 0.107 Void: 0.042***
F.99:2	10 m^3 steel boxes	–	Steam separators	18	23	Waste: 9.5 Void: 0.5
O.99:1	40 Concrete moulds	–	Ion-exchange resins	20	38	Waste: 3.37 Void: 0.18

* Number of packages Year 2050. ** Total packaging surface (except when indicated). *** from Zazzi (2011).

Table 2-8. Content of ion exchange resins, cement, concrete, stainless steel, Al, bitumen, cellulose and other organics in the waste package types deposited in the 2 BTF vault. Data from Almkvist and Gordon (2007).

Waste type	Ion exchange resin (kg)	Cement (kg)	Concrete (kg)	Steel (kg)	Aluminium (kg)	Bitumen (kg)	Cellulose (kg)	Other organics (kg)
B.07	1,400	–	10,300	647	–	–	–	116***
O.07	1,000	–	10,300	647	–	–	–	66
S.13	–	–	240	30*	6.5	–	–	–
O.99:1	130	–	–	1,220	–	–	8.3	–
F.99:2	–	–	–	4,900	–	–	–	–

* C-Steel & steel mould. ** concrete mould. *** from Zazzi (2011).

2.2.4 The BLA vault

The BLA is the vault for low-level waste, mainly trash and scrap. The rock vault has a length of 160 m and a width of 15 m. The vault has a concrete floor, and the walls and the roof are lined with shotcrete. A sketch from the vault is shown in Figure 2-5.

Most of the wastes are not conditioned, the containers being ISO shipping containers. The ionic exchange resins deposited in the BLA are stabilized with bitumen and located in steel drums inside the ISO containers (Table 2-9). As shown in Table 2-10, the content of cellulose, bitumen and other organic material is expected to be very high.

This vault, therefore, does not contain more concrete than the material used in the shotcreting of the walls and the roof, besides the concrete floor. For this reason, the redox processes occurring in this vault will have to consider the possibility of non-hyperalkaline conditions being developed.

A summary of the main characteristics of the vaults for the purpose of the present work is shown in Figure 2-6 and Table 2-11. The materials that *a priori* may be more active from a redox perspective are iron/steel, bitumen, cellulose, Al/Zn and other organic materials.

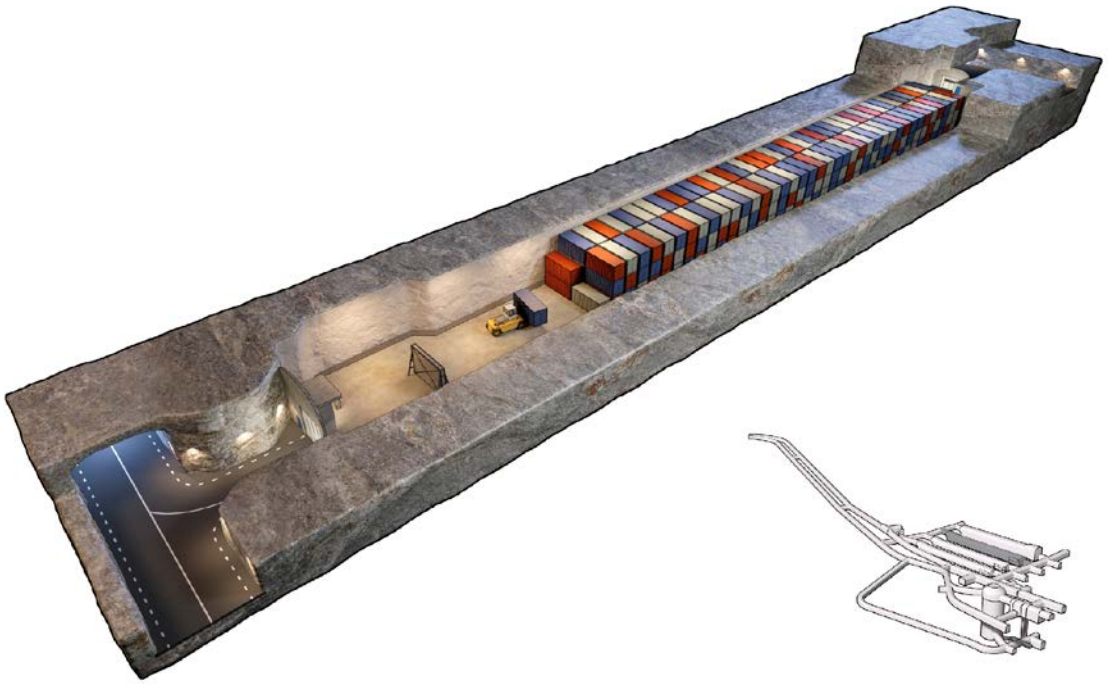

Figure 2-5. *Picture showing the BLA vault.*

Table 2-9. Description of the different waste types deposited in the BLA vault of the SFR 1 repository. Data from Almkvist and Gordon (2007).

Waste type	Packaging	Treatment and Conditioning	Waste	Number of packages*	Surface (m^2)**	Volume (m^3)
B.12	Standard steel ISO-container	–	Iron/steel, aluminium, cellulose and other organic materials	238	104/229(waste)	Waste: 11.5 Void: 7.5
B.20	Standard steel ISO-container	–	36 200-litre drums of steel with bitumen conditioned ion-exchange resins	12	104	Waste: 11.7 Void: 7.4
F.12	Standard steel ISO-container	–	Iron/steel, aluminium, cellulose and other organic materials	44	104/229(waste)	Waste: 11.5 Void: 7.5
F.20	Standard steel ISO-container	–	36 200-litre drums of steel with bitumen conditioned ion-exchange resins	15	104	Waste: 12 Void: 7
O.12	Standard steel ISO-container	–	Iron/steel, aluminium, cellulose and other organic materials	44	105/502(waste)***	Waste: 15*** Void: 7.5
R.12	Standard steel ISO-container	–	Iron/steel, aluminium, cellulose and other organic materials	167	104/229(waste)	Waste: 11.5 Void: 7.5
S.12	Standard steel ISO-container	–	Iron/steel, aluminium, cellulose and other organic materials	45	104/229(waste)	Waste: 11.5 Void: 7.5
S.14	Standard steel ISO-container	–	33 to 36 200-litre drums of steel with scrap metal and refuse	75	104/133(waste)	Waste: 12.7 Void: 6.4
O.99:3	Standard steel ISO-container	–	70 200-litre drums of steel with ion-exchange resins, filters and sludge in a concrete matrix	5	104/414(waste)	Waste: 23.5 Void: 16.5

* Number of packages Year 2050. **Total packaging surface (except when indicated). *** from Zazzi (2011).

Table 2-10. Content of ion exchange resins, cement, concrete, stainless steel, Al, bitumen, cellulose and other organics in the waste package types deposited in the 1 BTF vault. Data from Almkvist and Gordon (2007).

Waste type	Ion exchange resin (kg)	Cement (kg)	Concrete (kg)	Steel (kg)	Aluminium (kg)	Bitumen (kg)	Cellulose (kg)	Other organics (kg)
B.12	–	–	–	1,900*+4,500	100	–	500	3,000
B.20	1,800	–	–	2,728*	–	5,400	310	–
F.12	–	–	–	1,900*+4,500	100	–	500	3,000
F.20	4,680			2,800*	–	3,450	310	–
O.12	–	–	–	1,900*+4,500	100	–	500	3,000
R.12	–	–	–	1,900*+4,500	100	–	500	3,000
S.12	–	–	–	1,900*+4,500	100	–	500	3,000
S.14	–	–	–	2,980*+2,664	180	–	284	144
O.99:3	1,170	–	–	3,680*+190	–	–	–	320

* C-Steel.

In next chapter a discussion on the role that these materials may have in the short and long-term behaviour of the SFR 1 repository is presented.

Appendix 1 shows a cross reference table where package types are sorted in alphabetical order together with a list of the tables where to find their composition in this report.

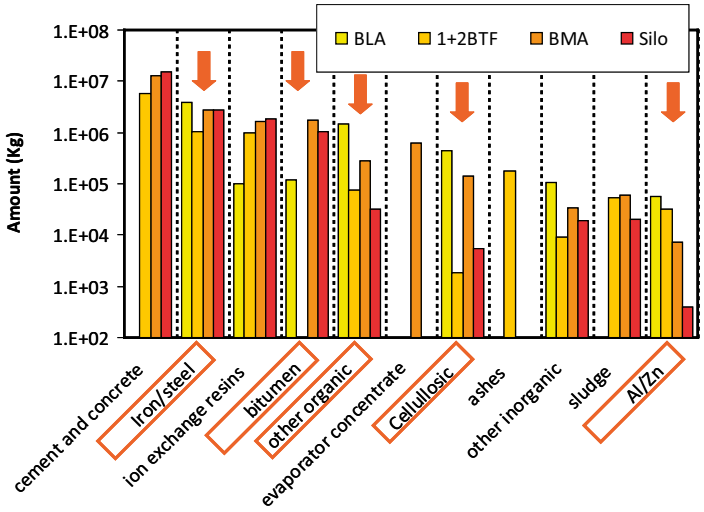

Figure 2-6. *Amounts of materials in each one of the vaults (data from Almkvist and Gordon (2007)). Materials indicated with an arrow and orange squares are those expected to be more redox active in the repository.*

Table 2-11. Summary of the general characteristics of the vaults in SFR 1. Most abundant materials listed in decreasing order of amounts in each vault. Materials in bold italics are those more likely to have an effect on the redox conditions of the repository.

Vault	Activity	Type of waste	Barriers	Most abundant materials
Silo	slightly below 80% of total in SFR 1	Intermediate-level, solidified	1. Waste matrix/containers 2. Concrete, compartment walls and silo walls 3. Bentonite 4 Surrounding rock	• Cement/concrete • ***Iron/steel*** • Ion exchange resins • ***Bitumen*** • ***Organics not cellullosic (plastics, rubber, cable)*** • Sludge • Non-metallic inorganic • ***Cellullosic materials (wood, paper, cloth)*** • ***Aluminium/Zinc***
BMA	below 20% of total in SFR 1	intermediate-level, mostly solidified	1 Waste package 2 Compartments in BMA 3 Surrounding rock	• Cement/concrete • ***Iron/steel*** • ***Bitumen*** • Ion exchange resins • Evaporator concentrate • ***Organics not cellullosic (plastics, rubber, cable)*** • ***Cellullosic materials (wood, paper, cloth)*** • Sludge • Other inorganic • ***Al/Zn***
1 BTF 2 BTF		Dewatered IE resins	1. Concrete walls 2. Surrounding rock	• Cement/concrete • ***Iron/steel*** • Ion exchange resins • Ashes • ***Organics not cellullosic (plastics, rubber, cable)*** • Sludge • ***Al/Zn*** • Other inorganic • ***Cellullosic materials (wood, paper, cloth)***
BLA		Low Level solid waste (trash and scrap)	1. Surrounding rock	• ***Iron/steel*** • ***Organics not cellullosic (plastics, rubber, cable)*** • ***Cellullosic materials (wood, paper, cloth)*** • ***Bitumen*** • Other inorganic • Ion exchange resins • ***Al/Zn***

3 Redox processes of relevance in the SFR 1 system

Many redox processes can be identified as being of relevance in the SFR 1 system: metal corrosion, degradation of organic matter, radiolysis, sulphate reduction, gases generation and fermentation.

Due to the huge amounts of materials such as metals and organic matter, it is unlikely that redox sensitive radionuclides drive the redox evolution of the system, although the implications that redox changes can have on their behaviour is an issue of concern and is also addressed in this report (see Chapter 9).

The level of radiation that may cause generation of oxidants in the repository is very low. Previous assessments on the influence that radiolysis can have on the oxidant balance of the repository, such as the one in Moreno et al. (2001) showed that the effect is expected to be minimal.

In this chapter the relevance of the main processes affecting redox conditions within the SFR 1 repository and the links and associations between them are discussed in order to select those processes identified as essential to be considered in the quantitative model. The modelled redox evolution will be used to assess the behaviour of the redox sensitive radionuclides included in this report (Se, Tc, Np and Pu).

The following processes, able to influence the redox evolution of the system are discussed in detail:

- Metal corrosion.
- Degradation of cellulose.
- Degradation of non-cellullosic organic matter, including bitumen.

3.1 Metal corrosion

Due to the large amounts of metals in the repository, and to their redox activity, metal corrosion is one of the main processes expected to affect the evolution of the redox state of SFR 1. Metals in SFR 1 are present in the wastes, used as base materials for waste packaging and also as reinforcement bars in concrete structures.

The corrosion of metals can produce oxygen depletion in the initial stages of the repository, and can potentially buffer possible oxidant intrusions in future evolutions of the system.

The most abundant metallic component in the SFR 1 is steel, although also some amounts of Al and Zn are present. Most of the reducing capacity in the repository will be given by Fe-containing material. Fe is not only present in carbon steel (C-steel), stainless steel (S-steel) and scraps in the wastes, but it is also a minor component of the cementitious materials present in the SFR 1, as well as an important component of the reducing groundwaters potentially intruding the repository in a future (in the form of dissolved Fe(II)).

Metal corrosion processes will be occurring from the onset of the process of packaging of the materials, during the period they are exposed to air. At repository closure, oxygen will be present in the system due to intrusion during the construction works and operational period (SKB 2008a). Oxic corrosion of metals is, thus expected to occur at least until this remaining oxygen is consumed. Therefore all metallic components, the ones from the packaging as well as the scrap present in the wastes will contribute to oxygen consumption through corrosion.

In the presence of oxygen, the corrosion of iron (steel) produces Fe(III) oxides and hydroxides, such as ferrihydrite ($Fe(OH)_3(s)$), goethite ($FeOOH(s)$) and hematite ($Fe_2O_3(s)$), according to Eq. 3-1.

$$Fe^0 + \tfrac{3}{4}\, O_2(g) + 3/2\, H_2O \rightarrow Fe(OH)_3(s) \qquad \text{Eq. 3-1a}$$

$$Fe^0 + \tfrac{3}{4}\, O_2(g) + \tfrac{1}{2}\, H_2O \rightarrow FeOOH(s) \qquad \text{Eq. 3-1b}$$

$$Fe^0 + 3\, O_2(g) + 6\, H_2O \rightarrow Fe_2O_3(s) \qquad \text{Eq. 3-1c}$$

As shown in Figure 3-1 hematite ($Fe_2O_3(s)$) is the thermodynamically stable Fe(III) oxide in the stability field of water (limited by dashed lines in the figure), followed by goethite (FeOOH) and ferrihydrite or hydrous ferric oxides ($Fe(OH)_3(s)$ or HFO). In the diagram, goethite appears only when the precipitation of hematite is suppressed and HFO only when both, hematite and goethite, are eliminated for the thermodynamic database. Despite their lower stability with respect to hematite, goethite and HFO can prevail as metastable solid phases for long time periods and they have faster formation kinetics when metallic iron oxidises in the presence of oxygen than hematite.

The rate at which steel corrodes under oxic conditions depends on many different parameters of the system, such as:

- the amount of oxygen initially present,
- the volume of water in contact with the metals and the exposed metallic surfaces,
- the temperature,
- the pH of the system, and, in general, the composition of the contacting water.

Figure 3-2 shows different rates of uniform corrosion measured for stainless steel covered with a passive film under oxic conditions (data from Blackwood et al. 2002 in Kursten et al. 2004). It is noticeable the effect that the temperature has on the uniform corrosion of this material and that the rates do not vary importantly between pH 6 and pH 11.

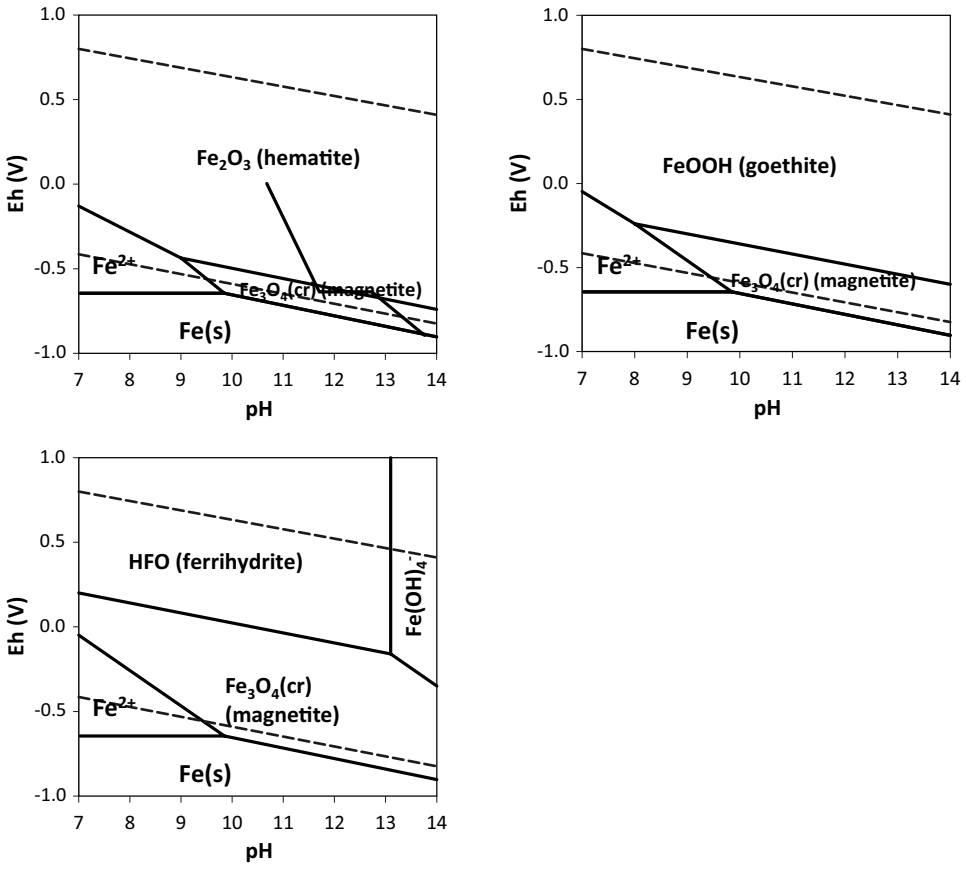

Figure 3-1. *Predominance Eh/pH diagrams of the Fe-O system showing the different stability fields of Fe(III) oxides and hydroxides. Hematite is the thermodynamically most stable Fe(III) oxide. When supressing its formation, the next stable Fe(III) oxide is goethite and in case of suppressing the formation of the later due to kinetic constraints, the metastable ferrihydrite (of hydrous ferric oxide, HFO) is formed.*

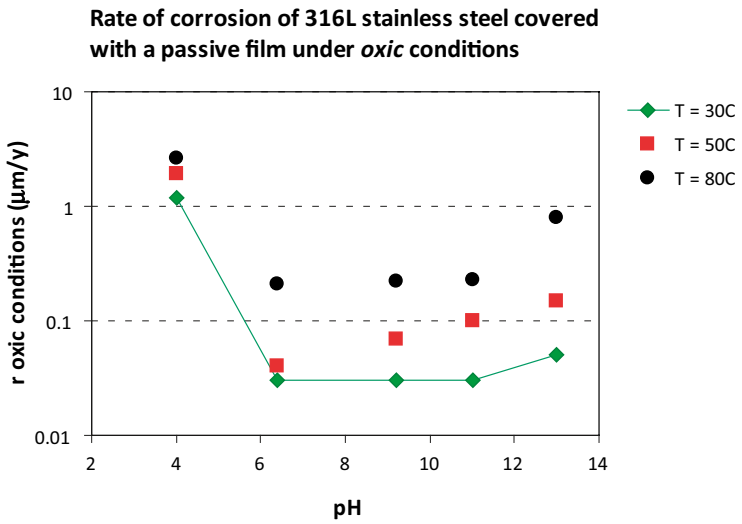

Figure 3-2. *Rate of corrosion of 316L stainless steel covered with a passive film under oxic conditions at different temperatures. Data from Blackwood et al. (2002) in Kursten et al. (2004).*

For pH values below 6 the corrosion rate increases sharply at all temperatures tested, while for pH above 11 the increase is less pronounced. Under the conditions of interest for the SFR 1, the rates would be around 0.03 µm/y in the initial stages of the repository evolution, this is, in the presence of oxidants. This value would compare with the 0.08 µm/y reported in Chambers et al. (1995) for carbon steel (see Table 3-1).

In SFR 1, the vault with the highest metal amount is BLA, containing mostly trash and scrap wastes. BLA is also the vault where wastes are mostly not conditioned. This means that the corrosion processes occurring in BLA will proceed at different conditions from those prevailing in the other vaults, where metals will mainly be in contact with cementitious materials. In BLA, metal corrosion will thus occur under near neutral conditions and this may change the corrosion rate.

Transforming the rates of steel corrosion to oxygen consumption rates in order to assess the length of the oxic period in the SFR 1 needs the use of different parametes, such as the density of the steel, which can be taken around 8,000 kg/m^3, the stoichiometry of the corrosion reaction of iron in the steel, and the average percentage of iron in the steel (for 316L one can considered around a 80% of Fe in wt. in steel). By taking Eq. 3-2 for the corrosion of iron in steel under oxic conditions, a rate of oxygen consumption by stainless steel of $2.57 \cdot 10^{-3}$ moles of O_2 per m^2 and per year can be calculated.

$$Fe^0 + \tfrac{3}{4}\, O_2(g) + 3/2\, H_2O \rightarrow Fe(OH)_3\,(s) \qquad \text{Eq. 3-2}$$

Table 3-1. Rate values for carbon-steel and stainless steel uniform corrosion under oxic hyperalkaline conditions at 30°C and 80°C. Data from Chambers et al. (1995).

Hyperalkaline conditions	T = 30°C	T = 80°C
C-steel, uniform corrosion	Rate = 0.08 µm/y	Rate = 1.6 µm/y
Stainless steel, uniform corrosion	Rate = 0.03 µm/y	Rate = 0.5 µm/y

By considering the surface area of iron/steel present in each one of the vaults from the inventory description, the calculated time needed for the consumption of all oxygen trapped in the different waste packages of the vaults is shown in Table 3-2 for the Silo and the BMA vaults.

This means that if the oxidation of steel accounts for the oxygen consumption it will only take a few years to consume the initial oxygen trapped in the repository and therefore to develop reducing conditions. In the case of using the oxidation rate of carbon steel, this time will be even reduced due to the faster corrosion rate of this material.

Al and Zn are also present in the SFR 1, and they present a fast corrosion rate under very alkaline conditions due to the re-dissolution of the passive layer formed on the surface of the metal. This would mean that the aerobic corrosion of Al and Zn would occur faster in the vaults containing a large amount of cementitious materials due to the reactivation of the metal surface, although the amount of Zn and Al in these vaults is smaller (Figure 2-6). Very simple preliminary calculations (see Appendix 2) show that the amount of Al present in the Silo and BMA vaults would be able to consume the initial oxygen trapped in these vaults, although only few types of waste packages contain Al (e.g. S.24, F.23, R.23, C.23, O.23 or S.23), that is, Al is present in very specific locations.

On the contrary, steel is ubiquitous in the repository (see Section 2.2 for a more detailed description); therefore the limitation of the presence of aluminium only in some very specific parts of the site does not apply to iron based materials.

At the end of the oxic period, metals will corrode in the absence of oxygen, under anoxic conditions. Fe(s) is thermodynamically unstable in water, its stability field falls below the stability line of water (dashed line in Figure 3-1) meaning that water can thermodynamically oxidise metallic iron.

In the absence of any other oxidant, metals corrode through water reduction, with subsequent hydrogen generation. In the case of iron corrosion by water, the initial hydrogen production proceeds according to Eq. 3-3.

$$Fe(s) + 2\ H_2O \rightarrow Fe(OH)_2\ (s) + H_2(g) \qquad \text{Eq. 3-3}$$

$Fe(OH)_2(s)$ is metastable and with time it evolves towards the formation of a spinel-like structure oxide, exemplified by magnetite, in the so-called Schikorr reaction (Eq. 3-4).

$$3\ Fe(OH)_2(s) \rightarrow Fe_3O_4 + H_2\ (g) + 2H_2O \qquad \text{Eq. 3-4}$$

The composition of the magnetite formed on the surface of iron is not exactly known, although it has been suggested that it consists of an oxide $Fe_{3-x}O_4$ with a spinel-like structure varying in composition from Fe_3O_4 (magnetite), in oxygen-free solutions, to $Fe_{2.67}O_4$ under the presence of oxygen (Stumm and Morgan 1996).

Iron/steel corrosion can also occur in the presence of carbonates and sulphides. In this case, the corrosion products may change from magnetite to iron sulphides and/or carbonates (siderite), and in the presence of chloride other phases such as the so-called green rusts may form.

Table 3-2. Calculation of the moles of O_2 (g) needed to corrode the steel present in the BMA vault and in the Silo of SFR 1 and of the time to consume the moles of O_2 (g) available in the repository. Surface area and total amount of iron/steel from Almkvist and Gordon (2007).

	BMA	Silo
Iron/steel (Kg)	2.68×10^6	2.79×10^6
Iron/steel (surface m^2)	1.24×10^5	$1.22E\times10^5$
mol O_2 consumed/year (stainless steel)	319	314
total moles O_2 from Table A2-1 and Table A2-2	515	800
Years for O_2 depletion	2	3

The global redox reaction for the transformation of iron into magnetite under anoxic conditions can then be written according to Eq. 3-5, indicating that 4 moles of water will be needed for the oxidation of 3 moles of iron, and consequently 4 moles of hydrogen will be produced.

$$3\ Fe(s) + 4\ H_2O \rightarrow Fe_3O_4(s) + 4\ H_2(g) \qquad \text{Eq. 3-5}$$

Many experiments in the literature report rates of anoxic corrosion of steel with subsequent hydrogen generation. Corrosion products may form a protective layer on the steel surface, and cause a decrease of the corrosion rate with time, as observed from experimental data and reported, for example in Smart et al. (2004) and references therein. Some uniform corrosion rates of carbon and stainless steel under anoxic conditions are shown in Table 3-3, from where the influence of pH can be also appreciated, as well as the different values obtained depending on the method used to determine the corrosion rate.

The model of gas generation developed in the previous safety assessment of the SFR 1 by Moreno et al. (2001) used uniform rates of anoxic steel corrosion between 0.1 and 1 μm/y.

Aluminum and zinc can also corrode under anoxic conditions, forming a very protective passive layer that prevents further oxidation, as shown in Eq. 3-6.

$$2\ Al(s) + 3\ H_2O \rightarrow Al_2O_3(s) + 3\ H_2(g) \qquad \text{Eq. 3-6}$$

At high alkalinity this oxide layer re-dissolves to form soluble aluminum species thus exposing the bare metal that further corrodes to produce aluminum hydroxide, also liberating hydrogen gas (Eq. 3-7).

$$2\ Al(s) + 2\ OH^- + 8\ H_2O \rightarrow 2\ Al(OH)_4^- + 3\ H_2(g) \qquad \text{Eq. 3-7}$$

In the presence of cementitious materials, the product of corrosion is less dense than the metal and hence it occupies more volume. This may lead to stress within cement matrix and possible creation of cracks.

Given the large amounts of concrete present in SFR 1, alkaline conditions are expected to prevail for those wastes conditioned with cement, thus favouring the fast corrosion of the metallic aluminium materials beyond passivation. The same is true for Zn.

As previously discussed, due to the much higher amounts and wider distribution of steel than of Al and Zn in the repository, steel is considered the metal having a most important effect on the redox evolution of the repository.

Typical iron-based alloy corrosion rates are below 1μm per year. Corrosion rates are influenced by many different variables of the media such as composition of the material, temperature, groundwater composition, presence and composition of gases, history of the surface (whether it has been corroded previously or not), etc.

Table 3-3. Rate values for carbon-steel and stainless steel uniform corrosion under different anoxic conditions.

C-steel, uniform corrosion		
pH	**Rate (μm/y)**	**Reference**
13	< 0.04	Naish et al. 2001
7	0.2	Naish et al. 2001
4	0.6	Naish et al. 2001
Stainless steel, uniform corrosion		
Method	**Rate (μm/y)**	**Reference**
Passive current	0.1	Blackwood et al. 2002
Hydrogen evolution	0.001	Naish et al. 1995
Hydrogen evolution	0.01	Mihara et al. 2002
Passive current	0.4	Sharland and Newton 1989

Cement acts as a physical barrier inhibiting the contact of steel with the most aggressive external species, thus stabilising the passivating layer. Montemor et al. (2003) and Soylev and François (2003) considered that cement properties (mineralogy, density) inhibit metal corrosion because they retard the movement of aggressive agents. Nevertheless cement properties such as porosity, permeability, water:cement ratio; pore water composition or cement and aggregates mineral composition will determine the alteration capacity of the passive layer formed on the steel surface.

The way in which metal corrosion has been implemented in a conceptual model to assess the evolution of the redox conditions with time in SFR 1 and the values of the parameters used in the numerical model are detailed in Chapter 5.

3.2 Degradation of organic matter

Organic wastes may degrade by a combination of physical, chemical and microbial processes. This degradation is likely to generate gases and a variety of organic compounds that may influence radionuclide solubilities.

According to previous assessments, the processes of degradation of organic matter account for an important part of the potential generation of gases in the short-term after the repository closure (see Moreno et al. 2001 for details).

Degradation of organic materials will mainly produce hydrogen and CO_2 as gaseous products (except at high pH, where CO_3^{2-} is formed instead).

Microbial processes degrade organic material and can contribute to the corrosion of metals and concrete. In this case, the effect that microorganisms can have on the redox state of the repository is due to their driving effect on oxidant consuming processes.

The activity and abundance of microbes in a repository are affected by different factors such as the supply of usable nutrients and energy sources; the availability of water, the temperature or the pore size of the media.

Organic carbon in wastes and inorganic molecules, such as hydrogen (from anaerobic corrosion processes) and methane (from geological sources or microbial origin) are possible electron donors and energy sources for microbial processes in the SFR 1 repository.

Microorganisms preferentially reduce electron acceptors in a particular order, in agreement with the redox ladder: oxygen, nitrate, manganese, iron, sulphate, sulphur and carbon dioxide sequentially (Figure 3-3). Simultaneously, fermentative processes supply the metabolizing microorganisms with, for example, hydrogen, methane and short-chain organic acids such as acetate.

Different type of organic matter can be found in the repository. Cellulose and bitumen are two of the different types but also non-classified organic matter occur, what we will refer to as “generic organic matter” in the text. Some of the specificities of the degradation processes of cellulose and bitumen follow.

3.2.1 Degradation of cellulose

Cellulose is only present in two types of waste packages in the Silo (C.24 and S.11) consistently with the safety criteria of minimizing the amount of organic matter in this vault (Table 2-2). Other organic materials in the Silo, such as polyethilene, are not present in massive amounts. In BMA, cellulose is present in some of the packages, and in this vault there is also a higher content of other organic matter available for oxidation (Table 2-4). The content of cellulose in BLA is important, as it is the presence of other organic materials that can contribute to oxygen and/or oxidants depletion (Table 2-10). In BLA, the degradation of the organic matter will probably happen in different conditions to those in the other vaults, due to the fact that concrete is not used for stabilization, but only for shot-creeting of the walls of the vault and in the floor, therefore the modeling of the initial evolution of the redox potential in BLA should not consider hyperalkaline conditions, at least at the initial stages, on contrary to the other vaults.

Within the repository, cellulose (wood, cotton cloth, card board, paper, tissues) is the most significant substrate for microbial growth. In order for cellulose to be available to microbes, the polymer must initially be broken to produce more metabolisable sub-units. This process can occur either biologically or chemically. Under high pH conditions such as those expected in most repository vaults, the chemical process will dominate, leading to the production of sugar acids such as isosaccharinid acid and similar compounds. Under neutral pH conditions the degradation of cellulose is likely to be mediated mainly by microorganisms and the process will be analogous to that occurring in landfills, producing glucose-type monomers (Askarieh et al. 2000).

Under oxic conditions cellulose hydrolyses to glucose-type monomers that react with oxygen to give CO_2 according to Eq. 3-8 and 3-9 where it can be seen that each mole of glucose-type monomer would consume 6 moles of oxygen to be completely oxidised to CO_2. The process of aerobic hydrolysis of cellulose has a high associated potential of gas generation.

$$(C_6H_{10}O_5)_n + H_2O \rightarrow n\ (C_6H_{12}O_6) \qquad \text{Eq. 3-8}$$

$$C_6H_{12}O_6 + 6\ O_2\ (g) \rightarrow 6\ CO_2(g) + 6\ H_2O \qquad \text{Eq. 3-9}$$

The released glucose units and their further non-complete oxidation products (aldehydes, ketones and/or carboxylates) and complete oxidation products (CO_2(g) and H_2O) will be the main degradation products.

Acetate has been chosen as representative of the non-complete oxidation of cellulose, in addition to CO_2 as shown in Eq. 3-10.

$$C_6H_{12}O_6 + 2\ H_2O \rightarrow 2\ CH_3COO^- + 2\ CO_2\ (g) + 8\ H^+ + 8\ e^- \qquad \text{Eq. 3-10}$$

Under anaerobic conditions, hydrolysed cellulose is degraded to alcohols, carboxylic acids, CO_2 and H_2, and the hydrolysis of alcohols yields hydrogen, according to Eq. 3-11 and 3-12 (Glaus et al.1999, Byrum 2006).

$$C_6H_{12}O_6 + H_2O \rightarrow C_2H_5OH + CH_3COOH + 2\ H_2 + 2\ CO_2\ (g) \qquad \text{Eq. 3-11}$$

$$C_2H_5OH + H_2O \rightarrow CH_3COOH + 2\ H_2\ (g) \qquad \text{Eq. 3-12}$$

Alkaline degradation of cellulose yields complexants, such as isosaccharinic acid (ISA), which have been found to have an important impact on the chemistry of radionuclides present in the repository, such as plutonium.

In their last publication Glaus and Van Loon (2008) suggest that the time needed for complete degradation of cellulose in a cementitious repository should be in the range between 1,000 and 5,000 years, given that although the initial degradation reaction is fast, the rate decreases with time, what the authors attribute to the change in the reaction responsible for the degradation of cellulose. In the mentioned work, these authors proposed a kinetic law based on an experiment on cellulose degradation under anoxic and abiotic conditions performed during 12 years (Glaus et al. 1999, Glaus and Van Loon 2004, 2008, Van Loon et al. 1999). They presented a mathematical equation able to explain the observed evolution of the concentration of ISA in the system (see Eq. 3-13) and parameterised the equation with values shown in Table 3-4.

$$celdeg_{cellulose} = 1 + e^{-k_h t}\left[\frac{k_1}{k_t}(G_t)_o\left(1 - e^{-k_h t}\right) - 1\right] \qquad \text{Eq. 3-13}$$

Table 3-4. Parameters used in the abiotic cellulose degradation rate equation. The data are from Glaus and Van Loon (2008).

$(G_r)_0$	5.6×10^{-4}
k_1 (h^{-1})	$(2.0\pm0.3)\times10^{-3}$
k_t (h^{-1})	$(3.3\pm0.5)\times10^{-4}$
k_h (h^{-1})	$(2.9\pm0.3)\times10^{-8}$

There is evidence that active microbial populations could be present in a repository and that they could evolve to degrade organic complexing agents such as ISA. Nevertheless, it is unlikely that such microbial populations will be widely distributed in the repository. There is considerable uncertainty about if, or when, active microbial populations would develop to the point where the removal of organic ligands by microbial action could have a significant impact on the release of dissolved radionuclides.

Investigations into the chemical stability of ISA have been carried out and reviewed by some authors (Glaus et al. 2007, Hurdus and Pilkington 2000). Hurdus and Pilkington (2000) carried out experiments at both room temperature and 80°C over 10 and 12 months respectively. Their results indicated that the chemical degradation of ISA only occurred in the presence of oxygen; acetic, lactic and formic acids were identified as degradation products. Similar results have been presented by Glaus et al. (2007) who showed that degradation of ISA occurred only in the presence of stoichiometric amounts of oxygen or a similar oxidant. The decomposition products were identified as a mixture of glycolic, formic and lactic acids. The authors concluded that the oxidative decomposition of ISA could not be included as a process of significance in reducing the concentrations of degradation products considered in the safety assessments of repositories due to limited period of oxidising conditions expected.

3.2.2 Degradation of bitumen

Given the stability of the bituminized matrix, as well as the evidences found for the stability of the ionic exchange resins (SKB 2014) these two materials are normally not considered to contribute importantly to the depletion of the initial oxygen present in the repository.

Bitumen as any organic material is prone to biodegradation in both aerobic and anaerobic conditions. The rate and extent of bitumen biodegradation is dependent on the amount and type of microorganisms present, the redox conditions (oxic or anoxic), the water composition, the chemical composition of the bitumen matrix itself and on some other physical properties (e.g. porosity and pore connectivity).

According to Pedersen (2001) a substantial amount of microorganisms may grow on bitumen surfaces exposed to water. The dependence of the rate of degradation on redox conditions is not totally clear; while some authors postulate that degradation is faster and more complete under oxic conditions (Wolf and Bachofen 1991) other give very similar biodegradation rates (Roffey and Norqvist 1991).

It is generally assumed that bitumen is stable under highly alkaline conditions because it is considered similar to “addition polymers” which are “insensitive to alkali” (Van Loon and Hummel 1995). Nevertheless, the description of bitumen as an addition polymer may not be entirely correct since it consists of mixtures in variable proportions of aliphatic and aromatic compounds, as well as resins and asphaltenes in a polydispersed colloidal fashion. Among these compounds, only the latter two may be considered as polymeric in nature. In fact, aliphatic and aromatic hydrocarbons, resins, and asphaltenes are the constitutive fractions of natural bitumen and petroleum (Faure et al. 1999), although they may be present in proportions, which are different than in the industrial bitumen (Pettersson and Elert 2001) such as that used in SFR 1.

Among the main aerobic degradation products of bitumen, oxalic acid, acetic and formic acids have been identified (Oude Elferlink et al. 1998, EPA 2000, Petterson and Elert 2001, SKB 2014).

There is increasing evidence for the generation of soluble organic compounds from natural organic matter under hyperalkaline conditions (Claret et al. 2003, Elie et al. 2004). Although it has been suggested that natural organic matter should not be considered as representative of industrial bitumen, the fact that industrial bitumen is prepared from natural petroleum may render natural organic matter a better analogue than previously recognized.

Kagawa et al. (1999) – cited in Pettersson and Elert (2001) – reported the production of 0.6–1.2 g C/L after leaching bitumen for 3 years under oxic conditions. The major alteration products were formic acid and acetic acid. Elie et al. (2004) found *n*-carboxylic acids to be the dominant degradation products of natural organic matter under hyperalkaline conditions.

By considering as representative of bitumen the following composition: C 88 wt.%, H 11 wt.%, and O 1 wt.% (Pettersson and Elert 2001), the degradation of bitumen under alkaline conditions can be written as a reaction of oxygen consumption, Eq. 3-14, if acetate is considered the main degradation product.

$$C_{7.33}H_{10.91}O_{0.06} + 3.67\ OH^- + 2.70\ O_2(g) \rightarrow 3.67\ CH_3COO^- + 1.79\ H_2O \qquad \text{Eq. 3-14}$$

Transforming the measurements of C production in the experiments of Kagawa et al. (1999) into rates of oxygen consumption by considering the former reaction of bitumen degradation, a vaue in the range of 0.01 moles O_2/L water per year is obtained for the rate of oxygen consumption. This means that time needed for completely consume the initial oxygen trapped in the repository in the vicinity of bitumen would be very short if this process is credited to occur at the initial stages after repository closure. It has to be indicated in this context that the oxidation of bitumen is a widely observed process in bituminised waste matrices.

3.3 Brief summary

Figure 3-3 summarises the different processes accounting for redox evolution within the frame of the SFR 1 repository. If the conditions under which the previous redox processes are occurring correspond to the pH imposed by a cementitious environment, and in the absence of oxidising perturbations in the system, the expected evolution of the redox potential can be conceptualised by the redox ladder shown in Figure 3-4.

Nevertheless, the conditions under which each one of the processes occur may vary importantly from sub-system to sub-system in the SFR 1, so that the understanding on how the environmental conditions will affect – and to which extent – to the redox evolution of the system is crucial.

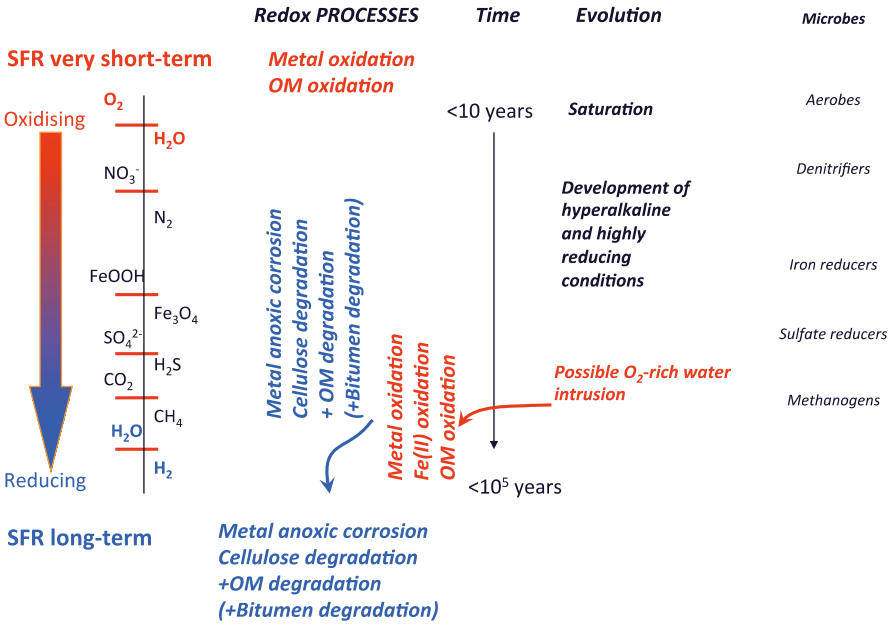

Figure 3-3. *Sketch of the redox evolution of the SFR 1. The time at which oxygen intrusion may happen will depend on the climatic evolution of the repository.*

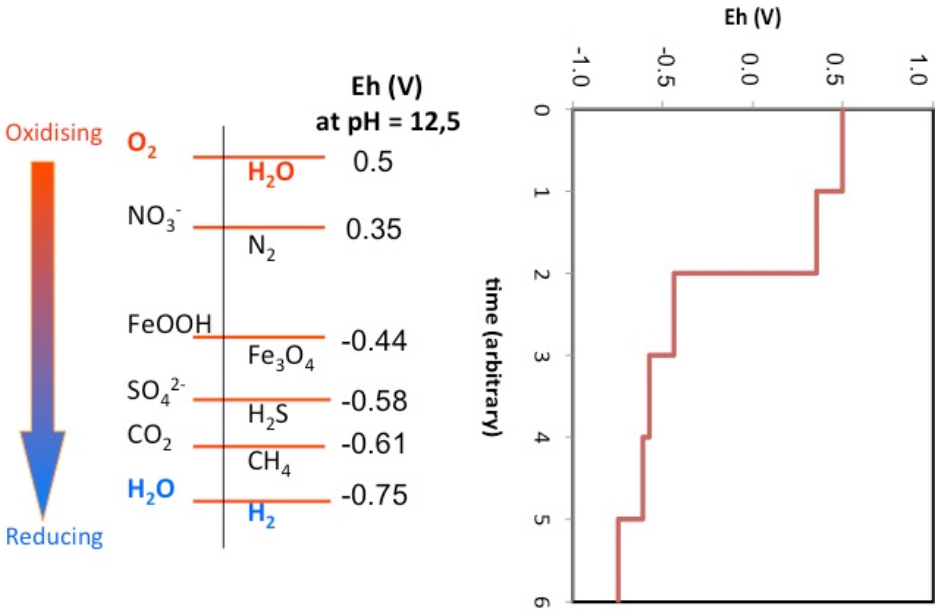

Figure 3-4. *Sketch of the evolution of the redox potential in SFR 1 in non-disturbed conditions depending on the redox couple governing the Eh at a pH controlled by cementitious environment conceptualised by portlandite ($Ca(OH)_2(s)$) equilibrium.*

4 General approach to the model

The objective of this project is the assessment of the evolution of the redox conditions of the SFR 1. As presented in Chapter 3, the system presents a high capacity to buffer an oxidant intrusion, given the amount of materials able to be oxidised in the repository. The main materials that can protect the repository from achieving oxidising conditions are metallic components and different organic matter materials (plastics, rubber, bitumen and cellulose).

When assessing the behaviour of this type of systems it is important to consider not only the theoretical capacity that the system has to accept oxidants, but also the relative rate of reduction *versus* the rate at which the oxidant intrusion occurs.

Under non-disturbed conditions, there will be an initial stage during which the oxidants initially present in the system due to the construction and operation works will be consumed. After this period, the system will reach anoxia and reducing conditions will develop. The groundwaters reaching the repository at long-term are not expected to contain appreciable concentrations of oxidising species, due to their prior interaction with soils and minerals that will cause oxidant consumption. According to the expected evolution of the SFR 1 environment, the only possibility of oxidising conditions to reach repository depths arises from an inflow of glacial oxygen-rich and diluted water. This situation would, if at all, happen during melting of water events. According to the current climatic evolution of the system, the earliest time at which melting water would reach the repository is 60 ky after its closure. This means that, once the system has reached reducing conditions, its capability to buffer an oxidising intrusion will basically remain the same until 60 ky and that after this time, it will be jeopardised only in the case of a melting water inflowing the system.

Although the reducing capacity of the repository is far larger than the one needed to account for total consumption of the oxygen initially trapped, the kinetics of the electron-transfer processes are among the most relevant parameters to estimate both the duration of the oxic period and the likeliness of the oxygen consumption to occur in all parts of the repository.

In order to account for how the system will behave during the 100 ky after repository closure the analyses will be undertaken from two different perspectives:

- Assessment of the time evolution of the system, i.e., the rate at which the system develops reducing conditions and how fast it reacts towards an oxidising intrusion.
- Assessment of the capacity remaining in the system to buffer any future oxidising disturbance, that is, the ReDucing Capacity of the system (RDC).

To this aim, the discussion presented in Chapter 3 must be transferred into a conceptual model to be implemented into a numerical model of the repository system.

The different vaults of the repository have been considered as a combination of generic waste package types. In this way, the combination of the evolution of the redox conditions in each generic waste package type will be useful to asses the evolution of the redox conditions in the vaults and this, in turn, in the complete repository system.

More than 50 different waste packages have been defined for the SFR 1. For the sake of model simplification, the most representative types of waste packages have been selected, in agreement with SKB (Zazzi 2011) and shown in Figure 4-1.

Each package type is conceptualised as a homogeneous mixture of waste, matrix and packaging materials (see Table 4-1).

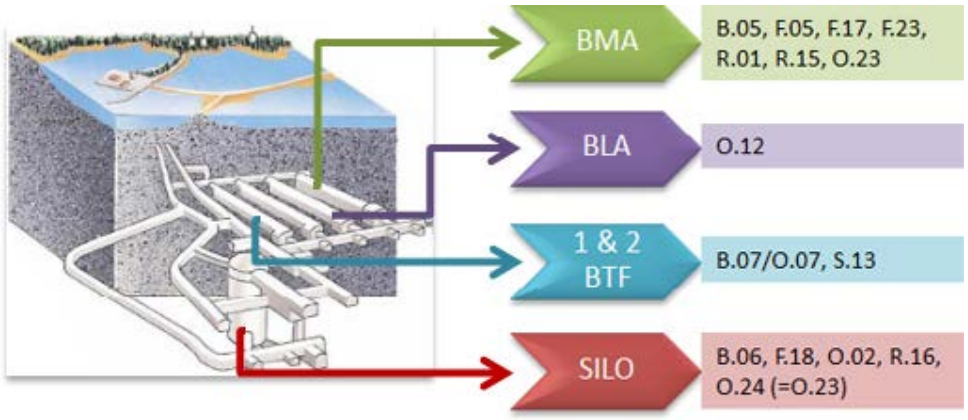

Figure 4-1. *Waste package types selected as the most representative for the BMA, BLA, 1 and 2 BTF vaults and for the Silo. Data from Zazzi (2011).*

Table 4-1. Waste types representative for Silo, and for BMA; BLA and 1&2 BTF vaults Zazzi (2011).

Waste type representative for Silo	
B.06	Steel packages containing ion-exchange resins in a bitumen matrix.
F.18	Steel packages containing ion-exchange resins in a bitumen matrix.
O.02	Concrete mould containing ion-exchange resins in a concrete matrix.
R.16	Steel packages containing ion-exchange resins in a concrete matrix.
O.24 (equal to O.23)	Concrete mould with scrap metal in a concrete matrix.
Waste type representative for BMA	
B.05	Steel packages containing ion-exchange resins in a bitumen matrix.
F.05	Steel packages containing ion-exchange resins in a bitumen matrix.
F.17	Steel packages containing ion-exchange resins in a bitumen matrix.
F.23	Steel packages with scrap metal in a concrete matrix.
R.01	Concrete mould containing ion-exchange resins in a concrete matrix.
R.15	Steel packages containing ion-exchange resins in a concrete matrix.
O.23	Concrete mould with scrap metal in a concrete matrix.
Waste type representative for BTF	
B.07/O.07	Concrete tank containing de-watered ion-exchange resins.
S.13	Steel drums with ashes in a concrete matrix.
Waste type representative for BLA	
O.12	ISO-container with metal scrap and other waste.

4.1 Methodology of the assessment

The methodology followed in the current assessment to estimate the evolution of the system has been:

a. To calculate the chemical evolution of each one of the 14 different types of waste packages presented in Table 4-1 by implementing the redox processes discussed in the previous section into a conceptual and numerical model.

b. From the results in a., the calculation of the temporal evolution of the Reducing Capacity (RDC) of each one of the 14 types of waste package according to Eq. 5-16 to 5-17.

c. Combination of the results from b. to obtain the RDC at each time at each one of the vaults Silo, BMA, BLA, 1 BTF, 2 BTF and BMA;

d. Combination of the results from c. to calculate the RDC of the SFR 1.

The implementation of the numerical model, as well as some results selected to describe the evolution of the system are presented in Chapters 5 to 8. The complete results for all the individual waste package types are shown in Appendix 5.

5 Conceptual model and numerical implementation

The model considers the calculation of the evolution of the redox conditions in each waste package individually.

The different key points to implement a conceptual and numerical model, as well as the initial state considered for the waste packages, are described below.

Base data from the SFR 1 description

- The packaging material can be concrete (e.g. waste type R.01) or steel (e.g. waste type R.15), as shown in Table 4-1.
- The waste material can be composed by steel, bitumen, ion exchange resins, cellulose, sludge, Al and Zn, and other organic or inorganic components.
- The wastes can be immobilised in a concrete matrix, a bitumen matrix or not conditioned.

General conceptual model

- For the sake of simplicity, concrete (from matrix or containers) is assumed to behave as portlandite. With this assumption, chemical changes due to cement and concrete degradation (chemical composition, porosity, sorption properties) are not included in the model. The coupling of the present model with concrete degradation could be considered for future developments although at this point it will increase the difficulty of the understanding of the results. Bounding cases are discussed in the assessment of the redox state of the system in subsequent chapters.
- Only steel, bitumen, cellulose and other generic organic materials are considered to be redox reactive. Although in Zazzi (2011) the degradation of ion exchange resins is pointed out, it was decided, in agreement with SKB, that these materials will be considered innert.
- Fast oxic corrosion of Al and Zn is pessimistically neglected. These metals are present only in very specific locations and are not thought to provide a general reducing capacity to the system.
- Sludge and other inorganic materials are not included in the model because they appear in very low amounts.
- Steel is considered to be homogeneous and no differences in composition are assumed between steels of different origins. Steel is considered to be carbon steel.
- Corrosion of steel is considered to be kinetically driven and bitumen, cellulose and other organic materials are assumed to degrade in the presence and in the absence of microbes, according to the kinetics presented in the following sections and resulting from literature review.
- The microbial communities are expected to have an important activity and to affect the degradation process of cellulose, bitumen and other organic materials.
- Generic organic matter is assumed to be CH_2O and to behave similarly to bitumen.
- The water saturation of the system is assumed to be very fast, therefore complete saturation of the system is always considered.
- Although steel corrosion products may cause expansion and generate cracks in the concrete material, no mechanical changes due to stresses have been considered in the assessment.
- When water flow is considered in the model, data from flow rates have been taken from Holmén and Stigsson (2001).
- Temperature is considered constant at 25°C due to the fact that temperature changes could only incorporate uncertainty to the results. Most thermodynamic databases are developed at this temperature, and the behaviour of the materials is much better known at 25°C.

Initial conditions

- Initially, the porewater of the waste package is considered to be in equilibrium with atmospheric O_2, at P_{O2} of 0.21 atm, due to the construction and operational periods.
- The groundwater considered to interact with the wastes is in equilibrium with portlandite (as proxy for concrete). Alternatively, in those waste package types not containing concrete or cement materials, porewater is also considered hyperalkaline given that groundwater will have interacted with repository structures (walls and floors) before reaching the waste package.
- Initial waste porewater has been assumed equal to the cementitious porewater for all cases except for waste package O.12, for which initial waste porewater is the granitic groundwater.
- The initial amount of portlandite of each waste package is recalculated to mol/L_{water} considering the porosity of the waste package fully saturated and assuming a mass of portlandite equal to the mass of concrete reported in Zazzi (2011).
- For the sake of simplicity the conceptual model does not consider the presence of radionuclides in the system (and thus, of their possible contribution to the Reductive Capacity of the system).
- Dissolution and precipitation of portlandite, goethite, FeS(ppt), magnetite, calcite and $Ca(CH_3COO)_2$ may happen, and will be thermodynamically driven as they are relatively fast processes. Also fast are gas-liquid equilibria.

Table 5-1. General overview of the conceptualisation and implementation of the different redox active processes in the model.

Process		Concept	Implementation
Metal corrosion	Al and Zn	• Fast corrosion under oxic cond. • Anoxic corrosion would generate H_2(g). • Only present in few type of waste packages.	• Al and Zn are not considered in the numerical assessment.
	Steel (Fe)	• Fast corrosion under oxic cond. to form Fe(III) oxides or hydroxides. • Slower corrosion by water with generation of H_2(g) and Fe(II)/Fe(III) oxides as corrosion product. • Ubiquitous in the repository and present in large amounts.	• Fe used as proxy for steel. • Fast oxidation in the presence of oxygen with the generation of goethite. This process is implemented according to equilibrium. • Kinetic corrosion under anoxic cond., with the formation of magnetite as corrosion product and generation of H_2(g) from water reduction. Steel corrosion rates used in the numerical model.
Organic matter	Ion-exchange resins	• Chemically inert.	• Not considered in the numerical assessment.
	Bitumen	• Slow degradation kinetics. • Microbially mediated. • Acetate as product.	• Monod-like rates for biotic degradation. • Linear rate for chemical degradation.
	Cellulose	• Microbially mediated giving acetate and CO_2 (g)as main degradation products. • In the absence of microbes, production of Acetate and CO_2 (g) in neutral pH conditions. • In the absence of microbes, production of ISA and acetate in alkaline conditions.	• During the biotic period kinetic degradation to form acetate and CO_2(g). Acetate also degrades to CO_2 (g) under these conditions (Monod-like rate law). • After microbes are not active, in alkaline conditions kinetic production (Van Loon and Glaus rate law) of ISA(80% yield) and acetate (20% yield).
	Other generic organic matter	• Treated as bitumen.	
Microbial processes		• Affect organic matter degradation.	• Bacterial mortality considered when e- acceptors fall below 10^{-6} M.
Gases		• During the oxic period gas generation is due to organic matter degradation, mainly CO_2(g). • During the anoxic period H_2(g) is formed due to the anoxic corrosion of steel.	• Gas allowed to form and leave the system when P > 6.87 atm.

Treatment of gases

- Gases generated from corrosion of steel and chemical or microbial degradation of cellulose, bitumen and other organic materials such as H_2, CH_4 and CO_2(g) in case of non-alkaline conditions can dissolve in the contacting water. Gases will be able to form an individual gas phase and leave the system only in case an overpressure is created. The hydrostatic pressure at 70 m depth is of 6.87 atm.
- The numerical model neither considers the transport or diffusion of gases through the container wall nor the mechanical effects on the system that the presence of these gases can produce.

A schematic overview of how the different processes are conceptualised in the model and the simplifications made is shown in Table 5-1.

5.1 Calculation code and thermodynamic database used

The cases presented in this report have been run with the code PHREEQC (Parkhust and Appelo 1999) and the thermodynamic database SKB_TDB_2009.

Prior to the calculations the database has been compared to the database ThermoChimie (Duro et al. 2010, 2012, issued together with PHREEQC code (Parkhurst and Appelo 1999)) for the S, Fe, C aqueous species and solid phases, main differences are related to the system Fe-carbonate and to ISA complexes. As a result of this comparison some modifications have been done to SKB_TDB_2009 before calculations:

- Aqueous species of Fe(III)-carbonate system from ThermoChimie have been added to SKB_TDB_2009 because of the importance of these species.
- A new equilibrium constant for ferrihydrite (log K = 1.2, from Grivé 2005) has been included in the database SKB_TDB_2009, because it is the reaction from which solubility of ferrihydrite in the presence of carbonate is described. Thermodynamic data for other ferrihydrites are kept because they cover other solubility ranges.
- ISA aqueous and solid complexes of ThermoChimie have been included in SKB_TDB_2009.
- Acetate aqueous complexes of ThermoChimie have been included in SKB_TDB_2009.
- A solid Ca-acetate phase has been included in SKB_TDB_2009 in case acetate concentrations become too high in a Ca-rich solution. Equilibrium constant for this solid has been estimated from its solubility in water (~25–35 g/100 mL) and it must be considered as an approximate value used only to avoid an infinite acetate aqueous concentration.

Table 5-2 summarises the reactions and thermodynamic data included in SKB_TDB_2009 previous to calculations.

Table 5-2. Thermodynamic data added to SKB_TDB_2009 in order to perform the calculations.

Reaction	Log K	Reference
$Fe^{3+} + CO_3^{2-} + H_2O \rightleftharpoons FeCO_3OH + H^+$	10.76	Grivé 2005
$Fe^{3+} + 3\ CO_3^{2-} \rightleftharpoons Fe(CO_3)_3^{3-}$	24.24	Grivé 2005
$Fe(OH)_3 + 3\ H^+ \rightleftharpoons Fe^{3+} + 3\ H_2O$	1.2	Grivé 2005
$H^+ + HIsa^- \rightleftharpoons H_2Isa$	4	Hummel et al. 2005
$Ca^{2+} + HIsa^- \rightleftharpoons Ca(HIsa)^+$	1.7	Hummel et al. 2005
$Ca^{2+} + HIsa^- \rightleftharpoons Ca(Isa) + H^+$	–10.4	Hummel et al. 2005
$Ca(HIsa)_2(cr) \rightleftharpoons Ca^{2+} + 2\ HIsa^-$	–6.4	Hummel et al. 2005
$HAcetate \rightleftharpoons Acetate^- + H^+$	–4.76	Stumm and Morgan 1996
$Acetate^- + Ca^{2+} \rightleftharpoons Ca(Acetate)^+$	1.12	De Robertis et al. 1995
$Ca(CH_3COO)_2 \rightleftharpoons Ca^{2+} + 2CH_3COO^-$	~0.8	Approximation. This report.

5.2 Groundwater composition

Initial waste porewater has been assumed equal to the cementitious porewater for all cases except for waste package O.12, for which initial waste porewater is the granitic groundwater. In both cases, O_2 concentration is in equilibrium with atmospheric O_2(g) (0.21 atm). Groundwater compositions are listed in Table 5-3.

Table 5-3. Composition of the cementitious and granitic groundwaters used in the calculations.

	Cement groundwater	Granitic groundwater
pH	12.5	7.49
S(VI)	2.0×10^{-5}	5.2×10^{-4}
Cl	2.0×10^{-3}	1.3×10^{-3}
Na	3.0×10^{-3}	4.4×10^{-3}
K	1.0×10^{-4}	1.0×10^{-4}
Ca	2.0×10^{-2}	8.7×10^{-4}
Al	2.0×10^{-6}	2.0×10^{-6}
Si	3.0×10^{-6}	9.8×10^{-5}
Mg	–	3.7×10^{-4}
C(IV)	–	4.9×10^{-3}
Al	–	–
O_2	In equilibrium with 0.21 atm O_2(g)	In equilibrium with 0.21 atm O_2(g)
Ref.	SKB 2008b	SKB 2008b

The conceptual model adopted for each one of the processes and their numerical implementation is described in more detail in the following sections.

5.3 Steel corrosion

5.3.1 Conceptual model

Fe^0 is the main and unique reactive component of steel.

No differences are assumed in steels from different package types in terms of corrosion rate, composition or corrosion mechanism. Only reactive area may differ from steels placed in different waste package types.

Under oxic conditions, Fe^0 corrodes kinetically, goethite forms if saturated.

Once anoxic conditions are achieved ($[O_2] < 10^{-6}$ M), steel corrosion continues at expenses of water reduction, kinetically governed.

Magnetite and H_2 (g) are considered the main corrosion products of the anoxic and reducing period.

During the development of anoxia, there is a transient period in which goethite is transformed to magnetite. Experimental observations by Hansel et al. 2003 indicated reductive dissolution of ferrihydrite ($Fe(OH)_3$), fast precipitation of goethite and subsequent precipitation of magnetite.

5.3.2 Numerical parameterisation

The values for steel corrosion rates used in this report are listed in Table 5-4 and are those suggested by PSU team. These values are in line with those values reported in literature and shown in Table 3-1 and Table 3-3.

For numerical implementation, rates in μm y^{-1} have been recalculated to mol_{Fe} m^{-2} s^{-1} by assuming a density of 7,860 kg m^{-3} for steel (Zazzi 2011) and a molecular weight of 55.85 g mol^{-1} for Fe^0. Carbon steel is considered to be 99% wt. Fe^0 (Zazzi 2011).

Table 5-4. Steel corrosion rates used in the calculations.

Hyperalkaline conditions	μm yr^{-1}	mol_{Fe} m^{-2} s^{-1}	Reference
Oxic corrosion rate	0.1	4.4×10^{-10}	Blackwood et al. 2002
Anoxic corrosion rate	0.05	2.2×10^{-10}	Smart et al. 2004
Near neutral conditions	μm yr^{-1}	mol_{Fe} m^{-2} s^{-1}	**Reference**
Oxic corrosion rate	60	2.7×10^{-7}	Kuron et al. 1985
Anoxic corrosion rate	2.8	1.2×10^{-8}	Simpson and Weber 1988, Schenk 1988, Simpson et al. 1985

5.4 Degradation of organic matter

5.4.1 Conceptual model

The development of different bacteria populations depends on the achievement of the optimal conditions for their growth. Besides nutrients availability and pH conditions, the redox value is an indicator of which type of bacterial population may dominate as conditions become reducing. The most common microbial communities are aerobes, denitrifiers, iron reducing bacteria (IRB), sulphate reducing bacteria (SRB) and methanogens. Denitrifiers are not considered in this study because nitrate aqueous concentration is not considered at this stage. Methanogens have not been explicitely included in the calculations, although during biotic conditions methane is left to be produced from carbonate reduction when thermodynamically allowed. The conceptual model thus, assumes that methanogens are present in the system, although their specific growth and mortality have not been considered. Fermentation has neither been considered.

In this conceptual model, thus, the unique bacterial communities whose growth and mortality have been considered have been aerobes, iron reducing bacteria (IRB) and sulphate reducing bacteria (SRB).

The threshold limiting the fields of activity of O_2-consumers, IRB and SRB communities has been fixed to 10^{-6} M of [O_2], [Fe(III)] and [S(VI)] respectively, which are in the range of values proposed in the literature, as shown in Table 5-5.

When biota is not active in the system, chemical degradation of organic matter occurs.

The detailed kinetic constraints on organic matter degradation are presented in the following subsections.

Table 5-5. Summary of concentration thresholds used by different authors to define the activity field of different oxidants.

McMahon and Chapelle (2008)				Small et al. (2008)	Appelo and Postma (2005)
Threshold	**mg/L**	**PM (g/mol)**	**Mol/L**	**Mol/L**	**Mol/L**
O_2	0.5	32	1.6×10^{-5}	1.0×10^{-6}	1.0×10^{-6}
SO_4	0.5	96	5.2×10^{-6}	1.0×10^{-6}	1.0×10^{-6}

5.4.2 Bitumen, "generic organic matter" and acetate degradation

The conceptual model assumes that generic organic matter and bitumen are degraded under alkaline and near neutral conditions. Degradation is microbially mediated under biotic conditions and organic matter and bitumen are chemically degraded once abiotic conditions are achieved. Acetate is considered the main representative product of both microbial and chemical degradation. The same model is considered for both "generic organic matter" and bitumen degradation (Eq. 5-1).

$$C_{7.33}H_{10.91}O_{0.06} + 7.28\ H_2O \rightarrow 3.67\ CH_3COO^- + 10.8\ e^- + 14.47\ H^+ \quad \text{Eq. 5-1}$$

The biotic degradation rates will be controlled by the growth rate of the different microbial communities and by the availability of O_2, Fe(III) or S(VI) in solution, following Monod-type expressions (Eq. 5-2 to 5-4). Each equation is only valid in the fields limited by the different thresholds shown in Table 5-5. Under abiotic conditions, that is, when electron acceptor concentrations are too low to keep microbes active, generic organic matter and bitumen are assumed to chemically degrade at a constant rate (Eq. 5-5), equal to 10^{-12} mol dm^{-3} s^{-1}. Table 5-6 shows the values of the parameters for these equations.

For $[O_2] > 10^{-6}$ M,

$$\boldsymbol{rate_i^{biotic,O_2} = [Biomass_O]\ K_i^{O_2} \frac{[O_2]}{k_{1/2}^{i,O_2} + [O_2]}} \quad \text{Eq. 5-2}$$

For $[O_2] < 10^{-6}$ M and $[Fe(III)] > 10^{-6}$ M,

$$\boldsymbol{rate_i^{biotic,Fe(III)} = [Biomass_{Fe}]\ K_i^{Fe(III)} \frac{[Fe(III)]}{k_{1/2}^{i,Fe(III)} + [Fe(III)]}} \quad \text{Eq. 5-3}$$

For $[O_2]$, $[Fe(III)] < 10^{-6}$ M and $[S(VI)] > 10^{-6}$ M,

$$\boldsymbol{rate_i^{biotic,S(VI)} = [Biomass_S]\ K_i^{S(VI)} \frac{[S(VI)]}{k_{1/2}^{i,S(VI)} + [S(VI)]}} \quad \text{Eq. 5-4}$$

For $[O_2]$, [Fe(III)], $S(VI) < 10^{-6}$ M

$$\boldsymbol{rate_i^{abiotic} = constant} \quad \text{Eq. 5-5}$$

where rates are given in mol dm^{-3} s^{-1} and the subindex i stands for Bitumen or Organic Matter parameters.

In the model it is assumed that acetate generated during organic matter degradation microbially degrades to carbonate according to Eq. 5-6. As in the case of bitumen and generic organic matter, acetate biotic degradation rate is controlled by the growth rate of aerobes, IRB and SRB and the availability of O_2, Fe(III) or S(VI) in solution (Eq. 5-2 to 5-4, *i* = acetate). The parameter values are listed in Table 5-6.

In this conceptual model it is assumed that acetate cannot degrade abiotically. Thus, once abiotic conditions are achieved, acetate accumulates in solution and can precipitate in the form of $Ca(CH_3COO)_2$ (s) if oversaturated, in agreement with Eq. 5-7.

$$CH_3COO^- + 4\ H_2O \rightarrow 2\ HCO_3^- + 10\ H^+ + 8\ e^- \quad \text{Eq. 5-6}$$

$$Ca(CH_3COO)_2 \rightarrow Ca^{2+} + 2\ CH_3COO^- \quad \text{Eq. 5-7}$$

5.4.3 Cellulose degradation

Degrading cellulose is considered from a monomer of cellulose already hydrolysed ($C_6H_{12}O_6$ in Eq. 5-8).

Under oxic conditions, ($[O_2] > 10^{-6}$ mol dm^{-3}), these previously hydrolysed cellulose monomers degrade to carbonate (Eq. 3-9). However, this reaction often is not complete leading to acetate and carbonate according to Eq. 5-9.

Acetate, in turn, can be also degraded to carbonate if microbes are active in the system (see Section 5.4.2).

Under anoxic conditions, approximately 80% of the products generated in the degradation process of cellulose are ISA. For the sake of simplicity, Eq. 5-10 is used for cellulose degradation under alkaline anoxic conditions and has been defined after assuming that 80% of cellulose degrades to ISA and 20% to acetate.

Given the high aqueous concentration of Ca under cementitious conditions and the increase of aqueous concentration of ISA foreseen because of cellulose degradation, Eq. 5-11 accounting for the precipitation of $Ca(Hisa)_2$ (cr) is also taken into account. This reaction is considered to occur in equilibrium.

As in the case of bitumen and acetate, cellulose degradation under biotic conditions is controlled by the growth of O_2-, Fe(III)- and S(VI)-reducing bacteria and the availabity of O_2, Fe(III) or S(VI) in solution (Eq. 5-2 to 5-4, *i* = cellulose). Table 5-6 shows the values of the parameters for these equations.

$(C_6H_{10}O_5)_n + H_2O \rightarrow n(C_6H_{12}O_6)$ Eq. 5-8

$C_6H_{12}O_6 + 2\ H_2O \rightarrow 2\ CH_3COO^- + 2\ CO_2\ (g) + 8\ H^+ + 8\ e^-$ Eq. 5-9

$C_6H_{12}O_6 + 0.40\ H_2O \rightarrow 0.8\ isa + 0.4\ CH_3COOH + 0.4\ CO_2(g) + 1.6\ H^+ + 3.2\ e^-$ Eq. 5-10

$Ca(Hisa)_2\ (cr) \rightarrow Ca^{2+} + 2\ Hisa^-$ Eq. 5-11

Under abiotic conditions, cellulose degrades according to the kinetic law proposed by Glaus and Van Loon (2008). A complete development of the cellulose degradation model is given in Appendix 4.

5.4.4 Biomass behaviour

The three different generic microbial communities present in the repository (O_2-, Fe(III)- and S(VI)-consumer bacteria) contribute to the degradation of bitumen, generic organic matter, acetate and/or cellulose and also depend on these substrates to survive.

The biological activity of each microbial group is modelled according to the extended Monod growth model (Rittmann and Van Briesen 1996, Sena 2009) as shown in Eq. 5-12 to 5-14. Table 5-7 shows the values of the parameters for these equations.

For $[O_2] > 10^{-6}$ M

$$rate_{O_2-consumer} = -Y_{acetate}^{O_2} rate_{acetate}^{biotic,O_2} - Y_{B/OM}^{O_2} rate_{B/OM}^{biotic,O_2} - Y_{cellulose}^{O_2} rate_{cellulose}^{biotic,O_2} - b_{O_2}[Biomass_O] \quad \text{Eq. 5-12}$$

For $[O_2] < 10^{-6}$ M and $[Fe(III)] > 10^{-6}$ M

$$rate_{Fe(III)-consumer} = -Y_{acetate}^{Fe(III)} rate_{acetate}^{biotic,Fe(III)} - Y_{B/OM}^{Fe(III)} rate_{B/OM}^{biotic,Fe(III)} - Y_{cellulose}^{Fe(III)} rate_{cellulose}^{biotic,Fe(III)} - b_{Fe(III)}[Biomass_{Fe}] \quad \text{Eq. 5-13}$$

For $[O_2]$, $[Fe(III)] < 10^{-6}$ M and $[S(VI)] > 10^{-6}$ M

$$rate_{S(VI)-consumer} = -Y_{acetate}^{S(VI)} rate_{acetate}^{biotic,S(VI)} - Y_{B/OM}^{S(VI)} rate_{B/OM}^{biotic,S(VI)} - Y_{cellulose}^{S(VI)} rate_{cellulose}^{biotic,S(VI)} - b_{S(VI)}[Biomass_S] \quad \text{Eq. 5-14}$$

where rates are given in mol $dm^{-3} \cdot s^{-1}$.

5.4.5 Numerical parameterization

Table 5-6 and Table 5-7 show the values of the parameters used in Eq. 5-2 to 5-4 to model the degradation of bitumen, generic organic matter, acetate and cellulose and the values of the parameters used in Eq. 5-12 to 5-14 to quantify the growth of O_2-, Fe(III)- and S(VI)-consumer bacteria.

Initial amounts of bitumen, cellulose, steel and other organic materials (originally in kg) are recalculated to mol/L_{water} by considering the waste package porosity fully saturated and the molecular weight of the material. Porosity is calculated from the void volume and the waste type volume values (Table 2-1, Table 2-3, Table 2-5 and Table 2-7).

A summary of the different processes considered depending on the environmental conditions is shown in Figure 5-1.

Table 5-6. Range of values for each parameter reported in literature and selected values used in the calculations. B/OM stands for Bitumen or generic Organic Matter parameters.

Parameter	Units	Range of values	Selected value
$K_{acetate}^{O_2}$	$mol_{acetate}\ mol^{-1}_{BiomassO}\ s^{-1}$	4.8×10^{-4} – 3.0×10^{-3} (a)	1.0×10^{-3} (b)
$K_{acetate}^{Fe(III)}$	$mol_{acetate}\ mol^{-1}_{BiomassFe}\ s^{-1}$	7.0×10^{-4} – 4.6×10^{-3} (a)	1.0×10^{-3} (b)
$K_{acetate}^{S(VI)}$	$mol_{acetate}\ mol^{-1}_{BiomassS}\ s^{-1}$	1.0×10^{-3} – 1.5×10^{-2} (a)	6.9×10^{-3} (c)
$K_{B/OM}^{O_2}$	$mol_{B/OM}\ mol^{-1}_{BiomassO}\ s^{-1}$	4.8×10^{-4} – 3.0×10^{-3} (a)	1.0×10^{-3} (b)
$K_{B/OM}^{Fe(III)}$	$mol_{B/OM}\ mol^{-1}_{BiomassFe}\ s^{-1}$	7.0×10^{-4} – 4.6×10^{-3} (a)	1.0×10^{-3} (b)
$K_{B/OM}^{S(VI)}$	$mol_{B/OM}\ mol^{-1}_{BiomassS}\ s^{-1}$	1.0×10^{-3} – 1.5×10^{-2} (a)	6.9×10^{-3} (c)
$K_{cellulose}^{O_2}$	$mol_{cellulose}\ mol^{-1}_{BiomassO}\ s^{-1}$	–	1.0×10^{-3} (g)
$K_{cellulose}^{Fe(III)}$	$mol_{cellulose}\ mol^{-1}_{BiomassFe}\ s^{-1}$		1.0×10^{-3}(g)
$K_{cellulose}^{S(VI)}$	$mol_{cellulose}\ mol^{-1}_{BiomassS}\ s^{-1}$		6.9×10^{-3}(g)
$k_{1/2}^{acetate,O_2}$	$mol\ dm^{-3}$	1.0×10^{-6} – 20×10^{-6} (d)	1.0×10^{-6} (a)
$k_{1/2}^{acetate,Fe(III)}$	$mol\ dm^{-3}$	1.0×10^{-10} – 3.7×10^{-6} (d)	1.0×10^{-10}(a)
$k_{1/2}^{acetate,S(VI)}$	$mol\ dm^{-3}$	1.0×10^{-5} – 1.0×10^{-3} (d)	1.7×10^{-4}(c)
$k_{1/2}^{B/OM,O_2}$	$mol\ dm^{-3}$	1.0×10^{-6} – 20×10^{-6} (d)	1.0×10^{-6}(a)
$k_{1/2}^{B/OM,Fe(III)}$	$mol\ dm^{-3}$	1.0×10^{-10} – 3.7×10^{-6} (d)	1.0×10^{-10}(a)
$k_{1/2}^{B/OM,S(VI)}$	$mol\ dm^{-3}$	1.0×10^{-6} – 1.0×10^{-5} (d)	1.7×10^{-4}(a)
$k_{1/2}^{cellulose,O_2}$	$mol\ dm^{-3}$	1.0×10^{-6} (f)	1.0×10^{-6} (f)
$k_{1/2}^{cellulose,Fe(III)}$	$mol\ dm^{-3}$		1.0×10^{-10}(g)
$k_{1/2}^{cellulose,S(VI)}$	$mol\ dm^{-3}$		1.7×10^{-4}(g)
$rate_{B/OM}^{abiotic}$	$mol\ dm^{-3}\ s^{-1}$	> 2 orders of magnitude smaller than biotic values (e)	1.0×10^{-12}

(a) Sena (2009). (b) Selected in this report to be within the reported range. (c) Lin and Lee (2001). (d) Omil et al. (1998), Puigdomenech et al. (2001). (e) Wolf and Bachofen (1991). (f) Rotter (2008). (g) In analogy to acetate parameters.

Table 5-7. Range of values for each parameter reported in literature and selected values used in the calculations. B/OM stands for Bitumen or generic Organic Matter parameters.

Parameter	Units	Range of values	Selected value
b_{O_2}	s^{-1}	2×10^{-6}–3×10^{-6} (a,b)	2.3×10^{-6}(b)
$b_{Fe(III)}$	s^{-1}	2×10^{-6}–3×10^{-6} (a,b)	2.3×10^{-6}(b)
$b_{S(VI)}$	s^{-1}	2×10^{-8}–3×10^{-5} (a,b)	1.3×10^{-5}(d)
$Y_{acetate}^{O_2}$	$mol_{BiomassO}/mol_{acetate}$	0.05–0.5 (a,b)	0.05 (c)
$Y_{B/OM}^{O_2}$	$mol_{BiomassO}/mol_{B/OM}$	0.05–0.5 (a,b)	0.05 (c)
$Y_{cellulose}^{O_2}$	$mol_{BiomassO}/mol_{cellulose}$		0.05 (e)
$Y_{acetate}^{Fe(III)}$	$mol_{BiomassFe}/mol_{acetate}$	0.006 (d)	0.006 (d)
$Y_{B/OM}^{Fe(III)}$	$mol_{BiomassFe}/mol_{B/OM}$	0.006 (d)	0.006 (d)
$Y_{cellulose}^{Fe(III)}$	$mol_{BiomassFe}/mol_{cellulose}$		0.006 (e)
$Y_{acetate}^{S(VI)}$	$mol_{BiomassS}/mol_{acetate}$	3.5×10^{-3}–8×10^{-1} (a,b)	0.085 (c)
$Y_{B/OM}^{S(VI)}$	$mol_{BiomassS}/mol_{B/OM}$	3.5×10^{-3}–8×10^{-1} (a,b)	0.085 (c)
$Y_{cellulose}^{S(V))}$	$mol_{BiomassS}/mol_{cellulose}$		0.085 (e)

(a) Vavilin and Lokshina (1996) (b) Small et al. (2008). (c) Selected in this report to be within the reported range. (d) Sena (2009). (e) in analogy to the B/OM and acetate parameters.

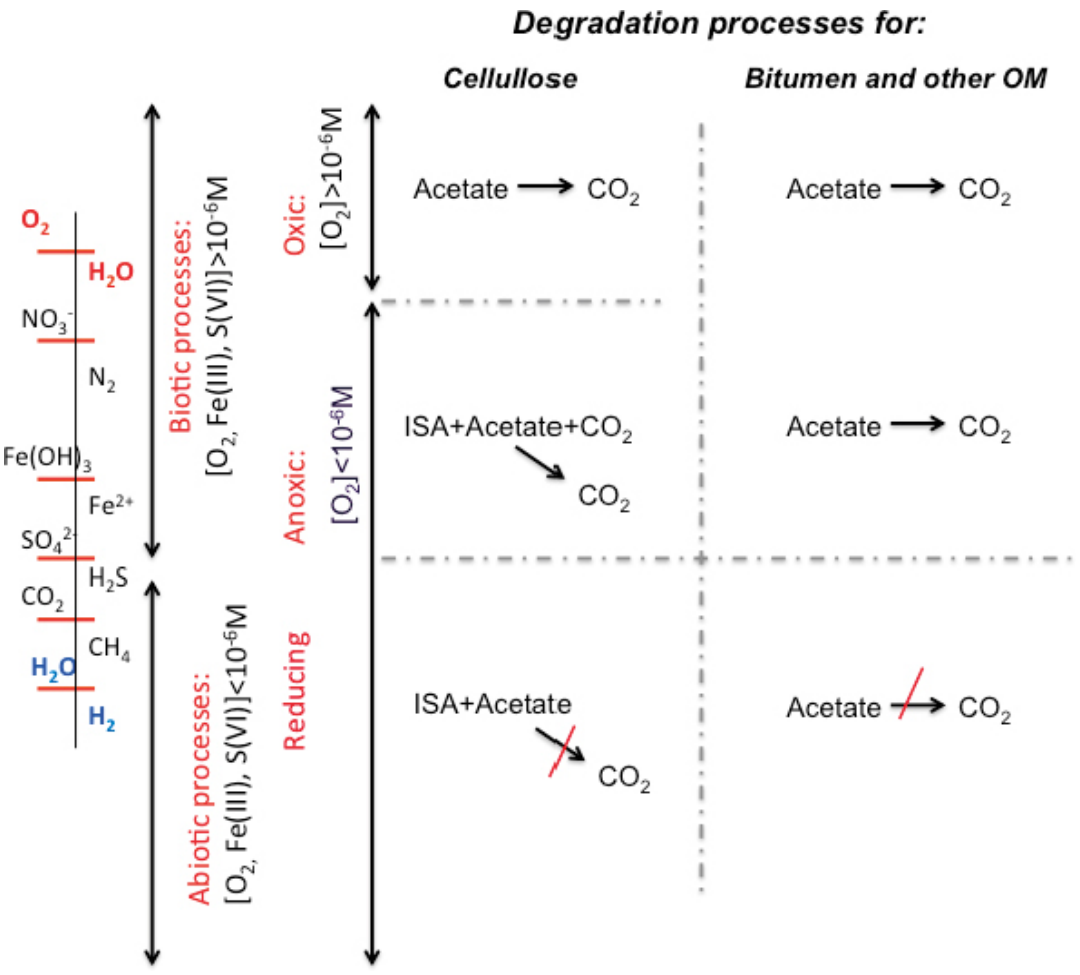

Figure 5-1. *Summary of the processes considered for organic matter degradation under diferent environmental conditions.*

5.5 Calculation strategy

Due to the complexity of the whole system considered in the model, the calculations have been performed in three steps:

a) Very short-term period, in which a very detailed modelling of the first 30 days is done. This model is useful to understand processes occurring under oxic and biotic conditions.

b) Short-term period, covering the first 5 years. This model is useful to see the connection between the very short term and the long term period.

c) Long-term period, in which the behaviour of the system is studied for 100,000 years. Given the long modelling time, the flow of groundwater through each waste package type has been considered to minimise the loss of mass water due to water reduction to $H_2(g)$ by iron corrosion. Initial groundwater is that obtained in the short-time model for the same case at 5 years; that is, at the end of the second step. Both groundwater flow rate and composition may differ from package to package as shown in next sections.

Figure 5-2 summarises the methodology followed to model the behaviour of the systems for each waste package type.

The results from calculations have been used to calculate the Reductive Capacity of each of the different types of waste package.

Two sensitivity analyses have been conducted with the system:

- Probabilistic sensitivity analyses on the steel corrosion rate implemented in the problem.
- Evolution of the system under the event of oxic water from deglaciation intruding the system.

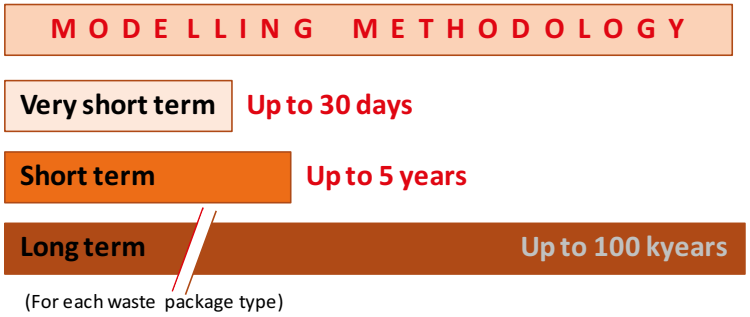

Figure 5-2. *Modelling methodology used to study the behaviour of each waste package type.*

5.6 Assessment of the ReDucing Capacity (RDC)

The most usual way to define the redox state of a system is based on the measure or determination of the redox potential, Eh, which can be related to the concentration of redox active species in the system. Due to the slow kinetics of redox processes, redox couples are usually not in equilibrium, what precludes in some cases the obtention of conclusions on the redox state of a system simply based on the determination of redox active species. Electron transfer reactions are known to be slow and in many cases they need the action of catalysts to proceed, despite being thermodynamically favoured. This is the case of many of the redox processes taken into account in the system of wastes we are dealing with in this work. It is well known that microbial activity catalyses reactions (as it is the case of the degradation of organic matter or the reduction of sulphate to sulphide, as discussed in the preceeding sections). This implies that the simple monitorization and calculation of redox potentials is sometimes not a very good indicator of the redox state of all redox couples in the system, and it has been proven from many groundwater analyses that different redox potentials can be determined depending on the redox couple considered to be in equilibrium in the system (Lindberg and Runnells 1984).

Due to the difficulty to obtain representative redox potentials, Scott and Morgan (1990) proposed the use of capacity magnitudes to define the redox state of geological systems. The authors proposed the concepts of of OxiDising and ReDucing Capacities (OXC and RDC) in analogy to magnitudes such as total acidity or alkalinity in the case of acid/base systems. Intensive parameters such as pH and Eh (or pe if we consider the activity of electrons in the system) rely on the determination of free concentrations, while capacity factors such as alkalinity or ReDucing Capacity (RDC) rely on the measurement of total concentrations of a given component of the system.

Scott and Morgan (1990) defined the reductive capacity as the sum of all reductants that can be oxidised by strong oxidants (e.g., O_2) to a preselected equivalence point, which is the electron reference level (ERL). The RDC of a system gives, thereof, an estimation of its capacity to accept oxidants, i.e., is a chemical sum of the maximum amount of oxidants that the system is able to buffer. The generic definition of RDC is given in Eq. 5-15, where [Red] and [Ox] are, respectively, the concentration of reducing and oxidising species present in the system, and n_i and n_j are the number of electrons involved in the redox reactions.

$$RDC = \sum_i n_i \times [Red] - \sum_j n_j \times [Ox] \qquad \text{Eq. 5-15}$$

Main *reducing* species, that is, electron donors, in the waste package types are:

- Iron from steel, that can corrode to form magnetite.
- Generic organic matter, that can be oxidised to acetate.
- Bitumen, that can be oxidised to acetate.
- Cellulose, that can be oxidised to acetate.

And once the system starts its evolution, new electron donors appear:

- Magnetite, that can be oxidised into goethite.
- Acetate, that can be oxidised into CO_2 under biotic conditions.
- Aqueous Fe(II), that can be oxidised to goethite.
- Aqueous S(-II), that can be oxidised to sulphate.

Main *oxidising species*, as electron acceptors, initially in the system we consider:

- Oxygen, consumed in the first stages of the evolution.
- Sulphate, that can be reduced into S(-II) during the biotic stages.
- Carbonate, that can be reduced into CH_4 during the biotic stages.

And once the system starts to evolve the following electron acceptors are generated:

- Goethite, that can be reduced to Fe(II).
- Aqueous Fe(III).

Given the relevance that the iron system has in the system, we have defined as electron reference level the most oxidised form of iron, Fe(III). In this way, if representing the redox ladder shown in Figure 3-4, all those reductants located in the right hand side of the redox ladderbelow Fe(III) will be contributing to the [Red] term in equation 5-21 while all those oxidants situated left above it will contribute to the term [Ox] in the same equation.

RDC is expressed as moles of electrons in a litre of water (mol/L) and is calculated with Eq. 5-16 and 5-17.

$$\Sigma n_i x[Red] = [Fe(0)] \times 2 + [Fe(II)(aq)] \times 1 + [magnetite] \times 1 + [HS^-] \times 8 + [bitumen] \times 11 + [organic\ matter] \times 11 + [cellulose] \times 3.2 + [acetate] \times 8 + 2\,x\,[H_2] \quad \text{Eq. 5-16}$$

$$\Sigma n_i x[Ox] = [O_2] \times 4 \quad \text{Eq. 5-17}$$

Given the uncertainty existing on the reactivity of H_2 (g) and bitumen, the contribution of H_2 (g) to the RDC of the system has not been included in the RDC calculation and in some cases the RDC has been calculated with and without considering bitumen in the formulae.

6 Results of the modelling of individual waste package types

This section summarises the results obtained in the modelling of individual waste package types. In order to understand how the different waste package systems behave and to evaluate the effect of the different processes, calculations have been done at three different time resolution levels (Section 5.5). Results will be discussed according to the same scheme:

- Very short-term (until 30 days).
- Short-term (until 5 years).
- Long-term (from 5 to 100,000 years).

Table 6-1 summarises the cases that have been run. Although they belong to different vaults, they have been grouped considering the main materials that will contribute to the reducing capacity of the waste packages.

6.1 Very short-term results (up to 30 days)

Given the short time period considered in this section, calculations have been done in static mode (batch) according to the conceptual and numerical models detailed in chapter 5.

6.1.1 Waste package types containing only steel as reducing material

In waste package types R.16, R.15 and S.13 steel corrosion is the only process affecting the redox evolution. These packages do not contain any type of organic matter. The microbial activity is thus not considered to affect the evolution of the system. All three waste packages are considered to contain portlandite as model for the cementitious conditions. Table 6-2 summarises the main differences between these three types of waste packages.

Table 6-1. Summary of cases modelled in this report. Cement groundwater has been used in all cases, except in O.12 waste, where granitic water has been used in calculations (Table 5-3). (For more information about packages see Appendix 1).

Steel	Steel + Org. Matter	Steel + Bitumen	Steel + cellulose + Org.Matter/Bitumen
R.16	O.02	B.06	O.23
R.15	R.01	F.18	F.23
S.13	B.07_O.07	F.05	B.05
		F.17	O.12

Table 6-2. Concentration of Carbon-Steel and portlandite and reactive area of C-Steel in R.16, R.15 and S.13 waste package types (see Section 2.2).

		R.16	R.15	S.13
C-Steel_P	moles/L	23.3	22	12.7
	area (m^2/L)	0.053	0.053	0.169
Portlandite	moles/L	88	88	77

No important differences have been observed among the behaviour of R.16, R.15 and S.13, hence results have been only plotted for the waste package R.16. pH is kept constant at 12.5 due to portlandite equilibration and does not change during these 30 days. Due to the presence of O_2 in groundwater, steel corrodes according to the oxic rate (Figure 6-1b). Fe^0 (steel) is oxidised to Fe(III) and forms goethite (Figure 6-2).

The amount of steel corroded is very small and only causes a very slight decrease in the value of Eh (Figure 6-1a).

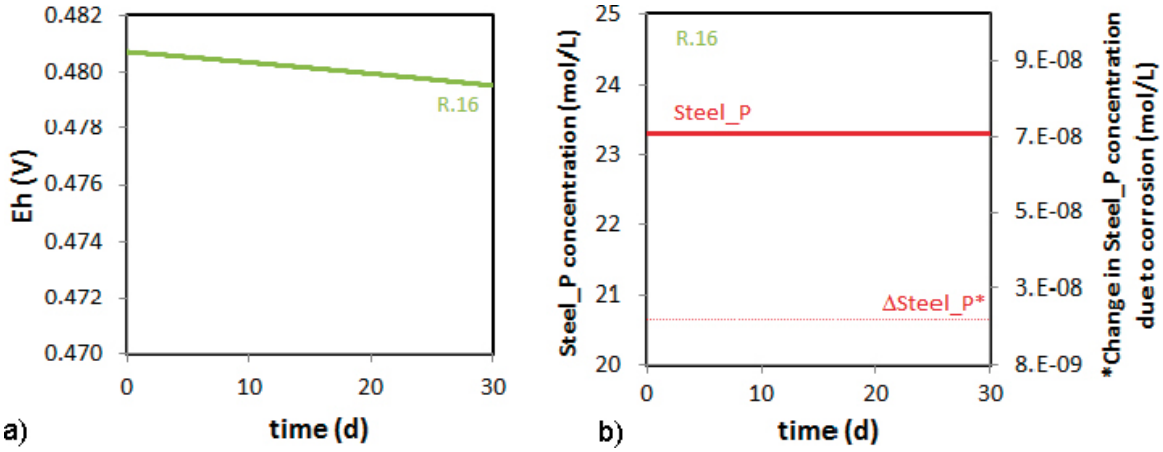

Figure 6-1. *a) Eh evolution of R.16 package during the very short term period. b) Evolution of the concentration of C-Steel and of the C-steel corroded at each time step.*

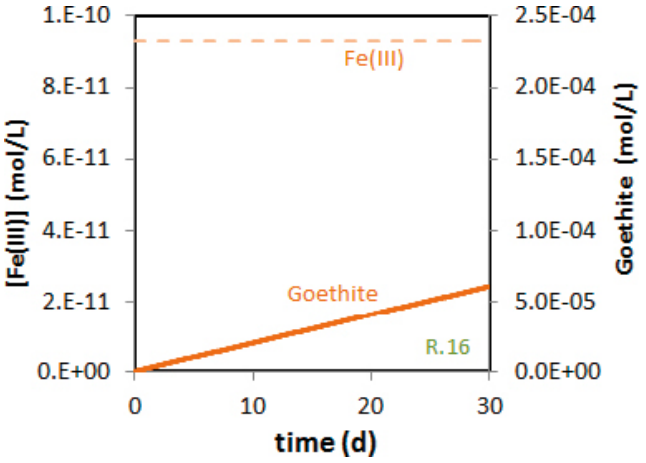

Figure 6-2. *Evolution of dissolved Fe(III) concentration and goethite amounts (expressed as mol/L porewater) during the first 30 days of the assessment.*

6.1.2 Waste package types containing steel and generic organic matter as reducing material

Waste package types O.02, R.01 and B.07_O.07 contain generic organic matter besides steel. In these packages, organic matter degrades kinetically to acetate under both biotic and abiotic conditions. Acetate is in turn oxidised to CO_2 (g) only when microbes are active in the system.

These three waste package types also contain cementitious materials, conceptualised as portlandite in this report. The initial amounts of steel, organic matter and portlandite in each waste package type are given in Table 6-3.

No significant changes in pH are observed with time because pH is controlled by equilibrium with portlandite. However, and as shown in Figure 6-3, the evolution of Eh in a package with organic matter (such as O.02) significantly differs from the evolution of Eh in a package containing only steel (Figure 6-1a) in this very short time period. The rate of consumption of oxygen by degradation of organic matter is much faster than by oxic steel corrosion. It can be appreciated that in the case of having organic materials and microbes, anoxia is reached at times close to 5 days (O.02 in the graph) while when steel is the only reducing agent in the system, O_2 is still present after one month of the simulation (R.16 in the graph) and anoxia is reached after 0.5 y (see Section 6.2).

During the oxic period, steel is corroded according to the oxic rate (Figure 6-4a), but once the $[O_2] < 10^{-6}$ M, the rate decreases to that corresponding to the anoxic corrosion, what causes also a decrease in the rate of generation of goethite (Figure 6-4b). Due to the presence of O_2, O_2-consumer bacteria grow and organic matter is degraded (Figure 6-4c). Acetate produced by organic matter degradation is also degraded to CO_2 (g) by aerobes (Figure 6-4e). This causes a fast consumption of the dissolved O_2. Once O_2 concentration falls below 10^{-6} M and, as detailed in Section 5.4.4, aerobes remain inactive.

Residual O_2 is consumed and, once it is exhausted, Eh drops significantly (Figure 6-3).

Table 6-3. Concentration and reactive area of C-Steel and concentration of organic matter and portlandite in O.02, R.01 and B.07_O.07 waste package types (see Section 2.2).

		O.02	R.01	B.07_O.07
C-Steel_P	moles/L	30.2	30.2	3
	area (m^2/L)	0.069	0.069	0.011
Org.matter	moles/L	1.96	1.96	1.02
Portlandite	moles/L	107	111	37

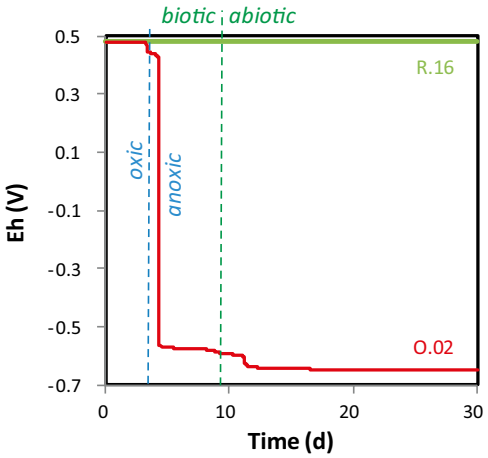

Figure 6-3. Eh evolution of O.02 package compared to that of R.16 package during the very short-term period.

After the oxic period, SRB increase their activity degrading the organic matter and the acetate present in the package (Figure 6-4c). Acetate degradation generates carbonate and precipitation of calcite (Figure 6-4e). As a result of this microbial activity, sulphate is reduced to sulphide (Figure 6-4d). This biotic period lasts until sulphate concentration falls below 10^{-6} M. During this time interval, the redox potential is controlled by the S(-II)/S(VI) redox pair.

After this period, the degradation of organic matter to acetate occurs only abiotically; but acetate is not allowed to degrade to carbonate and therefore accumulates in the system (Figure 6-4e). The redox potential decreases due to the corrosion of steel, what may cause the reduction of carbonate to methane with the subsequent dissolution of the precipitated calcite.

Figure 6-5 summarises the evolution of the Eh value in the O.02 waste package type.

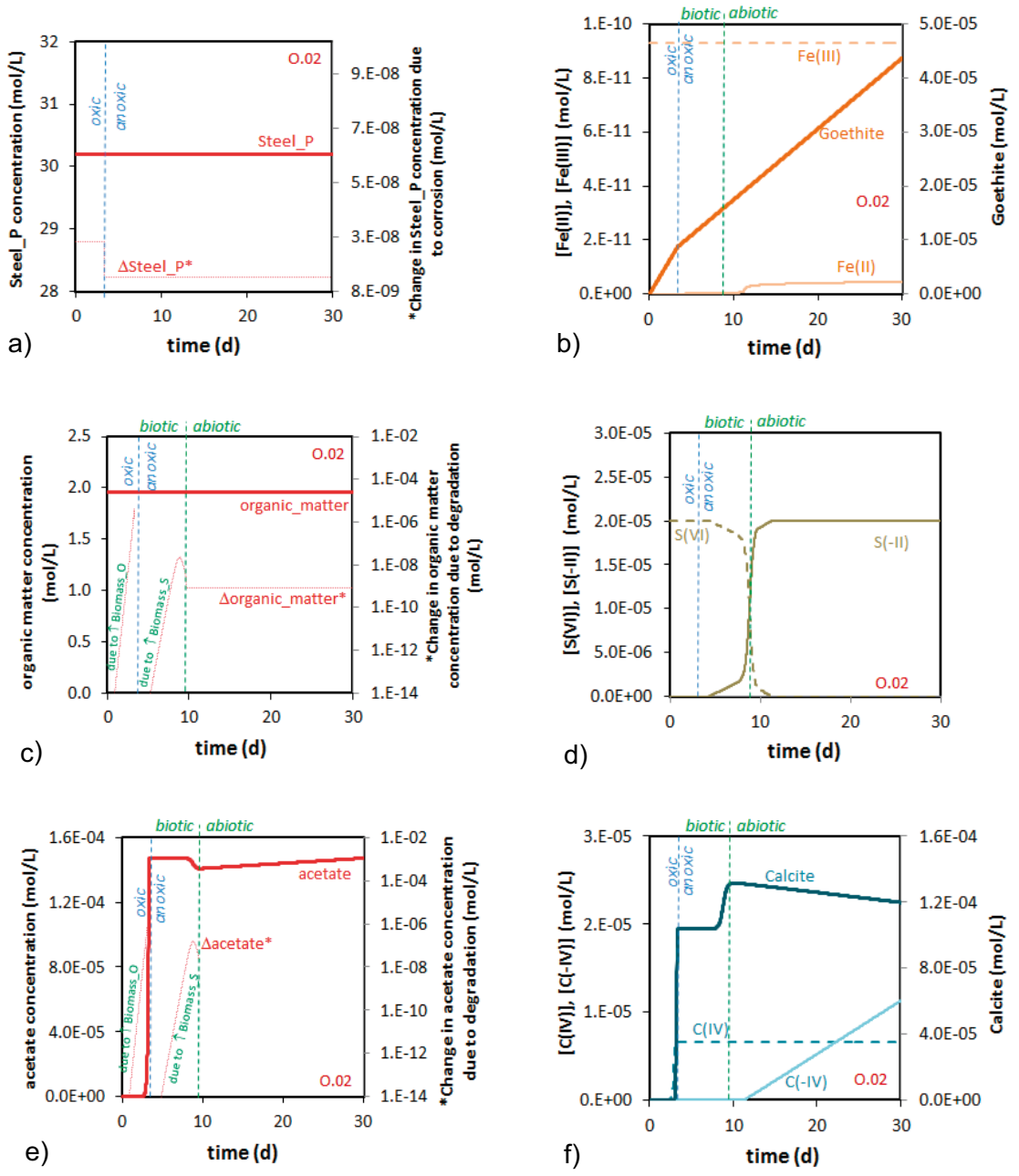

Figure 6-4. *Evolution of the first 30 days for O.02. Temporal evolution of a) concentration of C-Steel and of the C-steel corroded in each time step; b) goethite, Fe(II) and Fe(III) aqueous concentration; c) organic matter concentration and of the organic matter degraded in each time step; d) sulphide and sulphate aqueous concentration; e) acetate concentration and of the acetate degraded in each time step; f) calcite, and aqueous carbonate and methane concentration. Variables with a (*) are plotted in the right axis.*

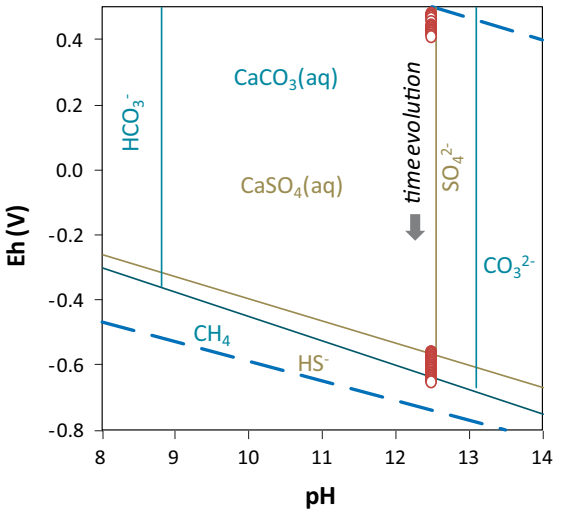

Figure 6-5. *Eh-pH predominance diagram of carbon and sulphur for O.02 waste package. Red dots show the Eh evolution calculated during the first 30 days of assessment.*

The influence of microbial activity through organic matter and acetate degradation in the Eh evolution of the waste package can be clearly seen in Figure 6-6, where the Eh evolution of waste package R.01 has been calculated considering the presence of only steel, only organic matter or steel and organic matter. When only steel is considered the Eh evolution of R.01 is similar to the Eh evolution calculated for the waste package types containing steel (R.16, R.15 and S.13, Section 6.1.1). As will be seen in Section 6.2, in the cases where only steel is modelled, Eh drops after 0.5 y. When organic matter is present, the value of Eh decreases faster. When both materials are considered, Eh value decreases even faster than with only organic matter because the effect of steel corrosion is added to the O_2 consumption by organic matter.

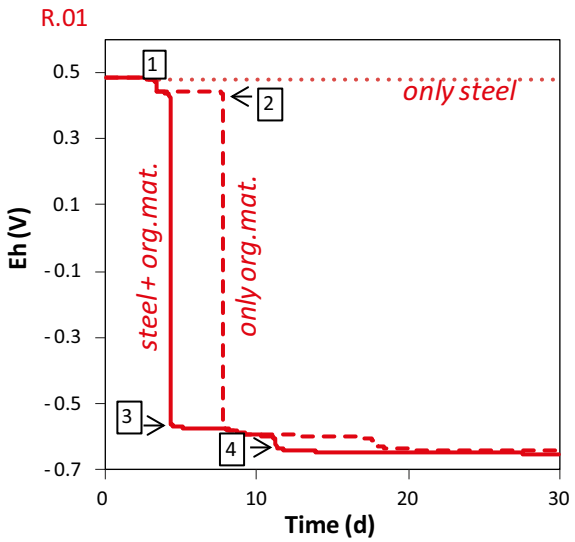

Figure 6-6. *Comparison of the Eh evolution of R.01 waste package type considering the presence of a) only steel, b) only organic matter and c) steel and organic matter in the waste. Numbers show the main periods identified: ① oxic period; ② $[O_2] < 10^{-6}$ M; ③ S(VI)/S(-II) equilibrium. ④ C(IV)/C(-IV) equilibrium.*

6.1.3 Waste package types containing steel and bitumen as reducing material

Waste package types B.06, F.18, F.05 and F.17 contain bitumen. These packages do not have concrete as immobilisation matrix (Table 6-4). Nevertheless, and as explained in the conceptual model, the composition of the groundwater used in the calculations is hyperalkaline because before reaching the waste, regional groundwater is expected to interact with the concrete and cementitious structures of the repository.

Results of the calculations show that, at least at this time interval, the behaviour of Eh in these waste package types is identical to the behaviour of Eh in the waste package types O.02, R.01 and B.07_O.07, with steel and organic matter (Figure 6-7).

The redox potential decreases at the end of the oxic period once the O_2 concentration decreases due to the microbial activity and bitumen and acetate degradation. After the oxic period, bitumen and acetate are degraded by SRB. When the sulphate concentration is so low that microbial mortality exceeds microbial growth, the abiotic period starts, and bitumen is degraded according to a constant rate given in Table 5-6 (see Figure 6-8).

Table 6-4. Concentration and reactive area of C-Steel packaging and concentration of bitumen in B.06, F.18, F.05, F.17 (see Section 2.2).

		B.06	F.18	F.05	F.17
C-Steel_P	moles/L	26.9	57.3	114.7	
	area (m^2/L)	0.137	0.059	0.118	
C-Steel_W	moles/L				36.9
	area (m^2/L)				0.175
Bitumen	moles/L	50.09	56.57	96.63	47.58

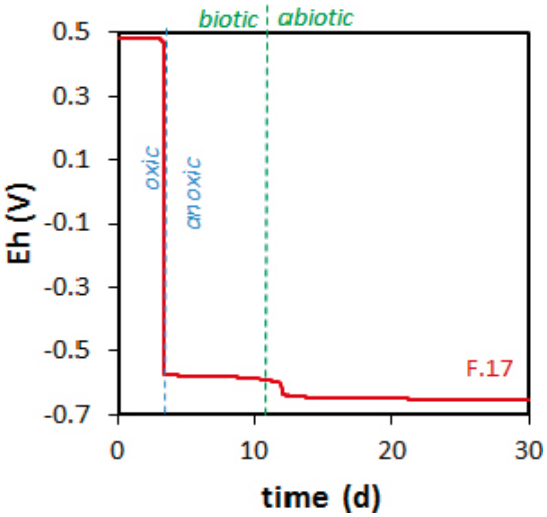

Figure 6-7. *Eh evolution of F.17 during the very short term period.*

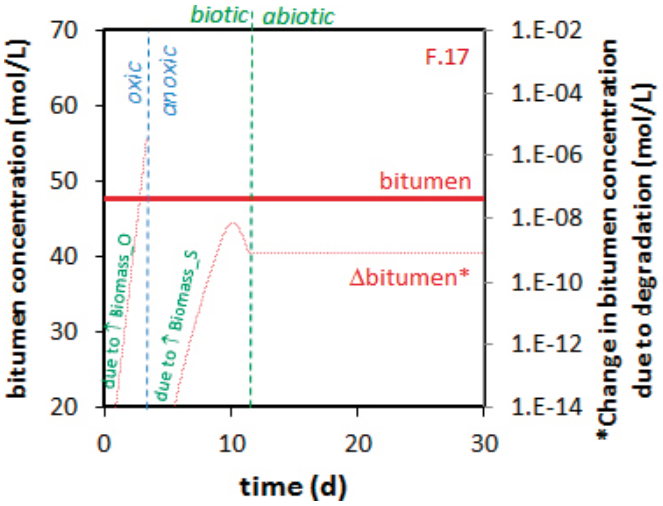

Figure 6-8. *Evolution of the concentration of bitumen and of the bitumen degraded in each time step. Δbitumen* stands for the change in bitumen concentration and is plotted in the right axis.*

6.1.4 Waste package types containing cellulose

The waste package types listed in Table 6-5 contain cellulose besides steel and bitumen or other generic organic matter. In the modelling of the Eh evolution of waste package types O.23, F.23 and B.05, hyperalkaline groundwater has been used in the calculations because O.23 and F.23 contain concrete (conceptualised by portlandite) and because in B.05, groundwater will have interacted with cementitious materials previous to the contact with the waste package. Only in the case of the waste package type O.12, granitic groundwater (near neutral pH) has been used in the calculations (Table 5-3).

Calculated trends of Eh, bitumen or organic matter consumption, goethite and calcite precipitation, and aqueous ion concentration in O.23, F.23 and B.05 waste package types are the same as those obtained in previous cases (Figure 6-9a,b,c). Cellulose is degraded following a biotic rate under oxic conditions due to the activity of aerobes. Acetate produced due to cellulose degradation is degraded to CO_2(g). Once the oxic period has finished, cellulose degrades to acetate and to ISA. Degradation of ISA is not considered, while acetate is assumed to degrade to CO_2 under biotic activity. Under abiotic conditions, cellulose degrades and acetate and ISA accumulate in solution (Figure 6-9d).

Table 6-5. Concentration and reactive area of C-Steel from packages and from the waste, and concentration of bitumen, organic matter, portlandite and cellulose in O.23, F.23, B.05 and O.12 waste package types (see Section 2.2).

		O.23	F.23	B.05	O.12
C-Steel_P	moles/L	26.8	96.3	23.2	4.5
	area (m^2/L)	0.072	0.235	0.127	0.014
C-Steel_W	moles/L	9.8	31.3		106
	area (m^2/L)	0.028	0.089		0.067
Bitumen	moles/L			50.1	
Org.matter	moles/L	11.7	176.5		13.3
Portlandite	moles/L	135	216		
Cellulose	moles/L	1.0	10.9	0.9	0.4

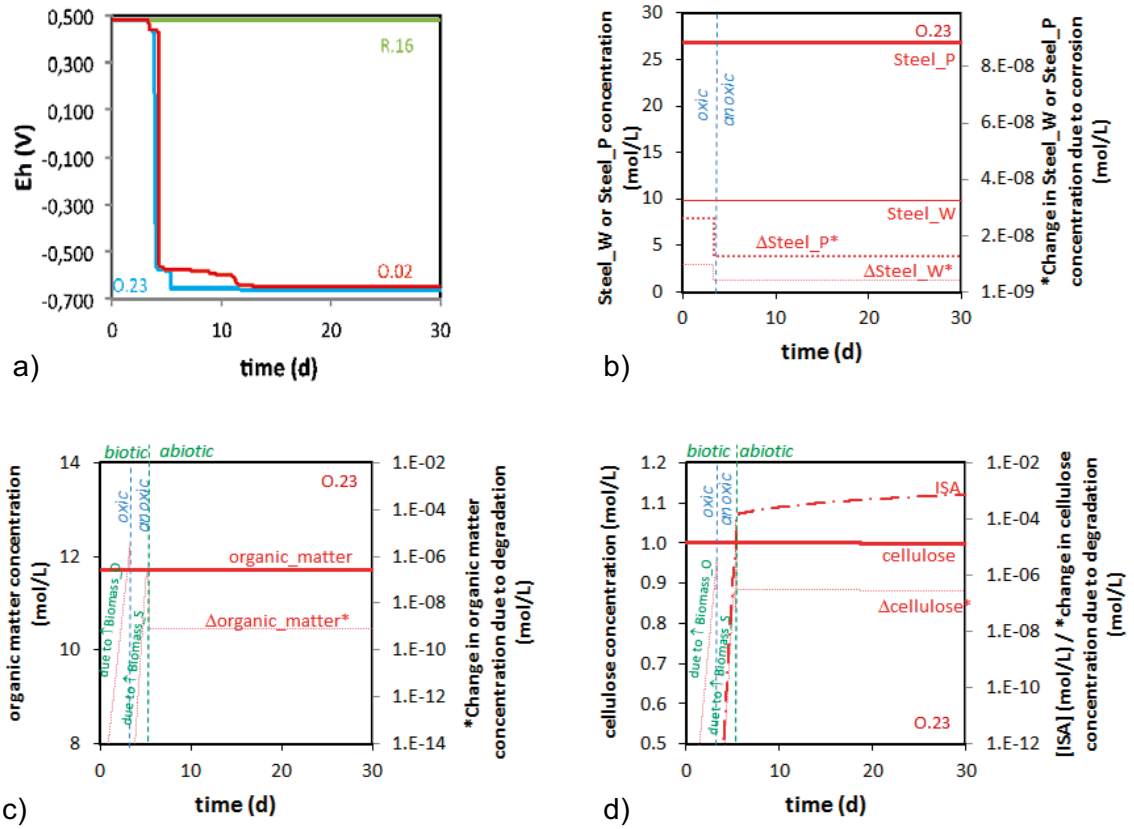

Figure 6-9. *Very short-term results for O.23. Temporal evolution of a) redox potential compared to the Eh evolution of R.16 and O.02 waste package types; b) steel and C-steel corroded in each time step; c) organic matter concentration and of the organic matter degraded in each time step; d) cellulose, cellulose degraded in each time step and aqueous ISA concentration. An asterisk (*) in a variable indicates that it is represented in the right axis.*

The evolution of O.12 is significantly different to that of the other packages. The reason for this different behavior is the composition of the groundwater contacting the waste, which presents a pH of 7.5. Under these conditions, the degradation of cellulose does not produce ISA. Both oxic and anoxic corrosion rates of steel at this pH are higher than under the pH conditions imposed by the presence of concrete (Table 5-4). These facts produce a higher Eh than that achieved in the other packages (Figure 6-11).

Two different cases have been considered for this waste package type, depending on whether or not the reduction of carbonate to form methane is considered. If methane is allowed to form, the pH of the system increases following the C(IV)/C(-IV) redox equilibrium. If methane formation is not allowed, the system follows the H_2/H_2O equilibrium boundary (Figure 6-10).

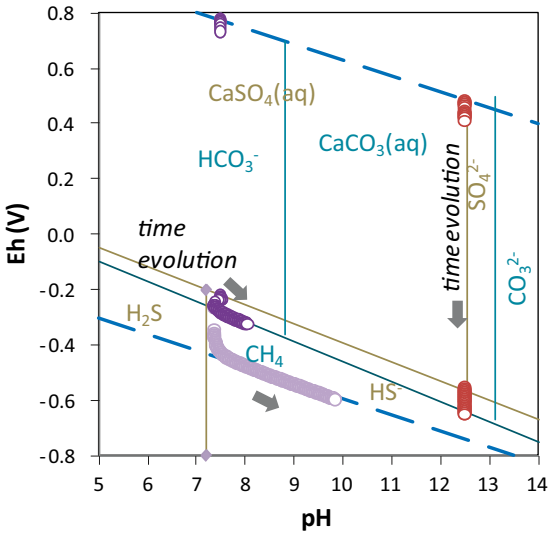

Figure 6-10. *Eh-pH predominance diagram of carbon and sulphur for the O.12 waste package type a) without considering methane formation (light purple dots), b) considering methane formation (dark purple dots) and c) for the very short term model of O.07 (red dots).*

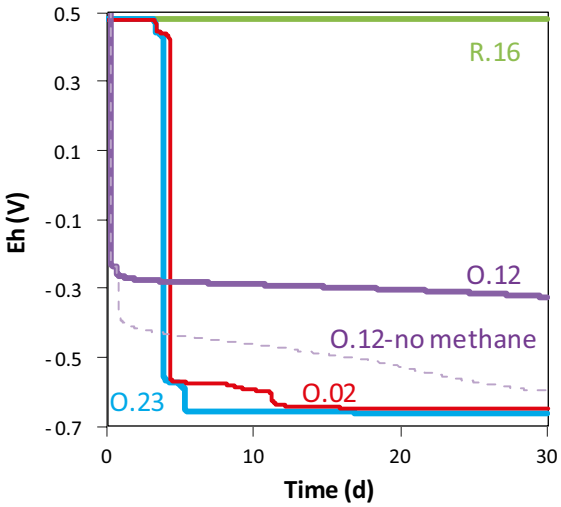

Figure 6-11. *Eh evolution of O.12 (with and without methane formation), O.23, O.02 and R.16 waste package types during the very short term period.*

6.1.5 Brief summary of the very short-term results

Figure 6-12 to 6-16 summarise the results calculated for all the packages at the end of this very short period of time. As can be seen, under hyperalkaline conditions (for all packages except O.12), pH is buffered to 12.5 (Figure 6-13). In all those waste package types containing organic matter, the oxic period is very short (about 3.3 days, Figure 6-12). In the absence of organic matter, the period exceeds 30 days, and in the case of O.12, the higher steel corrosion rates corresponding to near neutral pH shorten the oxic period to less than one day (Figure 6-12).

After 30 days, S(VI) dominates in the porewater of R.15, R.16 and S.13 waste package types, given that in these cases the system is still oxic. Total S concentration is $2 \cdot 10^{-5}$ M. Fe(III) prevails in all cases with a concentration ~$1 \cdot 10^{-10}$ M except in O.12 with a lower pH that produces the predominance of Fe(II) (~$1 \cdot 10^{-6}$ M).

O_2 is still present in the groundwater composition of R.15, R.16 and S.13 waste package types after 30 days (Figure 6-15). This is not the case of the other packages, where anoxic conditions prevail and H_2, H_2S and methane are formed, with concentrations about $5 \cdot 10^{-11}$ M H_2S and $1 \cdot 10^{-6}$ M H_2. Methane concentration is around $1 \cdot 10^{-5}$ M in those packages where organic matter is degraded and around $1 \cdot 10^{-4}$ M in those waste package types where cellulose degrades.

Figure 6-16 shows the total concentration of C(IV), C(-IV), Ca, ISA and acetate after 30 days for each waste package type. No important differences are observed in Ca concentration. In all cases, except O.12, portlandite controls the Ca concentration. The concentration of acetate is in the order of 10^{-4} M when organic matter or bitumen are degraded and it is 6 times higher ($6 \cdot 10^{-4}$ M) when organic matter includes cellulose.

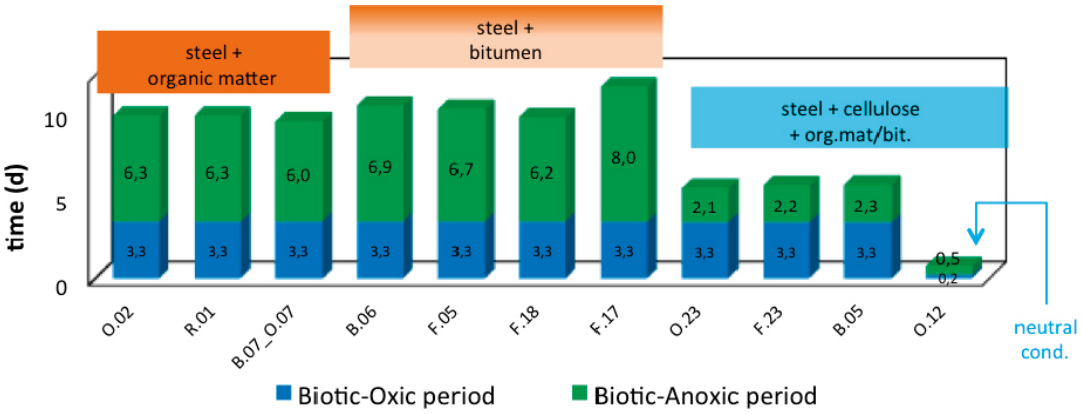

Figure 6-12. *Length of the biotic period (oxic and anoxic) calculated for each of the waste packages containing organic matter.*

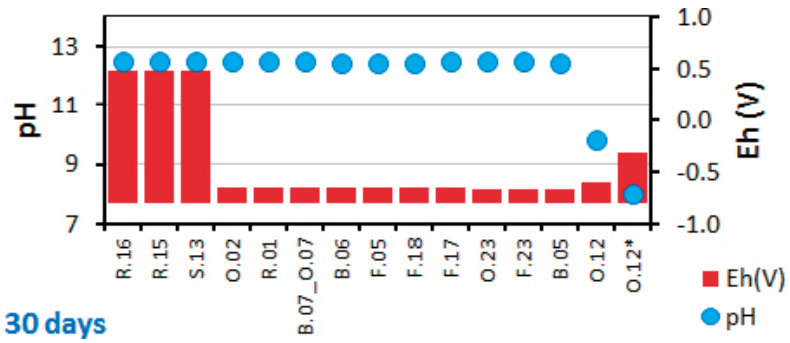

Figure 6-13. *Calculated pH and redox potential value after 30 days for each of the waste package types under the conditions specified in the text. *Production of methane is not allowed.*

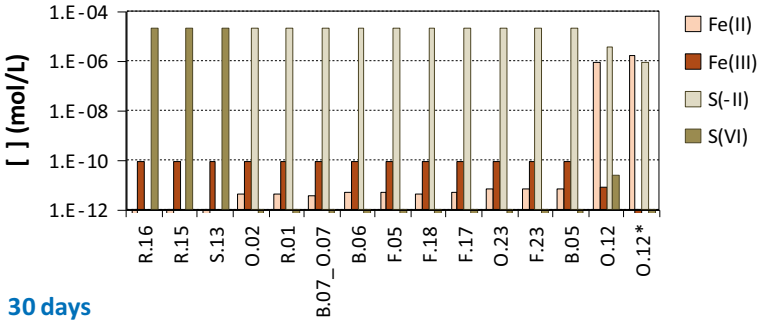

Figure 6-14. *Calculated Fe(II), Fe(III), S(-II) and S(VI) total aqueous concentration after 30 days for each of the waste package types under the conditions specified in the text. *Production of methane is not allowed.*

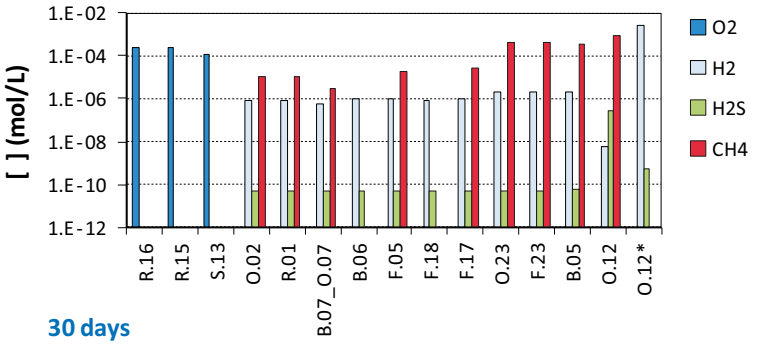

Figure 6-15. *Calculated O_2, H_2, H_2S and CH_4 aqueous concentration after 30 days for each of the waste package types under the conditions specified in the text. *Production of methane is not allowed.*

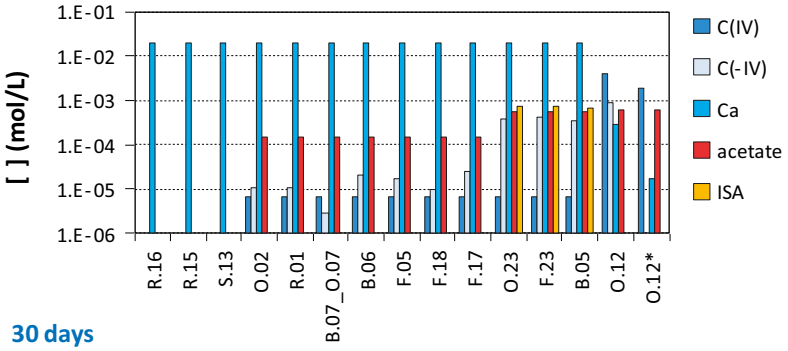

Figure 6-16. *Calculated C(IV), C(-IV), Ca, Acetate and ISA total aqueous concentration after 30 days of elapsed time for each of the waste package types under the conditions specified in the text. *Production of methane is not allowed.*

6.2 Short term results (up to 5 years)

This section discusses the results of the calculations after 5 years of evolution.

6.2.1 Waste package types containing only steel as reducing material

As seen in Section 6.1, redox potential in waste package types R.15, R.16 and S.13 was still oxic after 30 days. In Figure 6-17 it can be seen how this oxic period ends some time later for the case of R.15 (less than 1 year) with the subsequent Eh decrease (Figure 6-18). The evolution of Eh in R.16 and S.13 follows the same trend.

Goethite forms in the initial steps due to the initial corrosion of steel under oxic conditions. When oxygen is depleted, corrosion rate of steel decreases (anoxic rate is smaller than oxic rate, Table 5-4) and goethite precipitation is slower. As Eh decreases goethite becomes unstable and magnetite forms (Figure 6-19).

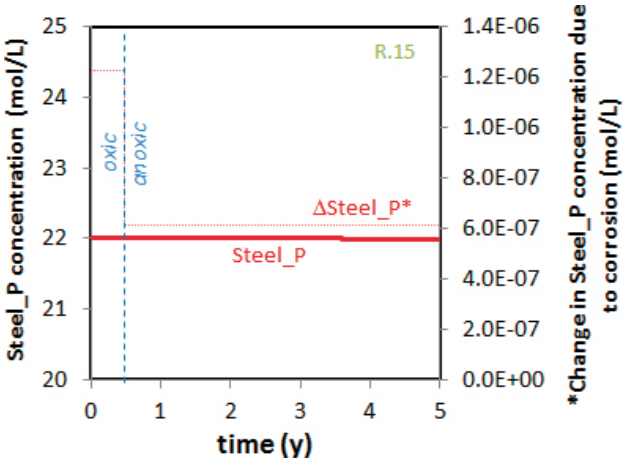

Figure 6-17. *Evolution of concentration of the steel concentration and of the steel corroded in each time step in of the R.15 package type during the short term period.*

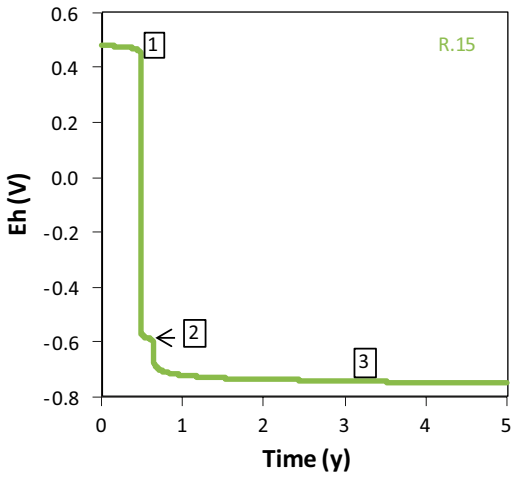

Figure 6-18. *Eh evolution of R.15 waste package type. Numbers show the main periods identified:*
① *oxic period.*
② *S(VI)/S(-II) equilibrium.*
③ *formation of magnetite and* H_2.

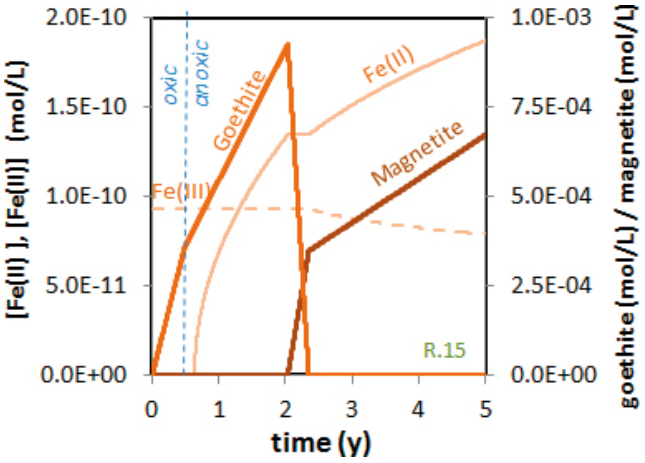

Figure 6-19. *Evolution of Fe(III), Fe(II), goethite and magnetite concentration during the short term period in R.15 package.*

6.2.2 Waste package types containing steel and generic organic matter as reducing materials

The oxic period in the waste package types containing organic matter was shorter than 30 days and therefore during this initial period of 5 years, steel corrosion and organic matter degradation occurs mostly under anoxic conditions. The redox potential decreases and achieves values controlled by the formation of magnetite and H_2 (Figure 6-20a); steel corrodes under anoxic conditions (Figure 6-20b); goethite initially precipitates and then becomes unstable and magnetite controls the Fe aqueous concentration (Figure 6-20c).

Organic matter degrades chemically (Figure 6-20d) but acetate accumulates given that its degradation is not considered to occur under these conditions (Figure 6-20e). Calcite dissolves completely due to the reduction of C(IV) to C(-IV) (Figure 6-20f).

6.2.3 Waste package types containing bitumen

The evolution of waste package types with bitumen (B.06, F.18, F.05, F.17) is very similar to the evolution of generic organic matter-bearing waste package types. Figure 6-21 shows the main results for F.17 waste package type. No important differences are observed between the different cases.

6.2.4 Waste package types containing cellulose

Results of the short-term period in waste package types containing cellulose are shown in Figure 6-22. As with the other packages, goethite dissolves and magnetite forms (Figure 6-22c). Under abiotic conditions, cellulose degrades chemically and ISA accumulates in solution (Figure 6-22b). The chemical degradation rate of cellulose decreases with time, as experimentally observed (Glaus and Van Loon 2008).

Again, the evolution of O.12 waste package type differs significantly to the evolution of the other packages due to the composition of the groundwater contacting the waste. Figure 6-23 and Figure 6-24 show the Eh evolution in this waste package type considering (or not) the reduction of carbonate to methane. Again, as pH is not buffered by portlandite, initial pH increases and Eh decreases. In both cases, the final Eh is controlled by the production of hydrogen, but buffered at higher values in the case where carbonate is not allowed to form methane.

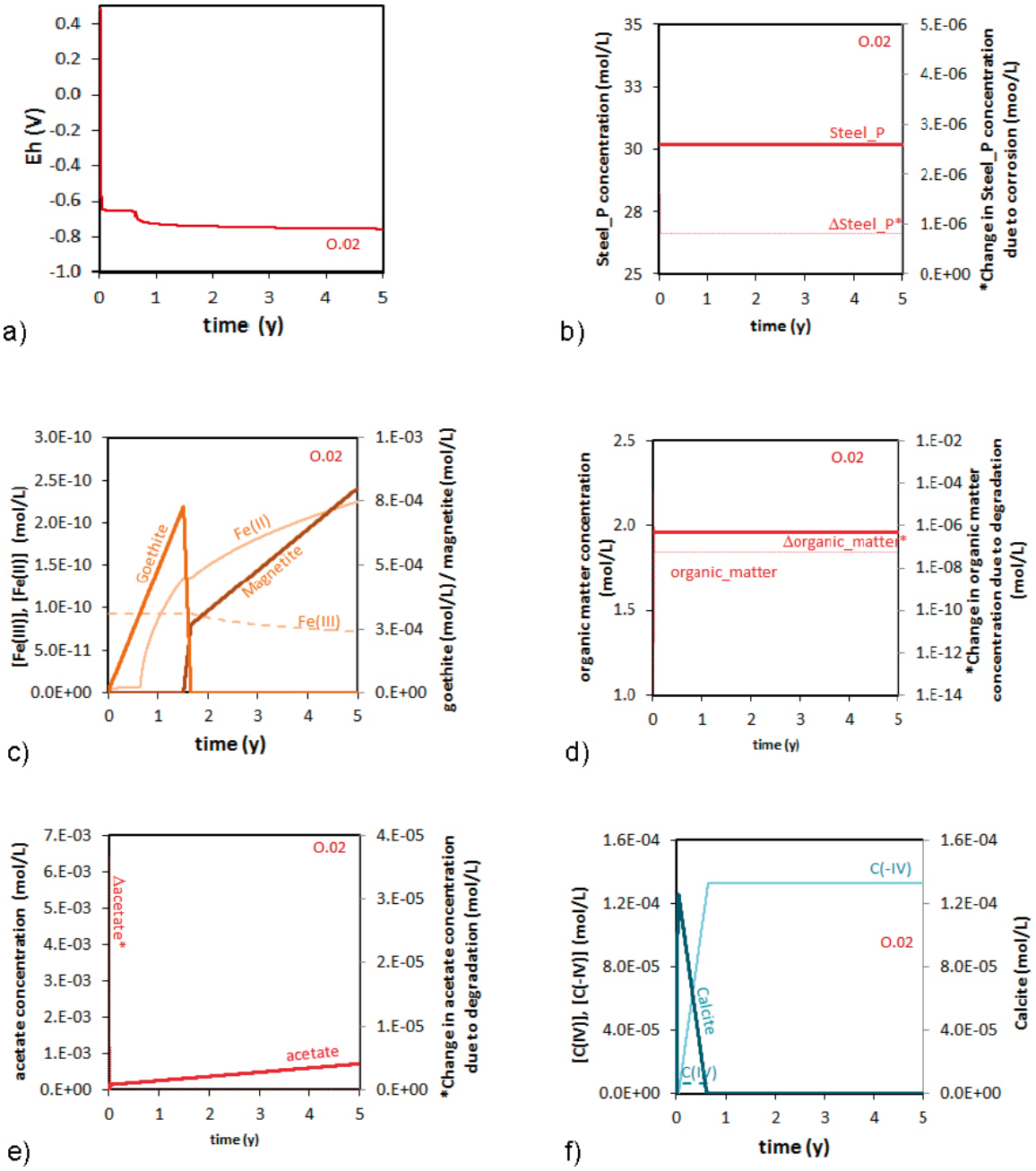

Figure 6-20. *Short term results for O.02. Temporal evolution of a) redox potential (Eh value); b) steel and steel corroded; c) goethite, magnetite, Fe(II) and Fe(III) aqueous concentration; d) organic matter concentration and organic matter degraded; e) acetate concentration and acetate degraded; e) calcite, and aqueous carbonate and methane concentration. An asterisk (*) in a variable indicates that it is plotted in the right axis.*

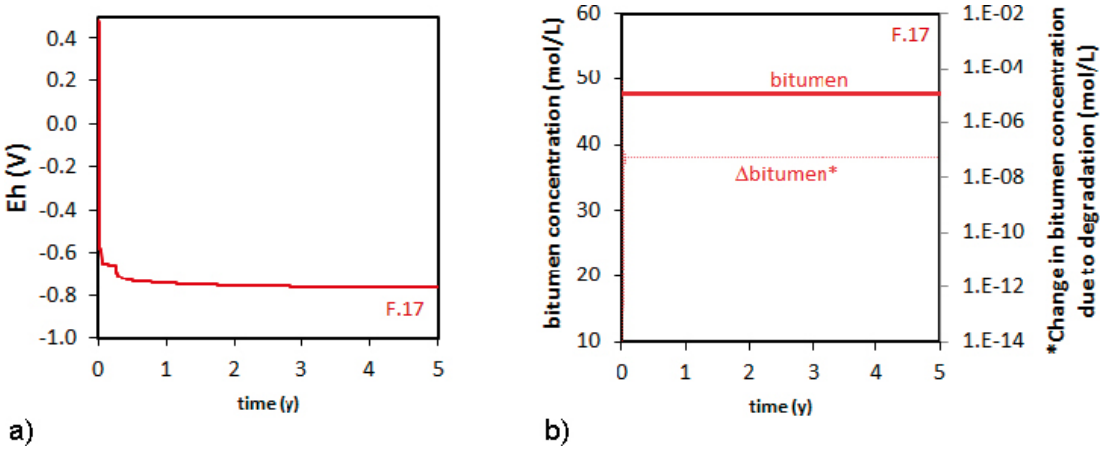

Figure 6-21. *a) Eh evolution of F.17 waste package type during the short term period. b) Evolution of the concentration of bitumen and of the amount of bitumen degraded in F.17 waste package type. An asterisk (*) indicates that the variable is plotted in the right axis.*

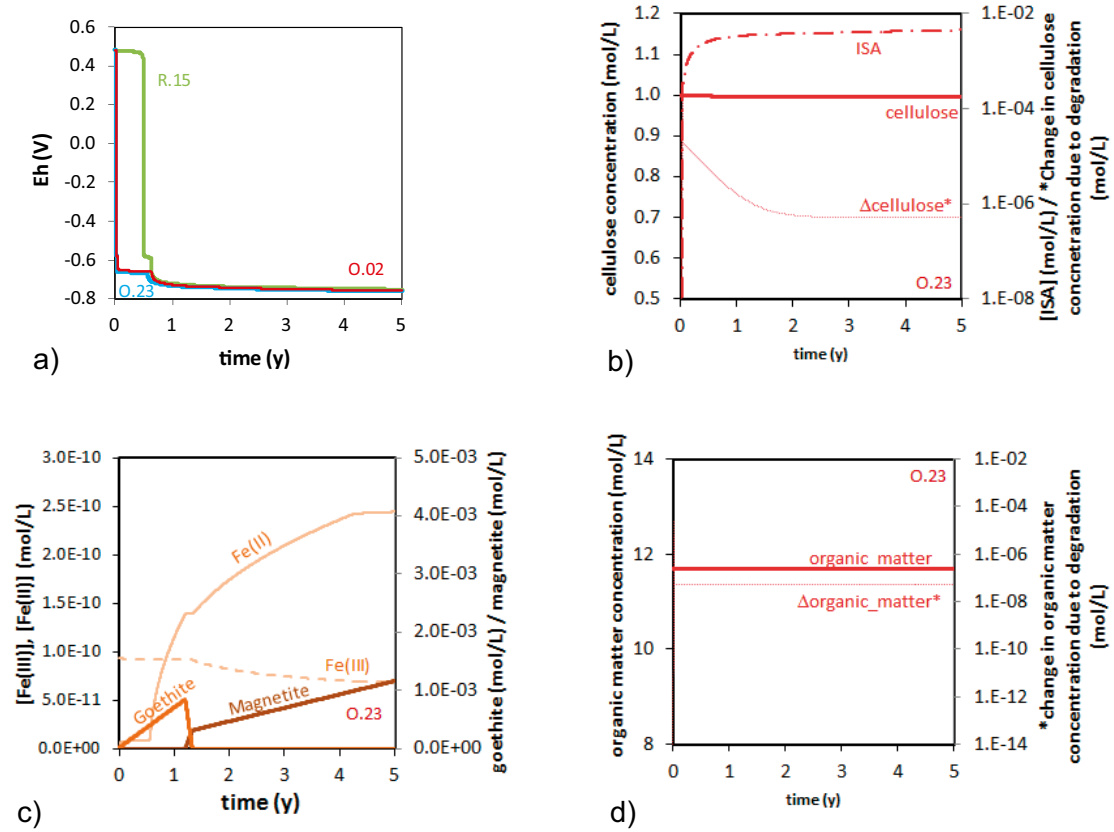

Figure 6-22. *a) Eh evolution of O.23 waste package type during the short-term period, compared to the Eh evolution of R.15 and O.02 waste package types. b) Evolution of cellulose, cellulose degraded and aqueous ISA concentration in O.23. c) Evolution of goethite and magnetite and Fe(II) and Fe(III) total aqueous concentration in O.23. d) Evolution of the concentration of organic matter and of the organic matter degraded in each time step in O.23 waste package type. An asterisk (*) indicates that the variable is plotted in the right axis.*

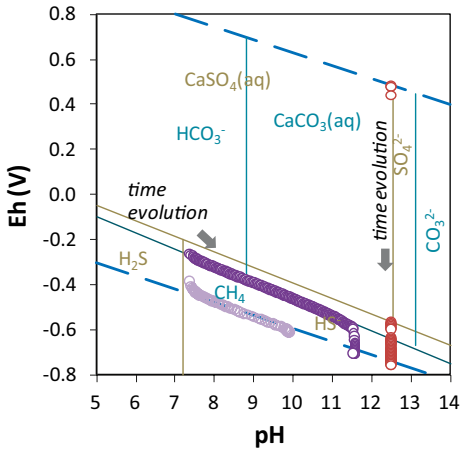

Figure 6-23. *Eh-pH predominance diagram of carbon and sulphur for O.12 waste package type without considering methane formation (light purple dots), considering methane formation (dark purple dots) and for the short term model of O.07 (red dots).*

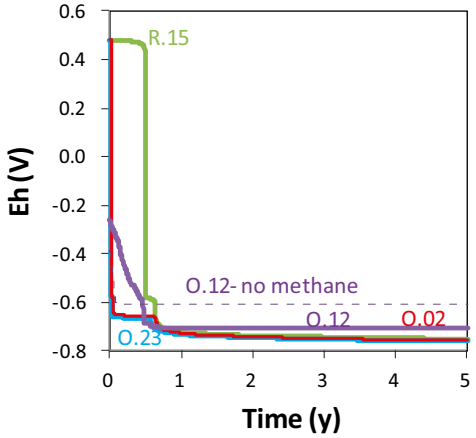

Figure 6-24. *Eh evolution of O.12 (with and without methane formation), O.23, O.02 and R.15 waste package types during the short term period.*

6.2.5 Brief summary of the short-term results

The results of this short-term period indicate that after 5 years, less than 0.1% wt of the steel, bitumen or organic matter has been corroded or degraded (Table 6-6). Around a 0.6 % wt. of the initial cellulose has been degraded, and only in the case of O.12, the percentage of steel corroded is as high as 0.6% wt.

Figure 6-25 to 6-28 summarise the results obtained for all the packages after 5 years.

After 5 years, the sulfur speciation is dominated by S(-II) species in all cases. Total S concentration is $2 \cdot 10^{-5}$ M. Fe total concentration is $\sim 1 \cdot 10^{-10}$ M in all cases (Figure 6-26). H_2, H_2S and methane are formed, with concentrations about $5 \cdot 10^{-11}$ M H_2S and $5 \cdot 10^{-3}$ M H_2. Methane concentration is about $1 \cdot 10^{-4}$ M in those packages where generic organic matter and bitumen are degraded and about $1 \cdot 10^{-3}$ M in those waste package types where also cellulose degrades (Figure 6-27).

Figure 6-28 shows the total concentration of C(IV), C(-IV), Ca, ISA and acetate after 5 years for each waste package type. No important differences are observed in Ca concentrations, controlled by equilibrium with portlandite. Acetate concentration is in the range $7 \cdot 10^{-4} - 6 \cdot 10^{-3}$ M when organic matter or bitumen are degraded. ISA concentration accumulates in solution up to values near $5 \cdot 10^{-3}$ M.

Table 6-6. Percentage of steel, bitumen, org.matter and cellulose degraded during the short term period (5 years) in each of the waste package types.

		Steel-P	Steel-W	Bitumen	Org.matter	Cellulose
Steel	R.16	0.01%	–	–	–	–
	R.15	0.01%	–	–	–	–
	S.13	0.05%	–	–	–	–
Steel + Org.matter	O.02	0.01%	–		0.01%	–
	R.01	0.01%	–		0.01%	–
	B.07_O.07	0.01%	–		0.16%	–
Steel + bitumen	B.06	0.02%	–	< 0.01%	–	–
	F.05	< 0.01%	–	< 0.01%	–	–
	F.18	< 0.01%	–	< 0.01%	–	–
	F.17	–	0.02%	< 0.01%	–	–
Steel + Org.matter/bitumen + cellulose	O.23	0.01%	0.01%	–	< 0.01%	0.57%
	F.23	0.01%	0.01%	–	< 0.01%	0.15%
	B.05	0.03%	–	< 0.01%	–	0.57%
	O.12	0.59%	0.12%	–	< 0.01%	–

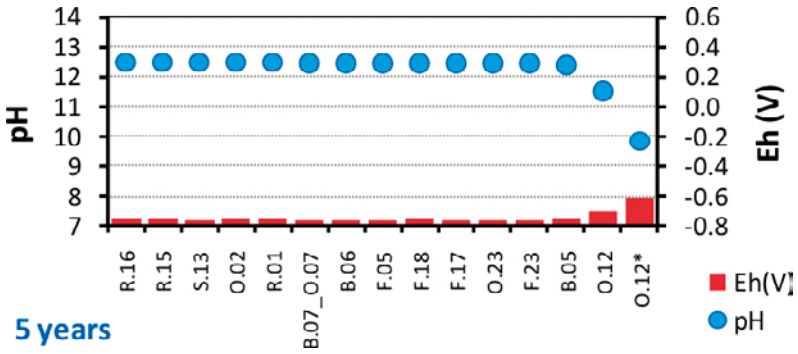

Figure 6-25 *Calculated pH and redox potential value after 5 years for each of the waste package types under the conditions specified in the text. *Production of methane is not allowed.*

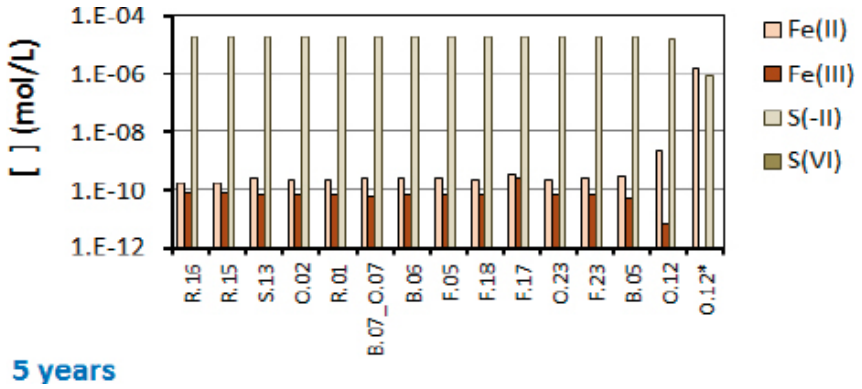

Figure 6-26. *Calculated Fe(II), Fe(III), S(-II) and S(VI) total aqueous concentration after 5 years for each of the waste package types under the conditions specified in the text. *Production of methane is not allowed.*

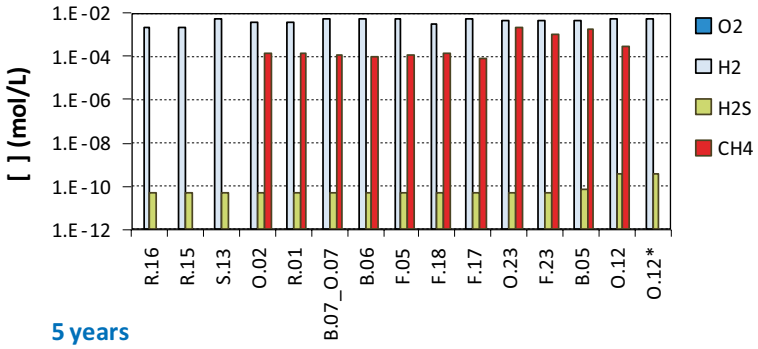

Figure 6-27. *Calculated O_2, H_2, H_2S and CH_4 aqueous concentration after 5 years for each of the waste package types under the conditions specified in the text. *Production of methane is not allowed.*

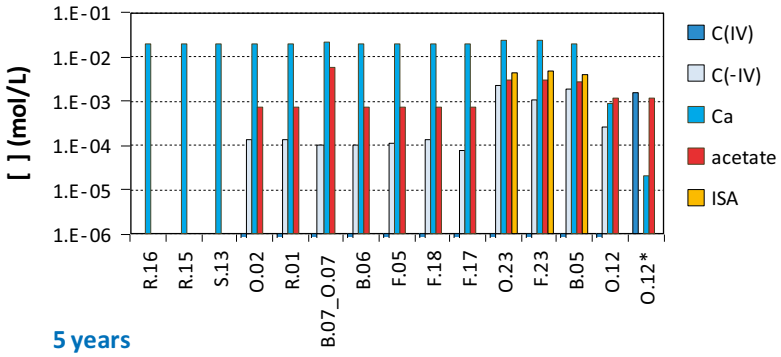

Figure 6-28. *Calculated C(IV), C(-IV), Ca, acetate and ISA total aqueous concentration after 5 years for each of the waste package types under the conditions specified in the text. *Production of methane is not allowed.*

6.3 Long term results (up to 100,000 years)

In this section we present the results of the calculations up to 100,000 years done for each waste package type.

The conceptual model assumes that the system is fully saturated. Even if water is consumed by the chemical processes occurring in the system, the system will remain fully saturated as a consequence of the suction pressure locally created.

Preliminary tests showed that in this long-term section, the mass of water was not kept constant if batch calculations were done. Therefore, and in order to keep the mass of water constant calculations in this section have been done considering that water flows through the waste packages. The reason for including this modification in this section and not in the very-short and short term calculations is precisely the modelling time.

This approach will prevent "artificial" changes on concentrations and ionic strength due to changes in the mass of water.

Flow fields for the waste package encapsulation areas were used in agreement with those calculated by Holmén and Stigsson (2001), as summarized in Table 6-7.

Table 6-7. Range of specific flows for the waste domain calculated by Holmén and Stigsson (2001).

in m/s	Silo	BMA	1 BTF	2 BTF	BLA
From	6.8×10^{-12}	9.3×10^{-13}	3.7×10^{-11}	3.7×10^{-11}	1.8×10^{-10}
To	1.3×10^{-11}	1.3×10^{-11}	1.2×10^{-10}	1.0×10^{-10}	1.9×10^{-9}

In the simulations we have used a different specific flow depending on the vault where the package is placed:

- a value of $6.8 \cdot 10^{-12}$ m/s for those packages contained in the Silo (B.06, F.18, O.02, R.16 and O.23),
- a value of $9.3 \cdot 10^{-13}$ m/s for those packages contained in the BMA vault (B.05, F.05, F.17, F.23, R.01, R.15 and O.23),
- a value of $3.7 \cdot 10^{-11}$ m/s for those packages contained in the 1&2 BTF vault (B.07_O.07 and S.13),
- a value of $1.8 \cdot 10^{-10}$ m/s for those packages contained in the BLA vault (O.12).

A default value of $1 \cdot 10^{-10}$ m^2/s has been used for molecular diffusion in all waste package types. As porosity and dimensions change within packages, time and space discretisation will be adapted to each packages type to fulfill Peclet and Courant conditions.

Each waste package type has been discretised in 8 cells whose length depends on the total length of the package. Water flow rate has been calculated considering the porosity of each waste package type (see Table 6-8). The time step is kept constant and equal to the time needed for water to travel a cell length in each case. Longitudinal dispersivity has been assumed equal to the half of the cell length in all cases.

Prior to reach the waste package cells, inflowing granitic groundwater flows through two cells of portlandite (in all cases except O.12) to simulate the circulation of groundwater through the cementitious structures of the repository. Granitic groundwater equilibrates with portlandite and pH increases up to values next to 12.5 before entering into the waste package.

In the case of O.12 waste package type, granitic groundwater enters directly to the waste package without reacting with cementitious materials.

In the long-term cases, methane has not been allowed to produce due to carbonate reduction. This consideration answers to the fact that biota is assumed to catalyse this process and microbial activity has been deactivated due to the decrease in the electron acceptors during the very early evolution of the repository, as shown in the previous sections, which is not considered to be relevant for the long-term simulations.

Table 6-9 and Table 6-10 list the initial porewater composition and mineral concentration of each waste package type. These values are those corresponding to the end of the short period calculation.

No significant changes in the chemistry of the different cells modelled have been identified in any of the cases run.

Table 6-8. Main transport values used in the calculations. Cell length has been calculated by assuming a discretisation of the waste height in 8 cells. Porosity has been calculated by considering the total and void volumes of waste packages. Water flow has been calculated from the specific flow and porosity.

Waste package type	Specific flow (m/s)	Height waste pack. (m)	Cell length (m)	Porosity (-)	Water flow (m/s)
O.23	6.80×10^{-12}	1.2	0.150	0.110	6.18×10^{-11}
F.23	9.30×10^{-13}	1.20	0.150	0.049	1.89×10^{-11}
B.05	9.30×10^{-13}	0.89	0.111	0.122	7.63×10^{-12}
O.12	1.80×10^{-10}	1.30	0.163	0.381	4.73×10^{-10}
B.06	6.80×10^{-12}	0.89	0.111	0.122	5.58×10^{-11}
F.18	6.80×10^{-12}	1.20	0.150	0.098	6.91×10^{-11}
O.02	6.80×10^{-12}	1.20	0.150	0.098	6.91×10^{-11}
R.16	6.80×10^{-12}	1.20	0.150	0.187	3.64×10^{-11}
F.17	9.30×10^{-13}	1.20	0.150	0.049	1.89×10^{-11}
F.05	9.30×10^{-13}	0.89	0.111	0.081	1.14×10^{-11}
R.01	9.30×10^{-13}	1.20	0.150	0.098	9.45×10^{-12}
R.15	9.30×10^{-13}	1.20	0.150	0.187	4.98×10^{-12}
B.07_O.07	3.70×10^{-11}	2.30	0.288	0.385	9.61×10^{-11}
S.13	3.70×10^{-11}	0.88	0.110	0.171	2.2×10^{-10}

Table 6-9. Initial porewater composition considered in the calculations of the long term period for each waste package type. They correspond to the final porewater compositions calculated in the short term model. Concentrations in mol/kgw.

	R.16	R.15	S.13	O.02	R.01	B.07_O.07	B.06	F.18	F.05	F.17	O.23	F.23	B.05	O.12
pH	12.5	12.5	12.5	12.5	12.5	12.5	12.5	12.5	12.5	12.5	12.467	12.5	12.4	9.8
Eh (mV)	–749	–749	–761	–736	–736	–760	–760	–753	–760	–760	–708	–759	–753	–607
Na	3.00×10^{-3}	3.00×10^{-3}	3.00×10^{-3}	3.00×10^{-3}	3.00×10^{-3}	3.00×10^{-3}	3.00×10^{-3}	3.00×10^{-3}	3.00×10^{-3}	3.00×10^{-3}	3.00×10^{-3}	3.00×10^{-3}	3.00×10^{-3}	4.40×10^{-3}
K	1.00×10^{-4}	1.00×10^{-4}	1.00×10^{-4}	1.00×10^{-4}	1.00×10^{-1}	1.00×10^{-4}	1.00×10^{-4}	1.00×10^{-4}	1.00×10^{-4}	1.00×10^{-4}	1.00×10^{-4}	1.00×10^{-4}	1.00×10^{-4}	1.02×10^{-4}
Ca	1.92×10^{-2}	1.92×10^{-2}	2.00×10^{-3}	1.95×10^{-2}	1.95×10^{-2}	2.16×10^{-2}	1.92×10^{-2}	1.92×10^{-2}	1.92×10^{-2}	1.92×10^{-2}	2.34×10^{-2}	2.34×10^{-2}	1.92×10^{-2}	2.01×10^{-5}
Mg														2.77×10^{-5}
Fe	2.66×10^{-10}	2.66×10^{-10}	3.24×10^{-10}	2.96×10^{-10}	2.96×10^{-10}	3.34×10^{-10}	3.27×10^{-10}	2.89×10^{-10}	3.27×10^{-10}	3.27×10^{-10}	3.13×10^{-10}	3.24×10^{-10}	3.53×10^{-10}	1.60×10^{-6}
Al	2.00×10^{-6}	2.00×10^{-6}	2.00×10^{-6}	2.00×10^{-6}	2.00×10^{-6}	2.00×10^{-6}	2.00×10^{-6}	2.00×10^{-6}	2.00×10^{-6}	2.00×10^{-6}	2.00×10^{-6}	2.00×10^{-6}	2.00×10^{-6}	
Si	3.00×10^{-6}	3.00×10^{-6}	3.00×10^{-6}	3.00×10^{-6}	3.00×10^{-6}	3.00×10^{-6}	3.00×10^{-6}	3.00×10^{-6}	3.00×10^{-6}	3.00×10^{-6}	3.00×10^{-6}	3.00×10^{-6}	3.00×10^{-6}	9.85×10^{-5}
Cl	2.00×10^{-3}	2.00×10^{-3}	2.00×10^{-3}	2.00×10^{-3}	2.00×10^{-3}	2.00×10^{-3}	2.00×10^{-3}	2.00×10^{-3}	2.00×10^{-3}	2.00×10^{-3}	2.00×10^{-3}	2.00×10^{-3}	2.00×10^{-3}	1.27×10^{-3}
S	2.00×10^{-5}	2.00×10^{-5}	2.00×10^{-5}	2.00×10^{-5}	2.00×10^{-5}	2.00×10^{-5}	2.00×10^{-5}	2.00×10^{-5}	2.00×10^{-5}	2.00×10^{-5}	2.00×10^{-5}	2.00×10^{-5}	2.00×10^{-5}	8.00×10^{-7}
C(IV)				1.33×10^{-4}	1.33×10^{-4}	1.06×10^{-4}	1.02×10^{-4}	1.34×10^{-4}	1.15×10^{-4}	7.87×10^{-5}	2.21×10^{-3}	1.09×10^{-3}	1.80×10^{-3}	1.50×10^{-3}
Acetate				7.13×10^{-4}	7.13×10^{-4}	5.89×10^{-3}	7.08×10^{-4}	7.14×10^{-4}	7.10×10^{-4}	7.06×10^{-4}	3.04×10^{-3}	3.06×10^{-3}	2.83×10^{-3}	1.00×10^{-3}
ISA											4.55×10^{-3}	4.66×10^{-3}		

Table 6-10. Initial mineral concentration considered in the calculations of the long term period for each waste package type. They correspond to the final mineral compositions calculated in the short term model. Concentrations in mol/kgw.

	R.16	R.15	S.13	O.02	R.01	B.07_O.07	B.06	F.18	F.05	F.17	O.23	F.23	B.05	O.12
Portl.	88	88	88	107	111	37					135	216		
C-Steel_P	23.3	22	12.7	30.2	30.9	3	26.9	57.3	114.7				23.2	4.5
C-Steel_W										36.9				105.8
Magnetite	6.74×10^{-4}	6.74×10^{-4}	2.02×10^{-3}	8.02×10^{-2}	8.02×10^{-4}	1.28×10^{-4}	1.59×10^{-3}	6.86×10^{-4}	1.37×10^{-3}	2.04×10^{-3}	1.16×10^{-3}	3.77×10^{-3}	1.48×10^{-3}	5.02×10^{-2}
FeS(ppt)														5.19×10^{-4}
Siderite														2.70×10^{-3}
Calcite														8.53×10^{-4}
Org. Matter				1.96	1.96	1.02				47.58	11.7	176.5		13.3
Bitumen							50.09	56.57	96.63				50.1	
Cellulose											1	10.9	0.9	0.4
Magnesite														3.42×10^{-4}

6.3.1 Waste package types containing only steel as reducing material

In those waste package types where only steel is considered (R.15, R.16 and S.13), Eh is constant and around –0.75 V during the long-term period (Figure 6-29). Steel corrodes and magnetite is the main corrosion product. When steel is completely corroded, the production of magnetite ceases (Figure 6-30 and 6-31). Steel is expected to corrode completely after 60 ky, 63.5 ky and 10.8 ky for cases R.15, R.16 and S.13, respectively. In the S.13 package, the initial amount of steel is lower and presents a higher specific surface area.

H_2 (g) is generated due to the anoxic corrosion of steel. It accumulates in solution until the total gas pressure overcomes 6.87 atm, which, as presented in the conceptual model, corresponds to the hydrostatic pressure foreseen for the repository. In R.15, R.16 and S.13 cases, H_2(g) is the main gas formed (29, 31 and 17 mol/L respectively). There is a slight formation of CO_2(g) which is not significant (< 10^{-12} mol/L).

There is a slight precipitation of FeS(ppt) due to the inflow of S(-II) with the inflowing water (Figure 6-31).

Carbonate behaviour is also different to that in the short-term simulations. In the long-term period, methane is not allowed to form, therefore, despite the reducing Eh, carbonate will be stable in solution.

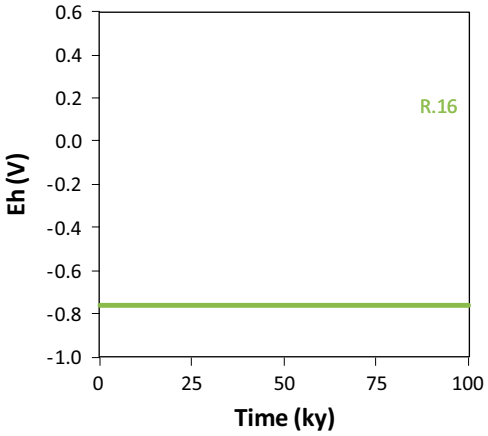

Figure 6-29. *Eh evolution of R.16 package during the long-term period.*

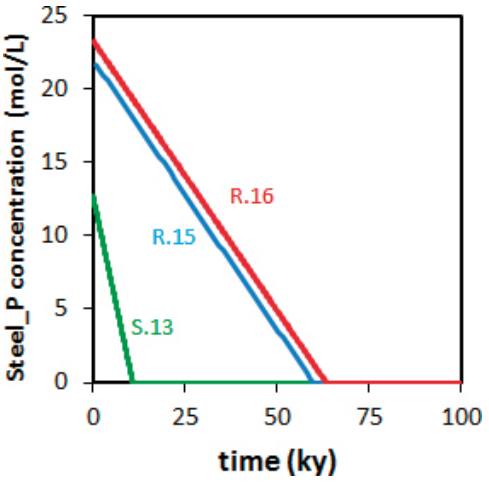

Figure 6-30. *C-Steel evolution of R.16, R.15 and S.13 waste package types during the long-term period.*

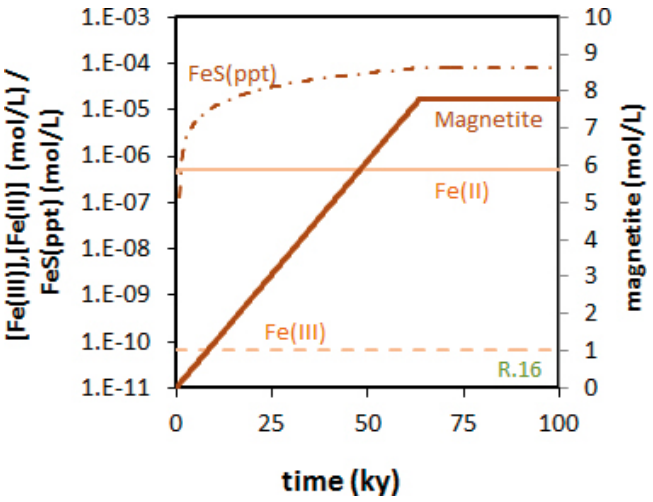

Figure 6-31. *Total aqueous Fe(II) and Fe(III) concentration and magnetite and FeS(ppt) evolution of R.16 during the long-term period.*

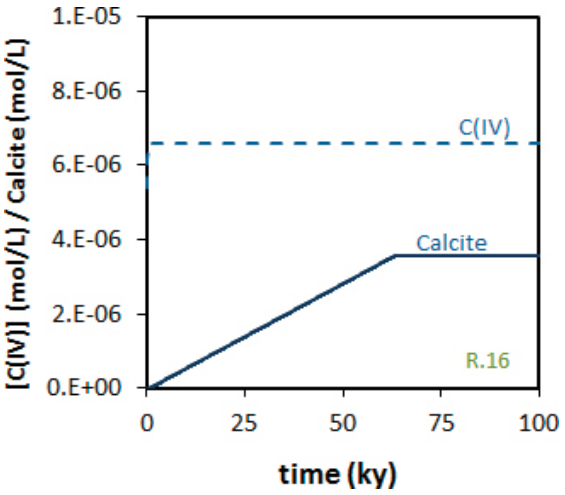

Figure 6-32. *Total aqueous C(IV) concentration and calcite evolution of R.16 during the long-term period.*

6.3.2 Waste package types containing steel and generic organic matter as reducing materials

The behaviour of waste package types O.02, R.01 and B.07_O.07 is not significantly different from that observed in packages R.16, R.15 and S.13 concerning Eh, steel behaviour and corrosion products. In O.02 and R.01 waste package types, steel is completely corroded after 63 ky and in B.07_O.07 steel finishes at 40 ky. Despite having only one tenth of the amount of steel of O.02 and R.01, in B.07_O.07 steel finishes at 40 ky because the reactive area is near 1/7 of the reactive area of the other two waste package types, so that the process is slower. Magnetite is the main corrosion product and there is also a small precipitation of FeS(ppt).

Organic matter degrades at a constant rate to acetate. Organic matter degradation proceeds for 63 ky for O.02 and R.01 and finishes before (because initial amount is lower) in B.07_O.07 (33 ky). Acetate does not degrade to CO_2 (g) under these conditions. The higher aqueous concentration of acetate is achieved in R.01, where the flow rate is slower (Table 6-8). The value is around 0.5 mol/L, while in the other cases it is around $7 \cdot 10^{-2}$ mol/L.

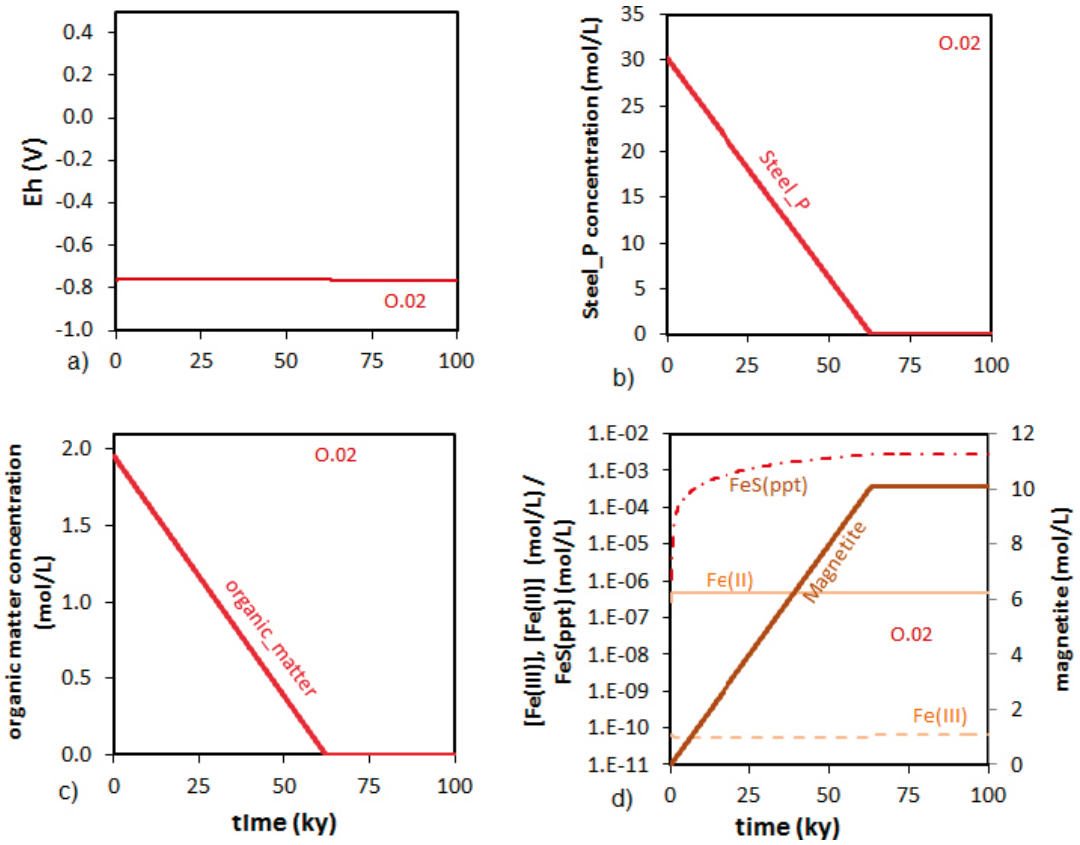

Figure 6-33. *Long-term results for O.02 waste package type. Temporal evolution of a) Eh; b) C-steel; c) organic matter; d) Fe(II) and Fe(III) aqueous concentration and magnetite and FeS(ppt).*

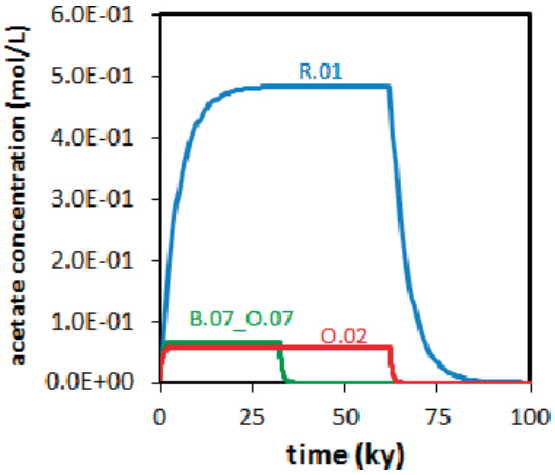

Figure 6-34. *Acetate long-term evolution of O.02, R.01 and B.07_O.07 waste package types.*

6.3.3 Waste package types containing bitumen

Waste packages types B.06, F.17, F.18 and F.05 contain bitumen and do not have cementitious matrix. Nevertheless, inflowing groundwater has a pH of 12.5 because it has been forced to equilibrate with portlandite before reaching the waste package to simulate the interaction with the cementitious structures of the repository.

In general terms, the processes occurring are the same than those in previous cases. Steel corrodes, magnetite and FeS(ppt) precipitate and bitumen is degraded generating acetate (Figure 6-35 and 6-36).

Because of the high amount of bitumen initially considered, it is never completely depleted in the time of the assessment (100 ky) for any of these four types of waste packages. The extent of degradation is of 7%, 6% and 3% of the intitial amount of bitumen for F.17, F.18 and F.05 respectively. In the case of B.06, the amount of degraded bitumen is as high as 63%. Acetate behaves similarly to the previous cases, achieving a maximum concentration of 0.5 mol/L in the B.06 package (Figure 6-36).

Only in the case of B.06 and F.17 waste package types, steel is completely corroded after 100 ky. In B.06 steel finishes at 600 y and in F.17 after 30 ky. In F.18 and F.05, after 100 ky, a 72% of the initial amount of steel has been corroded.

Magnetite and FeS(ppt) are the main corrosion products as in the previous cases. A slight precipitation of calcite is also observed due to the higher concentration of Ca in the inflowing groundwater. In F.17, the slope of calcite precipitation changes because once steel corrodes completely, FeS(ppt) can form from magnetite (Figure 6-37).

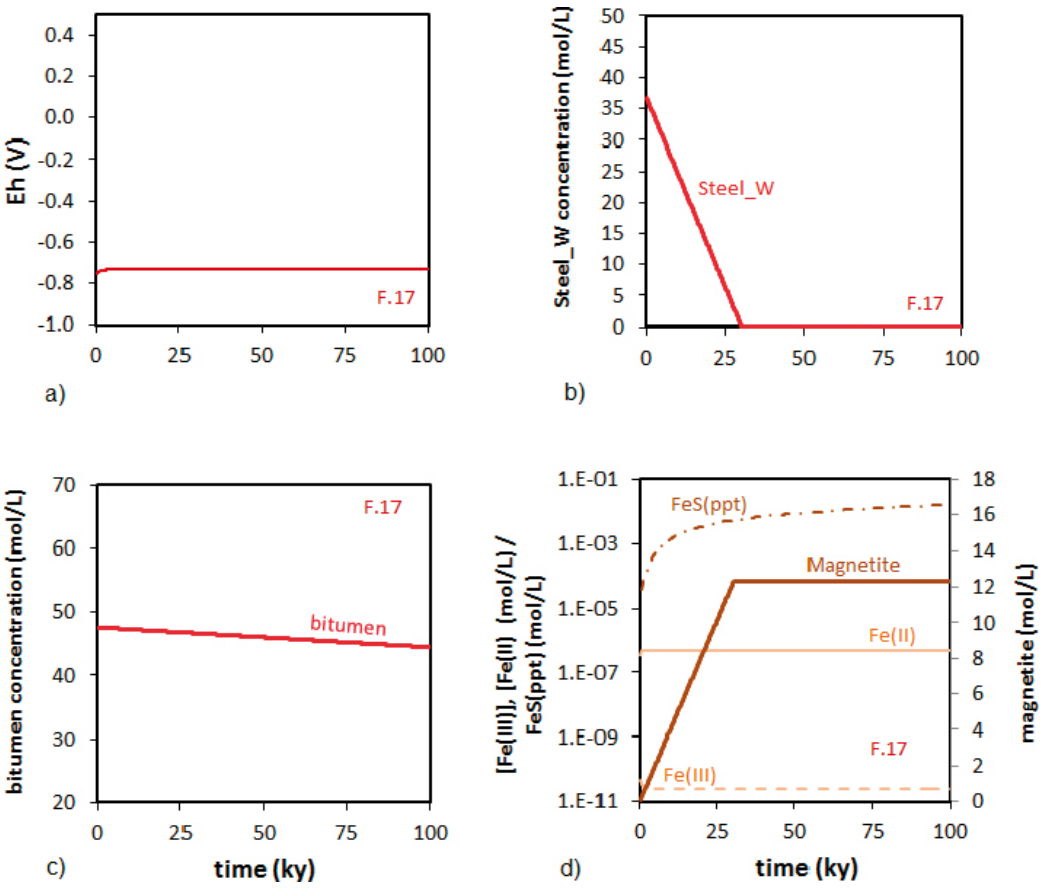

Figure 6-35. *Long-term results for F.17 waste package type. Temporal evolution of a) Eh; b) C-steel; c) bitumen; d) Fe(II) and Fe(III) aqueous concentration and magnetite and FeS(ppt).*

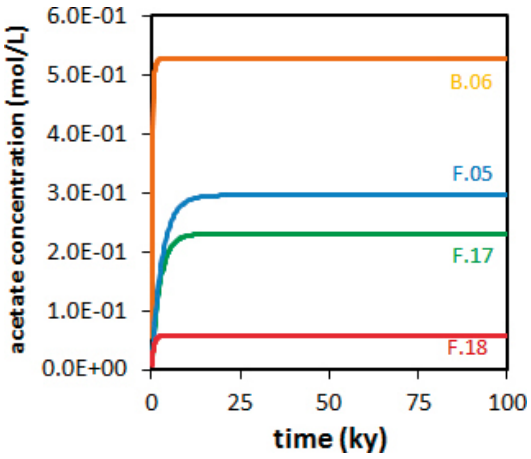

Figure 6-36. *Acetate long-term evolution of F.18, F.17, F.05 and B.06 waste package types.*

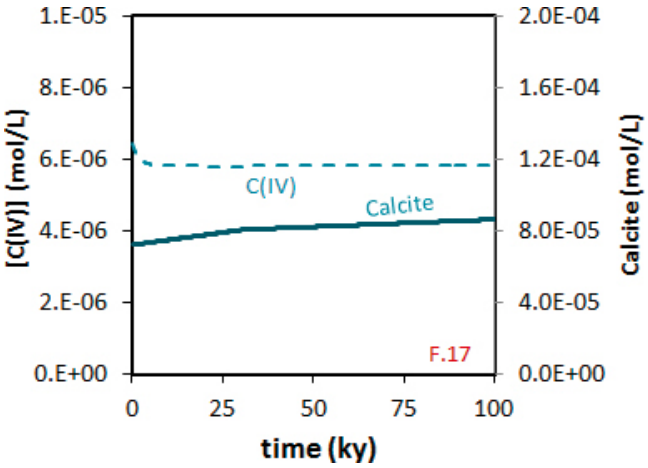

Figure 6-37. *Calcite and total aqueous carbonate long-term evolution F.17.*

6.3.4 Waste package types containing cellulose

O.23 and F.23 present very similar behaviour. Initially, both have C-steel from the package and from the waste, organic matter, portlandite and cellulose. The main difference is that concentrations are higher in F.23. Moreover, groundwater flow is three times slower in F.23 than in O.23 (see Table 6-8).

The time at which C-steel in O.23 is completely corroded is very similar to that in F.23 because, although the amount in O.23 is three times lower than in F.23, reactive area is higher, so that absolute corrosion rates are equivalent. C-Steel_P finishes at 54 ky in O.23 and at 59 ky in F.23, while C-steel_W finishes at 51 ky in both cases.

In both cases, magnetite is the main corrosion product although FeS(ppt) also precipitates. This behaviour is equivalent to that observed in previous cases. $H_2(g)$ is the main gas generated.

In both cases, only 3.16 mol/L of organic matter (CH_2O) have been degraded. However, this value represents near 27% of initial value in O.23 and only 1% of initial concentration of organic matter in F.23. Acetate is produced and accumulated in solution, reaching concentrations higher in F.23 (0.2 mol/L) than in O.23 (0.07 mol/L) because of the slower groundwater flow.

Concerning cellulose, in both cases it is abiotically degraded and generates CO_2 (g) and ISA as degradation products. In O.23 cellulose is totally degraded after 6.7 ky. In F.23, and due to the higher initial concentration of cellulose, it is not totally degraded within the timeframe of the assessment. Only 11% of cellulose is degraded (Figure 6-38). Due to the increase of ISA concentration and to high concentration of Ca^{2+} due to the presence of portlandite, $Ca(HISA)_2$(cr) precipitates. The aqueous concentration of ISA is fixed at $1.6 \cdot 10^{-2}$ mol/L by equilibrium with $Ca(HISA)_2$(cr) (see Table 5-2). The amount of $Ca(HISA)_2$(cr) precipitated in F.23 is 0.5 mol/L, while it is of 0.4 mol/L in O.23.

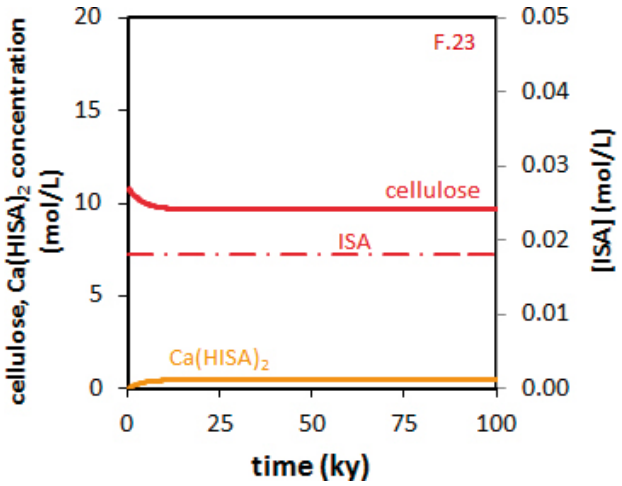

Figure 6-38. *Long-term evolution of cellulose, and Ca(HISA)$_2$(cr) and of total ISA aqueous concentration for F.23.*

About 5% of portlandite is dissolved in both cases during these 100 ky. Calcite precipitation increases because of the higher concentration of CO_2 produced by the degradation of cellulose.

The main difference of B.05 steel compared to the previous cases (O.23 and F.23) is that it only contains one steel type, and bitumen instead of organic matter. No portlandite is present in the waste because it is not stabilized with cementitious materials.

Despite these differences, its evolution does not differ significantly from those of O.23 and F.23. Steel is completely corroded after 27 ky. Despite having more or less the same amount of steel at initial conditions than O.23, the higher reactive area of this steel causes its earlier complete corrosion. Cellulose is totally degraded after 6 ky. Achieved ISA aqueous concentration is $1.6 \cdot 10^{-2}$ mol/L, in equilibrium with Ca(Hisa)$_2$(cr).

In the case of O.12, granitic groundwater flows through the waste packaging without being previously equilibrated with portlandite. That means that pH changes. The Eh is maintained at a value of –0.34 V (Figure 6-39).

In this case, C-steel_P is totally corroded after 900 y, and C-Steel_W after 4 ky. The main corrosion product is siderite, which precipitates due to the carbonate concentration of the inflowing groundwater.

3.16 mol/L of organic matter (CH_2O) are degraded, what represents near 23% of total initial organic matter concentration.

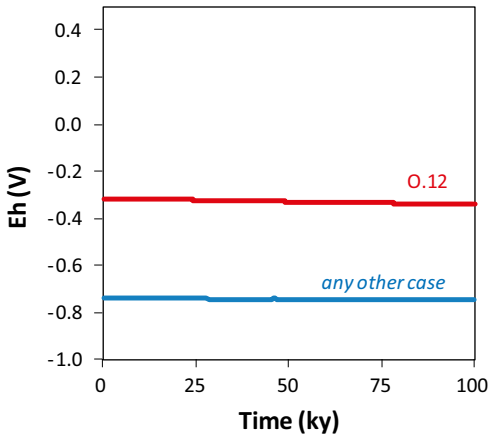

Figure 6-39. *Long-term temporal evolution of Eh in O.12 waste package type compared with the long term temporal evolution of any of the other waste package types studied.*

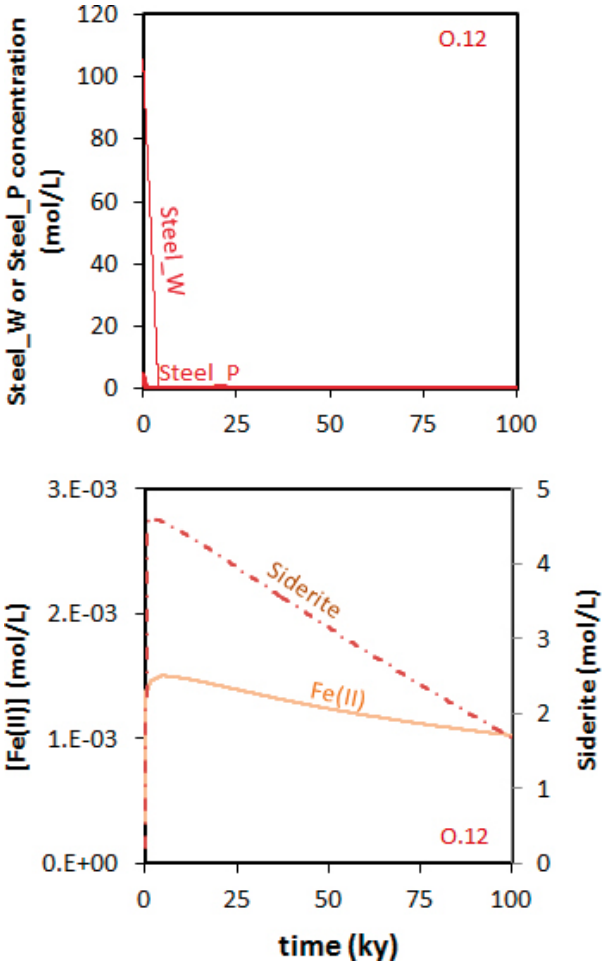

Figure 6-40. *Long term evolution of O.12 waste package type. In the upper diagram, evolution of C-steel_P and C-steel_W packages. In the bottom diagram, the evolution of Fe(II) aqueous concentration and of siderite compared with the long term temporal evolution of any of the other waste package types studied.*

6.3.5 Brief summary of the long-term results

Results indicate that in all waste package types but O.12 corrosion of steel, precipitation of magnetite and generation of $H_2(g)$ are the main processes controlling the Eh value of the system that takes a value around –0.75 V at the buffered pH of 12.5 (Figure 6-41). The pH is lower in the case of O.12 because it is not buffered by cementitious materials.

$H_2(g)$ is the most abundant gas generated. Only in the O.12 case, the amount of $CO_2(g)$ generated is significant (10% vol.) (Figure 6-42). All H_2 generated comes from the corrosion of the steel. In some cases the initial steel contained in the waste package has been completely corroded and in some cases there is still steel present after 100 ky (see Figure 6-43).

Figure 6-43 compares the time needed in each case to corrode the steel present in each waste package type. The time is mainly a function of the amount of steel but also of its reactive area and does not depend on the presence or not of generic organic matter, cellulose or bitumen.

Final aqueous concentrations of Fe(II), Fe(III), S(-II), Ca, and carbonate do not differ significantly between all those waste package types for which cementitious conditions control pH (Figure 6-45 and 6-46). Maximum acetate concentration reaches values around 0.5 M and ISA aqueous concentration about $1.6 \cdot 10^{-2}$ M.

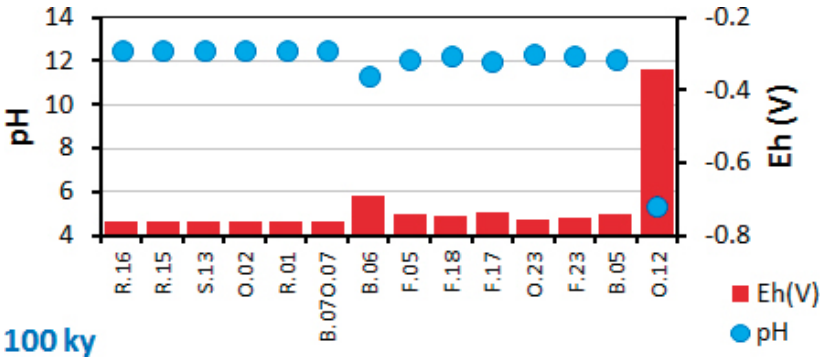

Figure 6-41. *Calculated pH and redox potential value after 100 ky for each of the waste package types under the conditions specified in the text.*

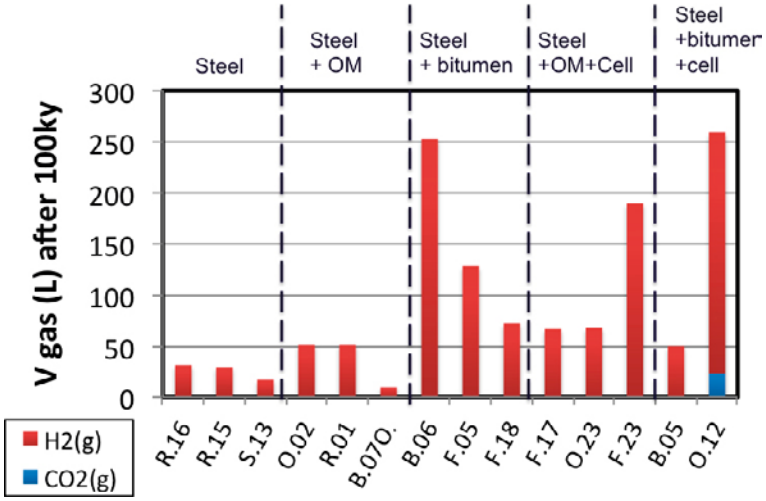

Figure 6-42. *Gas volume generated after 100 ky in each one of the waste package types.*

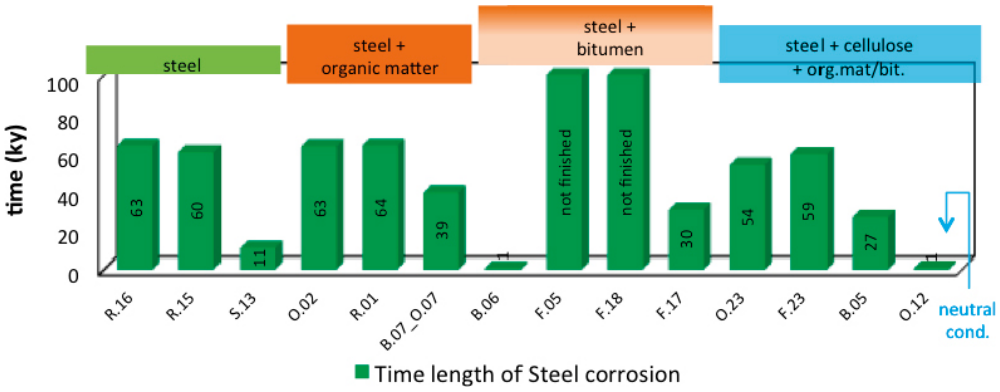

Figure 6-43. *Calculated time at which steel is completely corroded.*

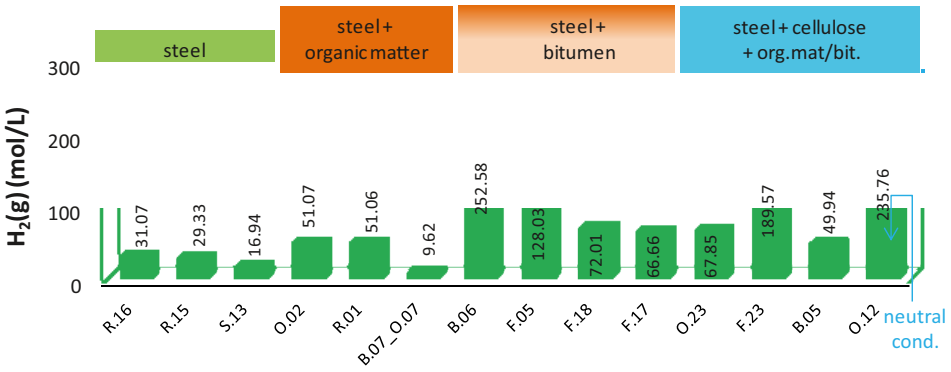

Figure 6-44. *Amounts of H_2(g) generated after 100 ky for each of the waste type packages.*

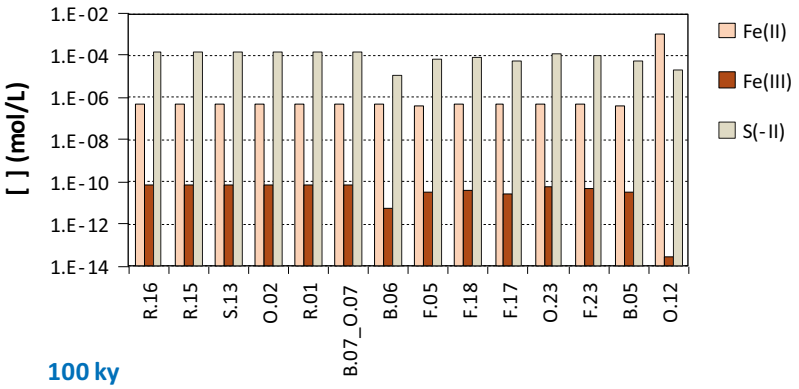

Figure 6-45. *Calculated Fe(II), Fe(III) and S(-II) total aqueous concentration after 100 ky for each of the waste package types under the conditions specified in the text.*

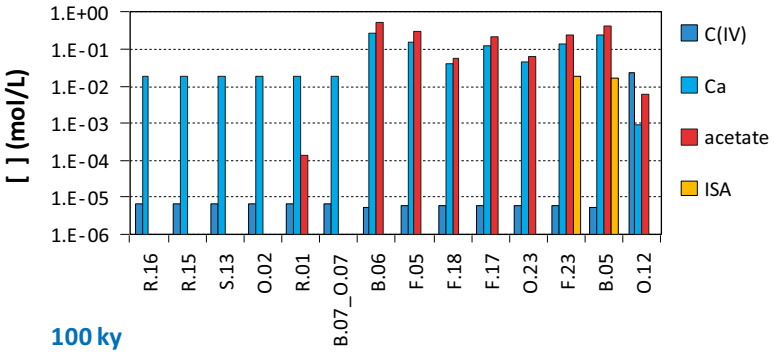

Figure 6-46. *Calculated C(IV), Ca, Acetate and ISA total aqueous concentration after 100 ky for each of the waste package types under the conditions specified in the text.*

6.4 Calculation of reducing capacity

The way to calculate the reducing capacity of the system has been presented in Section 5.6. In this section an analysis of the ReDucing Capacity RDC) of the individual waste package types and the vaults is presented. The calculations are based on the main contributors to the capacity that the system has to buffer an oxidant intrusion, which are, initially:

a) Steel.

b) Organic matter.

c) Bitumen.

d) Cellulose.

There are many uncertainties in this regard, such as whether the role of bitumen as reducing agent is fast enough as to occur in the timeframe and under the conditions of the assessment. For this reason, the RDC of those vaults containing bituminised wastes has been evaluated with and without considering the reducing capacity provided by bitumen. The same is true for organic matter. While under biotic conditions it seems clear that organic matter is easily oxidised, this does not apply to the conditions during which the system is not a proper environment for biota to be active. For this reason, the role of organic matter as reducing material has also been questioned in the analyses.

The RDC calculated for the individual waste package type has been combined in order to obtain the RDC for each one of the vaults, what gives an idea of the possibilities of combination and of applicability of the methodology to other spatial configuration of generic waste packages.

6.4.1 Results of the different waste package types

The reductive capacity of waste package types R.16, R.15 and S.13 (containing only steel as initial contributor to the RDC) is shown in Figure 6-47. In all cases an initial period of decrease of the RDC is observed, followed by a plateau with a constant RDC. During the first period, the main contributor to RDC is steel; as steel corrodes, the RDC of the system decreases. Once steel has been completed corroded, the RDC of the waste package is given mainly by magnetite, which is stable under the conditions of the simulations. The RDC of the system will then remain constant unless an inflow of oxidants intrudes the system.

The length of the period during which steel is the main contributor to the RDC depends on the rate of steel corrosion, which is in turn dependent on the reactive surface of the steel, as well as on the amount of steel in a given waste package type.

Figure 6-48 to 6-50 show the RDC of the waste package types containing organic matter besides steel. The RDC has been calculated with and without considering the contribution of organic matter remaining in the waste. Despite the potential role that organic matter can have in the reductive capacity of the system, as observed in the figures, the slow kinetics of its degradation reduces the effective role of organic matter down to insignificant values. Therefore, main contributors to the RDC are again steel and magnetite. Differences between the RDC of O.02, R.01 and B.07_O.07 waste package types depend on the amount of steel and its reactive surface.

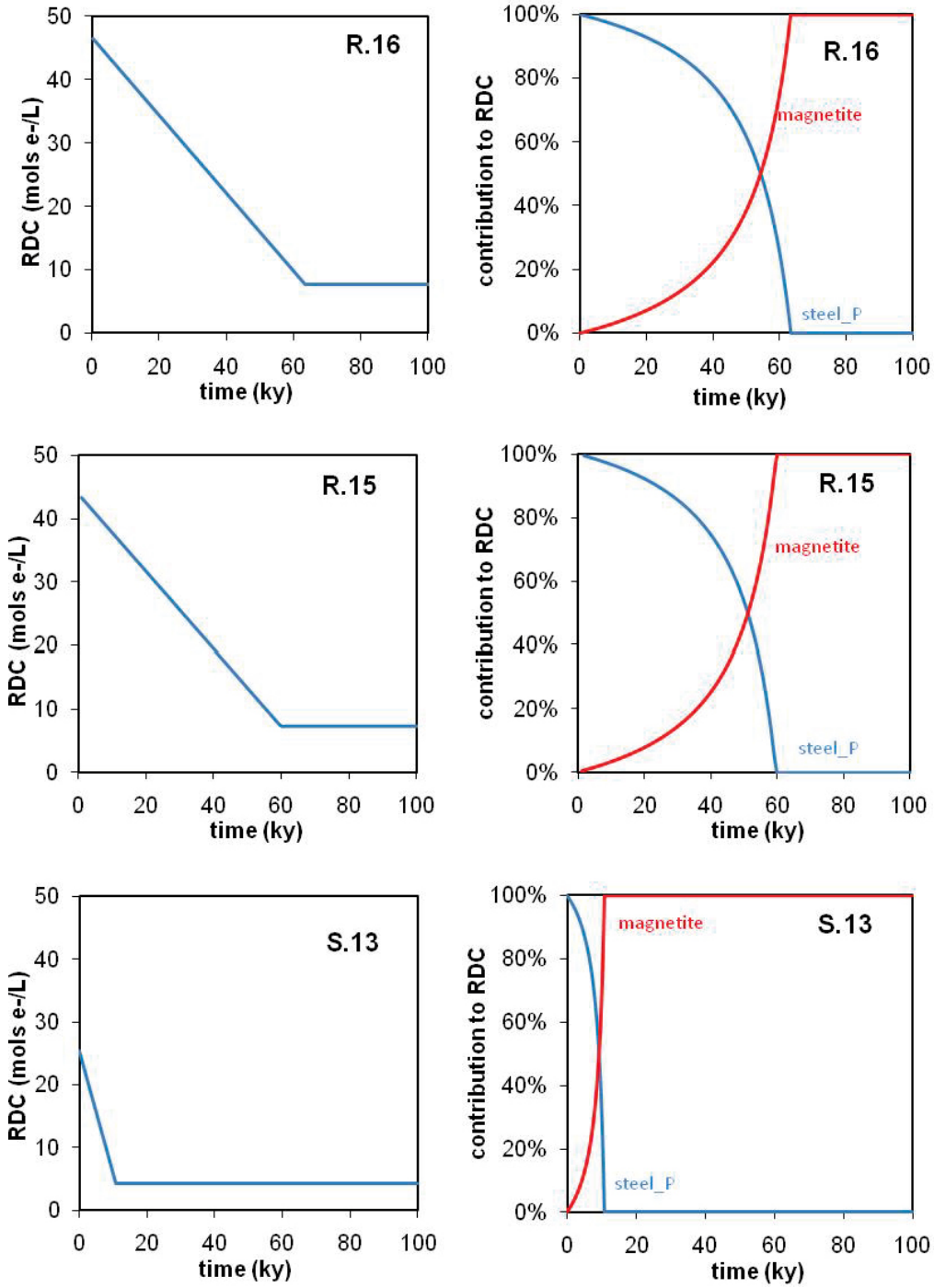

Figure 6-47. *Reductive capacity (RDC in mols e^-/L) calculated for R.16, R.15 and S.13 waste package types and contribution to RDC of steel and magnetite in percentage in each of the types.*

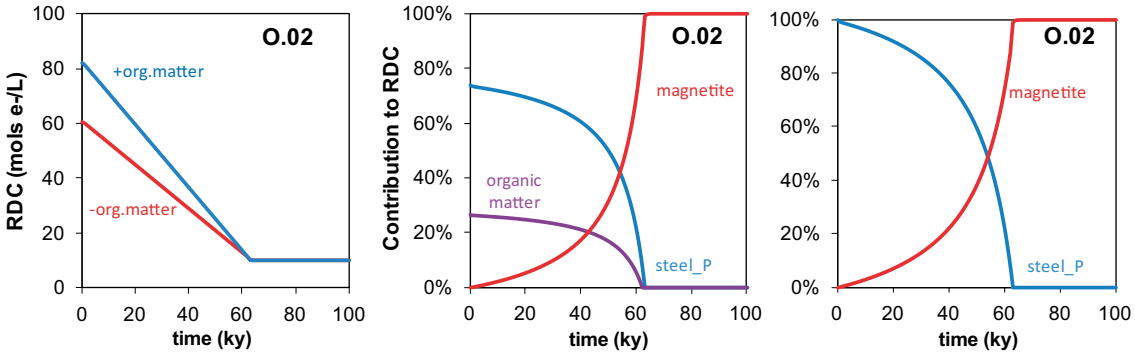

Figure 6-48. *Reductive capacity (RDC in mols e^-/L) calculated for O.02 waste package type with and without considering the contribution of organic matter (left), and contribution of organic matter, magnetite and steel_P to the calculated RDC (in %) in both cases: with (center) and withouth (right) considering the contribution of organic matter.*

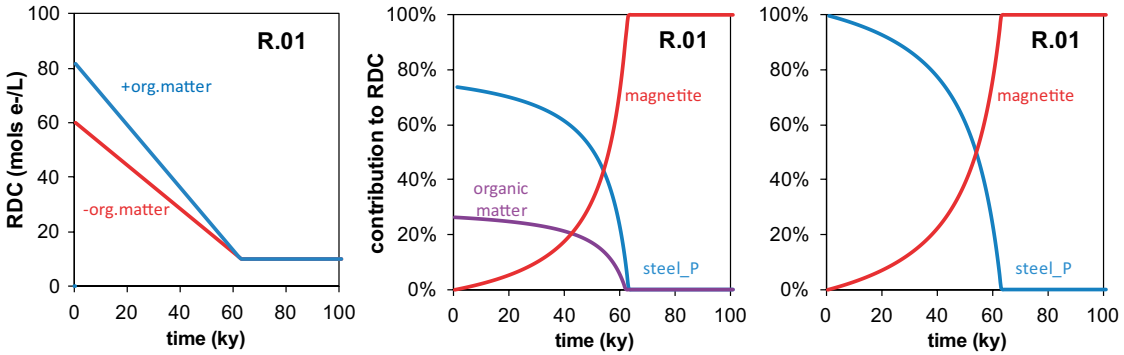

Figure 6-49. *Reductive capacity (RDC in mols e^-/L) calculated for R.01 waste package type with and without considering the contribution of organic matter (left), and contribution of organic matter, magnetite and steel_P to the calculated RDC (in %) in both cases: with (center) and withouth(right) considering the contribution of organic matter.*

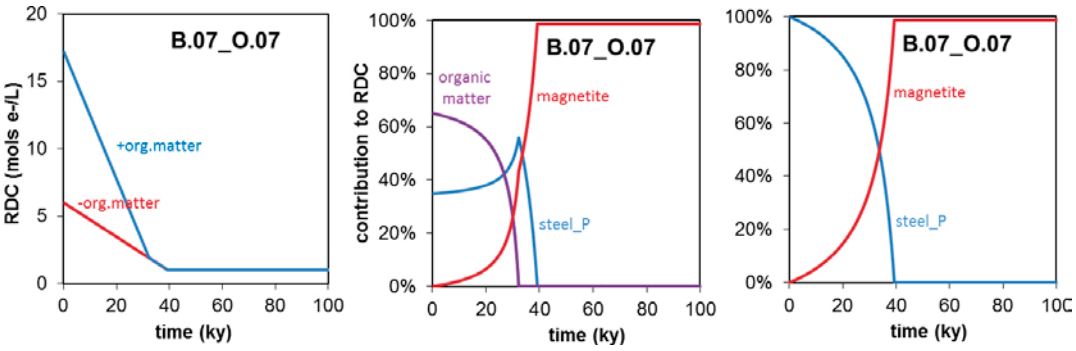

Figure 6-50. *Reductive capacity (RDC in mols e^-/L) calculated for B.07_O.07 waste package type with and without considering the contribution of organic matter (left), and contribution of organic matter, magnetite and steel_P to the calculated RDC (in %) in both cases: with (center) and withouth (right) considering the contribution of organic matter. Note the change of scale of the vertical axis compared to R.01 and O.02.*

The RDC of those packages containing bitumen are shown in Figure 6-51 to 6-54. Again, the contribution of bitumen to RDC might be significant, although, due to the slow kinetics of bitumen degradation, the role of bitumen is preferably discarded when calculating the effective RDC of the waste package types. The RDC of the package is then dependant on the amount of magnetite and steel.

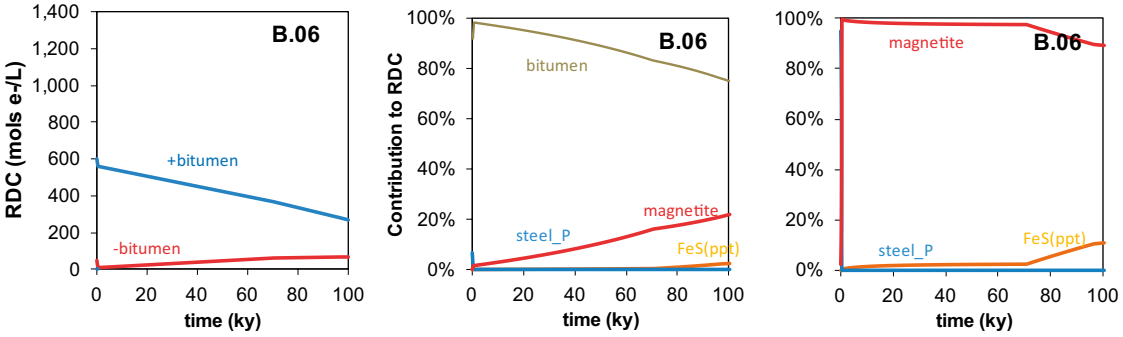

Figure 6-51. *Reductive capacity (RDC in mols e^-/L) calculated for B.06 waste package type with and without considering the contribution of bitumen (left), and contribution of bitumen, magnetite and steel_P to the calculated RDC (in %) in both cases: with (center) and withouth (right) considering the contribution of bitumen.*

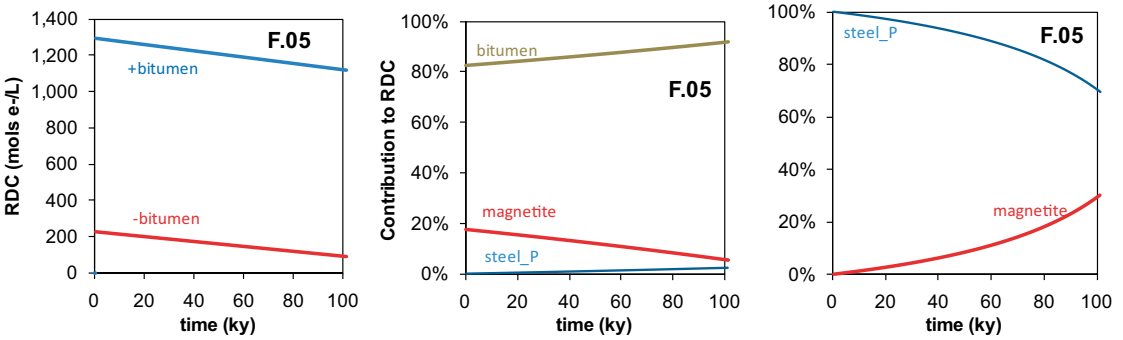

Figure 6-52. *Reductive capacity (RDC in mols e^-/L) calculated for F.05 waste package type with and without considering the contribution of bitumen (left), and contribution of bitumen, magnetite and steel_P to the calculated RDC (in %) in both cases: with (center) and withouth (right) considering the contribution of bitumen.*

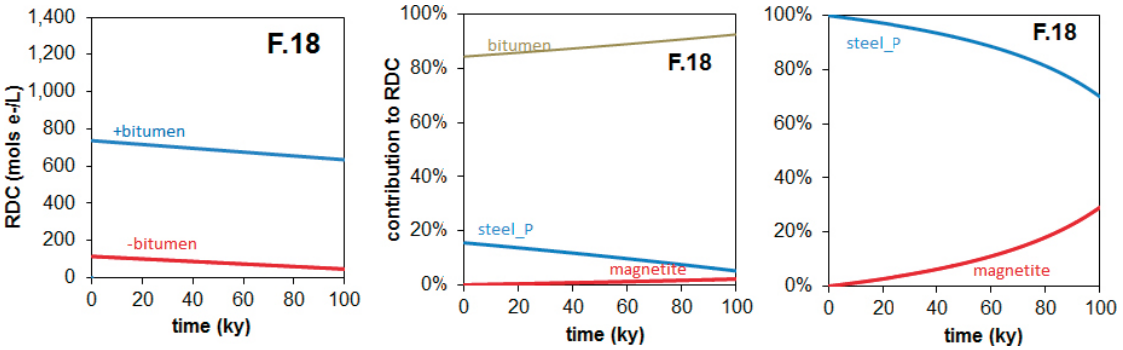

Figure 6-53. *Reductive capacity (RDC in mols e^-/L) calculated for F.18 waste package type with and without considering the contribution of bitumen (left), and contribution of bitumen, magnetite and steel_P to the calculated RDC (in %) in both cases: with (center) and withouth (right) considering the contribution of bitumen.*

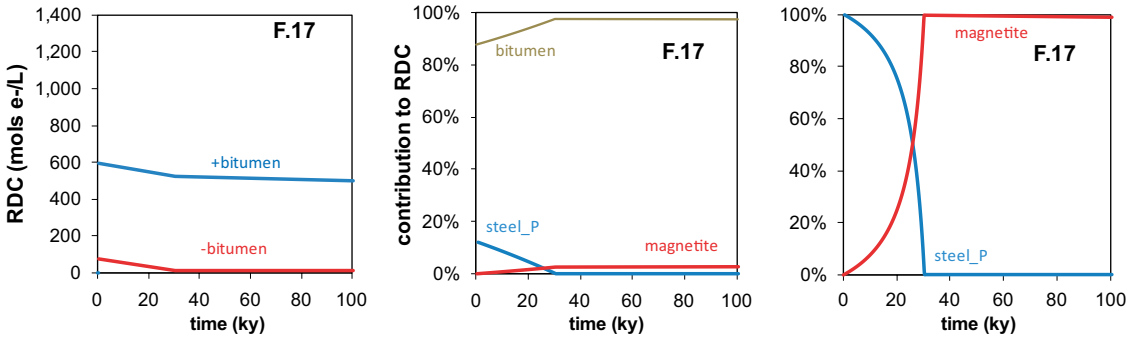

Figure 6-54. *Reductive capacity (RDC in mols e^-/L) calculated for F.17 waste package type with and without considering the contribution of bitumen (left), and contribution of bitumen, magnetite and steel_P to the calculated RDC (in %) in both cases: with (center) and withouth (right) considering the contribution of bitumen.*

F.23, O.23 and B.05 initially contain cellulose in their composition. In B.05 and O.23, cellulose is sooner exhausted while in F.23 waste package type, cellulose is not totally degraded because its initial amount is ten times higher. When the contribution of organic matter to RDC is not considered, cellulose contribution is significantly high in the F.23 RDC once steel has been totally corroded (Figure 6-55).

Figure 6-56 and 6-57 show the temporal evolution of RDC in O.23 and B.05 waste package types. As in these waste package types cellulose very soon totally degraded, the RDC behaves as in those cases not containing cellulose.

Finally, Figure 6-58 shows the RDC of the O.12 waste package type. The main difference of this case related to the previous cases is that RDC of the waste is due to siderite instead of magnetite.

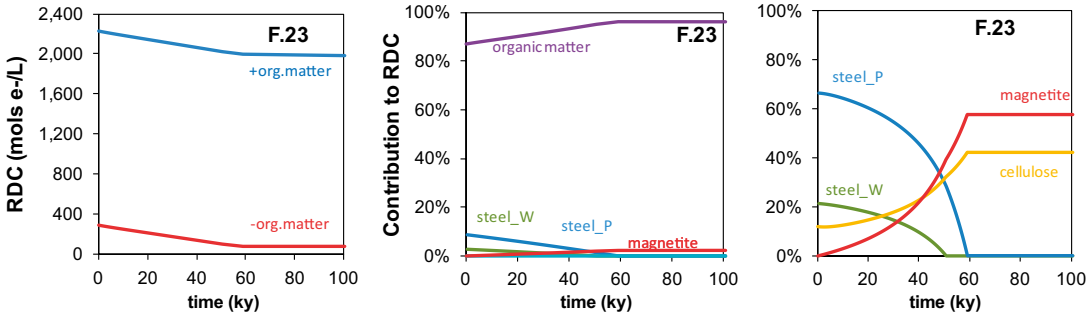

Figure 6-55. *Reductive capacity (RDC in mols e^-/L) calculated for F.23 waste package type with and without considering the contribution of organic matter (left), and contribution of organic matter, magnetite, cellulose and steel_P to the calculated RDC (in %) in both cases: with (center) and withouth (right) considering the contribution of bitumen.*

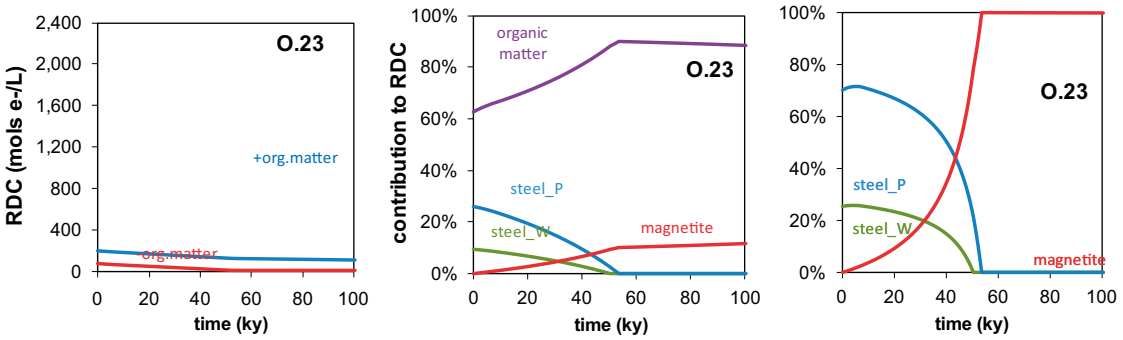

Figure 6-56. *Reductive capacity (RDC in mols e⁻/L) calculated for O.23 waste package type with and without considering the contribution of organic matter (left), and contribution of organic matter, magnetite and steel to the calculated RDC (in %) in both cases: with (center) and withouth (right) considering the contribution of organic matter.*

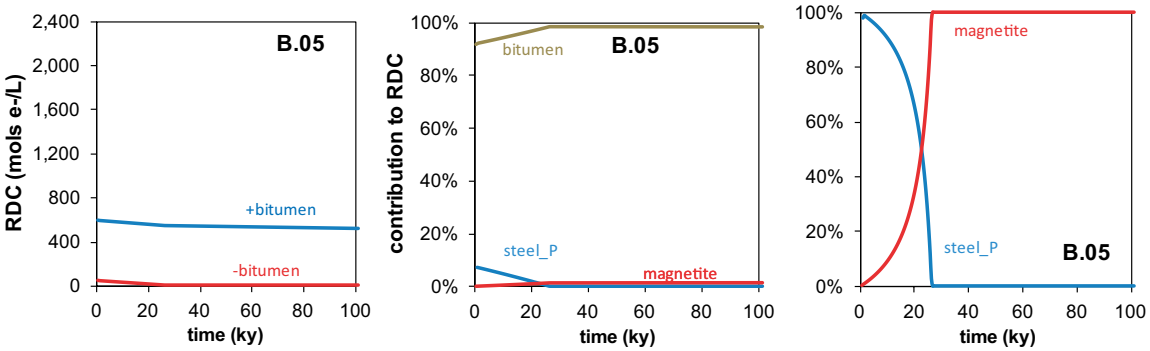

Figure 6-57. *Reductive capacity (RDC in mols e⁻/L) calculated for B.05 waste package type with and without considering the contribution of bitumen (left), and contribution of bitumen, magnetite and steel to the calculated RDC (in %) in both cases: with (center) and withouth (right) considering the contribution of bitumen.*

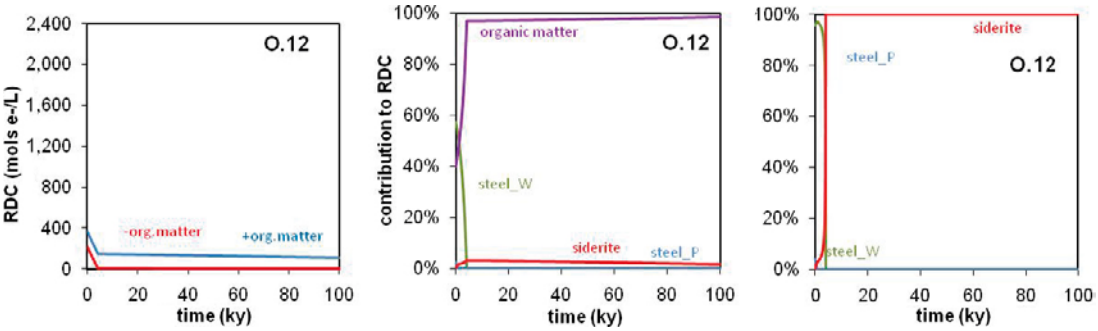

Figure 6-58. *Reductive capacity (RDC in mols e⁻/L) calculated for O.12 waste package type with and without considering the contribution of organic matter (left), and contribution of organic matter, magnetite and steel_P to the calculated RDC (in %) in both cases: with (center) and withouth (right) considering the contribution of organic matter.*

6.4.2 RDC of the vaults

Once the RDC of the different waste package types has been calculated considering the different chemical processes in agreement with the conceptual model described, the evolution of the overall RDC of the different vaults of the SFR 1 repository can be estimated by considering the number of each type of waste packages in each vault (Table 6-11). For BLA only the O.12 waste package type has been considered, as discussed in chapter 4.

Figure 6-60 shows the temporal evolution of the RDC for the four vaults and for the Silo of the SFR 1 repository. As can be seen, in early times of evolution, BLA presents the highest RDC of the repository. At intermediate and long term, BMA vault is the vault most contributing to the RDC of the repository.

1&2 BTF and BLA are the vaults with the lowest RDC values in the long-term, therefore the most susceptible of losing the reducing conditions under the event of an oxidant intrusion. The calculations of the RDC have pessimistically assumed that bitumen is not degraded and therefore, an important part of the potential reductive capacity of the system is neglected. The same approach has been applied to the organic matter, so that only steel has been credited as providing reducing capacity to the system (in these calculations).

The results of the individual vaults are shown in Figure 6-59, from where we can observe different steps:

- an initial step of linear decrease due to the corrosion of steel and production of magnetite,
- a second step where the main contribution to the RDC is the amount of magnetite because steel is completely corroded or the decrease induced by the corrosion of remaining steel is poor.

In none of the cases the RDC goes to zero, showing the after 100 ky, under non-disturbing conditions, the system is sufficiently robust as to keep the reducing conditions imposed by the process of steel corrosion.

As shown in Figure 6-60 most of the reducing capacity of the system is located in the BMA and in the Silo in the long-term.

Table 6-11. Number of waste package types considered in each vault to calculate the RDC. Data from Zazzi (2011).

	B.07_O.07	S.13	B.05	F.05	F.17	F.23	R.01	R.15	O.23	B.06	O.02	R.16	O.12
1 BTF	40	4,656											
2 BTF	683												
BLA*													180
BMA													
Comp. 1							*576*						
Comp. 2			*382*	*1712*			*142*						
Comp. 3			*1,438*		*144*		*140*						
Comp. 4						*49*	*219*	*132*	*175*				
Total			1,820	1,712	144	49	1,077	132	175				
Silo													
Shaft 55 (x9)										*320*	*12*		
Shaft gen (x63)											*24*	*28*	
Total										2,880	1,620	1,764	

*Expected deposition number given that no updated data from Studsvik and Svafo was available at the moment of vault description (Zazzi 2011).

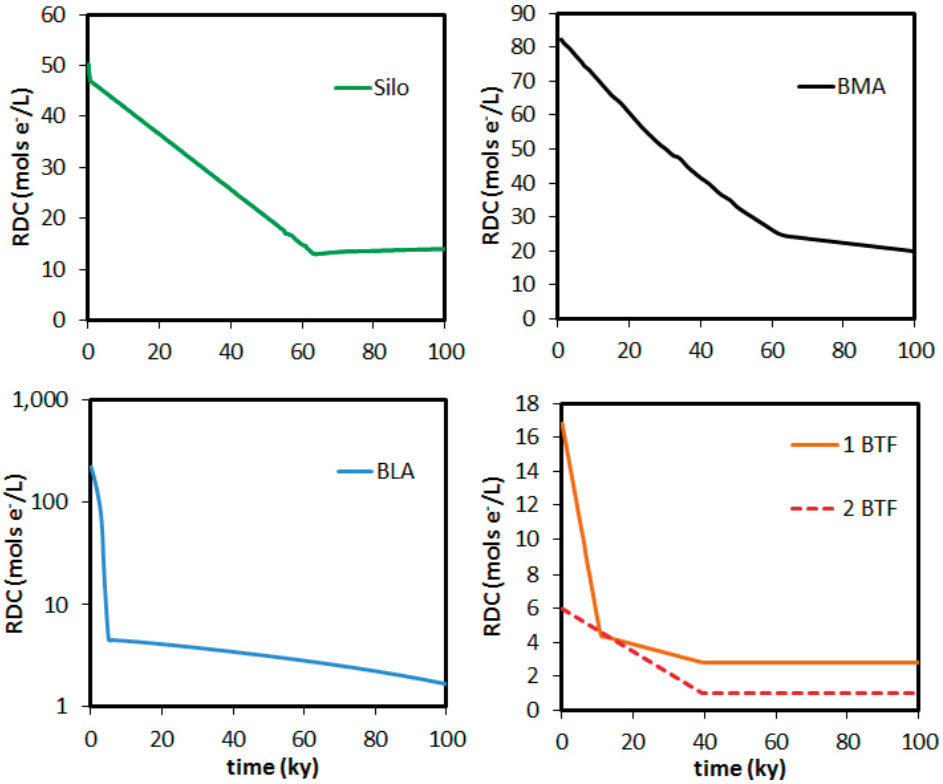

Figure 6-59. *Evolution of the reductive capacity (RDC in mols e⁻/L) of each one of the vaults with time. Bitumen and orgànic matter have not been considered as RDC contributors. Data for BLA has been represented in a log-scale to highlight that its RDC never goes to zero under undisturbed conditions.*

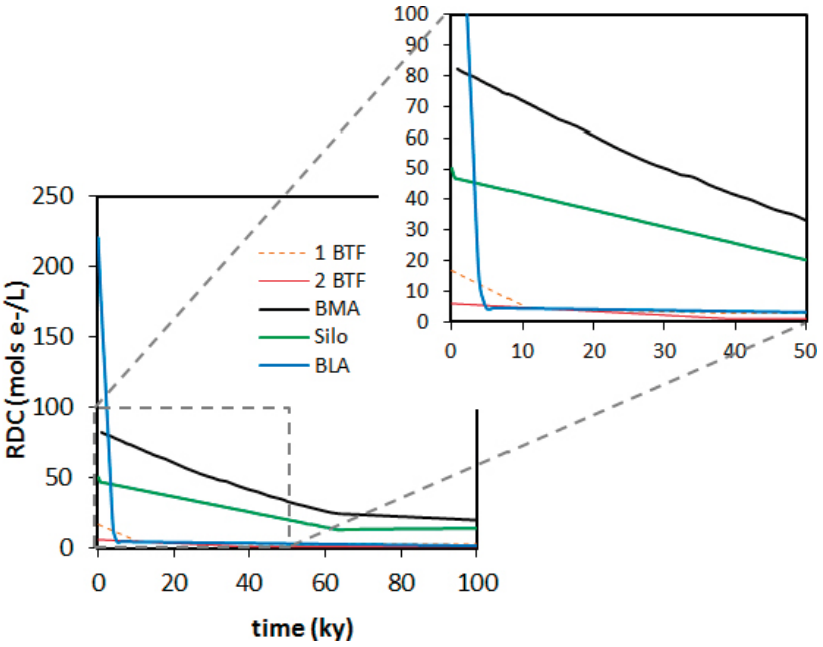

Figure 6-60. *Temporal evolution of the reductive capacity (RDC in mols e⁻/L) calculated for each of the vaults, 1&2 BTF, BMA, Silo and BLA. The contribution of bitumen and organic matter to the RDC has been pessimistically neglected.*

7 Sensitivity analyses

The calculated reducing capacity of the system is high after 100 ky, even neglecting the processes of degradation of organic matter and bitumen, that is, only considering the corrosion of steel. Anoxic steel corrosion proceeds at expenses of water consumption, what means that the limiting step for the kinetic corrosion will be water availability. In principle, according to the flow rates intruding the repository, once saturation is achieved, enough water will be available as to maintain the rate of anoxic steel corrosion.

We have discussed in previous chapters that the value of the corrosion rates in the literature spans over some orders of magnitude, thus being one of the uncertainties with higher influence on the amount of steel remaining after the assessment, on the rate of production of gases, as well as on the response of the system in front of an eventual oxidising perturbance. This section presents a probabilistic analysis of the effect that the uncertainty on the steel corrosion rate can have on the RDC of the system as well as a simple analysis on how would the system behave in front of an oxidising intrusion originated from melt water after a glacial episode.

7.1 Uncertainty on the steel corrosion rate

The different steel corrosion rates available in the literature span over more than 4 orders of magnitude depending on the type of material studied and the conditions imposed.

In the literature different methods are used to determine the rate of steel corrosion, such as measurement of the hydrogen evolution, corrent intensity, and metal loss or gain. Important differences in the same rates can be obtained depending on the method used for its determination as well as on the conditions of the experiments and type of material. The assumption of the stoichiometry of the corrosion process introduces limitations to the techniques, due to the consideration of different moles of hydrogen formed depending on whether the corrosion product is, for example, $Fe(OH)_2$ (s) or magnetite. The measurement of hydrogen evolution in the experiments also presents important limitations due to the fact that it is implicitely assumed that hydrogen gas is equilibrated with the solution, although this can introduce delays in the evolution of hydrogen due to the prior needed saturation of the solution with aqueous hydrogen. The explanation for this disagreement between corrosion rates determined by different methods is not clear, but it can be taken as an indication of the non-stoichiometry of the surface film formed on the iron-water interface, oxidation by other process besides water reduction or insufficient equilibration between the generated hydrogen in the solution and in the gaseous phase. A discussion on the adequacy of the different techniques for corrosion rate measurements is included in Kursten et al. (2004).

Different original data in the literature on corrosion rates of stainless steel under anoxic hyperalkaline conditions at room temperature are given in Smart and Hoch (2006). Although many discussions exist in the literature, data applicable under the specific conditions of interest are not abundant.

The approach followed in this work to asses how the uncertainty existing on the corrosion rate of steel will affect the assessment of the RDC is to apply a probabilistic Monte-Carlo analyses to the rate and see how it is mirrored in the RDC.

The analysis presented here has been conducted with the software MC-PHREEQC. This software has been developed at Amphos[21], and provides a way to do Monte-Carlo simulations automatically (www.amphos21.com). As input it needs a PHREEQC input file, a Probability Distribution Function (PDF) for each of the uncertain parameters, and the settings for the Monte-Carlo simulation. It can automatically generate histograms and scatter plots from the results.

We have used data from Tables 7 and 9 of Smart et al. (2004) to define the PDF for steel corrosion rate under alkaline conditions used in the calculations. After an expert judgement, the maximum value that the corrosion rate can reach (that with a cumulative distribution function equal to one, CDF=1), the minimum value (that with a cumulative distribution function equal to zero, CDF=0)

and the value representing 50 % of the values (CDF=0.5) have been selected from the experimental data reported in Smart et al. (2004) and from data used in this report (Table 5-4). Figure 7-1 defines the PDF and CDF (Cumulative Distribution Function) used in the sensitivity analyses, which are summarised in this report.

Results of the sensitivity analysis are shown in Figure 7-2.

The calculations are conducted in a way that the system samples values for the uncertain parameter (in this case the corrosion rate) in agreement with the Probability Distribution Function (PDF). Each time that a value is sampled, a run of simulation with PHREEQC is calculated, so that to obtain a simple result with the MC-PHREEQC hundreds of individual PHREEQC calculations are needed. Calculations of RDC have been done at different periods of time: 1, 5, 10 and 100 ky.

The calculations have been conducted with the waste package type S.13, which is the one presenting the lowest RDC based on steel.

The results can be seen in Figure 7-2 for 4 different times. The corrosion rate spans over the 4 order of magnitude obtained from the PDF. We observe that the RDC of S.13 waste package type after 100 ky is not very much affected by the uncertainty in the corrosion rate, given that steel has been already completely corroded and the remaining RDC is provided by magnetite. For a corrosion rate of $2 \cdot 10^{-10}$ mole/m^2/s after 5 ky the RDC remaining does only rely on magnetite, while when the rate is $1 \cdot 10^{-10}$ mole/m^2/s steel is still present in the system after 5 ky and provides additional RDC to the system. As expected, for short time periods, higher RDC are obtained for lower corrosion rates.

Table 7-1. Summary of the values defining the CDF and PDF used in the sensitivity analyses of the effect of alkaline steel corrosion uncertainty on RDC.

CDF selected values Ln rate (μm s^{-1} y^{-1})	CDF
–9.76	0
–8.76	0.01
–2.86	0.25
–2.61	0.50
–2.26	0.75
5.74	0.99
8.23	1.00

Log normal distribution parameters	
Average	–2.61
St.dev	0.60

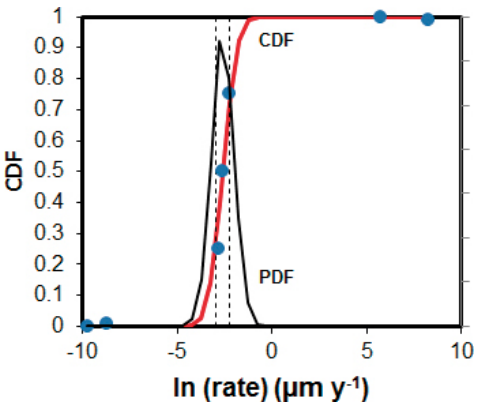

Figure 7-1. CDF and PDF used in the sensitivity analysis.

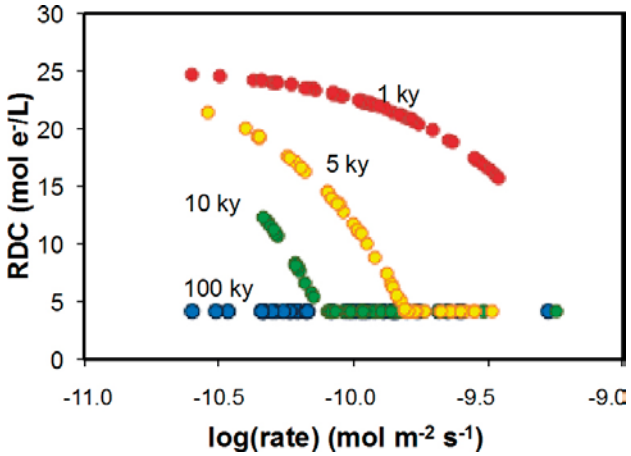

Figure 7-2. *Variation of the RDC calculated for S.13 waste package type at different times considering the PDF defined in Table 7-1.*

The uncertainty on the RDC is more relevant under the event of oxidant intrusion, because it is when the ability of the system to buffer reducing conditions is tested. In the following section the case of deglaciation water intrusion is simulated.

7.2 Glacial event scenario

The effect of a glacial event in the RDC of a waste package type has been tested with the S.13 package, which does neither contain bitumen or other organic matter. According to the calculations reported in the previous chapters, steel contained in S.13 is completely corroded around 11 ky after the closure of the repository. From this moment onwards, most of the reducing capacity of the system is provided by magnetite. The event of glacial melt water intrusion is one of the cases that have been considered as disruptive also for the high level waste deep geological repository of SKB given that glacial meltwaters are expected to be diluted and oxidising, that is, more aggressive for the stability of the safety functions than groundwaters that have been equilibrated with the host rock and fracture minerals.

Although the climatic evolution of the repository is currently under revision, it is not expected that the evolution cases will change importantly from the ones proposed for the SAR-08 assessment. The earliest melt water is expected to to occur after 60 ky AD (see Figure 7-3), therefore we have considered an intrusion of oxidising water after 60 ky of the closure of the repository.

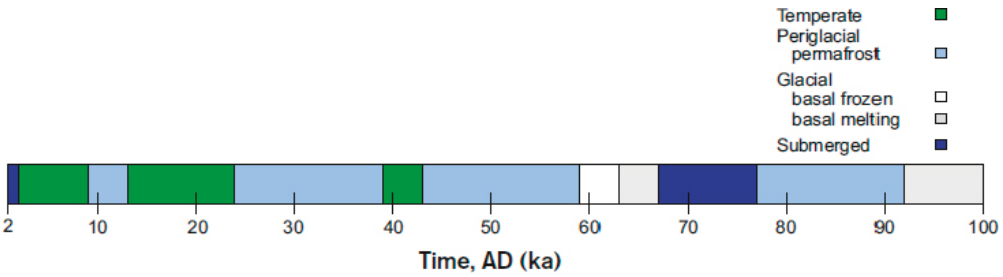

Figure 7-3. *Climate evolution according to the main scenario's Weichselian variant based on a reconstruction of the conditions during the latest glacial cycle, extracted from SAR-08 assessment (SKB 2008a).*

To simulate the mentioned glacial meltwater flow, we have used the code PHREEQC. Glacial groundwater has been assumed to flow through the S.13 after 60,000 y of the deposition of the wastes, for a period of 40,000 years, that is, from the moment of the glacial event to the end of the period of interest (from 60 ky to 100 ky after repository closure). The water flow rate, cell length, dispersivity and molecular diffusivity used in the calculations are shown in Table 7-2. They have not been changed with respect the values used and reported in Section 6.

The composition of the porewater of S.13 waste package type and the concentration of the minerals present in the package at the beginning of the glacial event (after 60,000 y of repository closure) are shown in Table 7-3, and have been taken from the results of the calculations shown in Section 6.

Glacial groundwater composition used in the calculations corresponds to a Finnish glacial groundwater. It is listed in Table 7-4 and has been taken from Salas et al. (2010). Oxygen aqueous concentration has been assumed given by equilibrium with atmospheric oxygen (0.21 atm) at 15°C.

Table 7-2. Main values used in the modelling of the glacial event in the S.13 waste package type (see Section 6.3).

Specific flow	**3.7×10^{-11} m/s**	**Porosity**	**0.171**
Water flow	2.2×10^{-10} m/s	Δx	0.111 m
Molecular diffusion, D_m	1×10^{-10} m^2/s	Longitudinal dispersivity, σ_L	0.055 m

Table 7-3. Composition of the cells (gases, minerals and porewater) considered as initial conditions for the glacial event.

pH	12.49
pe	–12.91

Aqueous concentration (in mol/L)		**Mineral composition (in mol/L)**	
C	6.60×10^{-6}	Portlandite	88
Ca	1.87×10^{-2}	Magnetite	4.24
Cl	1.27×10^{-3}	FeS(ppt)	4.32×10^{-5}
Fe(II)	4.95×10^{-7}	Calcite	1.93×10^{-6}
Fe(III)	6.86×10^{-11}		
H(0)	1.06×10^{-2}		
K	1.02×10^{-4}		
Mg	3.70×10^{-4}		
Na	4.35×10^{-3}		
S(-II)	1.50×10^{-4}		
S(VI)	1.21×10^{-28}		
Si	9.82×10^{-5}		

Table 7-4. Composition of the melt groundwater (Salas et al. 2010).

pH	5.8
pe	15.21

Aqueous concentration in mol/L	
C	2.6×10^{-6}
Ca	3.2×10^{-6}
Cl	2.0×10^{-5}
K	3.8×10^{-6}
Na	6.5×10^{-6}
S	5.2×10^{-7}
Si	1.7×10^{-7}
O_2	3.2×10^{-4}

A concentration of iron in the intruding groundwater of 3.8×10^{-7} mol/L, given by equilibrium with hydrous ferric oxide, has been considered.

The S13 waste package type contains 30 kg of steel, equivalent to 535.7 moles of Fe (steel 99% of Fe, and atomic weigh of Fe = 55.85 g/mol). This means that the maximum amount of magnetite that can be produced after total steel has been corroded is 177 moles, i.e. 1 mole of magnetite per mol of Fe. According to r. 7-1, 1 mole of oxygen is neede to oxidise 4 moles of magnetite, what means that for the oxidation of the 177 moles of magnetite in S.13 the intrusion of 44.3 moles of oxygen is needed.

$$4\ Fe_3O_4 + O_2\ (g) + 6\ H_2O \rightarrow 12\ FeOOH \qquad \text{r. 7-1}$$

By considering the specific flow of the intruding melt water (Table 7-2), and its dissolved oxygen concentration (Table 7-4), the complete oxidation of the magnetite contained in S.13 is not expected to occur until 0.5 million years, assuming fast magnetite oxidation, as soon as oxygen contacts it. This gives an idea on the fact that the reducing capacity of the system will last for long times under the conditions considered in the assessment.

A simple calculation aimed at reducing the calculation time has been done with a batch system where oxygen is added to a porous medium containing 1 L of water and the composition of S.13 waste package type at t = 60 ky. The result of this simple simulation is shown in Figure 7-4. As can be seen, magnetite oxidises to form goethite as oxygen is added to the system and, after 40 ky of oxygen intrusion (indicated by a vertical grey dashed line in the plot), there is still magnetite in the system, so that the system still has reducing capacity. When magnetite is completely oxidised (at t around 115 ky after closure) to goethite, the Eh of the system increases, as it is not able to buffer the oxidant intrusion.

The results shown in Figure 7-4 do not consider mass transfer out from the system, are simple batch calculations. Additional simulations, including transport of water and solutes, have been conducted (see Figure 7-5). The results indicate that, when oxygen starts to intrude the waste package, 60 ky after closure, oxygen is being consumed by transformation of magnetite into goethite (see Figure 7-5a) and the saturation index of goethite, which is initially negative reaches a value of zero, and goethite starts to form in the system. The calculated Eh of the system increases as oxygen intrudes the waste package until reaching a constant value, buffered by the transformation of magnetite into goethite. As this happens, also a decrease in the aqueous concentration of Fe(II) and S(-II) is calculated.

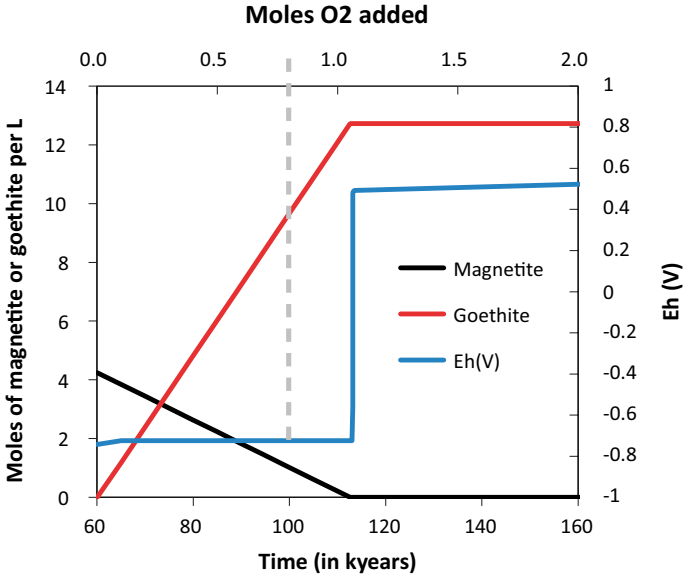

Figure 7-4. *Evolution of the moles of magnetite and goethite in S.13 and the value of the redox potential. Results of batch simulations. Time = 60 ky indicate the time at which the glacial groundwater intrudes the system. Vertical grey dashed line indicates the end of the period that must be covered by the performance assessment of the SFR 1.*

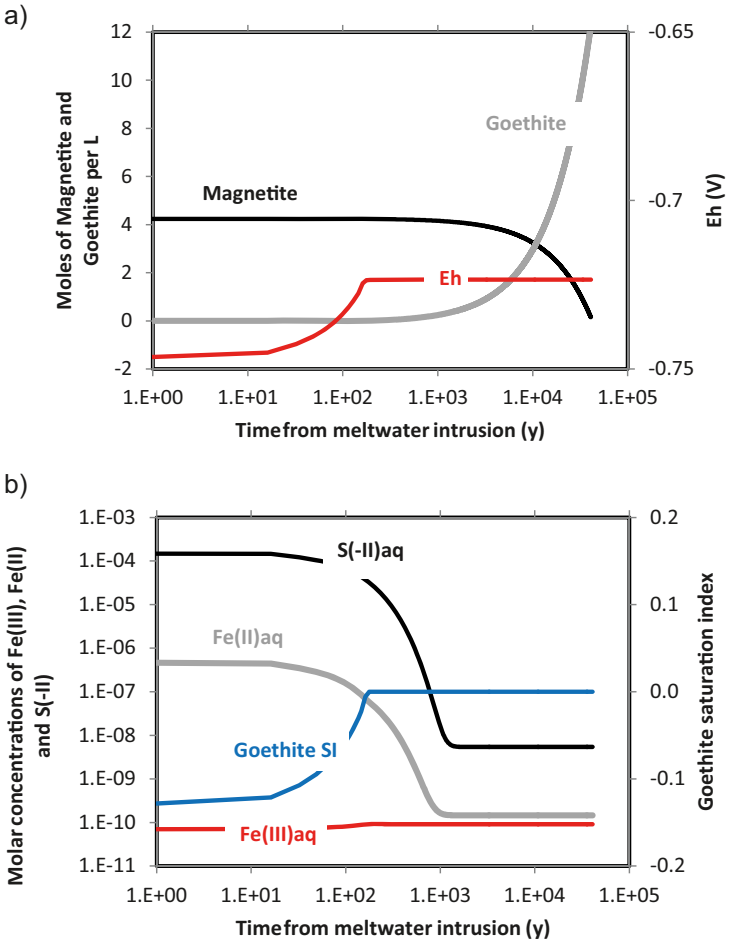

Figure 7-5. *Results of transport simulations in S.13 from the intrusion of meltwater in the system (t=0 corresponds to 60 ky after closure under non-disturbed conditions). a) Evolution of the moles of magnetite, goethite and Eh calculated. b) Evolution of the dissolved concentrations of Fe(II), Fe(III), S(-II) and Saturation index of Goethite.*

The results of the calculation indicate that at the end of the assessment period of interest (10^5 years) the system has not been depleted of its reducing capacity, which is equivalent in this simulation to say that not all magnetite has been transformed into goethite and, therefore, the system is still able to buffer an oxidant intrusion. After 40 ky of infiltration of meltwater, the amount of magnetite oxidised into goethite is of a 95%, and a 5% of the magnetite remains unoxidised.

8 Assessment of the redox potential and its influence on the radionuclide behaviour

The redox potential in the system is calculated to be given, for most of the length of the assessment, by the process of water reduction on the steel surface. In order to account for the formation of a surface layer of magnetite on the steel surface, what may difficult the contact between water and steel, the value for the rate of steel corrosion has been selected from the low range of data existing in the literature, as presented in Section 5.3.

In the calculations presented here, the redox potential reported is that given by the hydrogen concentration, that is, the simulations consider that hydrogen is chemically active.

Hydrogen activation has been proven not to occur in homogeneous solution, although its activation catalysed by metallic surfaces is a very well-known phenomenon reported in the literature. The effect of solid surfaces in the reduction of U(VI) to U(IV) in the presence of hydrogen, for example, has been pointed out in several investigations during the second half of the last century. As an example, the work of Forward and Halpern (1953) can be mentioned. These authors studied the process of uranium recovery from carbonate ore leaching solutions via reduction of U(VI) by $H_2(g)$ under the presence of metallic Ni(s) as catalyst. These results point towards an effect similar to the one observed for the catalytic hydrogenation of hydrocarbons. According to those authors, both reactants, Uranium and $H_2(g)$ were chemisorbed at the metal surface, where the electronic transference took place. As alternative, they tested several metals, such as Co and Pt, obtaining similar results.

In the last years, the effect of metallic surfaces on the activation of hydrogen from solution has been observed in many experiments. Among others, one can cite the work of Broczkowski (2008), Trummer and Jonsson (2010) and others, where the effect of metallic surfaces such as Pd in activating hydrogen has been observed. Also the reductive precipitation of different metals on the surface of magnetite under the presence of hydrogen has also been reported pointing towards the activation of hydrogen in the presence of steel/magnetite surfaces.

The observations of the activation of hydrogen on metallic surfaces previously cited, support the results that the system will be kept under reducing conditions, in agreement with the calculations presented in this report.

Nevertheless, it can be discussed that the value that the redox potential will take in the system will not correspond to that of the hydrogen formation but to that imposed by the magnetite surface, which will be the one in contact with the groundwater in the long term. This will cause the redox potential in the system to be higher than the one calculated in the present report (Figure 8-1). If the redox potential is controlled by water reduction, a value of –0.75 V at pH 12.5 is calculated, which is the one shown in the previous simulations. If, on the contrary, its value in the system is controlled by the interface between magnetite and goethite, the redox potential would be around –0.64 V at pH 12.5, that is, also very reducing. In the case of considering that the oxidation of magnetite forms hematite instead of goethite, the value of the redox potential would be of –0.66 V at pH 12.5.

Another case considering that the oxidation of magnetite can form ferrihydrite is also presented, which is the only case where less reducing redox potentials can be established at the boundary between ferrihydrite and hematite (Figure 8-2) and where the stability field of magnetite is increased due to the lower stability of ferrihydrite in comparison with goethite and hematite.

Another uncertainty that would affect the value of the redox potential is the pH achieved in the system. The calculations in this report have been conducted by assuming portlandite as a proxy for cement, without considering its degradation. If all degradation steps for cement are considered, the pH would vary from 13.3 in the initial stages of degradation, to 10.5 in the very degraded barrier case. The values of the redox potential that could develop in the system depending on the stage of degradation of the cementitious materials as well as on the redox couple assumed to control the redox conditions are presented in Table 8-1. There is one waste package (O.12) where low pH values are achieved (5.4), mainly due to the scarcity of cementitious materials both in the waste package as well as in the BLA vault where it is located. In the case of O.12, siderite ($FeCO_3(s)$) is formed, as seen in Figure 8-3.

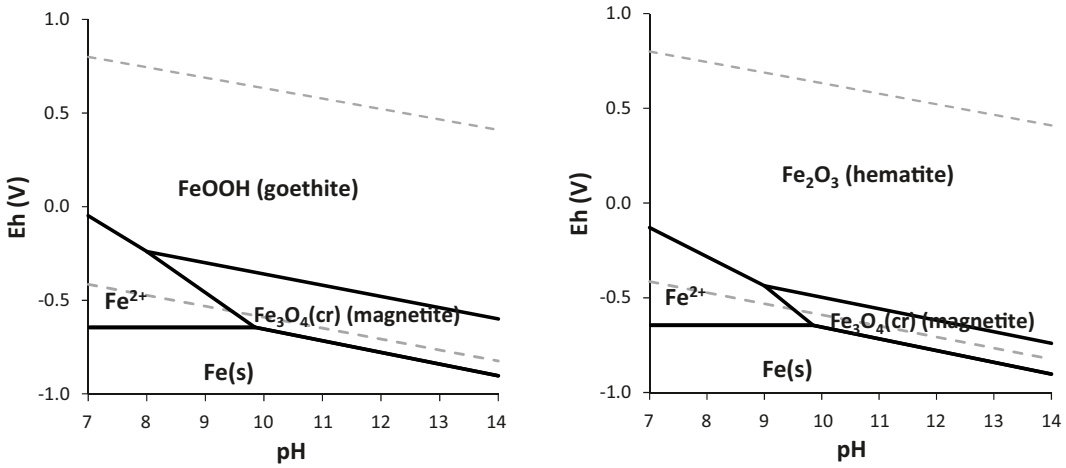

Figure 8-1. *Predominance Eh/pH diagram of the iron system calculated at concentration of iron of 10^{-6} M. The boundary between magnetite and two alternative Fe(III) solid phases are represented: left: magnetite/ goethite (FeOOH(cr)) and right: magnetite/hematite (Fe_2O_3(cr)). Dashed lines correspond to the stability field of water. Below the lower dashed line, water reduces with formation of hydrogen.*

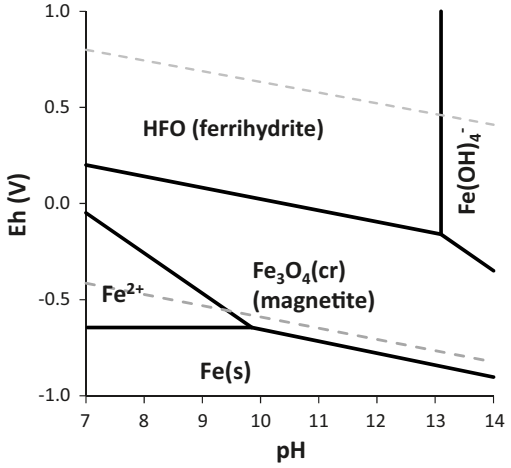

Figure 8-2. *Predominance Eh/pH diagram of the iron system calculated at concentration of iron of 10^{-6} M, by supressing the precipitation of goethite and hematite.*

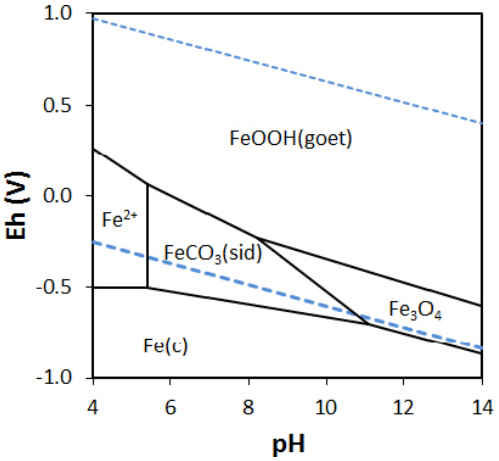

Figure 8-3. *Predominance Eh/pH diagram of the Fe system by considering the composition of the water evolved in O.12 waste package (pH = 5.4). $[S(VI)]_T=2\cdot10^{-5}$ M; $[C(IV)]_T=2.3\cdot10^{-2}$ M; $[Ca]_T=8.7\cdot10^{-4}$ M.*

Table 8-1. Range of redox potential calculated depending on the active couple considered to control the system and the pH marked by the degradation of cementitious materials. A specific calculation is indicated for O.12, with no cementitious materials present.

	Eh (V) given by equilibrium of the different compounds at the different pH given by the degradation of cementitious materials. Fe_2O_3: hematite; FeOOH: goethite; Fe_3O_4: magnetite; HFO: ferrihydrite			
pH	**H_2O/H_2**	**Fe_3O_4/Fe_2O_3**	**Fe_3O_4/FeOOH**	**Fe_3O_4/HFO**
13.5	–0.807	–0.721	–0.700	–0.190
12.5	–0.749	–0.663	–0.642	–0.132
10.5	–0.633	–0.547	–0.526	–0.016
O.12*	**H_2O/H_2**	**$FeCO_3/Fe_2O_3$**	**$FeCO_3$/FeOOH**	**$FeCO_3/Fe_3O_4$**
5.4	–0.344	–0.016	0.040	0.105

For those cases in italics in Table 8-1, the redox potential would be kept at reducing values, in a way that the implications for the mobility of the redox sensitive radionuclides would be bracketed in the pH/Eh range 10.5–13.5 / –0.526 – –0.807V. In the previous table, a case considering that the oxidation of magnetite can form ferrihydrite is also presented, which is the only case where less reducing redox potentials could be reached in those waste packages containing cementitious materials or located in the vaults that contain concrete in the structures. The case of O.12, with no massive amounts of cement in its inventory or as barriers in BLA, is also presented. In this case, it is noticeable that the redox potentials are bracketed in the range –0.344 to 0.105 V. The values in Table 8-1 are similar to the ones estimated by Wersin et al. (2003) when assuming that the iron system is the one controlling the redox state of the system.

The case of melting water intrusion has been calculated not to produce an increase in the redox potential of the system in the timeframe of the assessment (100,000 years) although it will be discussed when dealing with radionuclide behaviour for the sake of completeness.

According to the simulations presented in this report, the range of Eh/pH that can be developed in the system and conditioned by the most likely redox couples and considering the different steps in the degradation of the cementitious groundwaters can be bound by the shadowed insert in Figure 8-4, which will be discussed in the analyses of the radionuclide behaviour.

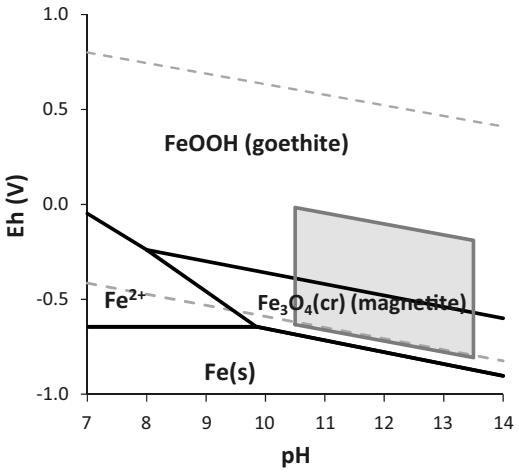

***Figure 8-4**. Predominance Eh/pH diagram of the iron system showing the insert that bounds the pH/Eh values conditioned according to the calculations presented in Table 8-1.*

9 Radionuclide behaviour

The main redox sensitive radionuclides present in SFR 1 are, besides U, Se, Tc, Np and Pu. The analysis presented here has been conducted by assuming that the concentration of the radionuclides in the system is given by the dissolution of the complete inventory (Table 9-1) in the total void volume of the vaults, assuming that the void volume is completely water saturated. The concentrations of the elements calculated for each vault are presented in Figure 9-1. Technetium is the element present in higher concentrations in all the vaults (in the order of 10^{-6} M) and Se shows the lower levels (from 10^{-12} M in the BLA to $2 \cdot 10^{-9}$ M in the Silo, BMA and 2 BTF).

The Pourbaix diagrams of the previous elements focused on the conditions expected to prevail in the system are shown in the following sections.

Table 9-1. Activity of Np, Pu, Tc and Se for each vault expressed in Bq (from Zazzi 2011).

Radionuclides	Silo	BMA	1 BTF	2 BTF	BLA
Np-237	5.07×10^{7}	1.53×10^{7}	8.02×10^{4}	1.89×10^{6}	7.90×10^{3}
Pu-238	2.02×10^{10}	1.63×10^{10}	1.73×10^{8}	6.55×10^{8}	1.83×10^{7}
Pu-239	4.38×10^{9}	1.91×10^{9}	6.00×10^{7}	1.48×10^{8}	2.96×10^{6}
Pu-240	8.76×10^{9}	3.81×10^{9}	1.20×10^{8}	2.96×10^{8}	5.96×10^{6}
Pu-241	7.15×10^{11}	1.83×10^{11}	7.82×10^{8}	2.08×10^{10}	3.31×10^{8}
Pu-242	3.94×10^{7}	1.72×10^{7}	9.64×10^{4}	1.33×10^{6}	1.84×10^{4}
Tc-99	1.40×10^{10}	5.14×10^{9}	1.78×10^{8}	6.31×10^{8}	1.97×10^{7}
Se-79	5.09×10^{8}	1.75×10^{8}	1.35×10^{6}	1.95×10^{7}	3.10×10^{5}

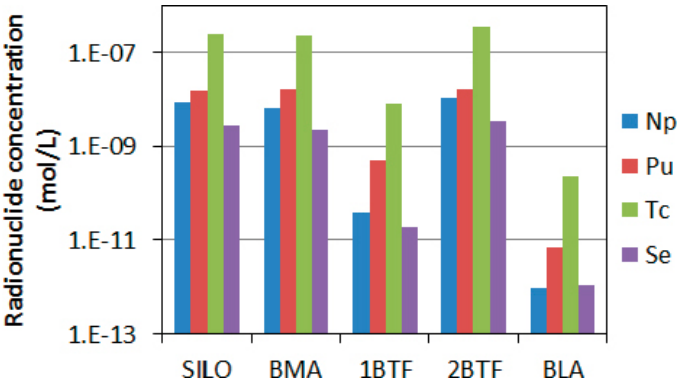

Figure 9-1. *Calculated concentrations of Np, Pu, Tc and Se resulting from dissolving the complete inventory in the saturated void volume.*

9.1 Neptunium

The predominance Eh/pH diagrams of Neptunium are shown in Figure 9-2 and 9-3. It is clear that the most stable solid phase under the conditions of the assessment is the tetravalent $NpO_2 \cdot 2H_2O(am)$ whose precipitation occurs at concentrations above 10^{-9} M in the absence of organic ligands.

Figure 9-3 shows the underlying aqueous speciation of Np.

As shown in Figure 9-4 the effect of acetate on the Np solubility is negligible at the acetate concentrations calculated in the SFR 1.

The speciation of Np in the presence of $1.6 \cdot 10^{-2}$ M of ISA is dominated by ISA species (see Figure 9-5).

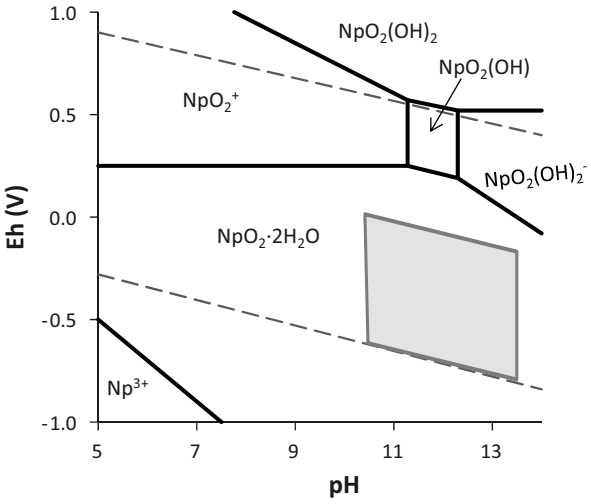

Figure 9-2. *Predominance diagram of Np at a total concentration of 10 nM. The precipitation of $NpO_2 \cdot 2H_2O(am)$ is favoured under the conditions developed in the redox model. $[S(VI)]_T = 2 \cdot 10^{-5}$ M; $[C(IV)]_T = 1 \cdot 10^{-6}$ M; $[ISA]_T = 0.0$; $[acetate]_T = 0.0$. The shadowed square indicates the range of Eh and pH calculated in Table 8-1.*

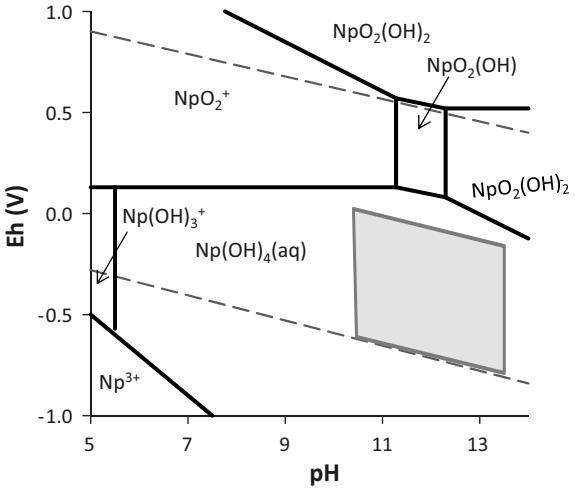

Figure 9-3. *The same diagram than Figure 9-2, but showing only the species present in solution. $Np(OH)_4(aq)$ dominates the speciation under the conditions of the assessment. $[S(VI)]_T = 2 \cdot 10^{-5}$ M; $[C(IV)]_T = 1 \cdot 10^{-6}$ M; $[ISA]_T = 0.0$; $[acetate]_T = 0.0$. The shadowed square indicates the range of Eh and pH calculated in Table 8-1.*

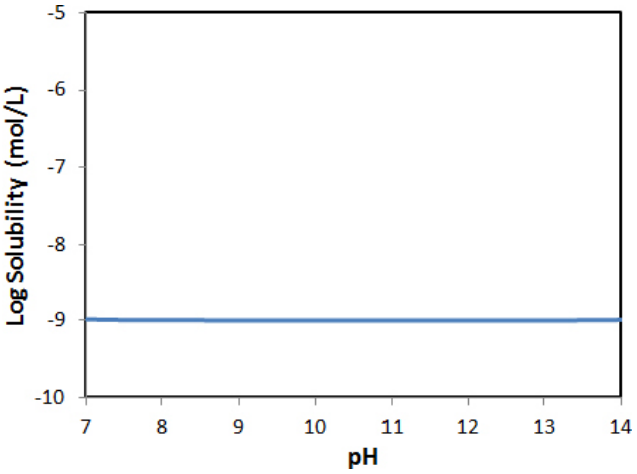

Figure 9-4. *Effect of 0.1 M of acetate on the solubility of $NpO_2 \cdot 2H_2O(am)$ at different pH values.*

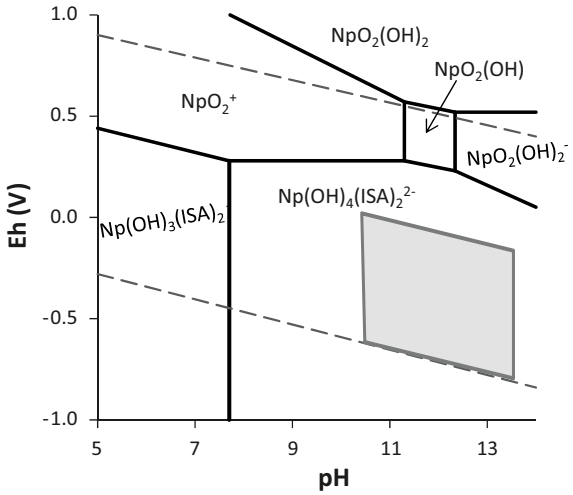

Figure 9-5. *Predominace diagram of Np showing the effect that $1.6 \cdot 10^{-2}$ M of ISA will have on the speciation of this element. $[S(VI)]_T = 2 \cdot 10^{-5}$ M; $[C(IV)]_T = 1 \cdot 10^{-6}$ M; [acetate]$_T$=0.0. The shadowed square indicates the range of Eh and pH calculated in Table 8-1.*

The effect that this complexing agent has on the solubility of $NpO_2 \cdot 2H_2O$ at pH = 12.5 and reducing Eh value is shown in Figure 9-6, where an important increase in the solubility is calculated when increasing the concentration of ISA. In the SFR 1 system this solubility increase is buffered by the presence of Calcium. In the same Figure 9-6 it is shown that, when allowing the system to be equilibrium with portlandite, the concentration of Ca in solution is sufficiently high as to favour the precipitation of Calcium isosacharinate and, therefore, limit the concentration of ISA in solution available for Np complexation. The fraction of ISA taken up by the precipitation of $Ca(ISA)_2(cr)$ is shown in Figure 9-7.

Under the range of conditions presented in Table 8-1, the most likely solubility limiting phase for Np is $NpO_2 \cdot 2H_2O$ (s). The calculated solubility for all the conditions of interest is shown in Table 9-2. In these calculations no ISA has been considered.

The comparison between the calculated solubilities in Table 9-2 and the concentrations of Np resulting from dissolving all the inventory in the total volume of water of the voids, as in Figure 9-1 is shown in Figure 9-8.

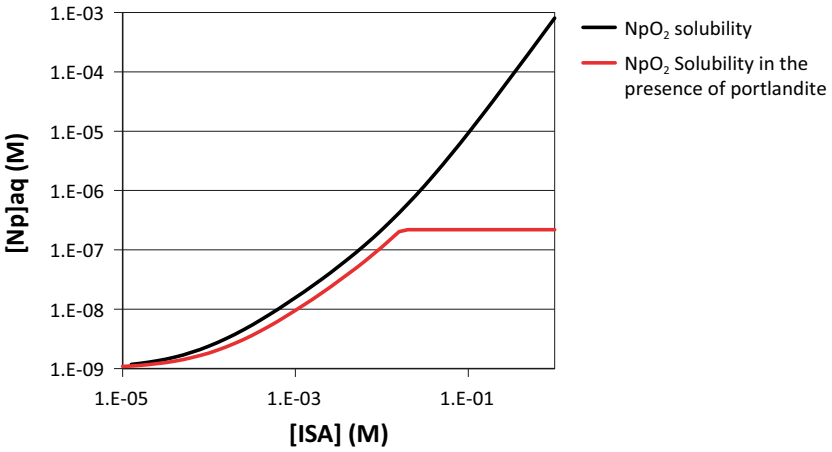

Figure 9-6. Effect of ISA on the solubility of $NpO_2 \cdot 2H_2O(am)$ at pH 12.5 and reducing Eh. A strong influence is observed, in agreement with the previously calculated speciation. When allowing portlandite in the system the precipitation of $Ca(ISA)_2(cr)$ limits the solubility of Np to $2.2 \cdot 10^{-7}$ M due to the limitation of the ISA concentration to $1.7 \cdot 10^{-2}$ M.

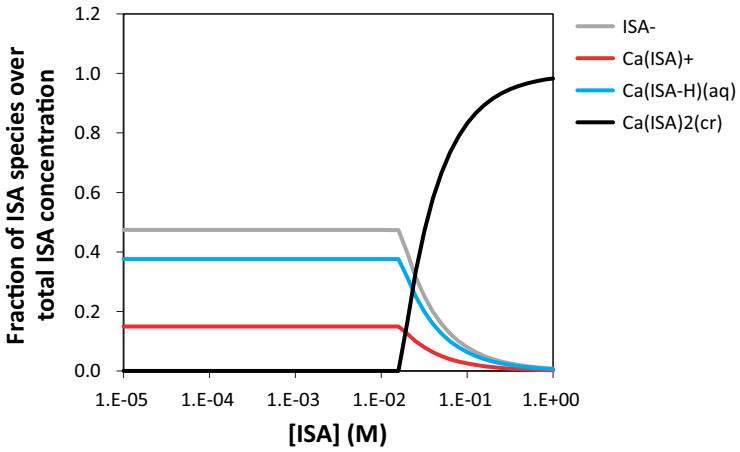

Figure 9-7. Fractional diagram showing the precipitation of Calcium isosaccarinate under the conditions of the assessment. Equilibrium with portlandite is assumed. $[ISA]_{tot} = 1.6 \cdot 10^{-2}$ M. pH = 12.5 and reducing Eh.

Table 9-2. Concentrations of Np in equilibrium with $NpO_2 \cdot 2H_2O$ (s) under the conditions of pH and Eh presented in Table 8-1.

Redox couple controlling Eh				
pH	**H_2O/H_2**	**Fe_3O_4/Fe_2O_3**	**Fe_3O_4/FeOOH**	**Fe_3O_4/HFO**
13.5	9.76×10^{-10}	5.62×10^{-8}	9.76×10^{-10}	1.00×10^{-9}
12.5	9.76×10^{-10}	9.76×10^{-10}	9.76×10^{-10}	9.81×10^{-10}
10.5	9.76×10^{-10}	9.76×10^{-10}	9.76×10^{-10}	9.86×10^{-10}
5.4*	4.33×10^{-9}	2.22×10^{-9}	2.27×10^{-9}	2.91×10^{-9}

* Conditions of the O.12 waste package.

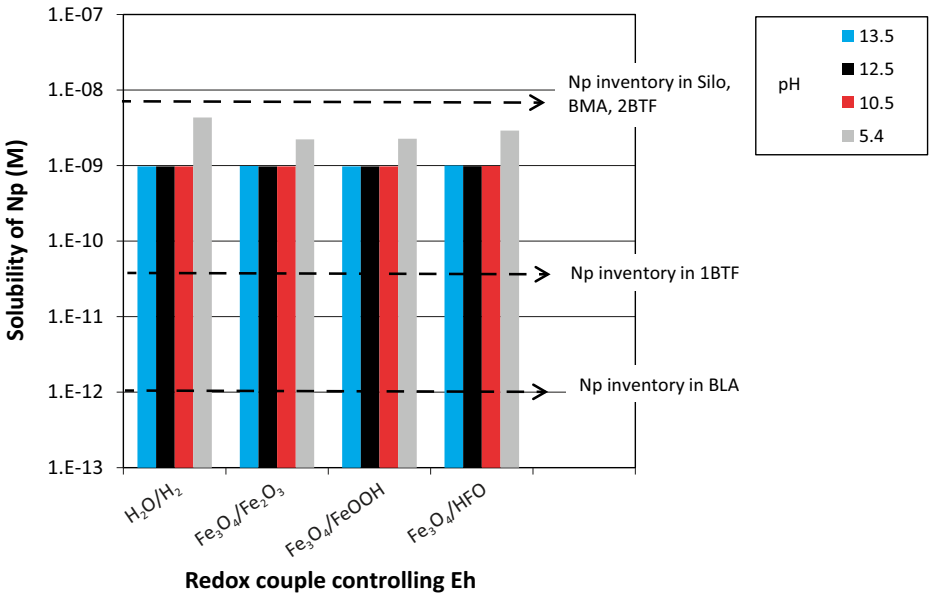

Figure 9-8. *Comparison between the dissolved inventory of Np (dashed arrows) and the solubility of Np shown in Table 9-2.*

As shown in Figure 9-8, the inventory of Np in 1 BTF and in BLA is below the solubility limit of Np under all the conditions of the assessment, what means that the most relevant retention processes in these cases will not be precipitation of secondary phases but sorption onto the surface of the major solid phases present in the system, presumably cement and its degradation products as well as iron oxides. The previous figure does not include the effect of complexing agents, what will result in an increase of the calculated solubility, thus decreasing the relevance of precipitation processes in Np retardation. In the case of the Silo, BMA and 2 BTF, the inventory of Np is slightly abover the calculated solubility of Np, thus setting the control of the Np concentration to values about 10^{-9} moles/L given by the solubility of Np(IV) oxides.

9.2 Plutonium

The behaviour of Plutonium is similar to that of Neptunium at the very alkaline and reducing conditions. Pu(IV) and Pu(III) species dominate the speciation and the precipitation of $PuO_2 \cdot 2H_2O$(am) is favoured under the conditions of the assessment (Figure 9-9).

Acetate complexes are only relevant in the case of being at pH below 9.5 and in the absence of calcium (Figure 9-10).

The effect of ISA on the solubility of Pu is shown Figure 9-11. As in the case of Np, when the system is left to equilibrate with portlandite, the precipitation of calcium isossacharinate limits the concentration of ISA available for the complexation with Pu and the solubility of Pu reaches a maximum corresponding to the maximum concentration of ISA in equilibrium with $Ca(ISA)_2$(cr).

Under the range of conditions presented in Table 8-1, the solubility limiting phases for Pu and the calculated solubility for all the conditions of interest are shown in Table 9-2. In these calculations no ISA has been considered.

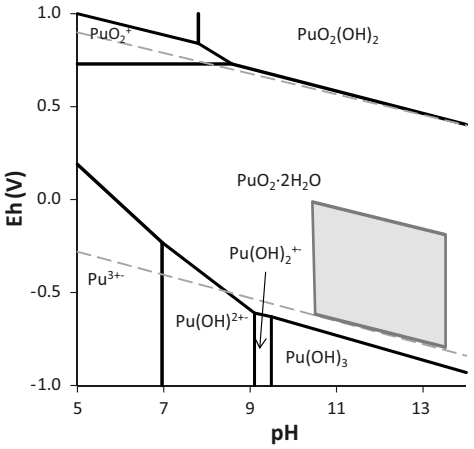

Figure 9-9. *Predominance diagram of Pu at a total concentration of 10 nM. The precipitation of $PuO_2{\cdot}2H_2O$(am) is favoured under the conditions developed in the redox model. $[S(VI)]_T = 1{\cdot}10^{-4}$ M; $[C(IV)]_T = 6{\cdot}10^{-6}$ M; $[ISA]_T = 0.0$; $[acetate]_T = 0.0$. The shadowed square indicates the range of Eh and pH calculated in Table 8-1.*

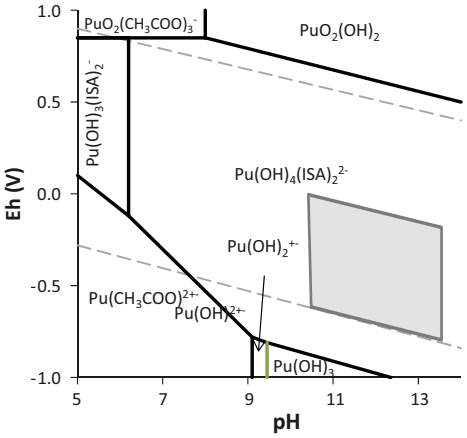

Figure 9-10. *Predominance diagram of aqueous species of Pu showing the dominance of Pu(III) acetate and Pu(IV) ISA species. $[S(VI)]_T = 1{\cdot}10^{-4}$ M; $[C(IV)]_T = 6{\cdot}10^{-6}$ M; $[ISA]_T = 0.0$; $[acetate]_T = 0.1$ M. The shadowed square indicates the range of Eh and pH calculated in Table 8-1.*

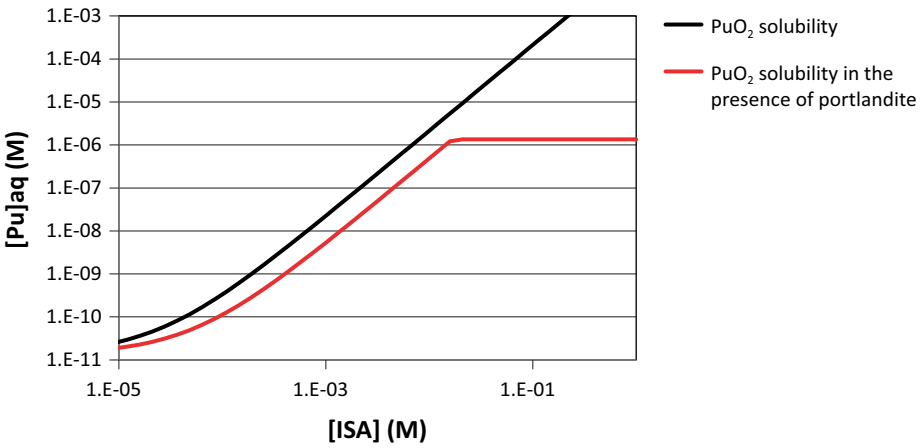

Figure 9-11. *Effect of ISA on the solubility of $PuO_2{\cdot}2H_2O$(am) at pH 12.5 and reducing Eh. A strong influence is observed, in agreement with the previously calculated speciation. When allowing portlandite in the system the precipitation of $Ca(ISA)_2$(cr) limits the solubility of Pu to $1.3{\cdot}10^{-6}$ M due to the limitation of the ISA concentration to $1.7{\cdot}10^{-2}$ M.*

Table 9-3. Concentrations of Pu in equilibrium with limiting solid phases (indicated) under the conditions of pH and Eh presented in Table 8-1.

	Redox couple controlling Eh			
pH	H_2O/H_2	Fe_3O_4/Fe_2O_3	Fe_3O_4/FeOOH	Fe_3O_4/HFO
13.5	3.38×10^{-10}	4.89×10^{-10}	5.68×10^{-10}	4.89×10^{-10}
12.5	3.37×10^{-10}	6.77×10^{-10}	5.72×10^{-10}	4.89×10^{-10}
10.5	3.60×10^{-10}	7.12×10^{-10}	5.87×10^{-10}	4.89×10^{-10}
5.4*	NSL	2.23×10^{-4}	2.52×10^{-5}	2.00×10^{-6}

*Conditions of the O.12 waste package. Shadowed rows indicate solubility limiting phase $PuO_2\cdot2H_2O$. Non shadowed cells indicate solubility controlled by $Pu(OH)_3$(s). NSL stands for no solubility limited.

As in the case of Np, the comparison with the complete dissolution of the inventory has been conducted (see Figure 9-12).

The previous comparison shows that the inventory is definitively over the calculated solubility limits for the Silo, BMA and 2 BTF vaults, while for the BTF and the BLA the most relevant retention processes are not likely to be precipitation of solid phases of the radionuclides. This is especially remarkable in the case of BLA, presenting the highest calculated solubility (pH = 5.4) and the lowest inventory of Pu. If not considering the effect of organics in the vaults, the maximum concentration of Pu in the Silo, BMA and 2 BTF can be limited to values around 10^{-9} M due to the precipitation of Pu(IV) oxides under the conditions of pH and Eh covered by this assessment. Nevertheless, as seen in Figure 9-11, the solubility of Pu in the presence of ISA would be increased to values around 10^{-6} M, thus the concentration of Pu in solution will be controlled either by the inventory or by sorption processes also in the case of the Silo, BMA and 2 BTF vaults.

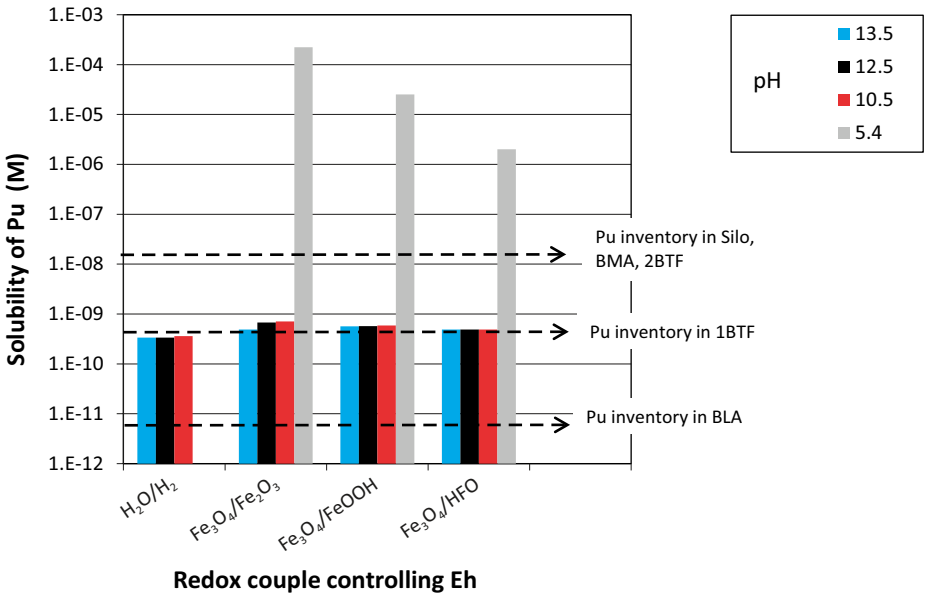

Figure 9-12. *Comparison between the dissolved inventory of Pu (dashed arrows) and the solubility of Pu shown in Table 9-3.*

9.3 Selenium

Se speciation is dominated by Se(-II) species, mainly HSe^- in the reducing part of the domain. The most favoured solid phase to be formed under the conditions of the assessment is Se(cr), if the concentrations of Se are high enough, which is a bit limited by the inventory of Se in the SFR 1, as will be discussed later (see Figure 9-13).

Depending on the concentration of Fe present in the system, Fe(II) selenides can form, reducing the mobility of Se. According to the available thermodynamic data, the precipitation of these phases will require concentrations of Fe in solution higher than the ones calculated to be present in the system. By keeping the concentration of Fe in solution to 10^{-7} M, we obtain the predominance diagram shown in Figure 9-14 where the precipitation of the different iron selenides is appreciated.

No direct influence of acetate or ISA is expected in the speciation of anionic Se species. In principle, for the low concentrations of Se calculated from the inventory it is very likely that under reducing conditions the main process accounting for its retardation is sorption and not precipitation. In the higher field of redox values, if the system is considered to be controlled by the magnetite/ferrihydrite redox couple (shadowed square in Figure 9-13) the dominant species is the oxidised selenite, which is more mobile than the reduced species (HSe^-) given that it does not form solid iron selenides.

In the presence of high concentrations of Ca, as it is the case of the conditions when equilibrated with portlandite, and under oxidising conditions, the solid phase $CaSeO_3$(s) can form.

Solubility calculations have been done for all the conditions in Table 8-1, as for the rest of radionuclides. The results and the limiting solid phase are shown in Table 9-4.

Table 9-4. Concentrations of Se in equilibrium with limiting solid phases under the conditions of pH and Eh presented in Table 8-1. (1): solid phase: $Fe_{1.04}Se$; (2) solid phase: $FeSe_2$; (3) solid phase: Se(cr); NSL stands for no solubility limited.

	Redox couple controlling Eh			
pH	H_2O/H_2	Fe_3O_4/Fe_2O_3	Fe_3O_4/FeOOH	Fe_3O_4/HFO
13.5	1.55×10^{-5}(1)	1.32×10^{-3}(2)	1.39×10^{-3}(2)	NSL
12.5	2.84×10^{-7}(1)	1.37×10^{-4}(2)	1.10×10^{-4}(2)	NSL
10.5	1.72×10^{-7}(1)	5.69×10^{-6}(2)	3.26×10^{-6}(2)	NSL
5.4*	1.37×10^{-7}(2)	2.00×10^{-14}(3)	3.00×10^{-16}(3)	3.00×10^{-16}(3)

* Conditions of the O.12 waste package. NSL stands for no solubility limited.

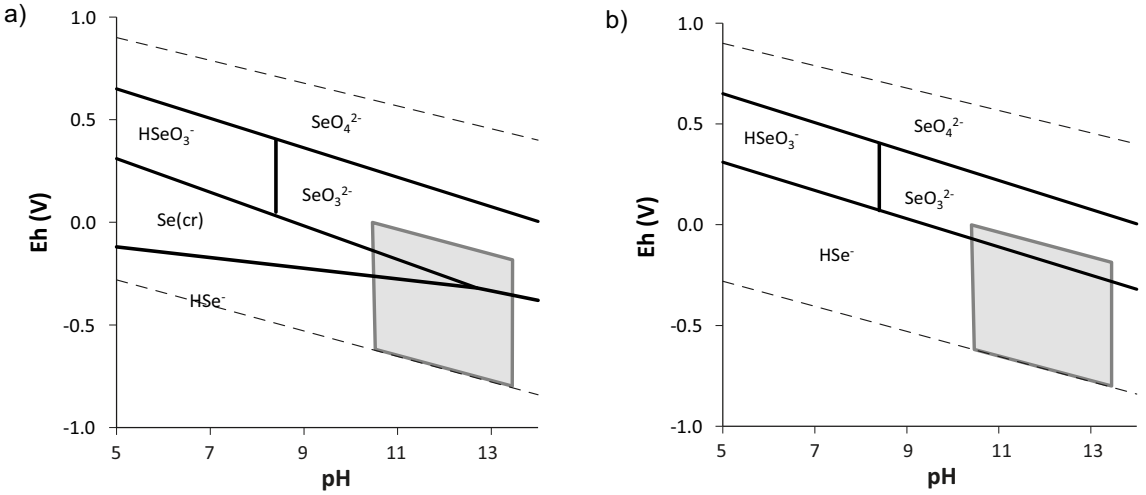

Figure 9-13. *Predominance diagram of Se (10^{-8} M) in the presence of 10^{-5} M of Fe under the conditions of the assessment. The shadowed square indicates the range of Eh and pH calculated in Table 8-1. Diagram b) shows only aqueous species.*

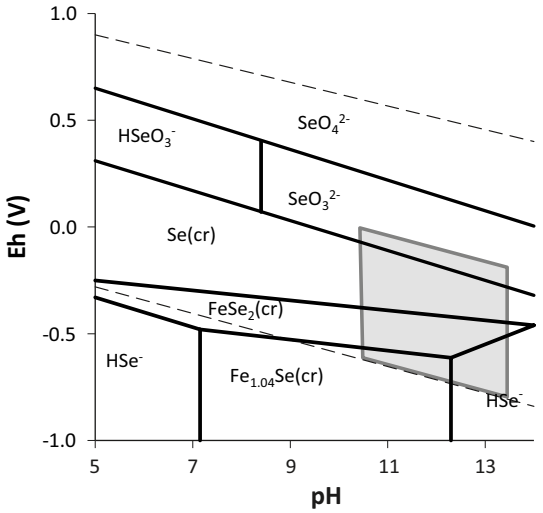

Figure 9-14. *Predominance diagram of Se calculated for a concentration of Fe in solution of 10^{-7} M and a total concentration of Se of 10^{-4} M, to see the formation of Fe selenides.*

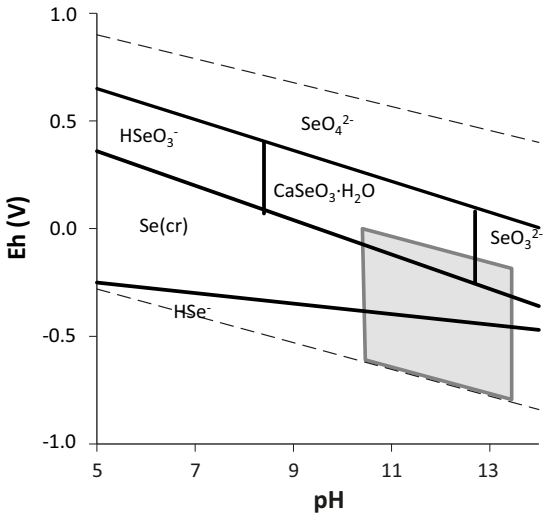

Figure 9-15. *Predominance diagram of Se calculated with a concentration of Ca of 0.01 M and a concentration of Se of 0.01 M to see the precipitation of Calcium Selenite.*

The comparison with the complete dissolution of the inventory has been conducted (see Figure 9-18).

From the previous figure it is clear that the calculated solubility is higher than the complete dissolution of the inventory in all cases except for the BLA, presenting a lower pH, in which case the formation of metallic Se could account for a more effective retardation mechanism than for the other vaults.

In most cases, the most likely retention mechanism for Se is not expected to be precipitation, but interaction with solid surfaces of the system.

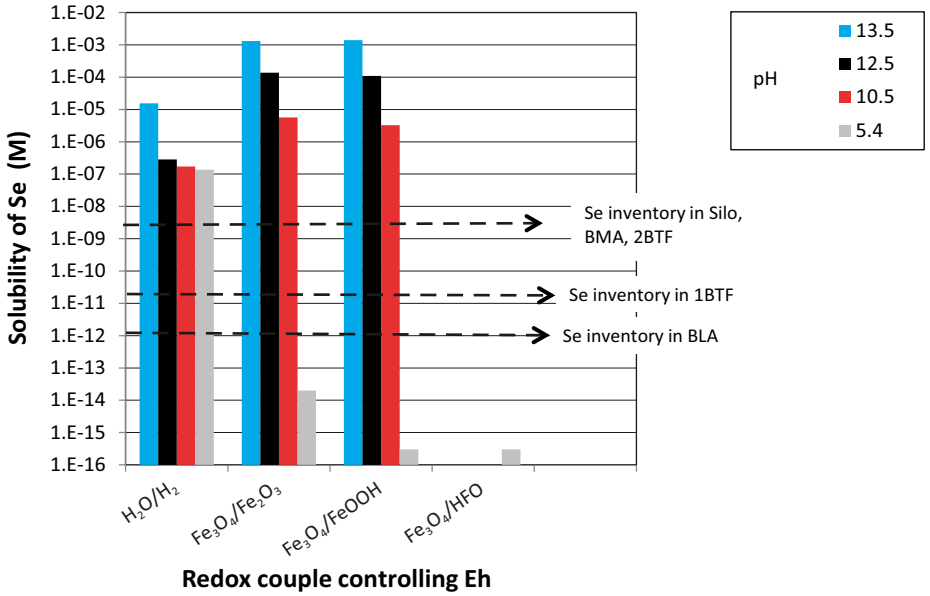

Figure 9-16. *Comparison between the dissolved inventory of Se (dashed arrows) and the solubility of Se shown in Table 9-4. Not solubility limited cases are not shown. Concentrations of Fe have been assumed in equilibrium with magnetite in all cases except for the case at pH = 5.4, where equilibrium with siderite has been assumed to calculate Fe concentration in solution.*

9.4 Technetium

As in the case of Se, no influence of ISA or acetate is observed in the chemical behaviour of Tc under the conditions of interest.

The predominance diagrams are shown in Figure 9-17a and b, from where it is seen that the precipitation of $TcO \cdot 1.63H_2O$ (s) can occur under reducing conditions, while under oxidising conditions Tc is maily soluble as Tc(VII), forming the oxyanion pertechnetate (TcO_4^-). Under reducing conditions the main aqueus species are $TcO(OH)_2(aq)$ and $TcO(OH)_3^-$.

Under the range of conditions presented in Table 8-1, the solubility limiting phases for Tc and the calculated solubility for all the conditions of interest are shown in Table 9-5.

The comparison with the complete dissolution of the inventory has been conducted (see Figure 9-18)

The previous comparison shows that the the inventory in BLA is definitively below the calculated solubility limits in all cases, thus implying that Tc will not be solubility limited in this vault. In the case of 1 BTF, the inventory is either below of very close to the solubility limit ($6.7 \cdot 10^{-9}$ M), indicating that solubility will neither be an important retardation process for Tc in this vault.

Regarding the Silo, BMA and 2 BTF vaults, the calculated solubility is below the inventory only in the case of pH = 10.5, that is when concrete has been degraded to CSH. This would also point towards other retardation processes, such as sorption on the surface of cement degradation phases or iron corrosion products, as mainly contributing to the retention of Tc in the system.

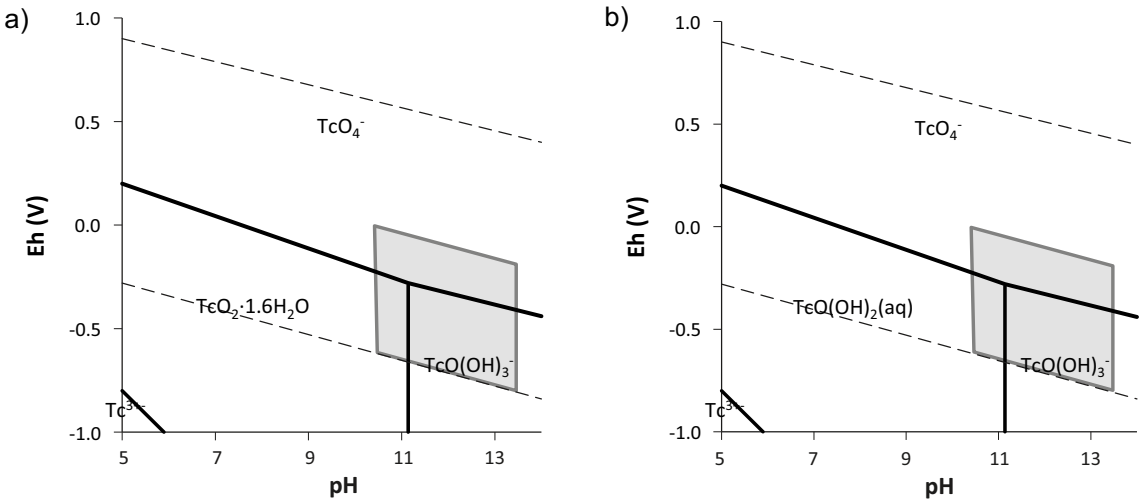

Figure 9-17. *Predominance diagram of Tc under the conditions of the assessment. A total concentration of Tc of 10^{-8} M has been used to calculate the diagram. In b) only aqueous species are shown. The shadowed square indicates the range of Eh and pH calculated in Table 8-1.*

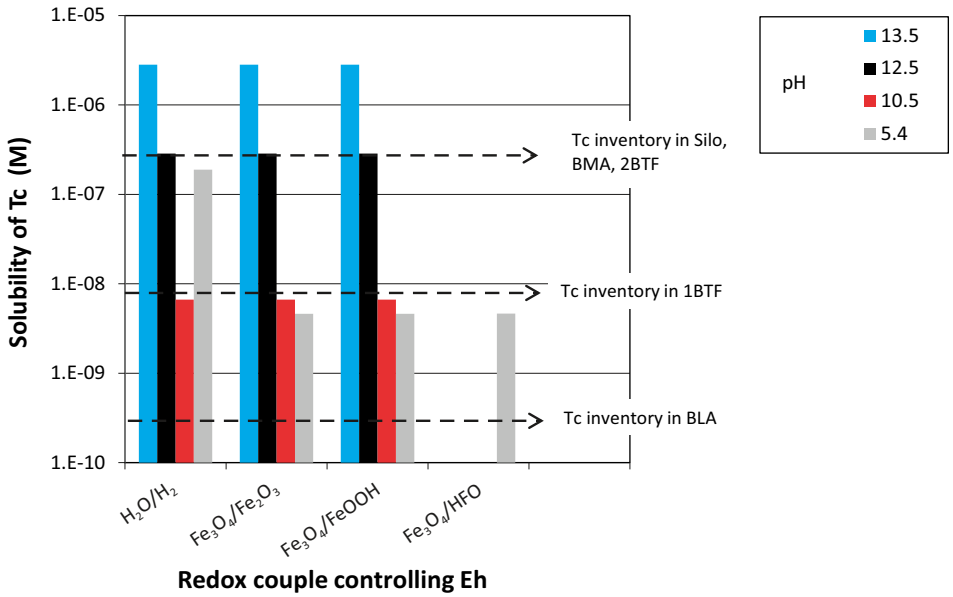

Figure 9-18. *Comparison between the dissolved inventory of Tc (dashed arrows) and the solubility of Tc shown in Table 9-5. Not solubility limited cases are not shown.*

Table 9-5. Concentrations of Tc in equilibrium with limiting solid phases ($TcO_2 \cdot 1.63H_2O$) under the conditions of pH and Eh presented in Table 8-1.

	Redox couple controlling Eh			
pH	**H_2O/H_2**	**Fe_3O_4/Fe_2O_3**	**Fe_3O_4/FeOOH**	**Fe_3O_4/HFO**
13.5	2.83×10^{-6}	2.83×10^{-6}	2.83×10^{-6}	NSL
12.5	2.86×10^{-7}	2.86×10^{-7}	2.86×10^{-7}	NSL
10.5	6.65×10^{-9}	6.65×10^{-9}	6.65×10^{-9}	NSL
5.4*	1.89×10^{-7}	4.62×10^{-9}	4.62×10^{-9}	4.64×10^{-9}

* Conditions of the O.12 waste package. NSL stands for no solubility limited.

10 Discussion and Conclusions

From the analyses presented the following conclusions are obtained:

- After repository closure, the reducing capacity is initially provided by the organic matter content and by the steel and its corrosion products.
- The duration of the oxic period is very short in all waste package types, in the order of days if organic matter degradation is credited and less than 1 year if steel corrosion is the only process accounting for oxygen depletion.
- The redox conditions imposed for all waste package types except O.12 in the long term indicate Eh values around –750 mV, corresponding to the hydrogen generation due to water reduction on steel under cementitious conditions. In case of O.12 waste package type, Eh value is around –0.34 V, given that pH is not controlled by cementitious phases. Corrosion of steel proceeds at expenses of water consumption once the initial oxygen is depleted. Under the expected repository flow conditions, water availability does not seem to be the limiting factor.
- According to the assessment, after 100 ky, the amount of magnetite present in the vaults and the remaining steel provide a good reducing capacity to buffer oxidant intrusions, although in some waste package types bitumen or organic matter can also contribute to the reducing capacity (B.06, F.05, F.18, F.17, F.23, O.23, B.05, O.12).
- Acetate is produced due to the processes of degradation of organic matter, bitumen and cellulose. During the prevalence of microbial activity acetate is degraded to CO_2. The maximum concentration of acetate accumulated in the system never exceeds 0.5 moles/L.
- ISA is generated through degradation of cellulosic materials under cementitious conditions. Maximum concentrations of ISA built up in the system are in the order of $1.6 \cdot 10^{-2}$ moles/L. This gives an indication of the range of concentrations to be included in the assessment of the influence of organic materials on radionuclide aqueous concentration.
- In the model, the formation of gas is allowed when the total gas pressure exceeds the hydrostatic load, which is estimated in 6.87 atm. The main gas generated is hydrogen. The volumes of gases produced in each of the vaults after 100 ky are shown in Figure 10-1. In order to compare with previous assessments the volumes have been calculated back to standard conditions. The volumes are lower than the ones obtained in the SAR-08 by Moreno et al. (2001) mainly due to the different corrosion rates used in both studies. In all cases hydrogen is the main component of the gaseous phase.

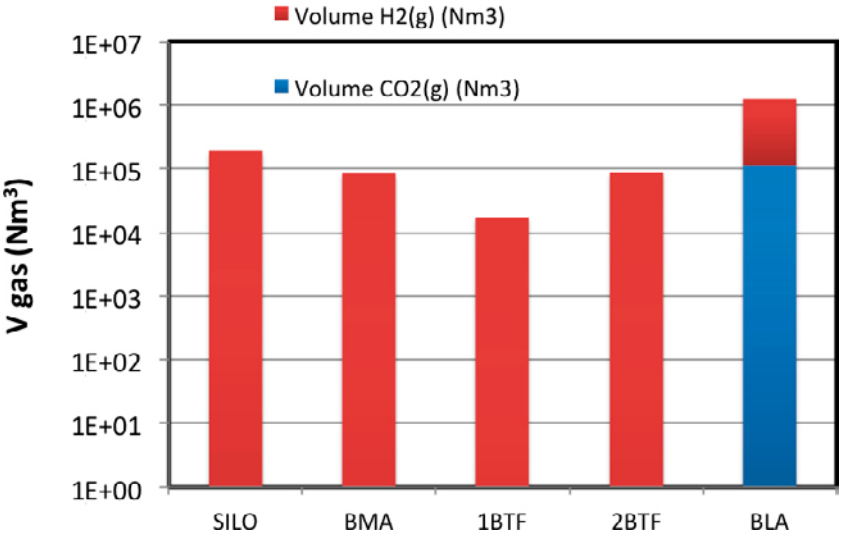

Figure 10-1. *Volume of gas generated in the vaults after 100 ky (calculated at Standard conditions of P and T).*

- The reducing capacity of the system is kept stable once all steel has been corroded, if there is not an intrusion of oxygen rich porewater.
- To test the ability of the system to buffer an oxidant intrusion, meltwater intrusion has been assumed after 60 ky of the closure. This is also the time at which all steel has been corroded in the repository; therefore the reducing capacity is given by magnetite. Magnetite is able to buffer the continuous supply of oxidising water during more than 40 ky through its oxidation to Fe(III) oxides, thus protecting the system from oxidation. The study of the behaviour of the radionuclides has been conducted assuming the concentration of the radionuclides provided by the complete inventory of the repository and the chemical conditions resulting from the modelling of the Eh behaviour.
- In 1 BTF and BLA vaults, the inventory of Np is below the solubility limit of Np under all the conditions of the assessment, what means that the most relevant retention processes will be sorption onto the surface of the major solid phases present in the system (cement and its degradation products as well as iron oxides). In the case of the Silo, BMA and 2 BTF, the Np concentration will be set to values about 10^{-9} moles/L given by the solubility of $NpO_2 \cdot 2H_2O$(am). The effect of acetate on the Np solubility is negligible at the acetate concentrations calculated to develop in the SFR 1. This is not the case of ISA, that causes an increase in the solubility of $NpO_2 \cdot 2H_2O$(am), although this effect is buffered by the precipitation of calcium isosacharinate.
- In 1 BTF and BLA the inventory of Pu is below the solubility limit of Pu under all the conditions of the assessment, what means, that the most relevant retention processes are not likely to be precipitation of solid phases**.** In the case of Silo, BMA and 2 BTF vaults, the inventory of Pu is over the calculated solubility limits of $PuO_2 \cdot 2H_2O$(am), that is the solid phase favoured under the conditions of the assessment. Under these conditions and if the effect of organics is not considered, Pu concentration is limited to values around 10^{-9} M. As for Np, the effect of acetate is negligible and the precipitation of calcium isossacharinate reduces the concentration of ISA available for the complexation with Pu limiting the increase of Pu solubility.
- In all cases except for BLA, the inventory of Se is below the solubility of the solid phase most likely to form under the corresponding conditions. This means that the most likely retention mechanism for Se is its interaction with solid surfaces of the system. In BLA the formation of metallic Se could account for a more effective retardation mechanism than for the other vaults. No direct influence of acetate or ISA is expected on the behaviour of Se.
- In the case of BLA and 1 BTF the inventory of Tc is below or very close to the solubility limit of $TcO \cdot 1.63H_2O$ (s), the solid phase likely to be formed. This is also expected to occur in the Silo, BMA and 2 BTF vaults, when concrete has been degraded to CSH (pH = 10.5). In all these cases, the processes most contributing to the retention of Tc in the system will be the sorption on the surface of cement degradation phases or iron corrosion products. $TcO \cdot 1.63H_2O$ (s) solubility ($6.7 \cdot 10^{-9}$ M) will limit Tc concentration in the other cases. As in the case of Se, no influence of ISA or acetate is observed in the chemical behaviour of Tc under the conditions of interest.

According the previous discussions, it seems that the likelihood of the system to oxidise is very low. Nevertheless both the conceptual and the numerical model developed have relevant uncertainties that must be considered. In order to systematize the uncertainties, a discussion on the likely impact that they will have on the conclusions follows.

Organic matter, bitumen and cellulose

Assumption: Organic matter has been considered to degrade under biotic conditions and form acetate, which in turn is degraded into CO_2 (g) only during the oxic period. The same processes have been considered for the degradation of bitumen and cellulose during the initial oxic period. Once the only oxidant present in the system is water bitumen and organic matter (except cellulose) is assumed to degrade according to a constant rate. Under anoxic and alkaline conditions cellulose is assumed to degrade according to the kinetic rate law provided by Glaus and Van Loon (2008).

Implementation in the model and uncertainties: The degradation occurring during the biotic period has been implemented by defining a series of Monod-like equations, whose parameter values have been selected from literature, and obviously contain some degree of uncertainty.

The uncertainty in these parameters is however not expected to largely affect the results because of the short-term impact that the degradation of organic materials will have in the overall redox behaviour of the repository.

The degradation in the long-term is assumed constant and for all organic materials (except cellulose) the degradation rate of bitumen has been used (from Wolf and Bachofen 1991). This hypothesis presents a high degree of uncertainty and for this reason the assessment of the RDC of the system has additionally been done by neglecting the capacity attributed to bitumen to keep the system under reducing conditions.

The uncertainty on the kinetic rate on cellulose degradation is mainly due to the type of cellulose considered to be present in the repository because rate law parameters depend on it. In this case, the type having the slower degradation has been chosen. A higher cellulose degradation rate will cause a higher ISA concentration.

The uncertainty on the concentration of acetate calculated to accumulate in the system will not importantly affect the behaviour of radionuclides, as shown by the speciation calculations. The increase of the concentration of ISA will affect the solubility of radionuclides but only to some extent given that even in the case of being produced in high amounts, the precipitation of the calcium salts in the presence of cementitious materials will keep their concentrations controlled at levels close to 0.016 M. This would imply solubility enhancement of Pu and Np in the order of 2 log units.

Steel

Assumption: Steel corrodes under oxic conditions to form goethite and once water is the only oxidant in the system, magnetite is allowed to form with the production of hydrogen from water. The corrosion rate of steel under anoxic conditions has been considered constant.

Implementation in the model and uncertainties: The rate of corrosion of steel in the literature, under the conditions likely to be found in the SFR 1, spans over 4 orders of magnitude. The probabilistic analyses conducted on the rate of steel corrosion indicate that under disturbed conditions the remaining reducing capacity of the system after 100 ky is provided by magnetite and, therefore, this uncertainty will not, a priori, have a large effect on the capacity of the system to buffer an oxidant intrusion. Its main impact will be on the time at which the steel is completely corroded and therefore, the time at which all RDC is provided by magnetite.

Other metals

Assumption: other metallic components, such as Al and Zn have not been credited as providing reductive capacity to the system.

Implementation in the model and uncertainties: Although this assumption can be considered pessimistic from the perspective that the system is attributed a lower reducing capacity that the actual one, the non-pessimistic implication is that the generation of hydrogen due to the corrosion of these metals by water is not considered. This fact is not expected to jeopardize the stability of the repository given that the oxidation of these metals during the oxic period is faster and, therefore, their contribution to the generation of hydrogen is not expected to be very relevant.

Concrete degradation

Assumption: Portlandite is the proxy considered for concrete in the model.

Implementation in the model and uncertainties: All waters of the waste package types containing concrete either as waste package material or as immobilisation matrix have been considered to equilibrate with portlandite. This has different effects: on the one hand the pH is buffered to 12.5 in all cases, and on another hand no degradation of the cementitious materials is considered. The buffering of the pH to 12.5 has implications on the redox potential of the system. The Eh of the system is for most of the period controlled by water reduction and H_2 (g) generation. The degradation of concrete and, therefore, the decrease of the pH of the system due to the formation of different CSH will buffer

the pH at lower values and therefore may result in higher redox potentials of the system. In any case, even by considering that the pH imposed by the degradation of concrete in the wastes reaches values as low as 10.5, the redox potential would be below –500 mV, thereof very reducing conditions would be also expected. If, as previously discussed, the system controlling the redox potential is that of magnetite and its possible oxidation products the Eh would vary in the range shown in Figure 8-4.

One of the uncertainties imposed by neglecting concrete degradation is that the hydrodynamics of the system are not considered to change in the time frame of the assessment. The impact that this simplification would have is thought to be minimum, given that transport will be mainly diffusion-controlled.

Oxidant intrusion

Assumption: the oxidant intrusion variant occurs after 60 ky of the repository closure.

Implementation in the model and uncertainties: A continuous ingress of water equilibrated with atmospheric oxygen is considered. The role of the fracture materials and the soils in consuming the oxidants in the infiltrating water has not been considered. It is also very unlikely that the melt water occurs continuously for 40 ky (from 60 ky after the closure until the 100 ky of the time frame of the assessment).

References

SKB's (Svensk Kärnbränslehantering AB) publications can be found at www.skb.se/publications. References to SKB's unpublished documents are listed separately at the end of the reference list. Unpublished documents will be submitted upon request to document@skb.se.

Almkvist L, Gordon A, 2007. Low and intermediate level waste in SFR 1. Reference waste inventory 2007. SKB R-07-17, Svensk Kärnbränslehantering AB.

Appelo C A J, Postma D, 2005. Geochemistry, groundwater and pollution. 2nd ed. Leiden: Balkema.

Askarieh M M, Chambers A V, Daniel F B D, FitzGerald P L, Holtom G J, Pilkington N J, Rees J H, 2000. The chemical and microbial degradation of cellulose in the near field of a repository for radioactive wastes. Waste Management 20, 93–106.

Blackwood D J, Gould L J, Naish C C, Porter F M, Rance A P, Sharland S M, Smart N R, Thomas M I, Yates T, 2002. The localised corrosion of carbon steel and stainless steel in simulated repository environments. Report AEAT/ERRA-0318, AEA Technology.

Broczkowski M E, 2008. The effects of hydrogen and temperature on the electrochemistry and corrosion of uranium dioxide. PhD thesis. The University of Western Ontario, London, Ontario.

Brush L H, 1990. Test plan for laboratory and modelling studies of repostitory and radionuclide chemistry for the waste isolation pilot plant. SAND90-0266, Sandia National Laboratories, New Mexico.

Brush L H, 1995. Systems prioritization method iteration 2, baseline position paper: gas generation in the waste isolation pilot plant. Sandia National Laboratories, Albuquerque, NM.

Byrum C O, 2006. Preliminary review of the degradation of cellulosic, plastic and rubber materials in the waste isolation pilot plant, and possible effects on magnesium oxide safety factor calculations. Contract n° EP-D-05-002. Washington, DC: U.S. Environmental Protection Agency. Available at: http://www.epa.gov/rpdweb00/docs/wipp/epa_mgo_report_91107.pdf

Chambers A V, Williams S J, Wisbey S J, 1995. Nirex safety assessment research programme. Nirex near field research: report on the current status in 1994. Nirex Science Report S/95/011, UK Nirex Ltd.

Claret F, Schäfer T, Bauer A, Buckau G, 2003. Generation of humic and fulvic acid from Callovo-Oxfordian clay under high alkaline conditions. The Science of the Total Environment 317, 189–200.

De Robertis A, Di Giacomo P, Foti C, 1995. Ion-selective electrode measurements for the determination of formation constants of alkali and alkaline earth metals with low-molecular-weight ligands. Analytica Chimica Acta 300, 45–51.

Duro L, Grivé M, Cera E, Domènech C, Bruno J, 2006. Update of a thermodynamic database for radionuclides to assist solubility limits calculation for performance assessment. SKB TR-06-17, Svensk Kärnbränslehantering AB.

Duro L, Grivé M, Giffaut E, 2010. ThermoChimie, the ANDRA thermodynamic database. In Buckau G, Kienzler B, Duro L, Grivé M, Montoya V (eds). 2nd annual workshop proceedings of the Collaborative Project "Redox Phenomena Controlling Systems" (7th EC FP CP RECOSY), Larnaca, Cyprus, 16–19 March 2010. Karlsruhe: Karlsruhe Institute of Technology, 275–283.

Duro L, Grivé M, Giffaut E, 2012. ThermoChimie, the ANDRA thermodynamic database. In Scientific basis for nuclear waste management XXXV. Warrendale, PA: Materials Research Society. (Materials Research Society Symposium Proceedings 1475), doi:10.1557/opl.2012.637

Elie M, Faure P, Michels R, Landais P, Griffault L, Mansuy L, Martinez L, 2004. Effects of water–cement solutions on the composition of organic compounds leached from oxidized Callovo-Oxfordian argillaceous sediment. Applied Clay Science 26, 309–323.

EPA, 2000. Engineered approaches to *in situ* bioremediation of chlorinated solvents: fundamentals and field applications. EPA 542-R-00-008, U.S. Environmental Protection Agency, Washington.

Faure P, Landais P, Griffault L, 1999. Behavior of organic matter from Callovian shales during low-temperature air oxidation. Fuel 78, 1515–1525.

Forward F A, Halpern J, 1953. Precipitation of uranium from carbonate solutions by reduction with hydrogen. Transactions of the Canadian Institute of Mining and Metallurgy and of the Mining Society of Nova Scotia 56, 645–648.

Glaus M A, Van Loon L R, 2004. Cellulose degradation at alkaline conditions: long-term experiments at elevated temperatures. PSI Bericht 04-01, Paul Scherrer Institute, Switzerland.

Glaus M A, Van Loon L R, 2008. Degradation of cellulose under alkaline conditions: new insights from a 12 years degradation study. Environmetal Science & Technology 42, 2906–2911.

Glaus M A, Van Loon L R, Achatz S, Chodura A, Fischer K, 1999. Degradation of cellulosic materials under the alkaline conditions of a cementitious repository for low and intermediate level radioactive waste. Part I: Identification of degradation products. Analytica Chimica Acta 398, 111–122.

Glaus M A, Van Loon L R, Schwyn B, Vines S, Williams S J, Larsson P, Puigdomenech I, 2007. Long-term predictions of the concentration of α-isosaccharinic acid in cement pore water. In Lee W E (ed). Scientific basis for nuclear waste management XXXI: symposium held in Sheffield, United Kingdom, 16–21 September 2007. Warrendale, PA: Materials Research Society. (Materials Research Society Symposium Proceedings 1107), 605–612.

Grivé M, 2005. The linkage between uranium, iron and carbon cycling, processes at interfaces: evidences from combined solution chemical and spectroscopic studies. PhD thesis. Universidad Politécnica de Catalunya, Spain.

Grivé M, Duro L, Domènech C, Salas J, 2011. Redox evolution of a cementitious geological disposal facility. In Proceedings of the 13th International High-Level Radioactive Waste Management Conference (IHLRWMC), Albuquerque, New Mexico, 10–14 April 2011. La Grange Park, IL: American Nuclear Society, 692–700.

Hansel C M, Benner S G, Neiss J, Dohnalkova A, Kukkadapu R K, Fendorf S, 2003. Secondary mineralization pathways induced by dissimilatory iron reduction of ferrihydrite under advective flow. Geochimica et Cosmochimica Acta 67, 2977–2992.

Holmén J G, Stigsson M, 2001. Modelling of future hydrogeological conditions at SFR. SKB R-01-02, Svensk Kärnbränslehantering AB.

Hummel W, Berner U, Curti E, Pearson F J, Thoenen T, 2002. Chemical thermodynamic data base (01/01). Parkland, FL: Universal Publishers.

Hummel W, Anderegg G, Rao L, Puigdomenech I, Tochiyama O, 2005. Chemical thermodynamics. Vol 9. Chemical thermodynamics of compounds and complexes Of U, Np, Pu, Am, Tc, Se, Ni And Zr with selected organic ligands. Paris: Nuclear Energy Agency, Organisation for Co-operation and Development.

Hurdus M H, Pilkington N J, 2000. The solubility and sorption of 2-C-(hydroxymethyl)-3-deoxy-D-pentanoic acid in the presence of Nirex reference vault backfill and its degradation under alkaline conditions. Report AEAT/ERRA-0153, AEA Technology.

Kagawa A, Fukumoto M, Kawamura K, 1999. Influence of chemical and radiolytic degradation of bitumen on disposal. In Proceeding of the International Workshop on the Safety and Performance Evaluation of Bitumenization Processes for Radioactive Waste, Prague, 29 June – 2 July 1999. Řež, Czech Republic, Nuclear Research Institute, 153.

Kuron D, Gräfen H, Batroff H-P, Fäußler K, Münster R, 1985. Einfluß des Chloridgehaltes in Trinkwasser auf die Korrosion von unlegiertem Stahl (Influence of chloride content in tap water on the corrosion of unalloyed steel). Materials and Corrosion 36, 68–79.

Kursten N, Smailos E, Azkarate I, Werme L, Smart N R, Santarini G, 2004. COBECOMA. State-of-the-art document on the COrrosion BEhaviour of COntainer MAterials. Final report. Contract n° FIKW-CT-20014-20138. European Commission.

Lin Y H, Lee K K, 2001. Verification of anaerobic biofilm model for phenol degradation with sulphate reduction. Journal of Environmental Engineering 127, 119–125.

Lindberg R D, Runnells D D, 1984. Ground water redox reactions: an analysis of equilibrium state applied to Eh measurements and geochemical modeling. Science 225, 925–927.

McMahon P B, Chapelle F H, 2008. Redox processes and water quality of selected principal aquifer systems. Groundwater 46, 259–271.

Mihara M, Nishimura T, Wada R, Honda A, 2002. Estimation on gas generation and corrosion rates of carbon steel, stainless steel and zircaloy in alkaline solutions under low oxygen condition. Saikuru Kiko Giho 15, 91–101. (In Japanese.)

Montemor M F, Simões A M P, Ferreira M G S, 2003. Chloride-induced corrosion on reinforcing steel: from the fundamentals to the monitoring techniques. Cement and Concrete Composites 25, 491–502.

Moreno L, Skagius K, Södergren S, Wiborgh M, 2001. Project Safe Gas related processes in SFR. SKB R-01-11, Svensk Kärnbränslehantering AB.

Nagra, 2008. Effects of post-disposal gas generation in a repository for low- and intermediate-level waste sited in the Opalinus Clay of Northern Switzerland. Nagra Technical Report NTB 08-07, Nagra, Switzerland.

Naish C C, Blackwood D J, Taylor K J, Thomas M I, 1995. The anaerobic corrosion of stainless steels in simulated repository backfill environments. Nirex Report NSS/R307, UK Nirex Ltd.

Naish C C, Blackwood D J, Thomas M I, Rance A P, 2001. The anaerobic corrosion of carbon steel and stainless steel. Report AEAT/R/ENV/0224, AEA Technology.

Neall F, 1994. Modelling of the near-field chemistry of the SMA repository at the Wellenberg site: application of the extended cement degradation model. Nagra NTB 94-03, Nagra, Switzerland.

NWMO, 2011. OPG's deep geological repository for low and intermediate level waste. Postclosure Safety Assessment. March 2011. NWMO DGR-TR-2011-25, Nuclear Waste Management Organization, Canada.

Omil F, Lens P, Visser A, Hulshoff Pol L W, Lettinga G, 1998. Long-term competition between sulphate reducing and methanogenic bacteria in UASB reactors treating volatile fatty acids. Biotechnology and Bioengineering 57, 676–685.

Oude Elferlink S J W H, Luppens S B I, Marcelis C L M, Stams A J M, 1998. Kinetics of acetate oxidation by two sulfate reducers isolated from anaerobic granular sludge. Applied and Environmental Microbiology 64, 2301–2303.

Park J B, Jung H, Lee E Y, Kim C L, Kim G Y, Kim K S, Koh Y K, Part K W, Cheong J H, Jeong C W, Choi J S, Kim K D, 2009. Wolsong low and intermediate level radioactive waste disposal center: progress and challenges. Nuclear Engineering and Technology 41, 477–492.

Parkhurst D L, Appelo C A J, 1999. User's guide to PHREEQC (version 2): a computer program for speciation, batch-reaction, one-dimensional transport, and inverse geochemical calculations. Water-Resources Investigations Report 99-4259, U.S. Geological Survey, Denver, Colorado.

Pedersen K, 2001. Project SAFE. Microbial features, events and processes in the Swedish final repository for low- and intermediate-level radioactive waste. SKB R-01-05, Svensk Kärnbränslehantering AB.

Pettersson M, Elert M, 2001. Characterisation of bitumenised waste in SFR 1. SKB R-01-26, Svensk Kärnbränslehantering AB.

Puigdomenech I, Ambrosi J-P, Eisenlohr L, Lartigue J-E, Banwart S A, Bateman K, Milodowski A E, West J M, Griffaut L, Gustafsson E, Hama K, Yoshida H, Kotelnikova S, Pedersen K, Michaud V, Trotignon L, Rivas Perez J, Tullborg E-L, 2001. O_2 depletion in granitic media. The REX project. SKB TR-01-05, Svensk Kärnbränslehantering AB.

Reed D T, Lucchini J F, Aase S B, Kropf A, 2006. Reduction of plutonium(VI) in brine under subsurface conditions. Radiochimica Acta 94, 591–597.

Reed D T, Lucchini J F, Borkowski M. Richmann M K, 2009. Pu(VI) reduction by iron under WIPP-relevant conditions: data summary and recommendations. Report LCO-ACP-09, LANL\ ACRSP, Los Alamos National Laboratory, New Mexico.

Rittmann B E, VanBriesen J M, 1996. Microbiological processes in reactive modelling. In Lichtner P C, Steefel C I, Oelkers E H (eds). Reactive transport in porous media. Washington, DC: Mineralogical Society of America, 311–332. (Reviews in Mineralogy 34)

Roffey R, Norqvist A, 1991. Biodegradation of bitumen used for nuclear waste disposal. Experientia 47, 539–542.

Rotter B E G, 2008. Modelling bioremediation of uranium contaminated aquifers. PhD thesis. University of Edinburgh, UK.

Salas J, Gimeno M J, Auqué L, Molinero J, Gómez J, Juárez I, 2010. SR-Site – hydrogeochemical evolution of the Forsmark site. SKB TR-10-58, Svensk Kärnbränslehantering AB.

Scott M J, Morgan J J, 1990. Energetics and conservative properties of redox systems. In Melchior D C, Basset R L (eds). Chemical modelling of aqueous systems II. Washington, DC: American Chemical Society, 368–378.

Schenk R, 1988. Untersuchungen über die Wasserstoffbildung durch Eisenkorrosion unter Endlagerbedingungen. Nagra Technischer Bericht 86-24, Nagra, Switzerland.

Sena C, 2009. Numerical modelling of radionuclide migration in near-surface systems. PhD thesis. Universidade de Aveiro, Portugal.

SKB, 2008a. Project SFR 1 SAR-08. Update of priority of FEPs from Project SAFE. SKB R-08-12, Svensk Kärnbränslehantering AB.

SKB, 2008b. Safety analysis SFR 1. Long-term safety. SKB R-08-130, Svensk Kärnbränslehantering AB.

SKB, 2014. Waste form and packaging process report for the safety assessment SR-PSU. SKB TR-14-03, Svensk Kärnbränslehantering AB.

Sharland S M, Newton C J, 1989. The long-term prediction of corrosion of stainless steel nuclear waste canisters. In Lutze W, Ewing R C (eds). Scientific basis for nuclear waste management XII: symposium held in Berlin, 10–13 October 1988. Pittsburgh, PA: Materials Research Society. (Materials Research Society Symposium Proceedings 127), 373–380.

Simpson J P, Weber J, 1988. Hydrogen evolution from corrosion in nuclear waste repositories. In Proceedings of UK Corrosion ’88 with EUROCORR, Brighton, 3–5 October 1988. Birmingham: Institution of Corrosion Science and Technology, 33.

Simpson J P, Schenk R, Knecht B, 1985. Corrosion rate of unalloyed steels and cast irons in reducing granitic groundwaters and chloride solutions. In Werme L O (ed). Scientific basis for nuclear waste management IX: symposium held in Stockholm, Sweden, 9–11 September 1985. Pittsburgh, PA: Materials Research Society. (Materials Research Society Symposium Proceedings 50), 429–436.

Small J S, Humphreys P N, Johnstone T L, Plant R, Randall M G, Trivedi D P, 2000. Results of an aqueous source term model for a radiological risk assessment of the Drigg LLW site. In Smith R W, Shoesmith D W (eds). Scientific basis for nuclear waste management XXIII: symposium held in Boston, Massachusetts, USA, 29 November – 2 December 1999. Warrendale, PA: Materials Research Society. (Materials Research Society Symposium Proceedings 608), 129–134.

Small J S, Abraitis P K, Beadle I R, Johnstone T L, Kelly P, Pettit C L, Stevens G A, 2004. A comparison of site characterisation data and modelling results from a radiological assessment of the Drigg low level radioactive waste disposal site. In Oversby V M, Werme L O (eds). Scientific basis for nuclear waste management XXVII: symposium held in Kalmar, Sweden, 15–19 June 2003. Warrendale, PA: Materials Research Society. (Materials Research Society Symposium Proceedings 807), 905–910.

Small J, Nykyri M, Helin M, Hovi U, Sarlin T, Itävaara M, 2008. Experimental and modelling investigations of the biogeochemistry of gas production from low and intermediate level radioactive waste. Applied Geochemistry 23, 1383–1418.

Smart N R, Hoch A R, 2006. A survey of steel and zircaloy corrosion data for use in the SMOGG gas generation model. Serco report SA/ENV/0841, Serco, UK.

Smart N R, Blackwood D J, Marsh G P, Naish C C, O'Brien T M, Rance A P, Thomas M I, 2004. The anaerobic corrosion of carbon and stainless steels in simulated cementitious environments: a summary review of Nirex research. Report AEAT/ERRA-0313, AEA Technology.

Soylev T A, François R, 2003. Quality of steel–concrete interface and corrosion of reinforcing steel. Cement and Concrete Research 33, 1407–1415.

Stumm W, Morgan J J, 1996. Aquatic chemistry, chemical equilibria and rates in natural waters. 3rd ed. New York: Wiley.

Telander M R, Westermann R E, 1993. Hydrogen generation by metal corrosion in simulated waste isolation pilot plant environments. SAND92-7347, Sandia National Laboratories, Albuquerque, NM.

Telander M R, Westermann R E, 1997. Hydrogen generation by metal corrosion in simulated waste isolation pilot plant environments. SAND96-2538, Sandia National Laboratories, Albuquerque, NM.

Trummer M, Jonsson M, 2010. Resolving the H_2 effect on radiation induced dissolution of UO_2-based spent nuclear fuel. Journal of Nuclear Materials 396, 163–169.

U.S. Department of Energy, 2006. Transuranic waste baseline inventory report – 2004 Revision 0. DOE/TRU-2006-3344, U.S. Department of Energy.

Van Loon L R, Hummel W, 1995. The radiolytic and chemical degradation of organic ion exchange resins under alkaline conditions: effect on radionuclide speciation. Nagra Technical Report NTB 95-08, Nagra, Switzerland.

Van Loon V R, Glaus M A, 1998. Experimental and theoretical studies on alkaline degradation of cellulose and its impact on the sorption of radionuclides. PSI Bericht 98-07, Paul Scherrer Institute, Switzerland.

Van Loon L R, Glaus M A, Laube A, Stallone S, 1999. Degradation of cellulosic materials under the alkaline conditions of a cementitious repository for low- and intermediate-level radioactive waste. II. Degradation kinetics. Journal of Environmental Polymer Degradation 7, 41–51.

Vavilin, V A, Lokshina L Y, 1996. Modeling of volatile fatty acids degradation kinetics and evaluation of mircroorganism activity. Bioresource Technology 57, 69–80.

Wang Y, Brush L, 1996. Estimates of gas-generation parameters for the long-term WIPP performance assessment. Sandia National Laboratories, Albuquerque, NM.

Wersin P, Johnson L H, Schwyn B, Berner U, Curti E, 2003. Redox conditions in the near field of a repository for SF/HLW and ILW in Opalinus clay. Nagra Technical Report 02-13, Nagra, Switzerland.

Wolf M, Bachofen L, 1991. Microbial degradation of bitumen. Experientia 47, 542–545.

Unpublished documents

SKBdoc id, version	Title	Issuer, year
1285831 ver 3.0	Input data for the redox-model	SKB, 2011

Appendix 1

Waste package types cross references

Waste type	Vault	Cited in
B.04	Silo	Table 2-1; Table 2-2; Table A2-1
B.05	BMA	Table 2-3; Table 2-4; Table 4-1; Table 6-1; Table 6-6; Table 6-5; Table 6-8; Table 6-9; Table 6-11; Table A2-2
B.06	Silo	Table 2-1; Table 2-2; Table A2-1; Table 4-1; Table 6-1; Table 6-8; Table 6-9; Table 6-10; Table 6-11
B.07	1 BTF, 2 BTF	Table 2-5; Table 2-6; Table 2-7; Table 4-1; Table 6-1; Table 6-3; Table 6-6; Table 6-8; Table 6-9; Table 6-10; Table 6-11
B.12	BLA	Table 2-9; Table 2-10
B.20	BLA	Table 2-9; Table 2-10
C.01	BMA	Table 2-3; Table 2-4;
C.02	Silo	Table 2-1; Table 2-2; Table A2-1
C.23	BMA	Table 2-3;
C.24	Silo	Table 2-1; Table 2-2;
F.05	BMA	Table 2-3; Table 2-4; Table 4-1; Table 6-1; Table 6-4; Table 6-6; Table 6-8; Table 6-9; Table 6-10; Table 6-11
F.12	BLA	Table 2-9; Table 2-10
F.15	BMA	Table 2-3; Table 2-4;
F.17	BMA	Table 2-3; Table 2-4; Table 4-1; Table 6-1; Table 6-4; Table 6-6; Table 6-8; Table 6-9; Table 6-10; Table 6-11
F.18	Silo	Table 2-1; Table 2-2; Table 4-1; Table 6-1; Table 6-4; Table 6-6; Table 6-8; Table 6-9; Table 6-10
F.20	BLA	Table 2-9; Table 2-10
F.23	BMA	Table 2-3; Table 2-4;; Table 4-1; Table 6-1; Table 6-5; Table 6-6; Table 6-8; Table 6-9; Table 6-10; Table 6-11
F.99:2	2 BTF	Table 2-7; Table 2-8
O.01	1 BTF, BMA	Table 2-3; Table 2-4; Table 2-5 Table 2-6;
O.02	Silo	Table 2-1; Table 2-2; Table 4-1; Table 6-1; Table 6-3; Table 6-6; Table 6-8; Table 6-9; Table 6-10; Table 6-11
O.07	1 BTF, 2 BTF	Table 2-5 Table 2-6; Table 2-7;
O.12	BLA	Table 2-9; Table 2-10Table 4-1; Table 6-1; Table 6-5; Table 6-8; Table 6-9; Table 6-10
O.23	BMA, Silo	Table 2-3; Table 2-4; Table 4-1; Table 6-1; Table 6-5; Table 6-6; Table 6-8; Table 6-9; Table 6-10; Table 6-11
O.99:1	1 BTF, 2 BTF	Table 2-5 Table 2-6; Table 2-7; Table 2-8
O.99:3	BLA	Table 2-9; Table 2-10
R.01	1 BTF, BMA	Table 2-3; Table 2-4; Table 2-5; Table 2-6; Table 4-1; Table 6-1; Table 6-3; Table 6-6; Table 6-8; Table 6-9; Table 6-10; Table 6-11
R.02	Silo	Table 2-1; Table 2-2;
R.10	1 BTF, BMA	Table 2-3; Table 2-4; Table 2-5; Table 2-6;
R.12	BLA	Table 2-9; Table 2-10
R.15	BMA	Table 2-3; Table 2-4; Table 4-1; Table 6-1; Table 6-2; Table 6-6; Table 6-8; Table 6-9; Table 6-10; Table 6-11
R.16	Silo	Table 2-1; Table 2-2; Table A2-1; Table 4-1; Table 6-1; Table 6-2; Table 6-6; Table 6-8; Table 6-9; Table 6-10; Table 6-11
R.23	BMA,1 BTF	Table 2-3; Table 2-4; Table 2-5; Table 2-6;
R.29	BMA	Table 2-3; Table 2-4
R.99:1	1 BTF	Table 2-5; Table 2-6
S.04	Silo	Table 2-1; Table 2-2;
S.09	BMA	Table 2-3; Table 2-4;
S.11	Silo	Table 2-1; Table 2-2;
S.12	BLA	Table 2-9; Table 2-10
S.13	1 BTF, 2 BTF	Table 2-5 Table 2-6; Table 2-7;Table 2-8; Table 4-1; Table 6-1; Table 6-2; ; Table 6-6; Table 6-8; Table 6-9; Table 6-10; Table 6-11
S.14	BLA	Table 2-9; Table 2-10;Table 4-1
S.23	BMA	Table 2-3; Table 2-4
S.24	Silo	Table 2-1; Table 2-2;

Appendix 2

Preliminary calculations: initial oxygen consumption by fast corroding metals

According to the reference inventory (Almkvist and Gordon 2007), from the 11 type of different waste package existing in the Silo, only one (S.24) contains Al (Table 2-2). The expected amount of S.24 waste package type in the Silo at year 2,050 is of 134 (Table 2-1), each of them containing 3.8 kg of Al with a surface area of 0.6 m^2 (Almkvist and Gordon 2007).

This type of waste packages has an estimated volume of waste of 0.95 m^3, with a void volume of 0.05 m^3 per waste package (Table 2-1). By assuming that all void volume will contain oxygen at the time of closure at the expected atmospheric percentage (21%), and that all this oxygen would dissolve in water once the Silo is saturated (expected to occur fast according to previous hydro-geological models), the maximum amount of oxygen expected to be trapped in 134 S.24 waste packages is 1.77 moles.

By assuming that the process of oxic corrosion of Al can be expressed by Equation A2-1, each mole of Al consumes ¾ moles of O_2. Therefore, the total consumption of 1.77 moles of O_2 in the existing S.24 waste packages will need of 4/3 moles of Al, that is, 2.4 moles of Al, or 63.6 g of Al, which is only a 0.013% of the Al present in this waste package type, and in all the Silo according to the inventory. Therefore there is sufficient Al to consume the trapped O_2 in S.24 packages.

$$2\ Al(s) + 3/2\ O_2 \rightarrow Al_2O_3(s) \qquad \text{Eq. A2-1}$$

If we extrapolate this calculation to the whole Silo, assuming that Al is homogeneously distributed, we will conclude that there is enough Al in the Silo (509.2 kg) as to consume all oxygen in the complete Silo system (800 moles O_2), as shown in Table A2-1, given that only 28.8 kg of Al are needed to consume 800 moles of O_2.

Nevertheless, it is important to bear in mind that Al is only present in 1% of the waste packages in the Silo, therefore other processes must be considered for the consumption of oxygen trapped in waste packages not containing Al.

Besides mass balance considerations, also kinetics must be taken into account. The waste package type S.24 contains concrete as stabilization matrix; therefore the oxidation of Al is expected to occur under hyperalkaline conditions. This means that the process is expected to be faster than if it were present in the absence of cement-related material, as per the reactivation of the surface expected under this condition.

In the case of BMA, aluminium is present in a 9% of the waste packages. Types F.23, R.23, C.23, O.23 and S.23 contain Al and also cellulose and other organic non-cellulosic materials (except for bitumen) and are packaged in 1.73 m^3 concrete moulds (Table 2-3). Therefore, the initial consumption of oxygen trapped in the BMA vault will be undertaken at the same waste package type, either by organic matter or by the oxic corrosion of aluminium if we exclude the effect of bitumen in the short-term.

Although in the discussed examples prevalence has been given to the corrosion of Al versus other metallic components due to the, in principle, faster corrosion of this metal in comparison with that of carbon or stainless steel, the fact is that in the SFR 1 repository massive amounts of steel are used, which is the reason why the bulk of the simulations have considered steel.

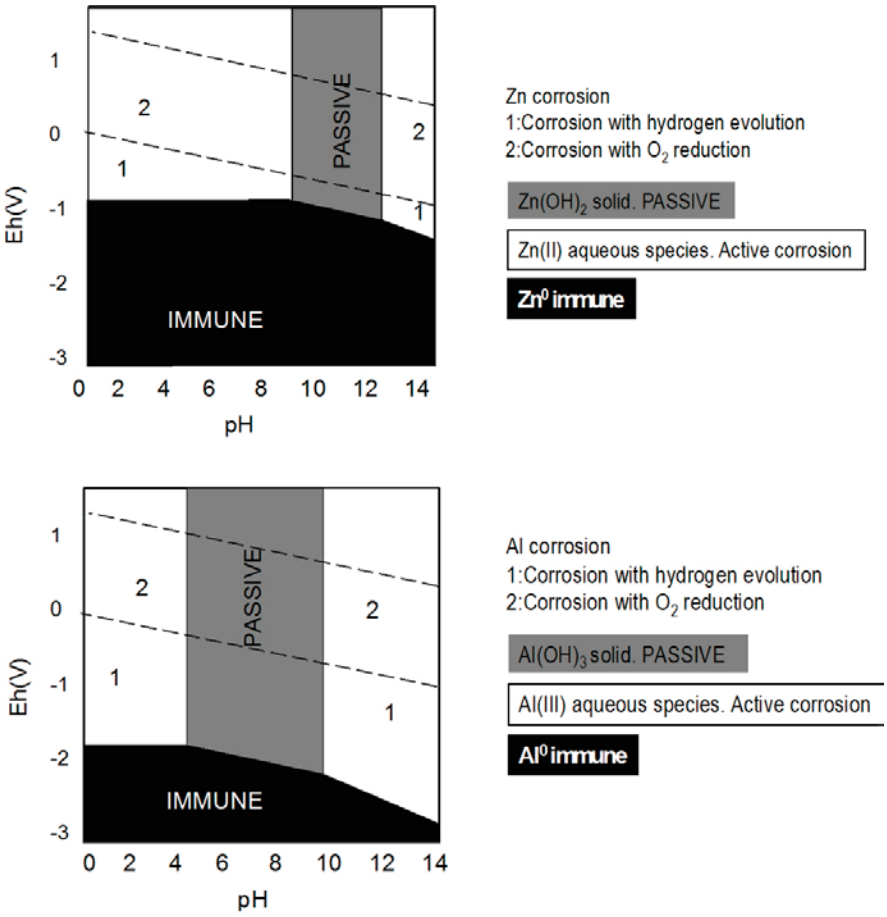

Figure A2-1. *Pourbaix diagrams of Zn and Al, showing the dissolution of the passive layer of oxide at pH above 12 for Zn (top) and above 9 for Al (bottom), giving rise to an increase of the rate of corrosion process.*

Table A2-1. Calculation of the maximum moles of oxygen trapped in the Silo waste packages at repository closure. Figures calculated from data in the waste inventory (Almkvist and Gordon 2007) and listed in Table 2-1 and Table 2-2.

Silo				
Waste package	**Total internal void volume (m^3)**	**Maximum moles of O_2 inside the waste packages**	**Al (kg) present in the waste**	**Al (kg) needed to consume all oxygen**
B.04	20	5.28		
B.06	55	14.6		
C.02	219	57.8		
C.24	2	0.51		
F.18	169	44.5		
O.02	351	92.7		
R.02	56	14.7		
R.16	292	77.1		
S.04	2	0.58		
S.11	5	1.35		
S.24	7	1.77	3.8	
Total in Silo	3,029	800	509.2	28.8

Table A2-2. Calculation of the maximum moles of oxygen trapped in BMA waste packages at repository closure. Figures calculated from data in the waste inventory (Almkvist and Gordon 2007) and listed in Table 2-3.

BMA				
Waste package type	**Total internal void volume (m^3)**	**Maximum moles of O_2 inside the waste packages**	**Al (kg) present in the waste**	**Al (kg) needed to consume all oxygen**
B.05	126	33.2		
C.01	10	2.69		
C.23	10	2.67	3.5	
F.05	34	9.04		
F.15	2	0.49		
F.17	136	36		
F.23	40	10.5	5	
F.99	0	0.08		
O.01	34	8.91		
O.23	32	8.45	3.5	
R.01	253	66.8		
R.10	15	3.85		
R.15	14	3.66		
R.23	52	13.6	**4**/1	
R.29	163	43.1		
S.09	11	2.85		
S.23	22	5.81	3.8	
Total in BMA	1,952	515	9,396	18.5

Appendix 3

Redox considerations in similar repository systems

There are different types of LILW repositories in the world, managed by different organizations. Some of them are located in surface facilities and some others in the underground, as it is the case of the SFR 1. Most of them use backfills based on cementitious materials, which are also used in waste stabilization processes (conditioning of the wastes). Although the cases of the surface deposits are not so similar from the point of view of water intrusion to the deposit, as well as on other particularities, we present below some of the systems based on the criteria on how the redox conditions or related issues have been considered in the safety assessment, environmental impact assessment, or feasibility studies of the repositories.

The current status of the underground repositories for low and intermediate level wastes is shown in Table A3-1.

Below, a short description of the underground repositories for LILW is given, together with references to the way in which the redox evolution has been dealt with in the associated safety assessments, if possible.

Although the Drigg deposit presented below is a surface facility, some of the models applied to assess redox evolution of underground LILW repositories are based on the model developed for this site, and this is why it is included in this chapter.

Also the modelling of the redox evolution of a generic site conducted for the NDA is briefly summarized as a study case in order to provide an example of a complementary way of assessing the evolution of an underground repository.

A3-1 The Drigg deposit, UK

In 1957 the site was developed for the disposal of LLW. Most of the material handled at Drigg comes from Sellafield, the rest is made up of materials from other sites, nuclear power stations, hospitals, research sites and other industries. The majority of wastes are compacted and put in containers before being transferred to Drigg. Wastes that cannot be compacted are placed directly into the disposal containers. At Drigg the waste is immobilised within the disposal containers by the addition of grout in the Drigg Grouting Facility before being placed in the engineered concrete vaults.

The Drigg site presents two types of deposition: trenches, where the wastes are not conditioned, and vaults where the wastes are conditioned in a similar way to the ones in SFR 1.

Table A3-1. Current status of the underground repositories for low and intermediate level wastes.

Facility	Country	Waste type	Depth	Host rock	Status
VLJ, Olkiluoto	Finland	L&ILW	60 m	Crystalline	Operating
SFR 1	Sweden	L&ILW	50 m	Crystalline	Operating
WIPP	US	ILW (TRU)	650 m	Sedimentary salt	Operating
Konrad	Germany	L&ILW	~1000 m	Sedimentary carbonate	Licensed
Gyeongju	Korea	L&ILW	~100 m	Crystalline	Under construction
Bataapati	Hungary	L&ILW	250 m	Crystalline	Under construction
Bruce	Canada	L&ILW	680 m	Clay	EIA and PSR submitted April 2011
Opalinus Clay	Switzerland	L&ILW	300 m	Clay	Siting process

A Generalised Repository Model (GRM) was used in the Drigg site to simulate the evolving geochemistry of the Drigg trenches and vaults. The model, described in Small et al. (2000), considered corrosion of steel kinetically controlled and cellulose degradation microbially mediated. These processes are simulated and their results are used to describe the redox evolution of the site by assuming that the system is in equilibrium with the most oxidising redox couple. The calculated redox potential is then used as an input data for the calculation of speciation and mineral equilibrium. To this aim a routine based on PHREEQE was used.

The results of the application of the model by Small et al. (2000) to the vaults systems indicated:

- Establishment of reduced conditions as a result of cellulose degradation and steel corrosion reactions.
- Re-oxidation occurring over a period of 2,000 to 10,000 years.
- Under alkaline conditions different secondary mineral phases are produced with Fe(II) hydroxide and FeS being formed as main corrosion products.

The main uncertainties of the model were recognized as being:

- Steel corrosion rate.
- The assumed levels of acetate.
- The lack of methanogenesis.

A3-2 Underground deposit in Olkiluoto, Finland

The VLJ repository for LILW in Olkiluoto, Finland, contains reactor-operating wastes emplaced in drums and located in an underground cavern. It is assumed that after the closure of the repository the system will re-saturate and the waste will submerge in water.

A large-scale Gas Generation Experiment (GGE) has been in operation in the VLJ repository since 1997. The model presented in the previous section for the Drigg site was applied to the results obtained from the GGE (Small et al. 2004, 2008). The modelling code consists on a 2-dimensional finite difference grid, used to model the transport of chemical species under an imposed flow field in saturated groundwater coupled sequentially to an equilibrium chemical speciation calculation using the PHREEQE code.

As in the previous case, several criteria are defined to calculate the redox potential from the "controlling redox couple". The results of the model indicate that the redox potential is well predicted during the first 4 years, controlled apparently by sulphate reduction processes at values around –400 mV. At longer times, from 4 to 9 years, the measured Eh increases to –200 mV while pH decreases to values close to 8, although in some cases this decrease is discussed to be a consequence of CO_2 absorption by the system. The lowest pH values measured, around 6, occur in waste drums with high content of biodegradable waste.

The model is not able to predict the Eh increase, given that the process assumed to control the Eh in this period is fermentation, what would result in Eh values going down to –550 mV. It must be highlighted that in this model the assumption of water reduction is never considered as able to control the redox potential due to the fact that at these short-term the process of organic matter oxidation is more effective in consuming oxidants trapped in the system, and water reduction is not expected to occur.

A3-3 Underground deposit in the WIPP Site for LILW and TRU wastes, USA

The Waste Isolation Pilot Plant (WIPP) is a deep geological repository licensed to permanently dispose of transuranic radioactive waste for 10,000 years that is left from the research and production of nuclear weapons.

SOTERM-2009 (Actinide Chemistry Source Term) is a summary of the U. S. Department of Energy's (DOE's) understanding of the Waste Isolation Pilot Plant (WIPP) chemical conditions, assumptions, and processes; the underlying actinide chemistry; and the resulting dissolved actinide concentrations that were calculated based on this repository chemistry. What is explicitly said is:

The WIPP repository will contain a large quantity of reduced iron due to the use of iron-based containers for much of the emplaced TRU waste

Currently, it is estimated that the WIPP will contain upwards of 51,000 metric tons of iron (U.S. Department of Energy 2006) when all the waste is emplaced. The presence of this reduced metal will have an important role in the establishment of reducing conditions in the WIPP by removing oxygen. Reduced iron species (aqueous Fe(II) and Fe(0, II)-valent minerals) are important because they will reduce higher-valent actinides in the WIPP, leading to lower actinide solubilities (Reed et al. 2006, 2009). It is expected that oxic corrosion of steels and aerobic microbial consumption of CPR (cellulose, plastic and rubber) materials will quickly consume the limited amount of oxygen (O_2) trapped within the repository at the time of closure. After O_2 is consumed, anoxic corrosion of metals will occur (Brush 1990, 1995, Wang and Brush 1996). WIPP-specific experiments (Telander and Westerman 1993, 1997) showed that steels and other Fe-based alloys will corrode and three important reactions of iron are considered for the WIPP PA:

a) The first is the reaction of metallic iron with carbon dioxide to form insoluble ferrous carbonate. This suggests that the presence of iron will likely remove CO_2 from the repository more effectively than MgO due to its lower solubility product. This reaction is not included in the WIPP PA because the CO_2 reacts with MgO before iron does.

b) The second is the reaction of iron and ferrous ions with the hydrogen sulphide that could be generated in the repository by sulphate-reducing microbes. This reaction is assumed to occur instantaneously in the PA.

c) Finally, iron species form strong complexes with organic ligands. The strongest of these complexes is EDTA. The net effect is that dissolved iron species will compete with actinides for organic ligands, and in many cases out-compete the actinides to counteract the potential enhancement of actinide solubility that would otherwise occur. This reaction is not currently included in the PA.

The chemistry of iron will have a pronounced effect on WIPP-relevant actinide chemistry in many ways. Iron will establish reducing conditions conducive to the overall reduction of higher-valent actinide species and precipitate an iron sulphide phase that removes sulphide from solution. Additionally, iron species could sequester carbon dioxide and compete with actinides for organic and inorganic ligands (complexing agents).

Lead is present in the repository in the metallic form as part of the waste

The reactivity of zero-valent lead is greatly mitigated by the formation of a thin, coherent, protective oxide, oxycarbonate, chloride, or sulphate protective layer. Metallic lead also reacts slowly with water at room temperature and undergoes corrosion to form oxides and oxyhydroxides. Lead, as was the case with iron, can influence the redox chemistry and precipitate carbonate and sulphide from the WIPP brine. This leads to a redox chemistry that will help maintain reducing conditions and effectively lower carbonate concentration. Both of these will potentially lower actinide solubility in the WIPP.

Concerning organic chelating agents in WIPP, there are two final but important observations.

a) Microbial activity, based on many general observations with soil bacteria, will likely readily degrade citrate, oxalate, and acetate to very low (sub-micromolar) steady-state concentrations. This important degradation pathway is not as certain for EDTA, which tends to resist biodegradation in most groundwaters. These degradation pathways have, however, not been demonstrated for the halophiles typically present in the WIPP, and it is currently assumed in the WIPP PA that no degradation pathways for these organic complexing agents, microbiological or chemical, exist.

b) The second important observation is that these chelating agents, under WIPP-relevant conditions, are expected to help establish reducing conditions in the WIPP because they tend to reduce higher-valence actinides. These potentially beneficial effects of organic chelating agents on actinide speciation are also currently not included in the WIPP PA.

Microbial activity, if it occurs, will consume CPR (cellulose, plastic and rubber) materials

Besides other effects, such as production of CO_2 and colloids, it is discussed that after 100 years, the repository will have a reducing environment. This is, in part, established by the post closure microbial consumption of oxygen, but is also due to the corrosion of steel. This combined effect leads to the formation of an anoxic reducing environment in the WIPP.

A3-4 Underground deposit in the Bruce Site for LILW, Canada

The Environmental Impact Statement (EIS), Preliminary Safety Report (PSR) and supporting documents for OPG's Deep Geologic Repository for low and intermediate level waste were submitted by OPG to the Canadian Nuclear Safety Commission (for the Joint Review Panel) on April 14, 2011.

Currently all of the low and intermediate level wastes (L&ILW) generated from the operation of the CANDU reactors are being stored at OPG's Western Waste Management Facility (WWMF) which is located on the Bruce site, located about 225 km north-west of Toronto.

Although current storage practices are safe, these wastes will eventually need to be transferred to a long-term management facility, as some of the wastes remain hazardous for thousands of years.

Low-level wastes include contaminated clothing, rags, plastics, papers and similar lightly contaminated materials. WWMF receives about 5,000–6,000 m^3 per year of low-level waste. This is incinerated or compacted if possible, and the remainder is stored. Approximately 2,000–3,000 m^3 is stored each year. There is currently about 60,000 m^3 in storage.

Intermediate-level waste includes contaminated resins, filters and reactor core components. It has generally higher activity, and a significant proportion of long-lived radionuclides. Approximately 200–400 m^3 of intermediate-level waste is received each year at WWMF, where it is stored. There is currently about 8,500 m^3 in storage.

The DGR is presently being designed with a capacity of 160,000 m^3 of as-stored waste, corresponding approximately to the volume of operational and refurbishment L&ILW from the existing Ontario reactors through their present scheduled life. After some overpacking for disposal, the total as-disposed volume would be approximately 200,000 m^3.

The repository is planned to be located in an argillaceous limestone formation (the "Cobourg Formation") at a depth of about 680 m below surface. In principle, the storage rooms will be arranged in parallel rows on either side of central access tunnels. Some of them would be reserved for LLW and the rest for ILW. The floor of the rooms would be built with concrete. Each room would be isolated with a concrete wall when full, but not sealed or backfilled. The shafts would be sealed with a combination of concrete caps and low-permeability materials, in particular bentonite-sand.

According to the Post-closure safety assessment recently submitted (NWMO 2011), during the years following closure it is assumed that there will occur corrosion of the carbon steel containers and degradation of organic materials in the wastes. This will cause a depletion of oxygen and thus the development of an anaerobic atmosphere in the repository. Subsequent slow anaerobic degradation of the wastes and of the packaging materials will generate various decomposition products, especially gases: H_2 from the corrosion of metals and CO_2 and CH_4 from the microbial decomposition of organics. No specific assessment of the evolution of the redox state of the repository has been done or has been found in the associated literature.

A3-5 Underground deposit for LILW, Switzerland

The region of Northern Aargau has been proposed as one of the siting regions for a LILW geological repository in Opalinus Clay. The repository would be located at a depth of around 300 m. The assessment works that have been made are based on a generic repository for LILW. Very detailed assessment of gas generation processes has been conducted (Nagra 2008), where the corrosion of metals was considered as the main process responsible for gas generation. Although in the mentioned report no redox implications are specifically discussed, the generation of hydrogen is assumed to keep the system under reducing conditions.

Previous assessment by the Swiss agency were focused on the Wellenberg deposit for LILW in Switzerland, which has been never been built due to several reasons, although several investigations were conducted aimed at showing its feasibility.

Of the materials which make up the Swiss UILW repository for short-lived low- and intermediate-level wastes, around 95 weight percent consists of concrete, around 4% of steel and around 1 % of high molecular weight organic waste components.

We will present here the main conclusions of the redox assessment of the non-existing Wellenberg because the discussion on the redox active materials and the redox stages of the repository can be of relevance for the work we are undertaking within SFR 1.

Redox active materials in the repository (Neall 1994) were defined as:

- **Metals**, mainly steel of the containers, contained in the waste itself and used as concrete reinforcement. Other metals present in minor amounts are Al, Zn, zircaloy, inconel and Pb in the waste.
- **Cement**. In the assessment of the redox evolution of Wellenberg it is assumed that cement does not contribute to the oxidant consumption. The presence of iron in the cement composition is assumed to be in its highest oxidation state, so that in any case it would be possible for iron in the cement to be reduced but not oxidized. In some cases the oxidizing properties of cement have been used to state that the presence of cement imposes oxidizing conditions, although due to the small percentage of iron(III) in cement in comparison with the amount of steel, this is not very likely to impose an oxidizing environment.
- **Organics and other waste materials**. Cellulose, plastics and ion exchange resins present in the wastes can constitute a source of reducing capacity in the system as well as nutrients for microbes contributing to oxidant consumption. In the case of Wellenberg, ashes from the incineration of organic materials are also considered as likely to influence the redox state of the system due to their high content of remaining reduced carbon, although their effect is not considered in the assessment of the Eh evolution in the repository.

Despite highly uncertain, rates for anaerobic microbial degradation of organic materials in the repository in the order of 0.002 to 0.05 moles gas/kg.y for most organic materials and 0.05 to 0.7 moles gas/kg.y for cellulose have been considered. This means that after 10^3 or even 10^4 years not all the organic matter had been oxidised. Organic matter could last longer than steel and therefore it could contribute to the maintenance of reducing conditions in the repository at long-term through oxidant consumption.

- **Radiolytic oxygen**. According to Neall (1994) the amount of radiolytic oxygen produced is around $1.25.10^5$ moles during the first 500 years. This amount could oxidise 10.5 tonnes of steel to iron oxides over that period in the case this is the only process for oxygen consumption. Taking into account that the total amount of steel in the repository is around 100,000 tonnes, the presence of radiolytic oxygen is not predicted to have any important effect on the redox evolution of the repository.
- **Groundwater dissolved oxygen**. In the same study, it is said that the amount of dissolved oxygen, although being more important than that radiolytically generated, will not be very important due to the low groundwater fluxes

According to the modelling of the near field of the repository presented by Neall (1994) the redox conditions in the disposal caverns are mainly controlled by the corrosion of steel.

A first aerobic phase is defined in the repository, lasting for few decades and producing the consumption of all oxygen initially trapped in the repository until anoxia is reached. This oxygen consumption is mainly attributed to the corrosion of the metals present in the repository, oxidation of organic matter and of cellulose specifically. According to their results, an oxic period of 1–5 years length is assessed if steel oxidation is the only process accounting for oxygen consumption (total porosity initially filled with air); in the case of considering that oxygen is only used for Al oxidation, the oxic period would last for 3 years and in the case of considering also cellulose oxidation the duration of this stage will be reduced to 1.5 years.

Once the oxygen has been consumed, anaerobic corrosion of steel and other metal components is predicted to occur for several thousands of years; causing very reducing redox conditions in the system, until all metals in the repository have been corroded. Sharland and Newton (1989) assume that the time to reach very reducing environment is around 100 years, and the Eh would be around –700 mV, due to the conditions imposed by the generation of H_2 from anoxic metal corrosion. This fact is questioned in the Wellenberg assessment because of the time needed to reach equilibrium between hydrogen gas and water, and it is suggested that it is more likely that the redox potential is buffered by the Fe(II)/Fe(III) system, what will also keep the redox values in the reduced field.

After the exhaustion of the material susceptible of corrosion, the redox state is predicted to adjust gradually to that of the inflowing groundwater.

A3-6 Underground deposit for LILW in Konrad, Germany

The basis for the Safety Analyses/Safety Case for the Konrad disposal have been elaborated between 1977 and 1982. At that time, evolution of the near-field was only related to leach rates of waste forms and or sorption coefficients. Evolution of the redox state was not considered explicitly. Also the production, fate and behaviour of H_2 gas has been considered only with respect to advective processes (Kienzler B 2011, pers. comm.).

A3-7 Underground deposit for LILW in Gyenjou, Korea

Two alternative disposal methods, the rock cavern and the engineered vault disposal, have been considered, and the rock cavern type was determined in consideration of site conditions. Conceptual design studies and preliminary safety assessments for rock-cavern type were completed in 1993.

Construction started in April 2008 and in December 2010 KRWM commenced operation of the facility, accepting the first 1,000 drums of wastes there from the Ulchin plant. These will be held in outdoor storage until the underground repository itself (80~130m below ground) is commissioned in 2012.

A rock cavern type disposal facility initially scheduled to dispose of 100,000 waste packages (and ultimately 800,000 waste packages) was conceptualized. The current licensing application for a 100,000 waste package (waste volume of 35,200 m^3) facility was approved simultaneously for operation and construction. For 100,000 waste packages, the total radioactivity is about $5.63 \cdot 10^{15}$Bq. The disposal facility consists of six silos, and the capacity of each silo is approximately 16,000 drums.

The type and quantity of waste packages for each waste producer are reported in Park et al. (2009) although they consist of miscellaneous radioactive solid wastes, concentrates, spent resins, and cartridge filters. A large portion of solid wastes is compressed, but non-compressible miscellaneous radioactive solid wastes are kept in 200L drum without waste processing. Cement appears to be one of the main components used a matrix of the wastes although asphalt is also used in some cases. Waste containers are foreseen to be steel drums, concrete containers, HIC, and polyethylene containers with drums of of 200L and 320L capacity.

No assessment of the redox evolution of the repository has been conducted to our knowledge, although the information is slightly more difficult to find than in other cases, and we are still investigating on possibilities to get access to the information.

A3-8 Assessment of the redox evolution of a generic underground deposit for LILW developed for the NDA, UK

The generic concept for the underground repository of LILW developed in the UK assumes the emplacement of the wastes in a similar manner as the SFR 1, by using steel drums/containers and a cementitious-based backfill. Within the assessments undertaken by the NDA, the redox evolution of the near field of the repository has been modelled by Grivé et al. (2011).

The model assumes a heterogeneous repository, formed by a homogenous mixture of ILW or ILW+LLW waste isolated from the NRVB backfill by a stainless steel container. The evolution of the Eh is modelled in a batch fully saturated system. Temperature is considered equal to 25°C. Microbial activity is not occurring in the repository. Initially, both backfill and waste pore water are considered to be in equilibrium with $O_2(g)$ atmospheric pressure (0.21 atm).

The reference case is modelled in two stages. In Stage I, the Eh evolution is modelled without the inclusion of radionuclides. Stage I model comprises the assessment of the Eh evolution in the waste, the Eh evolution in the backfill and the assessment of the Eh obtained if both waste and backfill pore waters mix or if waste pore water is mixed with regional pore water. Stage II models the repository Eh evolution considering the presence of radionuclides.

Stage I model concludes that waste Eh evolution can be considered representative of the repository Eh evolution. This evolution is characterized by the identification of three redox buffer periods: Fe^{2+}/goethite equilibrium, goethite to magnetite transformation and Fe(0)/magnetite equilibrium with $H_2(g)$ generation. Stage II model conclusions are that changes in radionuclide redox states slightly influence the Eh evolution of the system in the first 50 years, and that only the transformation of $CaU_2O_7{:}3H_2O$ to $UO_2(s)$ may control the Eh value for a significant period of time.

Sensitivity analyses have been done to analyse the influence of different factors on the repository Eh evolution: vault and repository features (SILW or UILW vaults, groundwater composition), steel corrosion properties (rate, surface area, corrosion products), kinetically hindered processes (S(VI) to S(-II) reduction, chemical effect of $H_2(g)$) or radionuclide sorption or organic aqueous complexation.

Sensitivity cases results show that steel corrosion properties greatly influence the timescale of the different redox buffer periods identified but do not affect the achieved Eh value. Moreover, they also show that the chemical role of $H_2(g)$ is an important key parameter in determining both the repository long-term Eh value and the time needed to achieve it. Important changes of the calculated Eh in the different redox buffer periods are mainly linked to changes in the pH of the pore water.

Appendix 4

Algorithm of cellulose degradation implemented in PHREEQC

In this section we describe in detail the algorithm of cellulose degradation we have used in the modelling exercise reported in this document.

The conceptual model on which this algorithm is based assumes that:

- Under alkaline and oxic conditions, cellulose is degraded to acetate and the degradation rate is microbially controlled by O_2-consuming bacteria.
- Under alkaline and anoxic but still biotic conditions, cellulose is degraded to ISA and to acetate and the degradation rate is microbially controlled by Fe(III) and S(VI)-consumer bacteria.
- Under alkaline abiotic conditions, cellulose is degraded to ISA and acetate and the degradation rate is controlled according to the mechanism proposed in Glaus and Van Loon (2008).
- Under neutral conditions, ISA is not produced by cellulose degradation.

The procedure followed in the algorithm development has consisted on:

1. Definition of reactions taking place at each step.
2. Definition of the kinetic rate to be used in each step.

A4-1 Definition of reactions

It is assumed that reacting cellulose is a monomer of cellulose already hydrolysed (r. A4-1). Under oxic conditions, the monomer of cellulose is degraded to acetate and to CO_2, according to r. A4-2, which can be expressed as the semi reaction r. A4-3.

$(C_6H_{10}O_5)_n + H_2O \rightarrow n(C_6H_{12}O_6)$ r. A4-1

$C_6H_{12}O_6 + O_2 \rightarrow 2\ CH_3COOH + 2\ CO_2 + 2H_2O$ r. A4-2

$C_6H_{12}O_6 + 2\ H_2O \rightarrow 2\ CH_3COOH + 2\ CO_2 + 8\ H^+ + 8\ e^-$ r. A4-3

Under anoxic and alkaline conditions, cellulose is degraded to ISA. It is considered that the degradation of a monomer of cellulose to ISA implies an oxidation of an aldehyde type group of cellulose to a carboxilic acid but also a reorganisation of the molecule Figure A4-1). The simplified reaction can be expressed as r. A4-4. However, as it is known that ISA is not the only product of cellulose degradation (Glaus et al. 1999), in the algorithm we have supposed that under alkaline and anoxic conditions, cellulose degrades to ISA and to acetate. From experimental data, we have considered that 80% of cellulose degrades to ISA and 20% to acetate. r. A4-5 expresses the final reaction of cellulose degradation considered under anoxic and alkaline conditions.

$C_6H_{12}O_6 \rightarrow isa + 2\ e^-$ r. A4-4

$C_6H_{12}O_6 + 0.40\ H_2O \rightarrow 0.8\ isa + 0.4\ CH_3COOH + 0.4\ CO_2 + 1.6\ H^+ + 3.2\ e^-$ r. A4-5

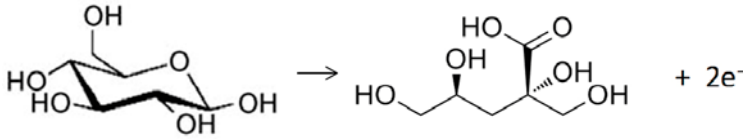

Figure A4-1. *Reaction showing the oxidation of a cellulose monomer unit to ISA.*

A4-2 Definition of kinetic rates

Degradation of cellulose proceeds according to Eq. A4-1–A4-3 under biotic conditions (rates given in mol dm^{-3} s^{-1}).

For $[O_2] > 10^{-6}$ M

$$rate_{cellulose}^{biotic,O_2} = [Biomass_O]\, K_{cellulose}^{O_2} \frac{[O_2]}{k_{1/2}^{cellulose,O_2} + [O_2]} \quad \text{Eq. A4-1}$$

For $[O_2] < 10^{-6}$ M and $[Fe(III)] > 10^{-6}$ M

$$rate_{cellulose}^{biotic,Fe(III)} = [Biomass_{Fe}]\, K_{cellulose}^{Fe(III)} \frac{[Fe(III)]}{k_{1/2}^{cellulose,Fe(III)} + [Fe(III)]} \quad \text{Eq. A4-2}$$

For $[O_2]$, $[Fe(III)] < 10^{-6}$ M and $[S(VI)] > 10^{-6}$ M

$$rate_{cellulose}^{biotic,S(VI)} = [Biomass_S]\, K_{cellulose}^{S(VI)} \frac{[S(VI)]}{k_{1/2}^{cellulose,S(VI)} + [S(VI)]} \quad \text{Eq. A4-3}$$

Under abiotic and alkaline conditions, the rate provided by Glaus and Van Loon (2008) has been used in the calculations. This rate is shown in Eq. A4-4, where $(celdeg)_t$ is the fraction of cellulose degraded as a function of time, k_h a normalized first-order reaction rate constant of the mid-chain scission, $(G_r)_0$ is the number of end reducing groups (estimated as the reciprocal of the initial degree of polymerisation) and k_l and k_t the reaction rate constants related to the peeling-off process.

$$(celdeg)_t = 1 + e^{-k_h t}\left[\frac{k_l}{k_t}(G_r)_0\left(1 - e^{-k_t t}\right) - 1\right] \quad \text{Eq. A4-4}$$

Glaus and Van Loon (2008) studied the degradation of four different cellulosic materials (Aldrich cellulose, tissue, cotton and paper) under alkaline and anaerobic conditions over a period of 12 years and at 25°C in an artificial cement pore water. This work was the continuation of previous studies (Van Loon and Glaus 1998, Van Loon et al. 1999) showing data for 3 years.

Glaus and Van Loon (2008) observed that cellulose degradation proceeds according to:

1. A fast reaction phase dominated by the conversion of a terminal glucose monomeric unit to ISA
2. A very slow reaction phase during which ISA was also produced.

Glaus and Van Loon (2008) showed that previous models on cellulose degradation under alkaline conditions did not properly describe the evolution because they predicted that cellulose degradation stopped after some years. Experimental data of Glaus and Van Loon (2008) demonstrated that after the short period with a fast rate controlled by the peeling-off process, there was a slower process controlling the rate of cellulose degradation. The degradation process did not stop but was slower. They could not distinguish the origin of this second process, although they postulate two different alternatives:

- Mid-chain scission of the polysaccharide chain combined with the peeling-off process.
- Temporary transition of crystalline to amorphous cellulose structures.

They derived Eq. A4-4 and used values of Table A4-1 to fit their experimental data (Figure A4-2).

Previous to the use of Eq. A4-4 in the algorithm of cellulose, we implemented Eq. A4-4 in PHREEQC to reproduce the results of Glaus and Van Loon (2008). As can be seen in Figure A4-2 results obtained with PHREEQC satisfactorily reproduced the experimental data and the analytical solution of Eq. A4-4 of Glaus and Van Loon (2008).

After testing the good behaviour of Eq. A4-4 in PHREEQC we implemented the whole system in the cellulose algorithm to calculate cellulose degradation (Figure A4-3). The system has been completed by allowing the precipitation of $Ca(HISa)_2(cr)$ in case it becomes oversaturated.

Table A4-1. Best-fit parameters for fitting the experimental data on alkaline degradation of cellulose (from Glaus and Van Loon 2008).

Cellulose type	$(G_r)_0$	$k_1(h^{-1})$	$k_t(h^{-1})$	$k_h(h^{-1})$
Aldrich Cellulose	8.5×10^{-3}	$(8.8\pm0.4)\times10^{-3}$	$(3.2\pm0.2)\times10^{-4}$	*
Tela tissues	9.0×10^{-4}	$(1.0\pm0.1)\times10^{-2}$	$(2.9\pm0.5)\times10^{-4}$	$(1.0\pm0.2)\times10^{-7}$
Cotton	5.6×10^{-4}	$(2.0\pm0.3)\times10^{-3}$	$(3.3\pm0.5)\times10^{-4}$	$(2.9\pm0.3)\times10^{-8}$
Paper	3.5×10^{-3}	$(4.3\pm1.3)\times10^{-3}$	$(4.3\pm1.5)\times10^{-4}$	$(1.6\pm0.5)\times10^{-7}$

* No value determined because the uncertainty was larger than the value itself ($(1.0\pm0.2)\cdot10^{-7}\ h^{-1}$).

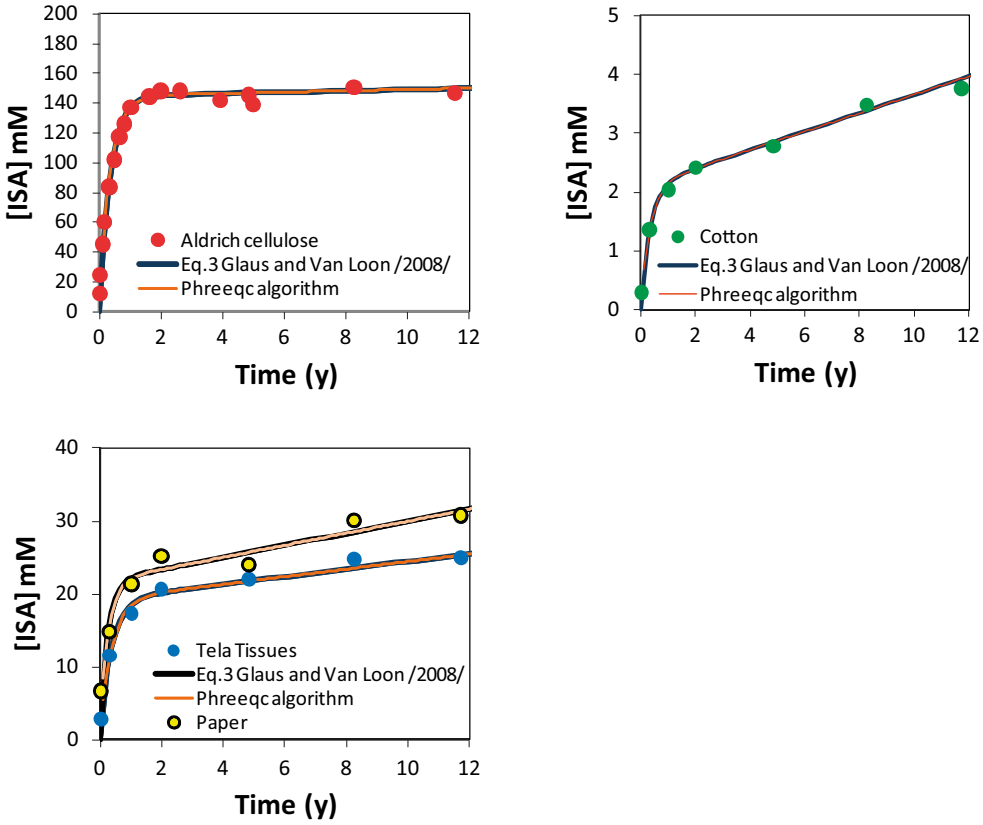

Figure A4-2. Experimental data (dots) reported in Glaus and Van Loon (2008) of concentration of ISA generated due to cellulose degradation under anoxic and alkaline conditions, for the four types of cellulosic materials used in the experiment. Lines represent the analytical solution of Eq. A4-4 (in black) and the concentrations calculated with the code PHREEQC (in red). Values of Table A4-1 are used in the calculations.

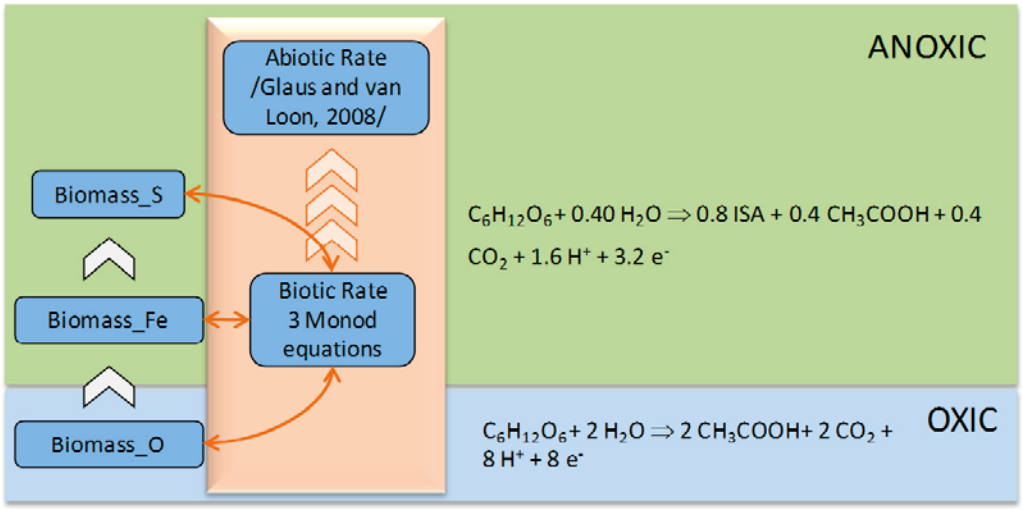

Figure A4-3. *Main outline of the algorithm implemented in PHREEQC for cellulose degradation.*

Appendix 5

Results for all cases

A5-1 Very short term results. Steel cases. R.15, R.16 and S.13 waste package types

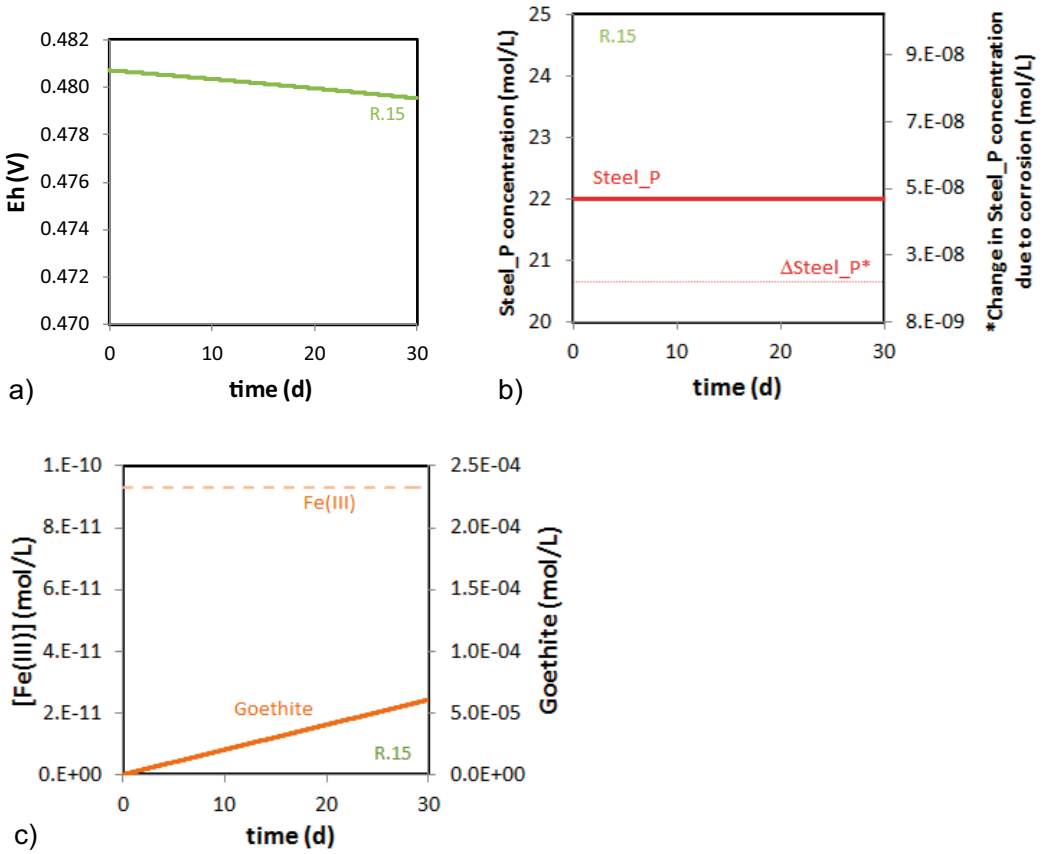

Figure A5-1. *a) Eh evolution of R.15 package during the very short term period. b) Evolution of the concentration of C-Steel and of the C-steel corroded in each time step. c) Evolution of Fe(III) and goethite concentration during the very short term period.*

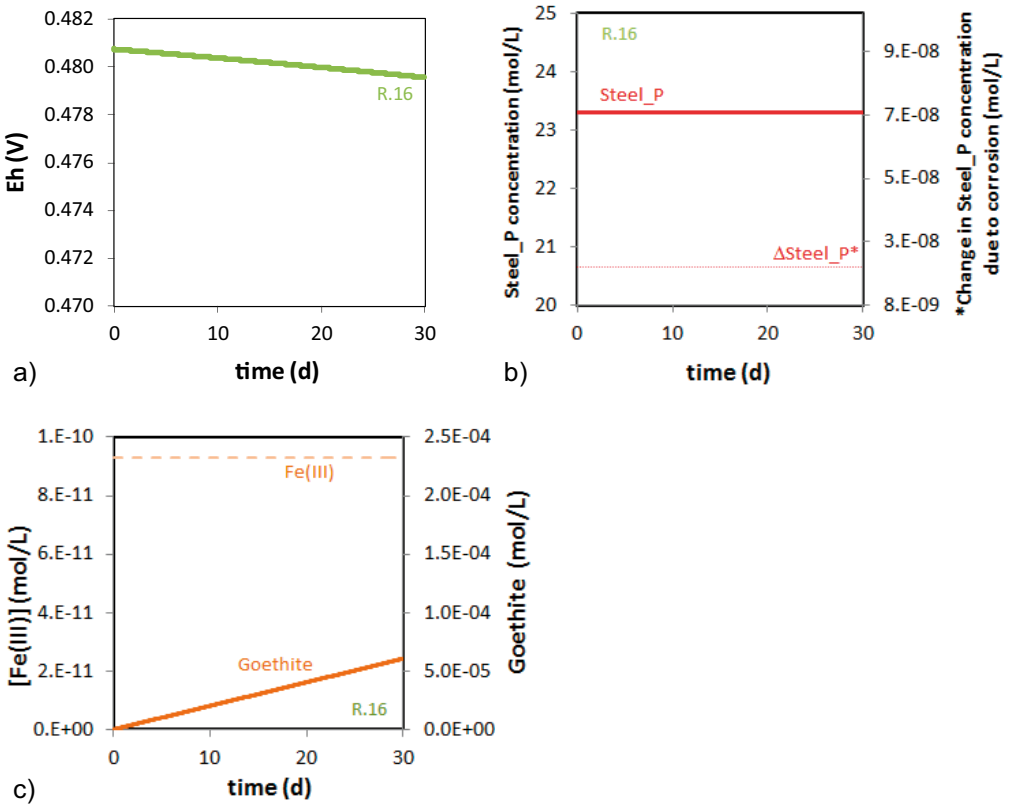

Figure A5-2. *a) Eh evolution of R.16 package during the very short term period. b) Evolution of the concentration of C-Steel and of the C-steel corroded in each time step. c) Evolution of Fe(III) and goethite concentration during the very short term period.*

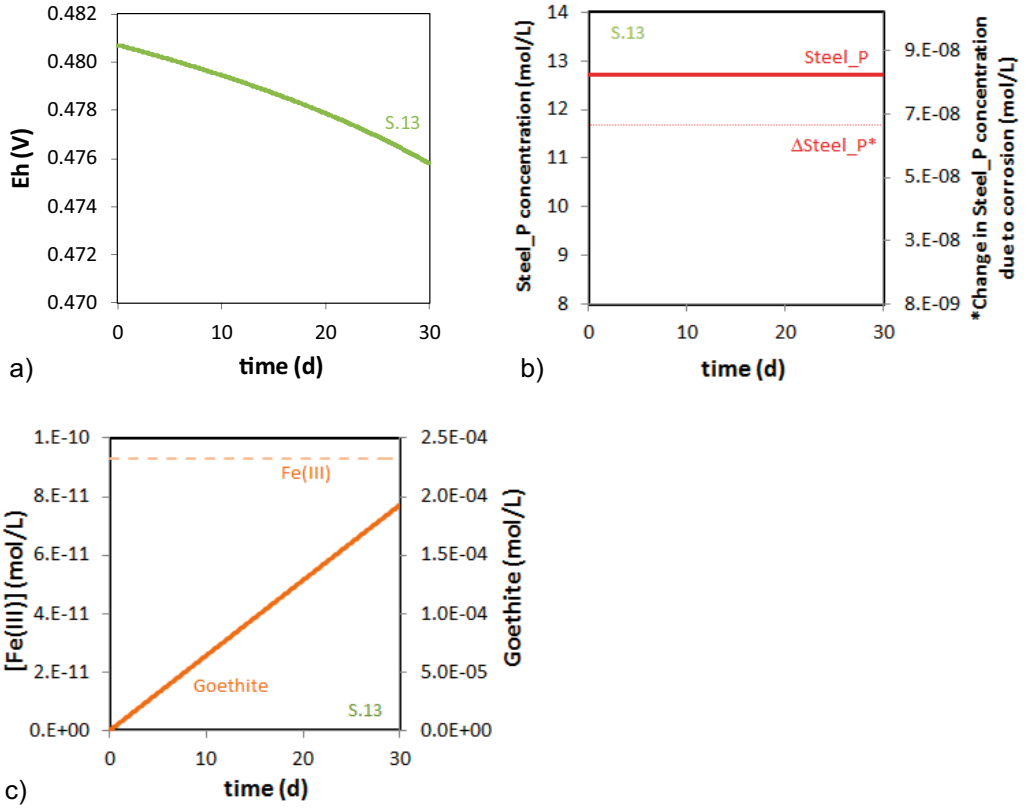

Figure A5-3. *a) Eh evolution of S.13 package during the very short term period. b) Evolution of the concentration of C-Steel and of the C-steel corroded in each time step. c) Evolution of Fe(III) and goethite concentration during the very short term period.*

A5-2 Very short term results. Steel and organic matter cases. O.02, R.01 and B.07_O.07 waste package types.

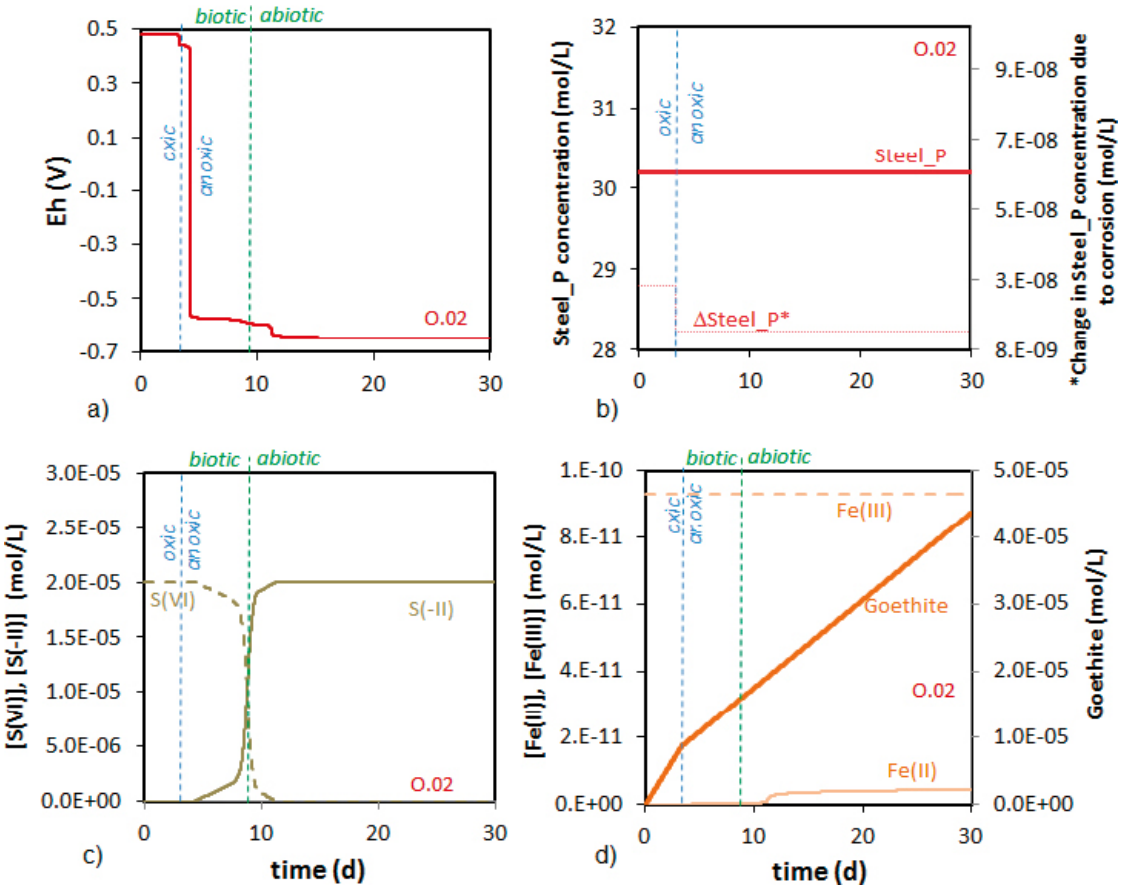

Figure A5-4. *Very short term results for O.02. Temporal evolution of a) Eh; b) concentration of C-Steel and of the C-steel corroded in each time step; c) S(-II) and S(VI) total aqueous concentration; d) goethite, Fe(II) and Fe(III) aqueous concentration.*

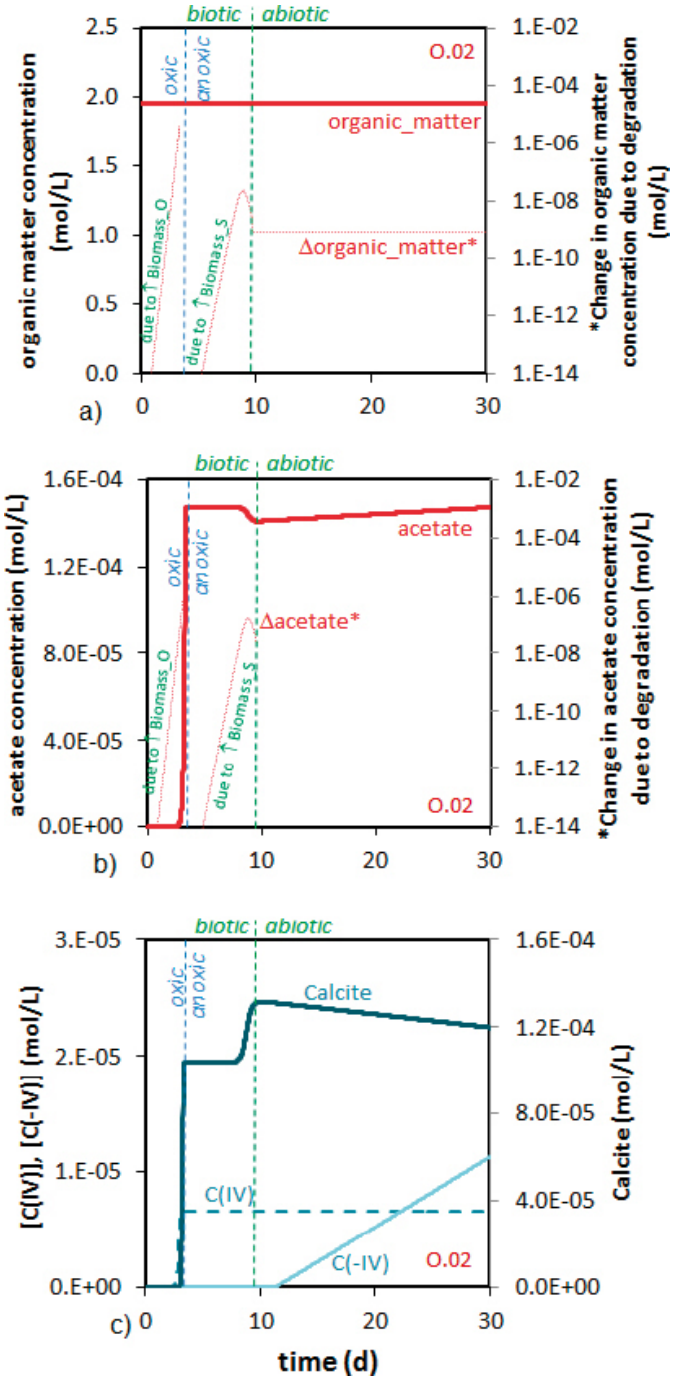

Figure A5-5. *Very short term results for O.02. Temporal evolution of a) organic matter concentration and of organic matter degraded in each time step; b) acetate concentration and of acetate degraded in each time step; c) calcite, and aqueous carbonate and methane concentration.*

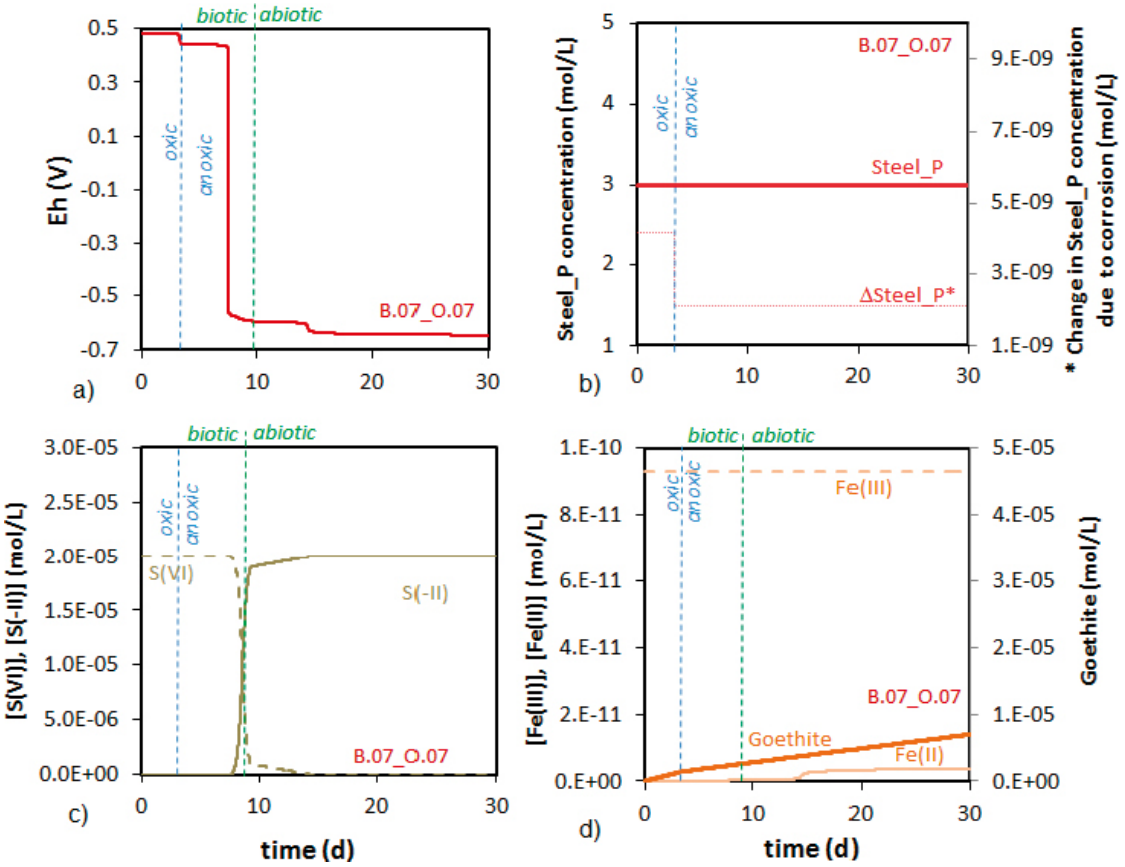

Figure A5-6. *Very short term results for B.07_O.07. Temporal evolution of a) Eh; b) concentration of C-Steel and of the C-steel corroded in each time step; c) S(-II) and S(VI) total aqueous concentration; d) goethite, Fe(II) and Fe(III) aqueous concentration.*

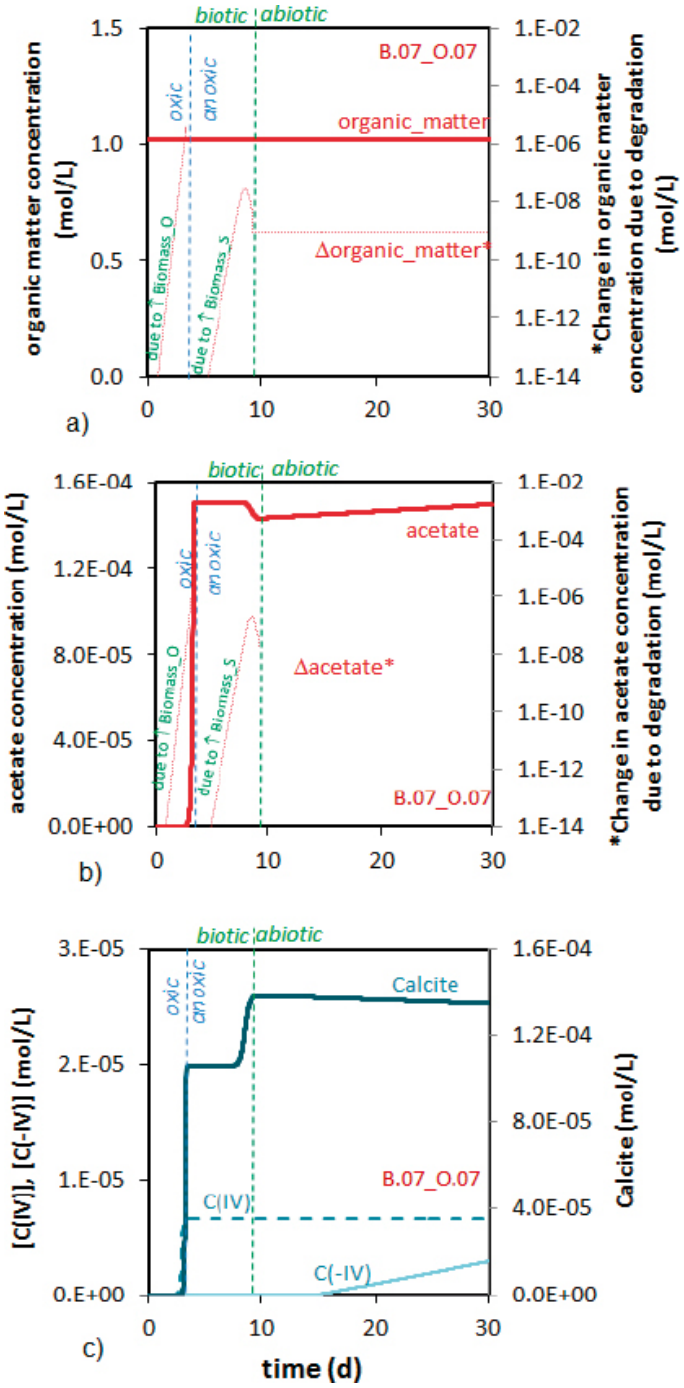

Figure A5-7. *Very short term results for B.07_O.07. Temporal evolution of a) organic matter concentration and of organic matter degraded in each time step; b) acetate concentration and of acetate degraded in each time step; c) calcite, and aqueous carbonate and methane concentration.*

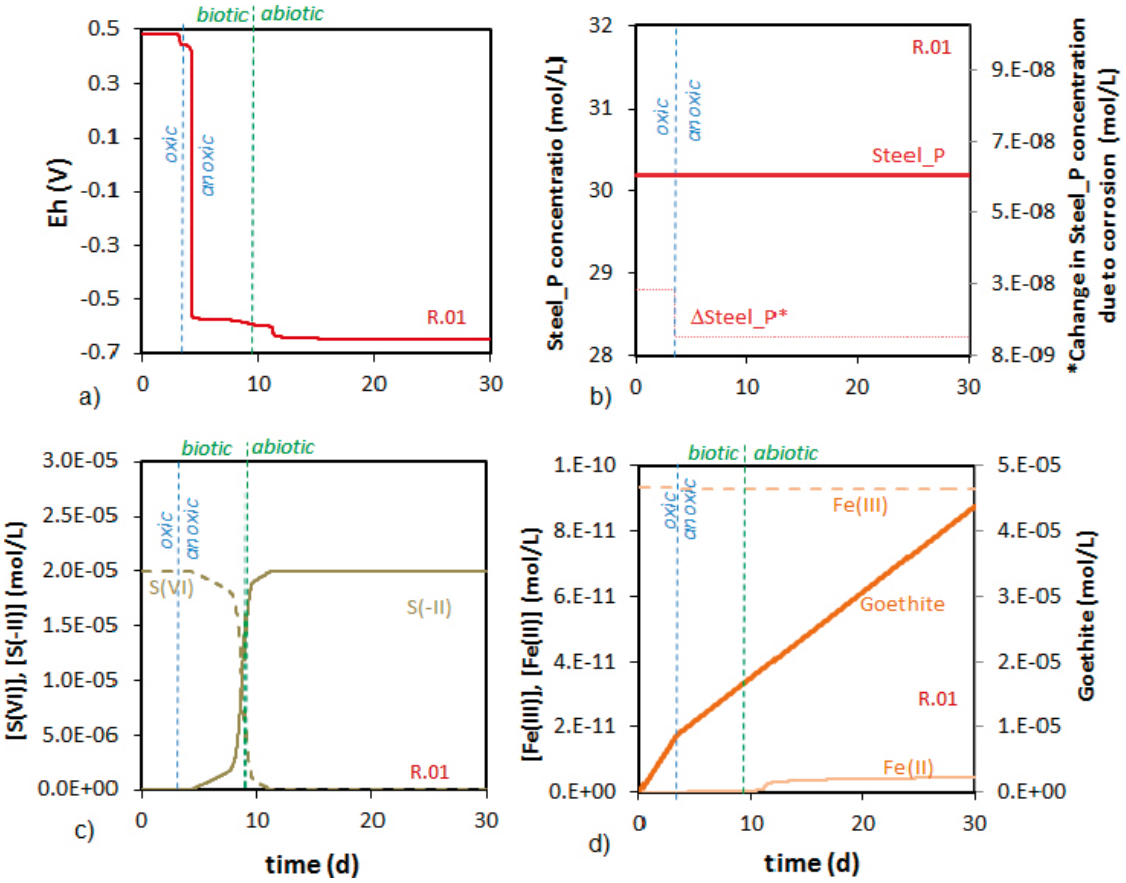

Figure A5-8. *Very short term results for R.01. Temporal evolution of a) Eh; b) concentration of C-Steel and of the C-steel corroded in each time step; c) S(-II) and S(VI) total aqueous concentration; d) goethite, Fe(II) and Fe(III) aqueous concentration.*

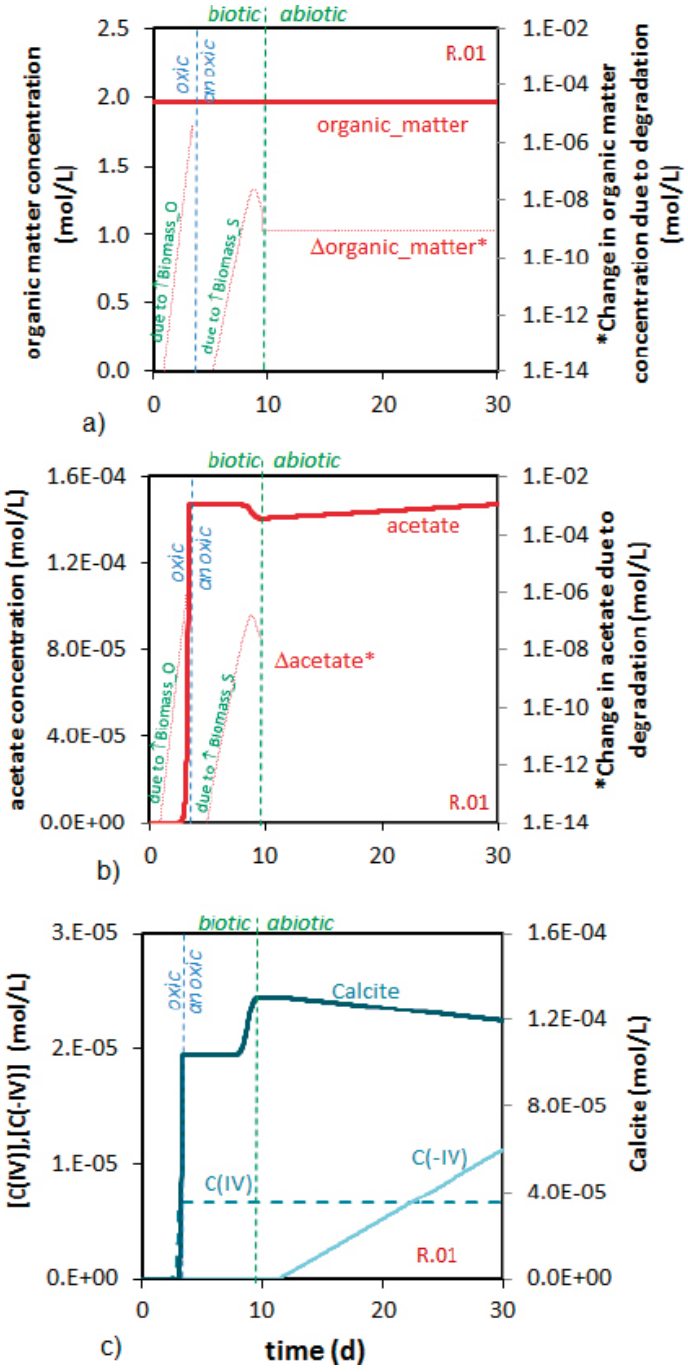

Figure A5-9. *Very short term results for R.01. Temporal evolution of a) organic matter concentration and of organic matter degraded in each time step; b) acetate concentration and of acetate degraded in each time step; c) calcite, and aqueous carbonate and methane concentration.*

A5-3 Very short term results. Steel and bitumen cases. B.06, F.18. F.05 and F.17 waste package types.

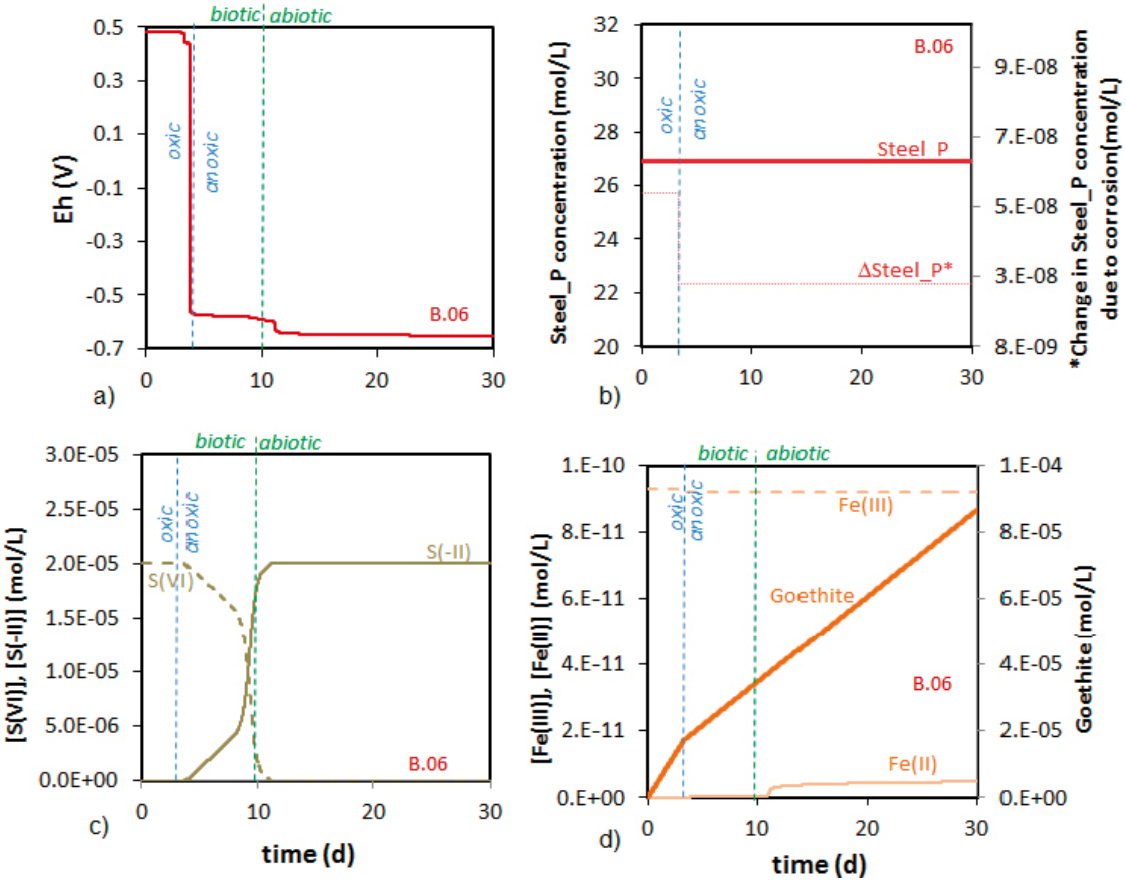

Figure A5-10. *Very short term results for B.06. Temporal evolution of a) Eh; b) concentration of C-Steel and of the C-steel corroded in each time step; c) S(-II) and S(VI) total aqueous concentration; d) goethite, Fe(II) and Fe(III) aqueous concentration.*

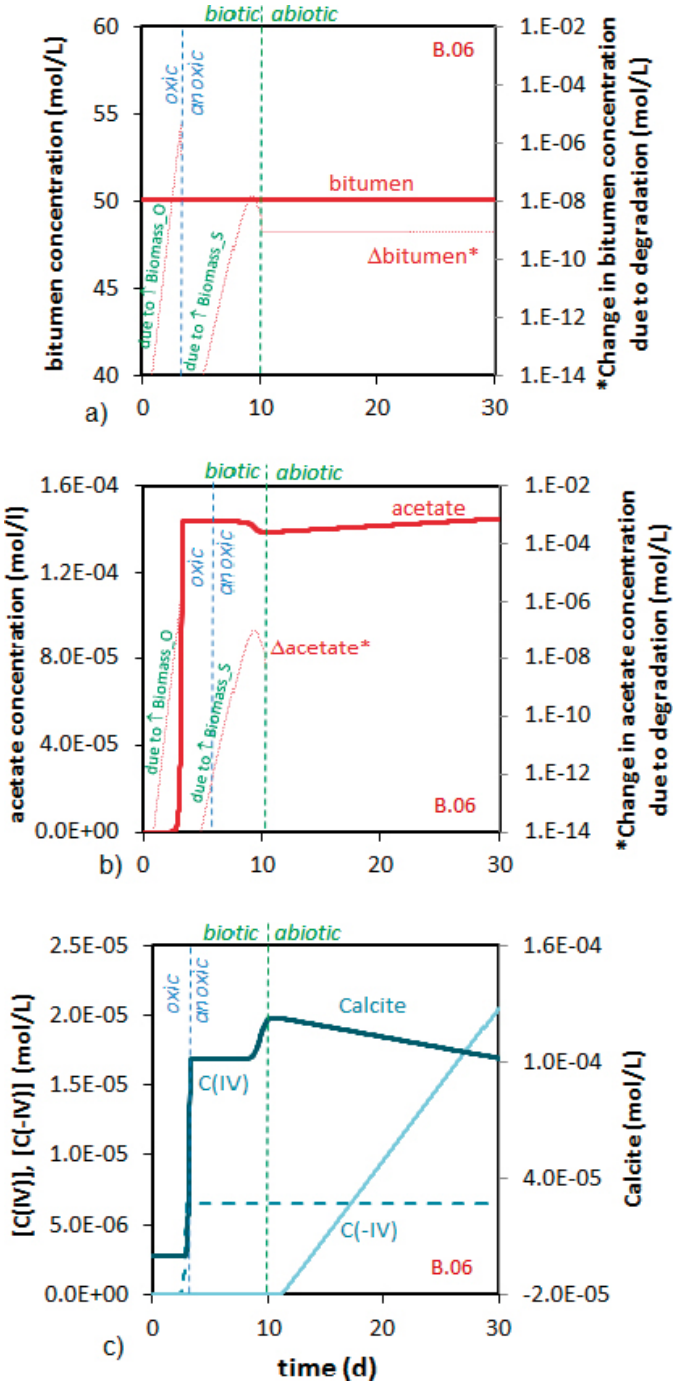

Figure A5-11. *Very short term results for B.06. Temporal evolution of a) organic matter concentration and of organic matter degraded in each time step; b) acetate concentration and of acetate degraded in each time step; c) calcite, and aqueous carbonate and methane concentration.*

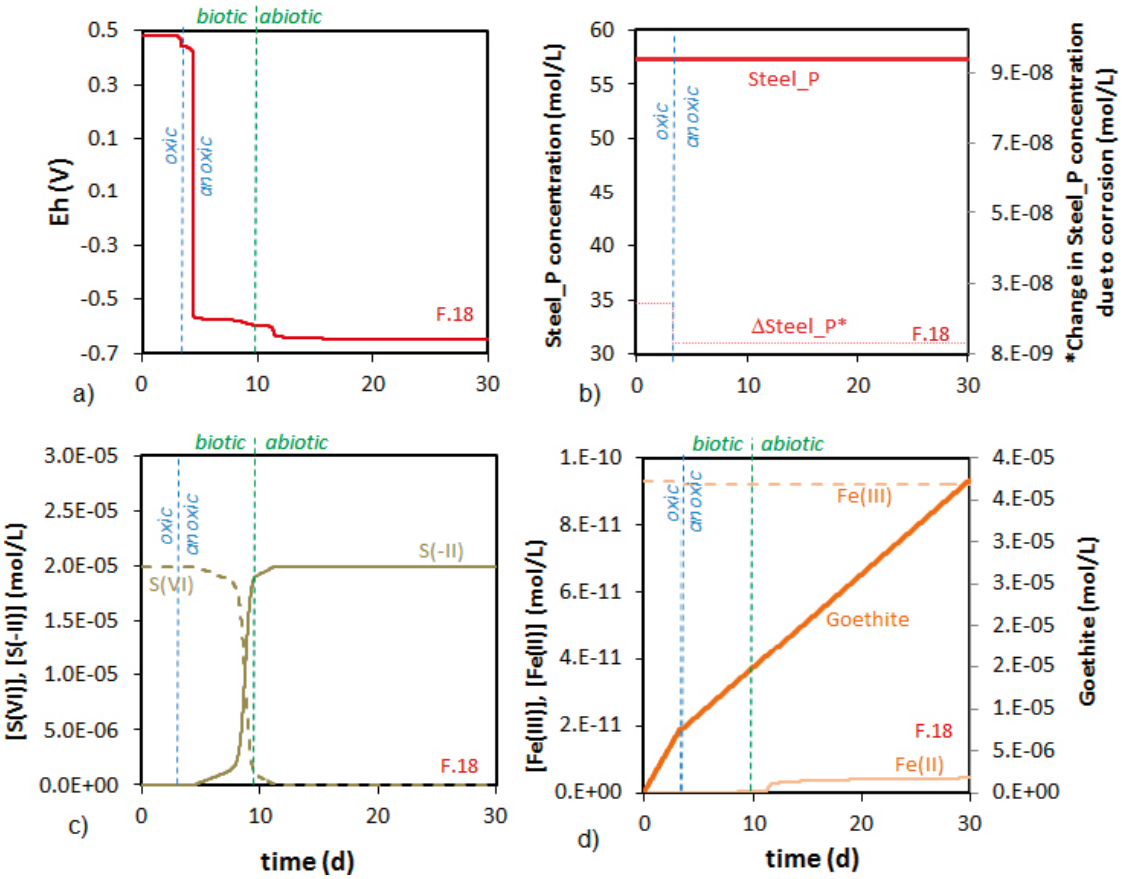

Figure A5-12. *Very short term results for F.18. Temporal evolution of a) Eh; b) concentration of C-Steel and of the C-steel corroded in each time step; c) S(-II) and S(VI) total aqueous concentration; d) goethite, Fe(II) and Fe(III) aqueous concentration.*

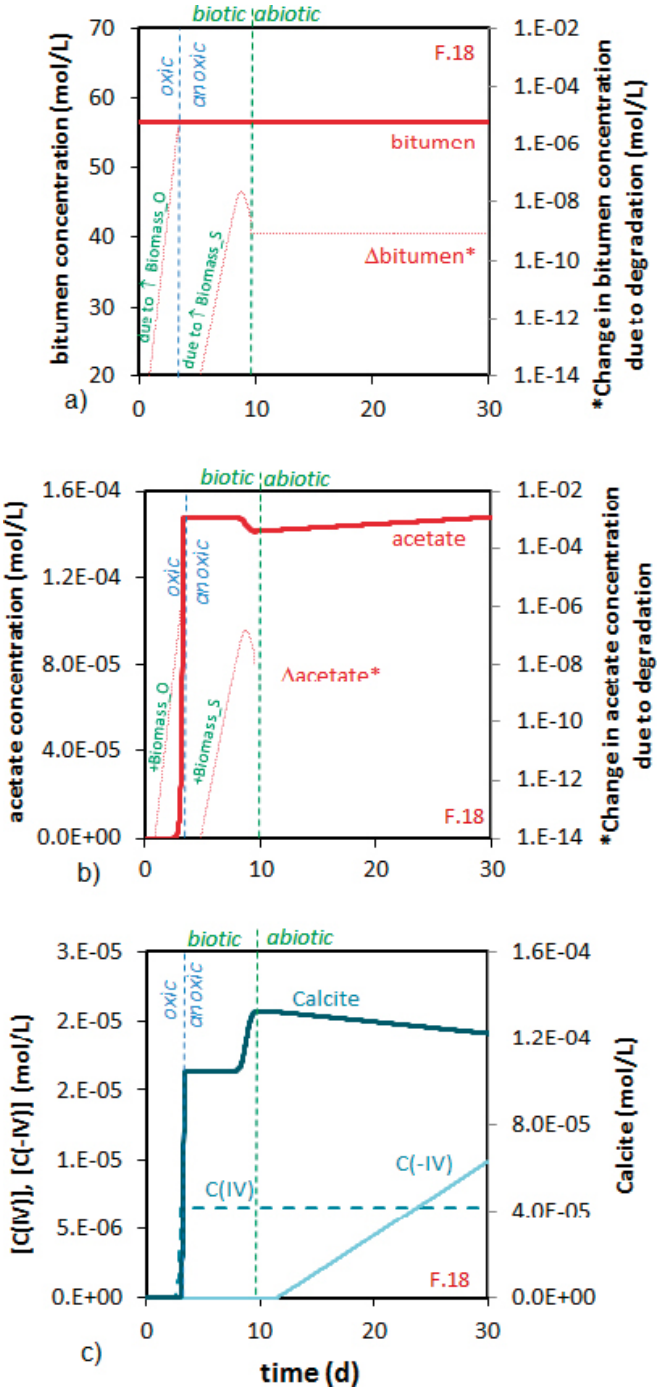

Figure A5-13. *Very short term results for F.18. Temporal evolution of a) organic matter concentration and of organic matter degraded in each time step; b) acetate concentration and of acetate degraded in each time step; c) calcite, and aqueous carbonate and methane concentration.*

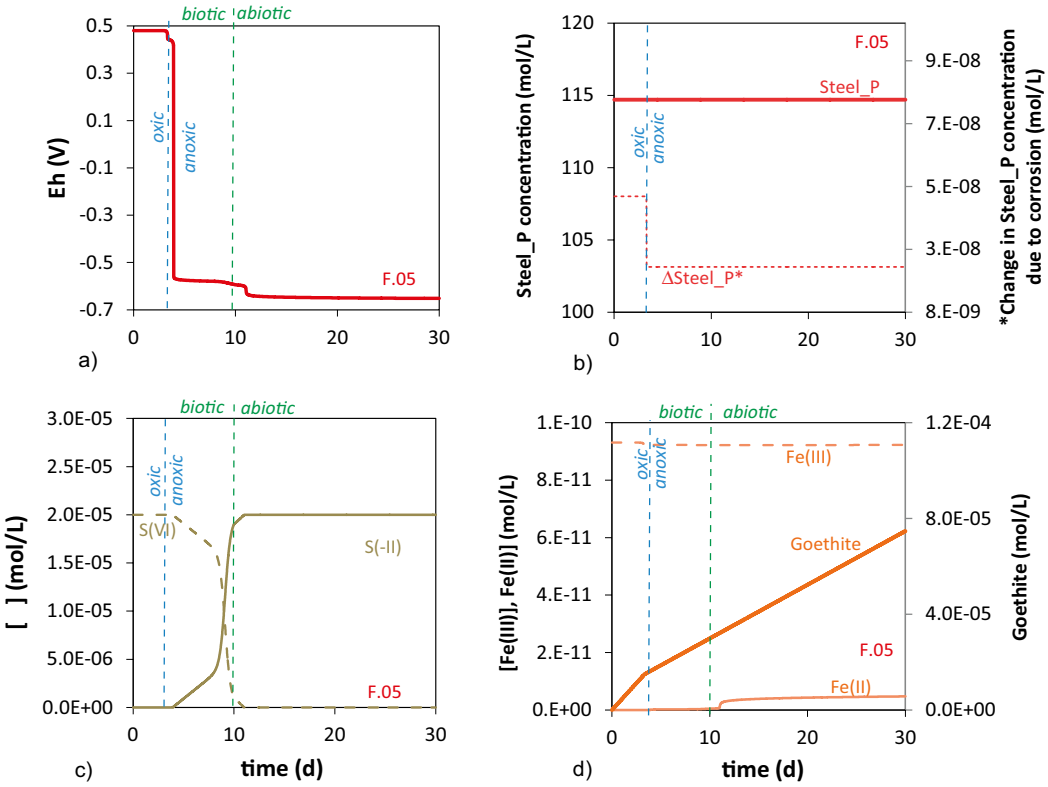

Figure A5-14. *Very short term results for F.05. Temporal evolution of a) Eh; b) concentration of C-Steel and of the C-steel corroded in each time step; c) S(-II) and S(VI) total aqueous concentration; d) goethite, Fe(II) and Fe(III) aqueous concentration.*

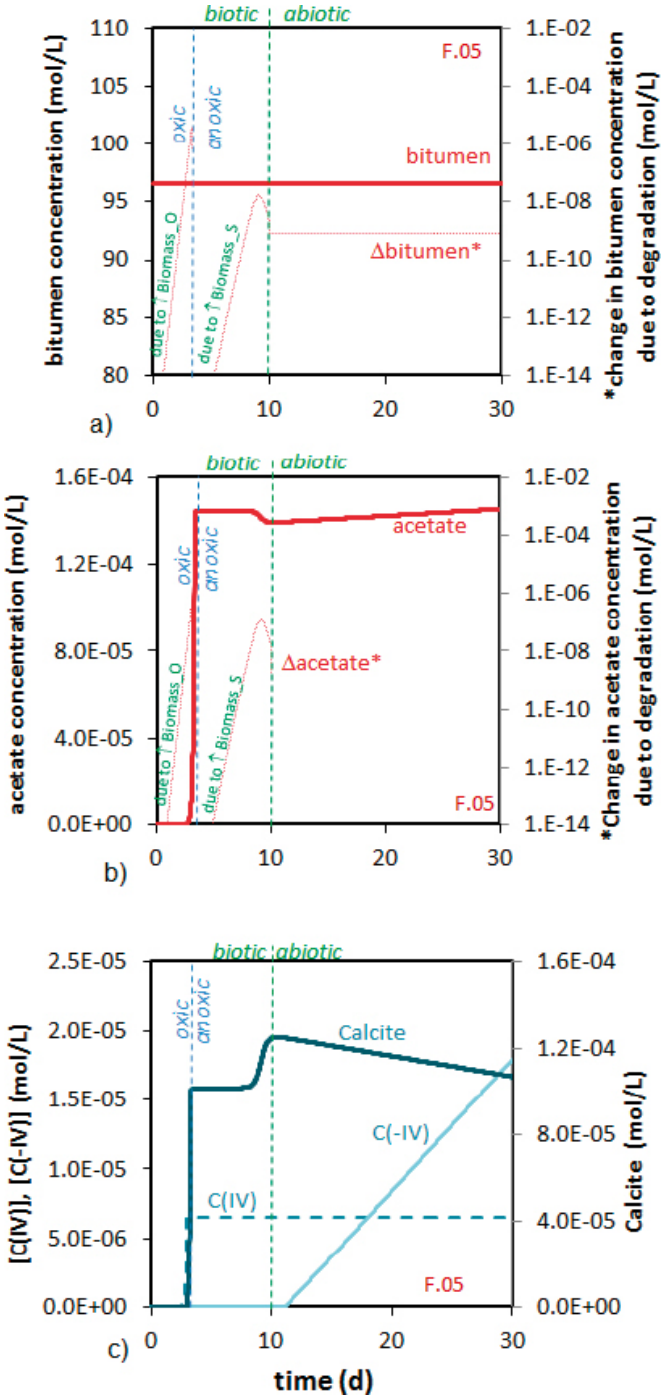

Figure A5-15. *Very short term results for F.05. Temporal evolution of a) organic matter concentration and of organic matter degraded in each time step; b) acetate concentration and of acetate degraded in each time step; c) calcite, and aqueous carbonate and methane concentration.*

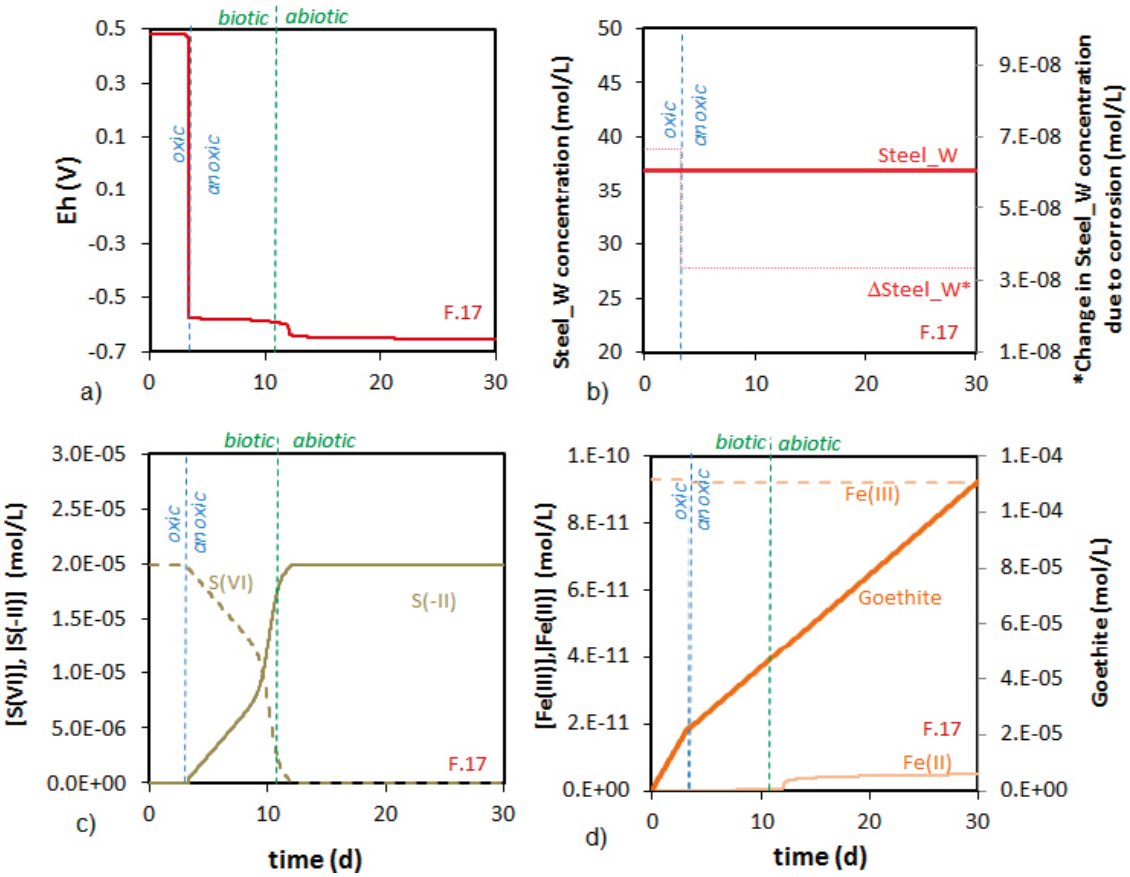

Figure A5-16. *Very short term results for F.17. Temporal evolution of a) Eh; b) concentration of C-Steel and of the C-steel corroded in each time step; c) S(-II) and S(VI) total aqueous concentration; d) goethite, Fe(II) and Fe(III) aqueous concentration.*

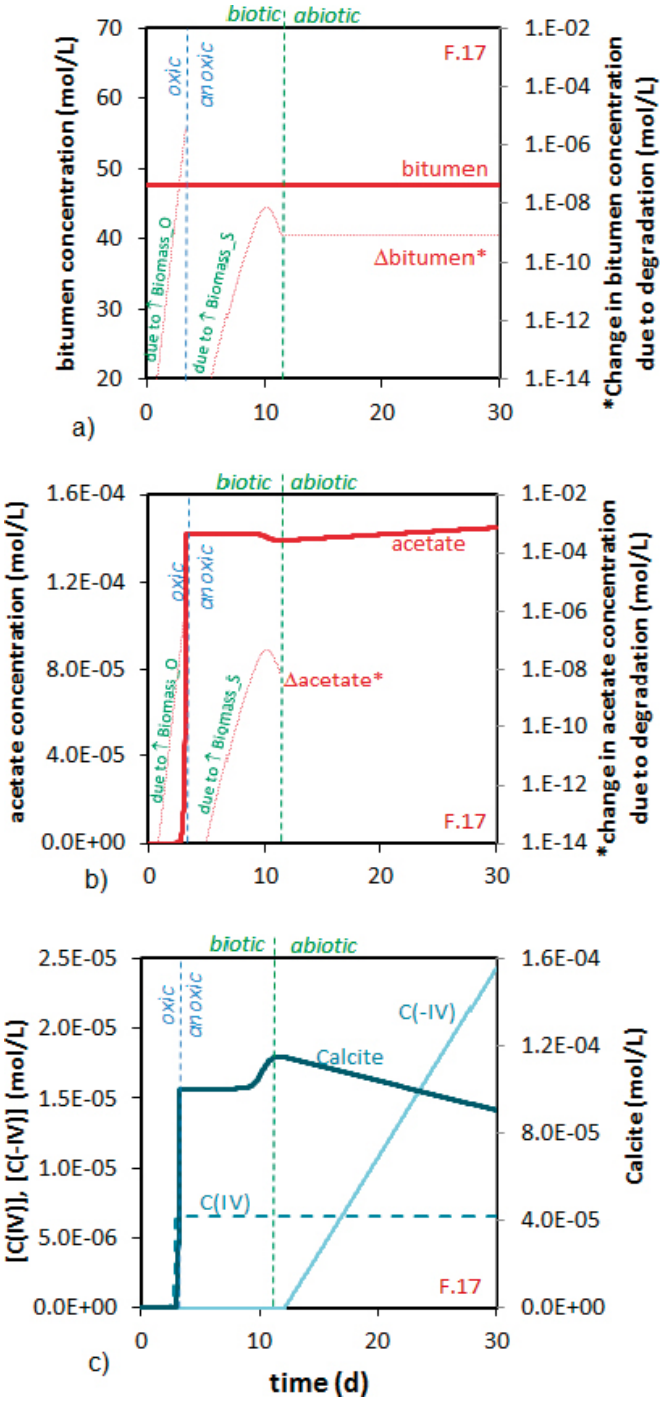

Figure A5-17. *Very short term results for F.17. Temporal evolution of a) organic matter concentration and of organic matter degraded in each time step; b) acetate concentration and of acetate degraded in each time step; c) calcite, and aqueous carbonate and methane concentration.*

A5-4 Very short term results. Steel and cellulose cases with bitumen or organic matter. O.23, F.23, B.05 and O.12 waste package types.

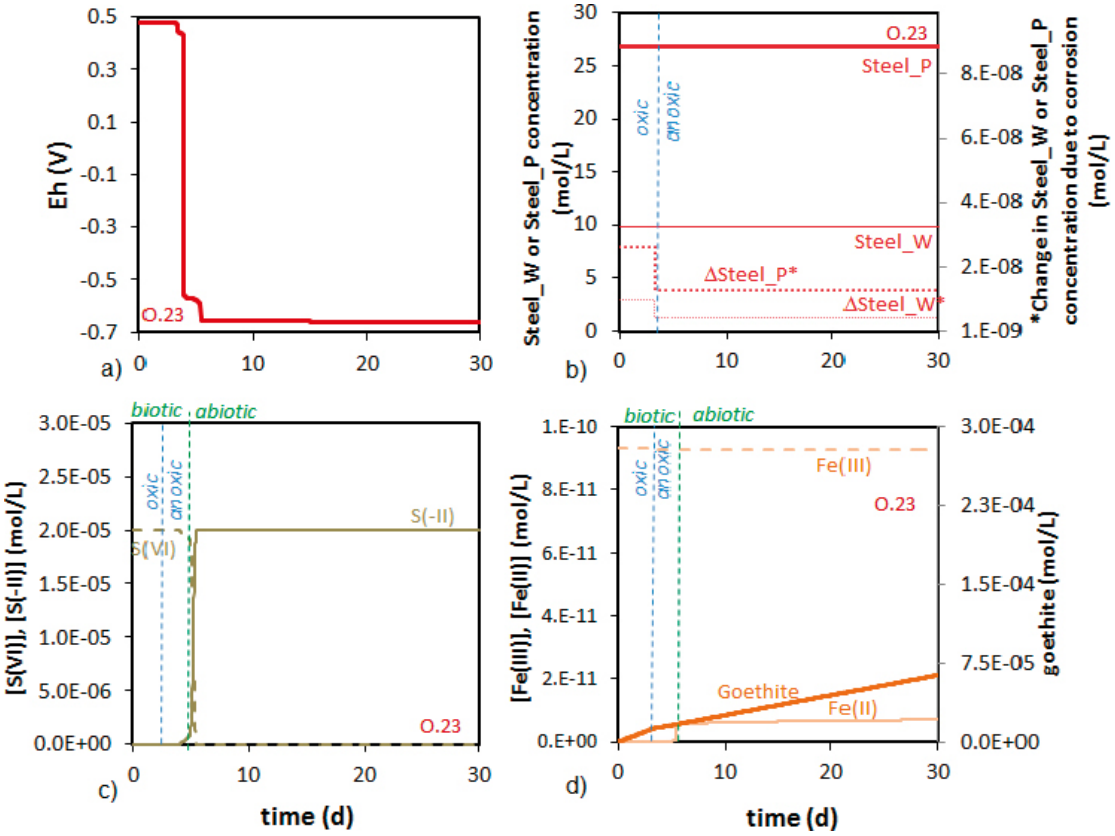

Figure A5-18. Very short term results for O.23. Temporal evolution of a) Eh; b) concentration of C-Steel and of the C-steel corroded in each time step; c) S(-II) and S(VI) total aqueous concentration; d) goethite, Fe(II) and Fe(III) aqueous concentration.

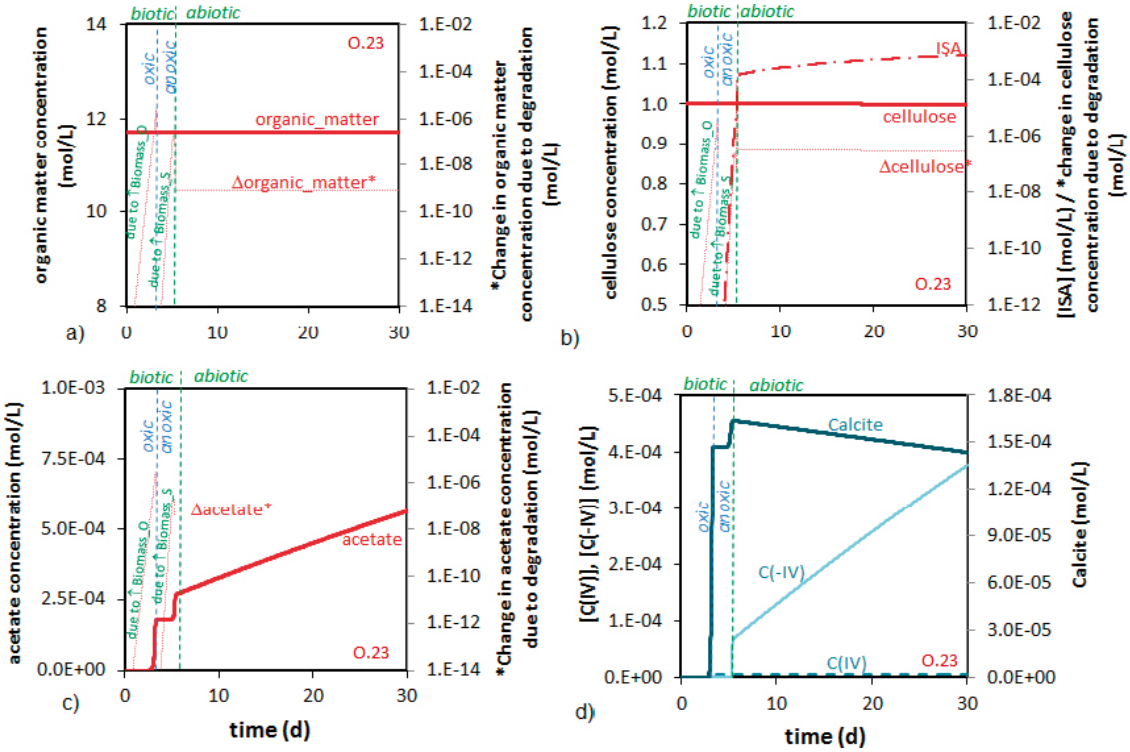

Figure A5-19. *Very short term results for O.23. Temporal evolution of a) organic matter concentration and of organic matter degraded in each time step; b) cellulose and ISA aqueous concentration and cellulose degraded in each time step; c) acetate concentration and of acetate degraded in each time step; d) calcite, and aqueous carbonate and methane concentration.*

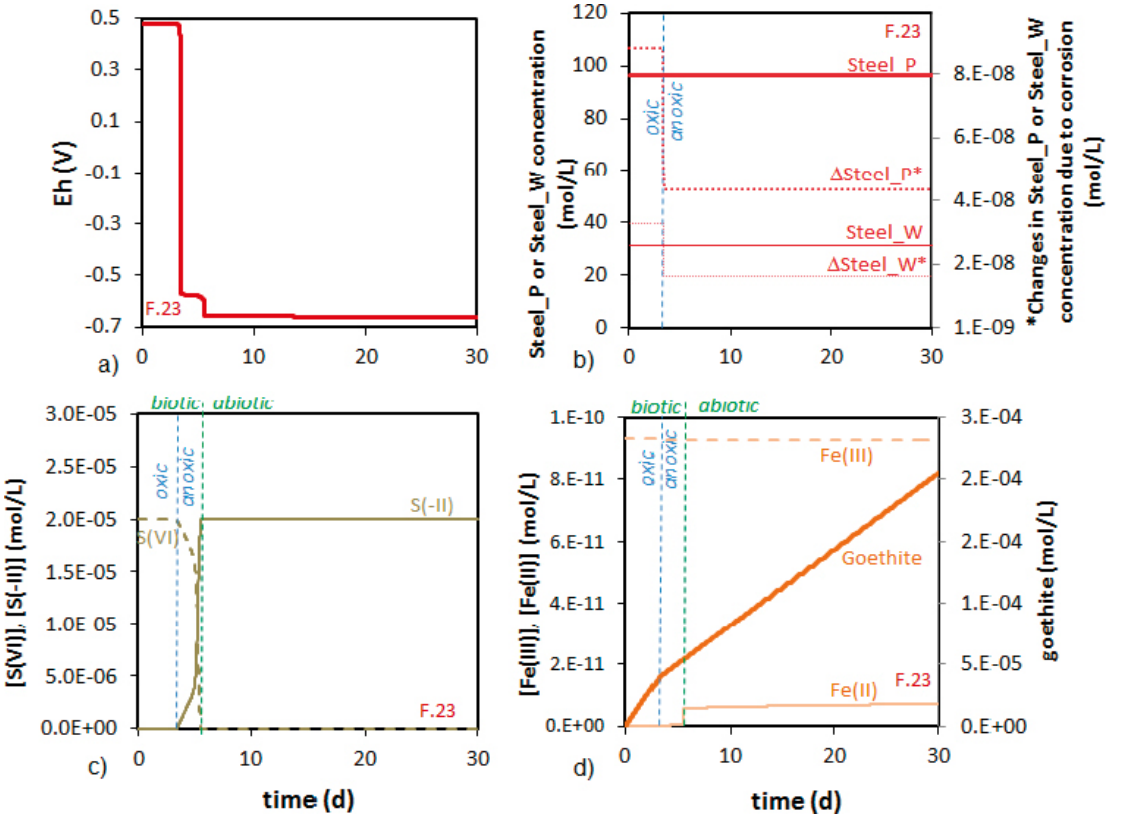

Figure A5-20. *Very short term results for F.23. Temporal evolution of a) Eh; b) concentration of C-Steel and of the C-steel corroded in each time step; c) S(-II) and S(VI) total aqueous concentration; d) goethite, Fe(II) and Fe(III) aqueous concentration.*

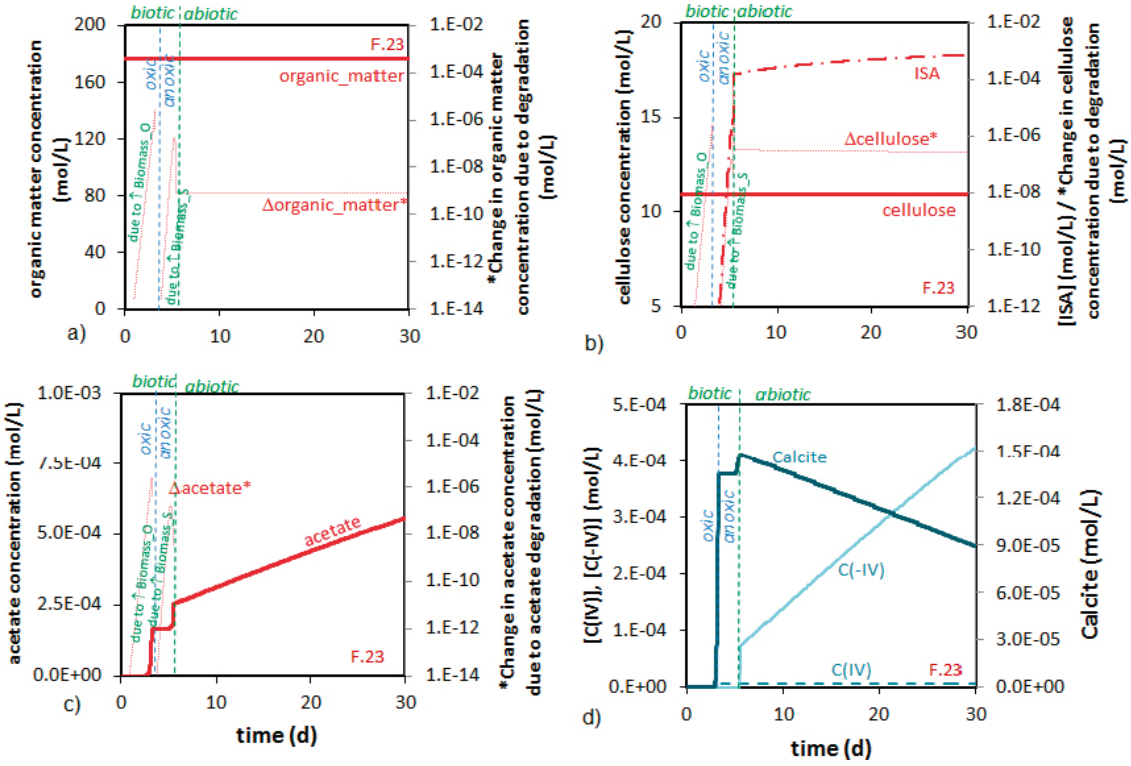

Figure A5-21. *Very short term results for F.23. Temporal evolution of a) organic matter concentration and of organic matter degraded in each time step; b) cellulose and ISA aqueous concentration and cellulose degraded in each time step; c) acetate concentration and of acetate degraded in each time step; d) calcite, and aqueous carbonate and methane concentration.*

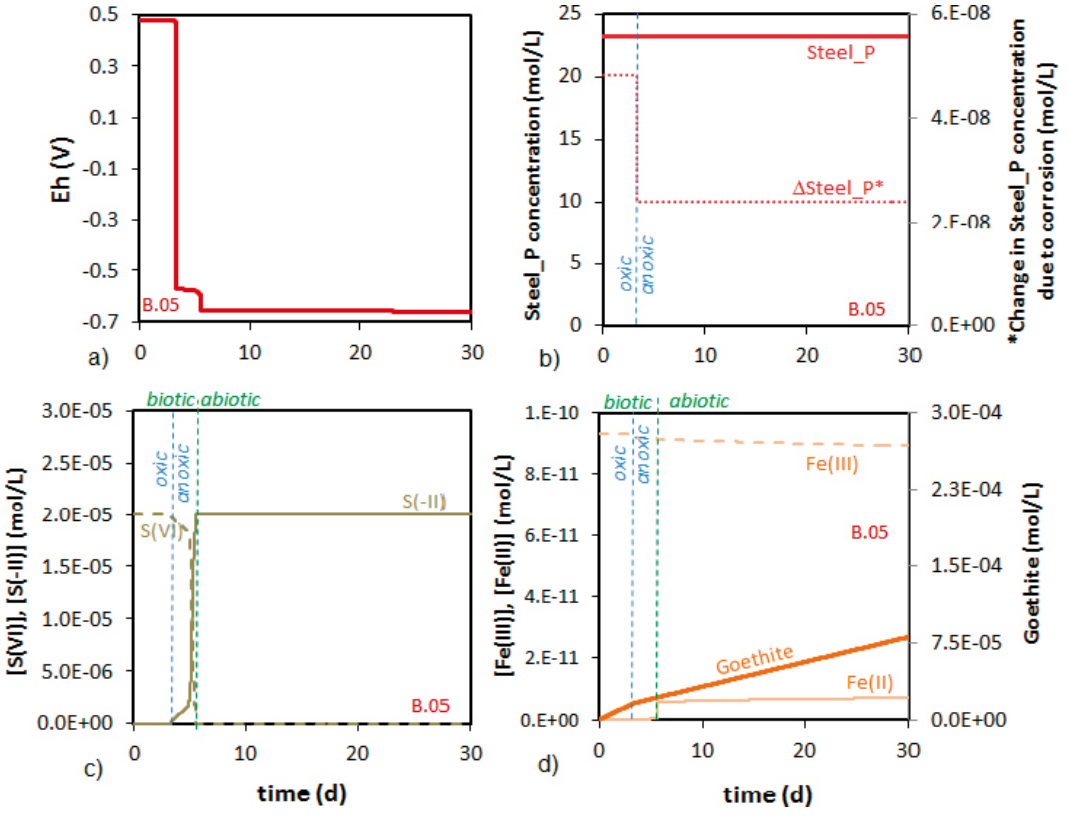

Figure A5-22. *Very short term results for B.05. Temporal evolution of a) Eh; b) concentration of C-Steel and of the C-steel corroded in each time step; c) S(-II) and S(VI) total aqueous concentration; d) goethite, Fe(II) and Fe(III) aqueous concentration.*

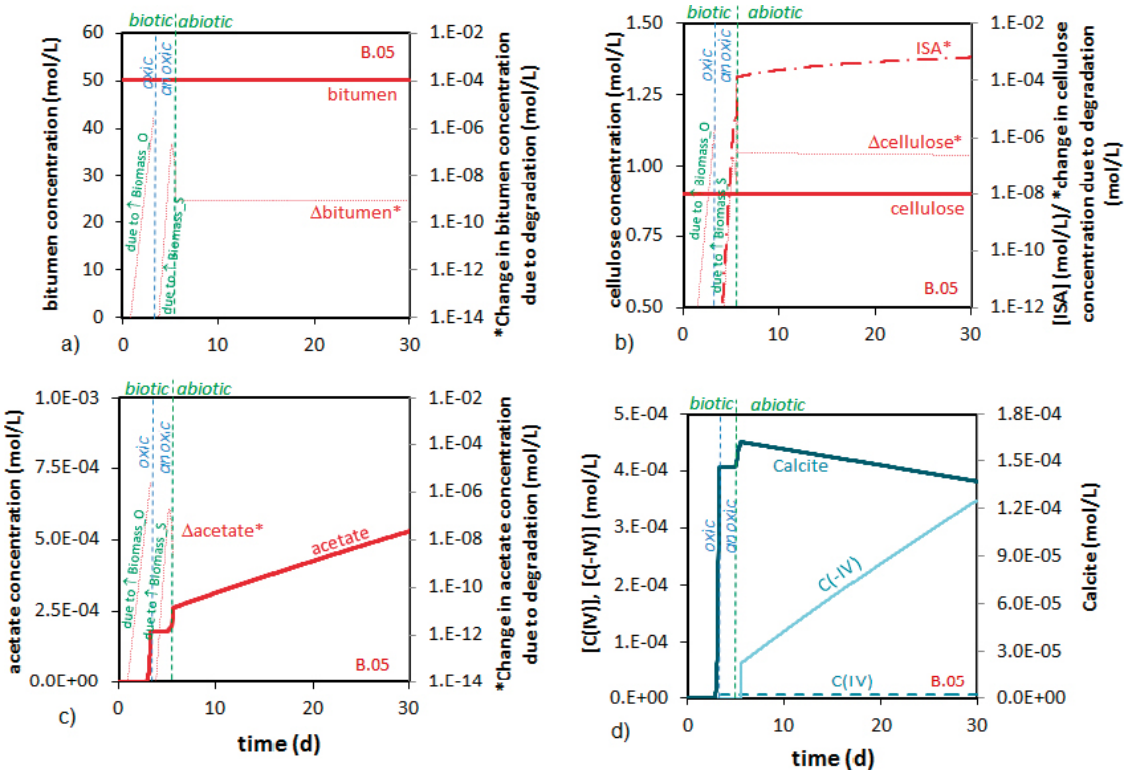

Figure A5-23. *Very short term results for B.05. Temporal evolution of a) bitumen concentration and of bitumen degraded in each time step; b) cellulose and ISA aqueous concentration and cellulose degraded in each time step; c) acetate concentration and of acetate degraded in each time step; d) calcite, and aqueous carbonate and methane concentration.*

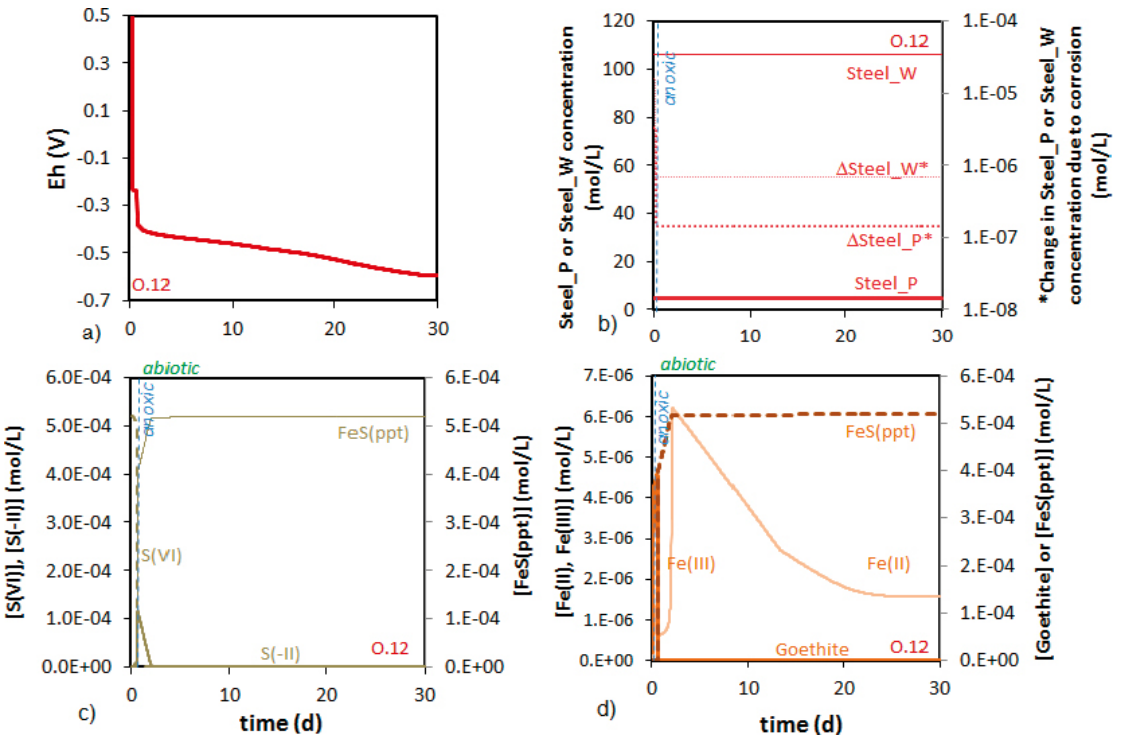

Figure A5-24. *Very short term results for O.12 (methane not considered). Temporal evolution of a) Eh; b) concentration of C-Steel and of the C-steel corroded in each time step; c) FeS(ppt), S(-II) and S(VI) total aqueous concentration; d) FeS(ppt), goethite, Fe(II) and Fe(III) aqueous concentration.*

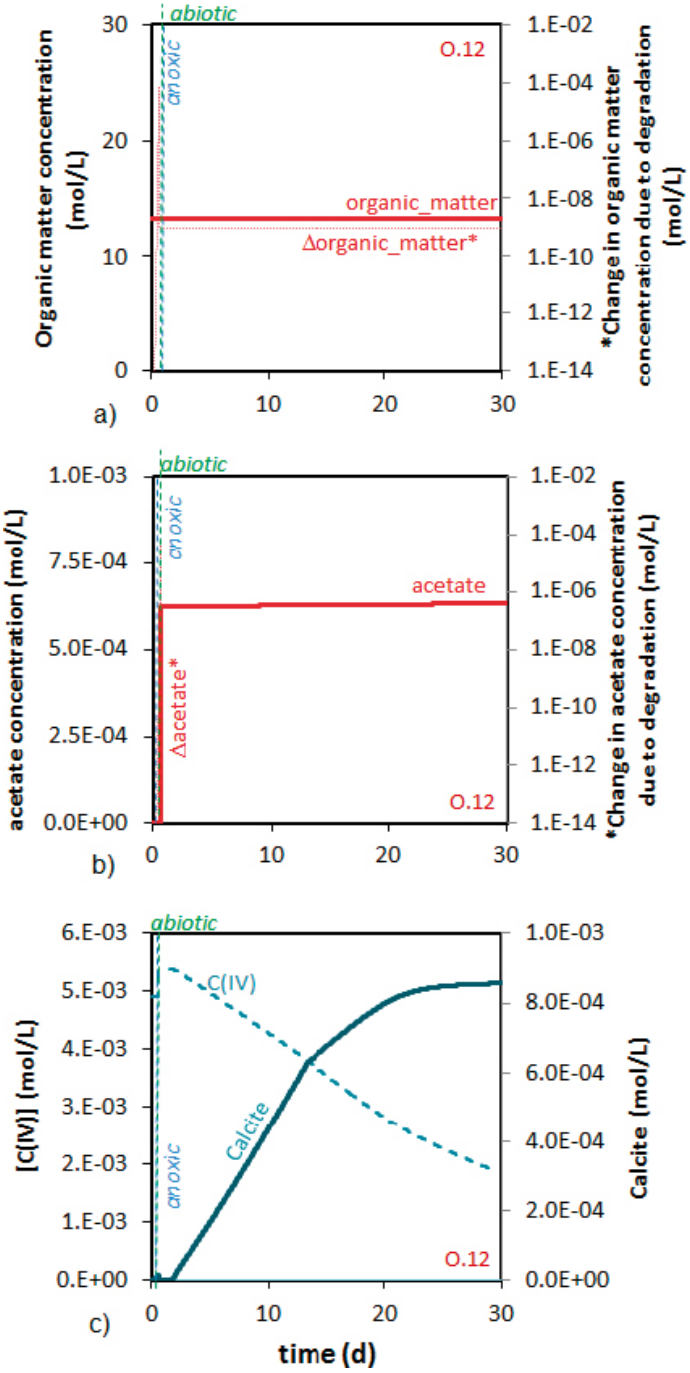

Figure A5-25. *Very short term results for O.12 (methane not considered). Temporal evolution of a) organic matter concentration and of organic matter degraded in each time step; b) acetate concentration and of acetate degraded in each time step; c) calcite, and aqueous carbonate concentration.*

A5-5 Short term results. Steel cases. R.15, R.16 and S.13 waste package types

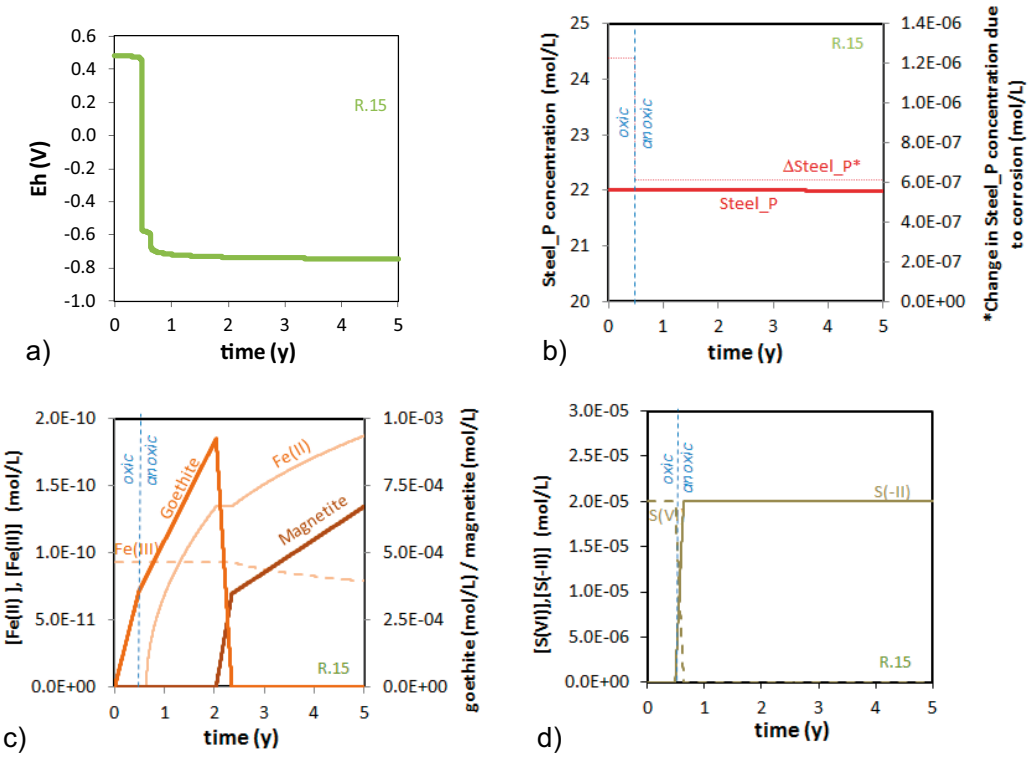

Figure A5-26. *a) Eh evolution of R.15 package during the short term period. b) Evolution of the concentration of C-Steel and of the C-steel corroded in each time step. c) Evolution of Fe(III), Fe(II), goethite and magnetite concentration during the short term period. d) Evolution of S(VI) and S(-II) aqueous concentration during the short term period.*

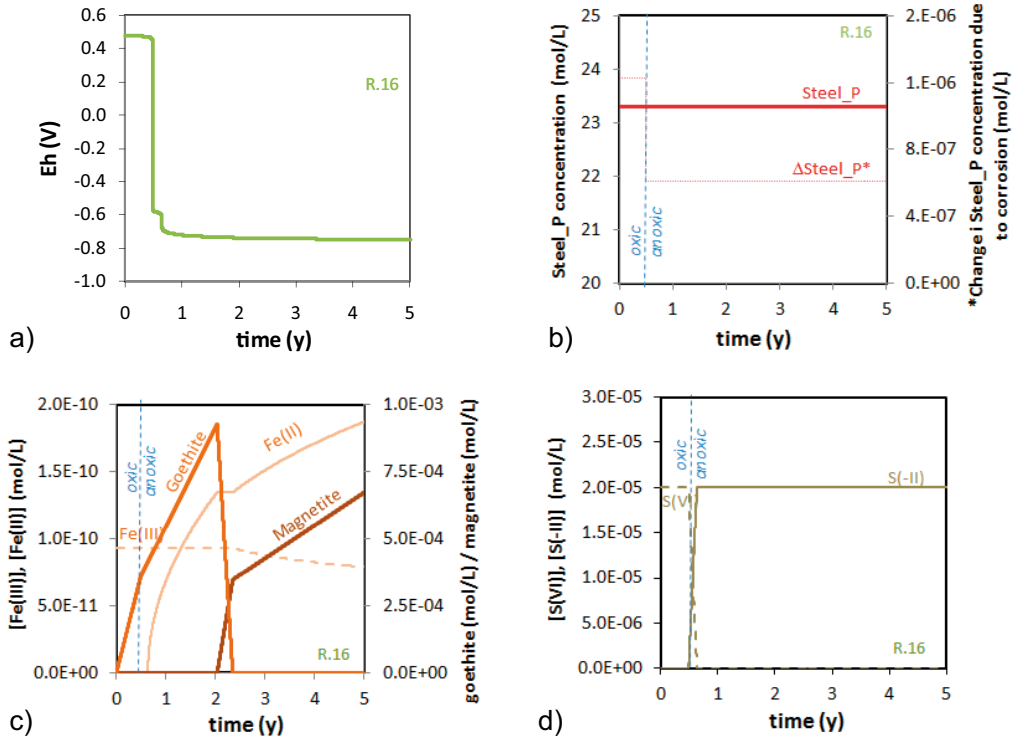

Figure A5-27. *a) Eh evolution of R.16 package during the short term period. b) Evolution of the concentration of C-Steel and of the C-steel corroded in each time step. c) Evolution of Fe(III), Fe(II), goethite and magnetite concentration during the short term period. d) Evolution of S(VI) and S(-II) aqueous concentration during the short term period.*

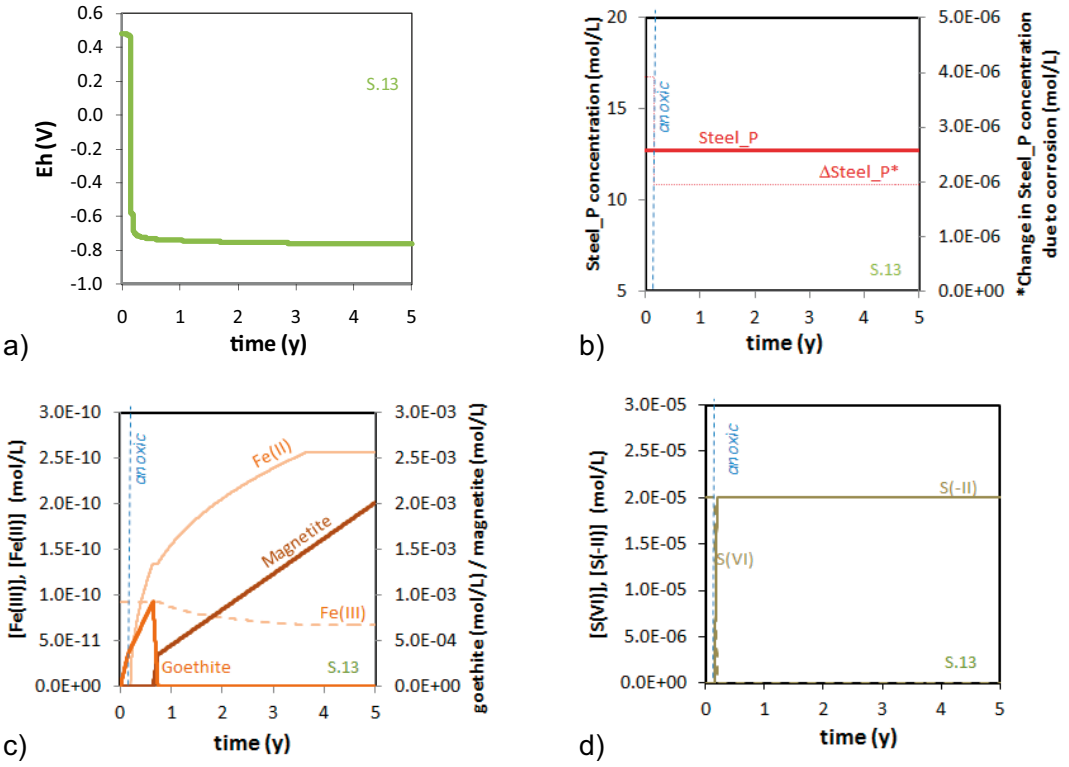

Figure A5-28. *a) Eh evolution of S.13 package during the short term period. b) Evolution of the concentration of C-Steel and of the C-steel corroded in each time step. c) Evolution of Fe(III), Fe(II), goethite and magnetite concentration during the short term period. d) Evolution of S(VI) and S(-II) aqueous concentration during the short term period.*

A5-6 Short term results. Steel and organic matter cases. O.02, R.01 and B.07_O.07 waste package types.

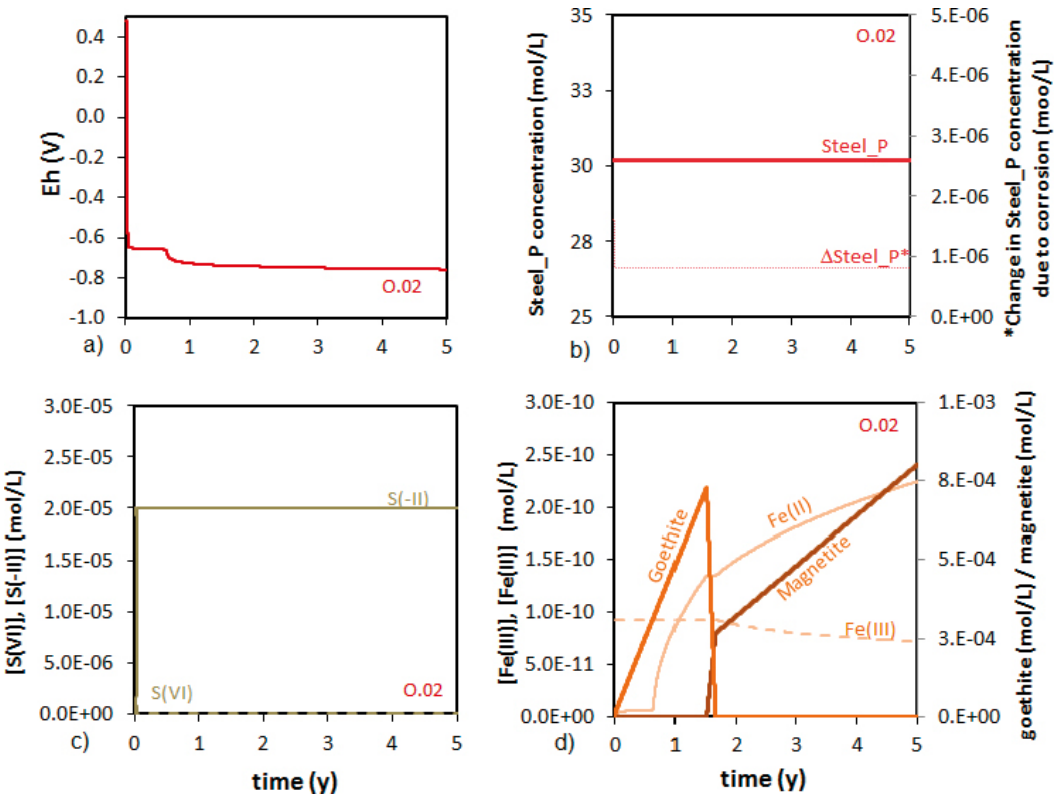

Figure A5-29. Short term results for O.02. Temporal evolution of a) Eh; b) concentration of C-Steel and of the C-steel corroded in each time step; c) S(-II) and S(VI) total aqueous concentration; d) goethite, magnetite, Fe(II) and Fe(III) aqueous concentration.

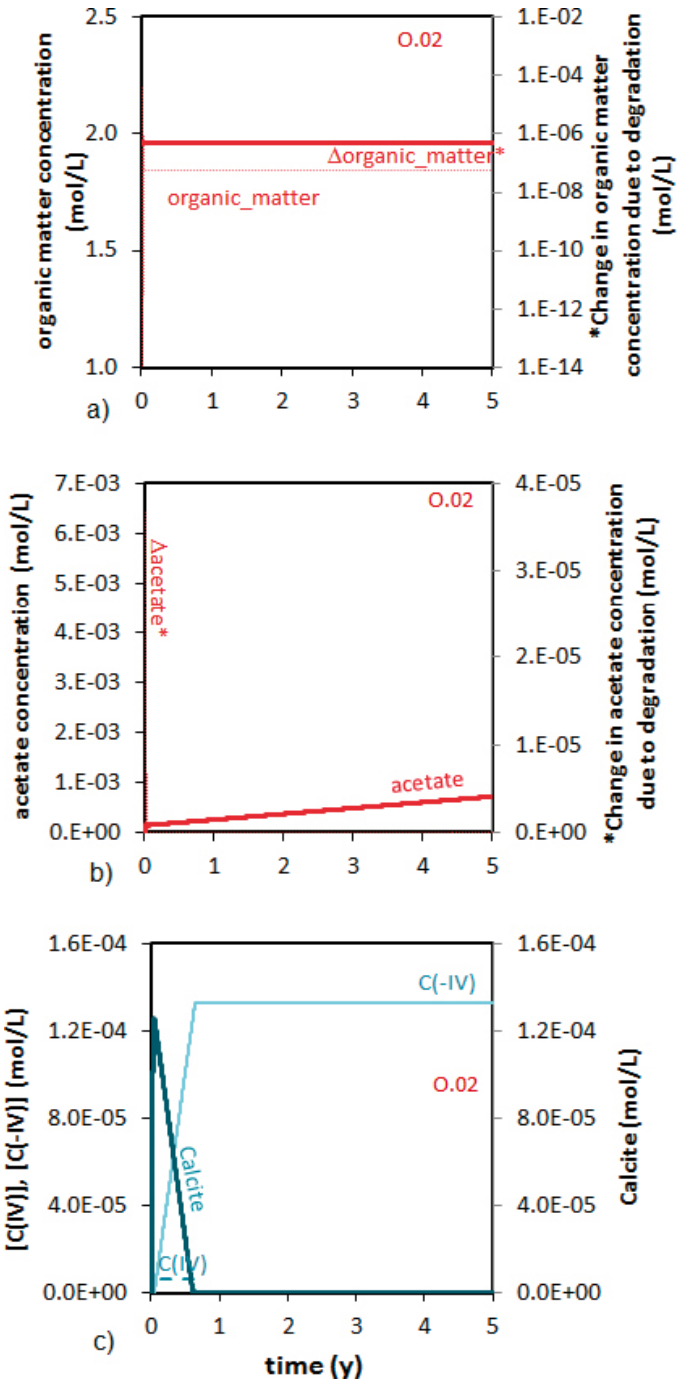

Figure A5-30. *Short term results for O.02. Temporal evolution of a) organic matter concentration and of organic matter degraded in each time step; b) acetate concentration and of acetate degraded in each time step; c) calcite, and aqueous carbonate and methane concentration.*

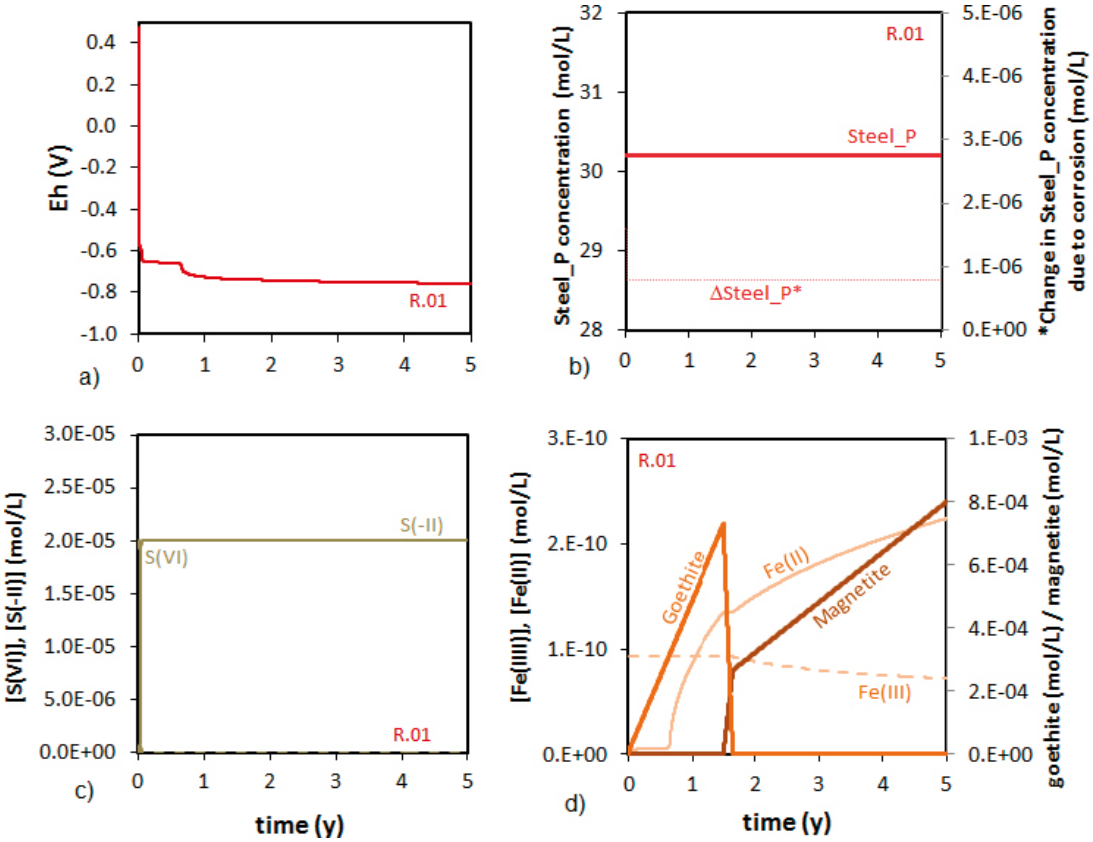

Figure A5-31. *Short term results for R.01. Temporal evolution of a) Eh; b) concentration of C-Steel and of the C-steel corroded in each time step; c) S(-II) and S(VI) total aqueous concentration; d) goethite, magnetite, Fe(II) and Fe(III) aqueous concentration.*

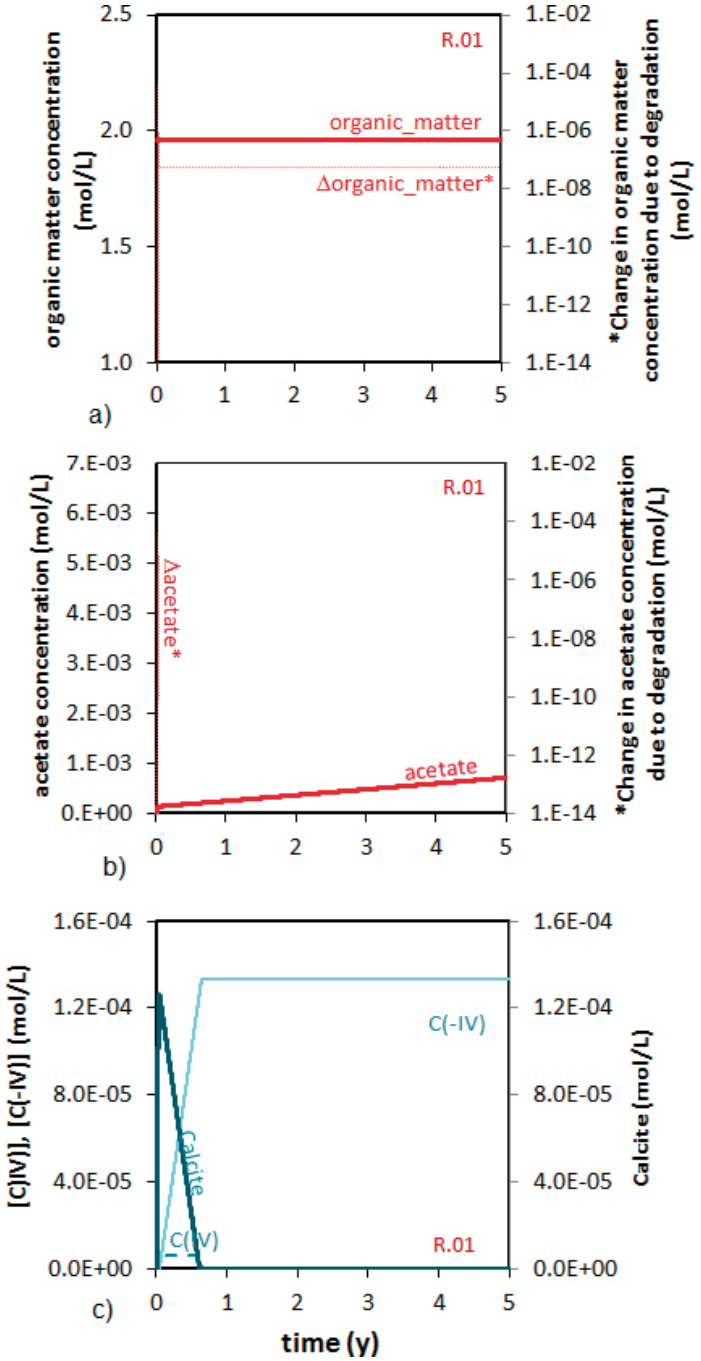

Figure A5-32. *Short term results for R.01. Temporal evolution of a) organic matter concentration and of organic matter degraded in each time step; b) acetate concentration and of acetate degraded in each time step; c) calcite, and aqueous carbonate and methane concentration.*

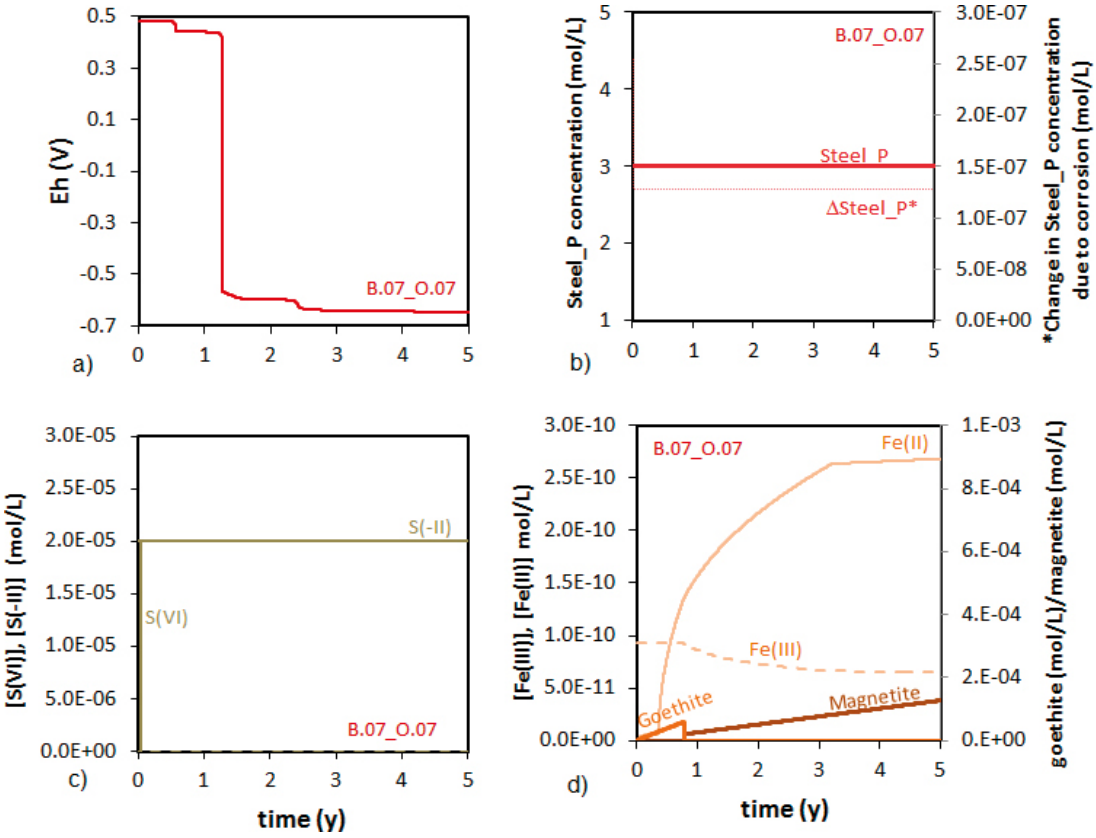

Figure A5-33. *Short term results for B.07_O.07. Temporal evolution of a) Eh; b) concentration of C-Steel and of the C-steel corroded in each time step; c) S(-II) and S(VI) total aqueous concentration; d) goethite, magnetite, Fe(II) and Fe(III) aqueous concentration.*

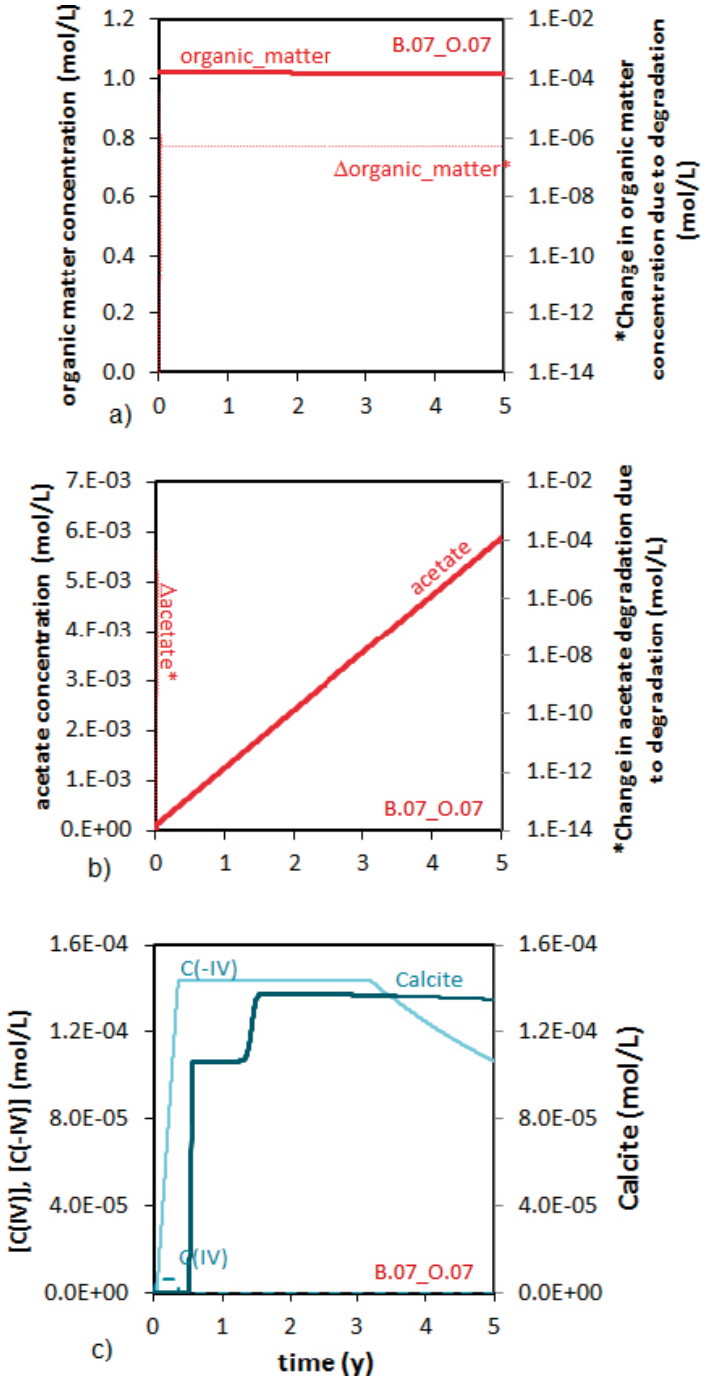

Figure A5-34. *Short term results for B.07_O.07. Temporal evolution of a) organic matter concentration and of organic matter degraded in each time step; b) acetate concentration and of acetate degraded in each time step; c) calcite, and aqueous carbonate and methane concentration.*

A5-7 Short term results. Steel and bitumen cases. B.06, F.18. F.05 and F.17 waste package types.

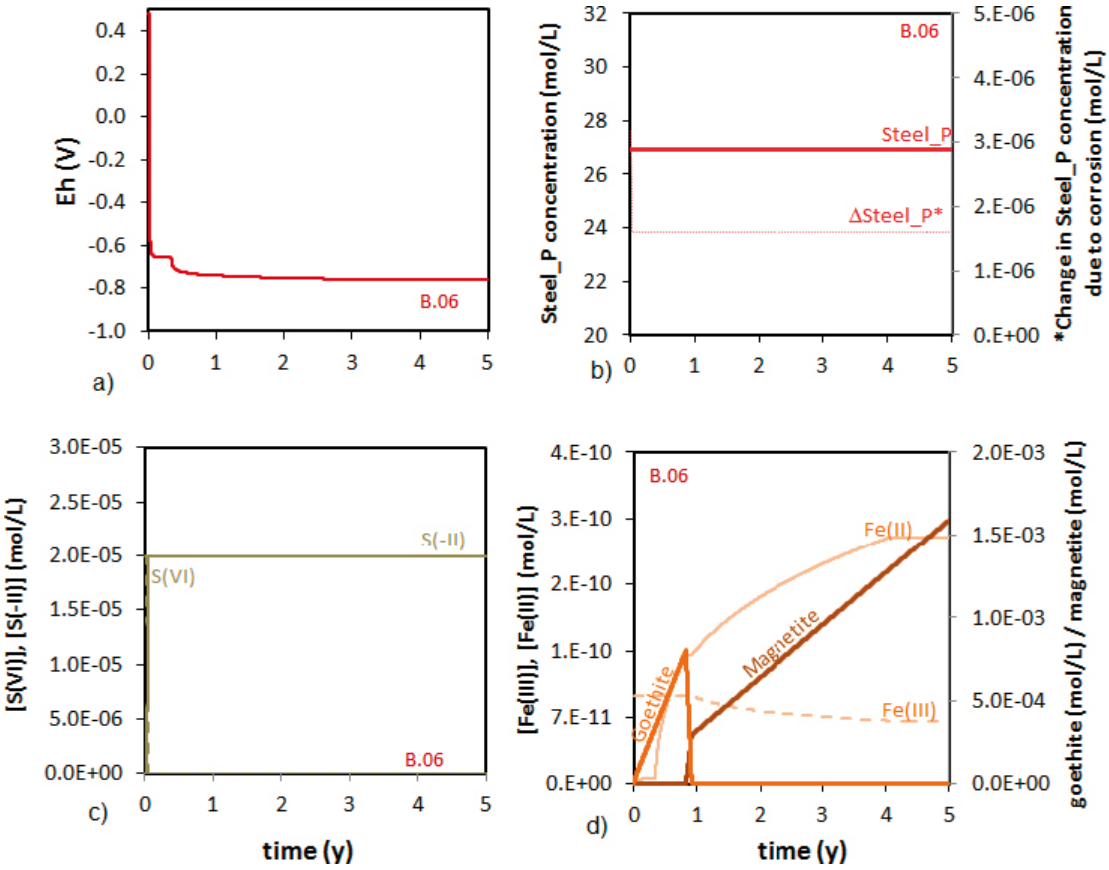

Figure A5-35. Short term results for B.06. Temporal evolution of a) Eh; b) concentration of C-Steel and of the C-steel corroded in each time step; c) S(-II) and S(VI) total aqueous concentration; d) goethite, magnetite, Fe(II) and Fe(III) aqueous concentration.

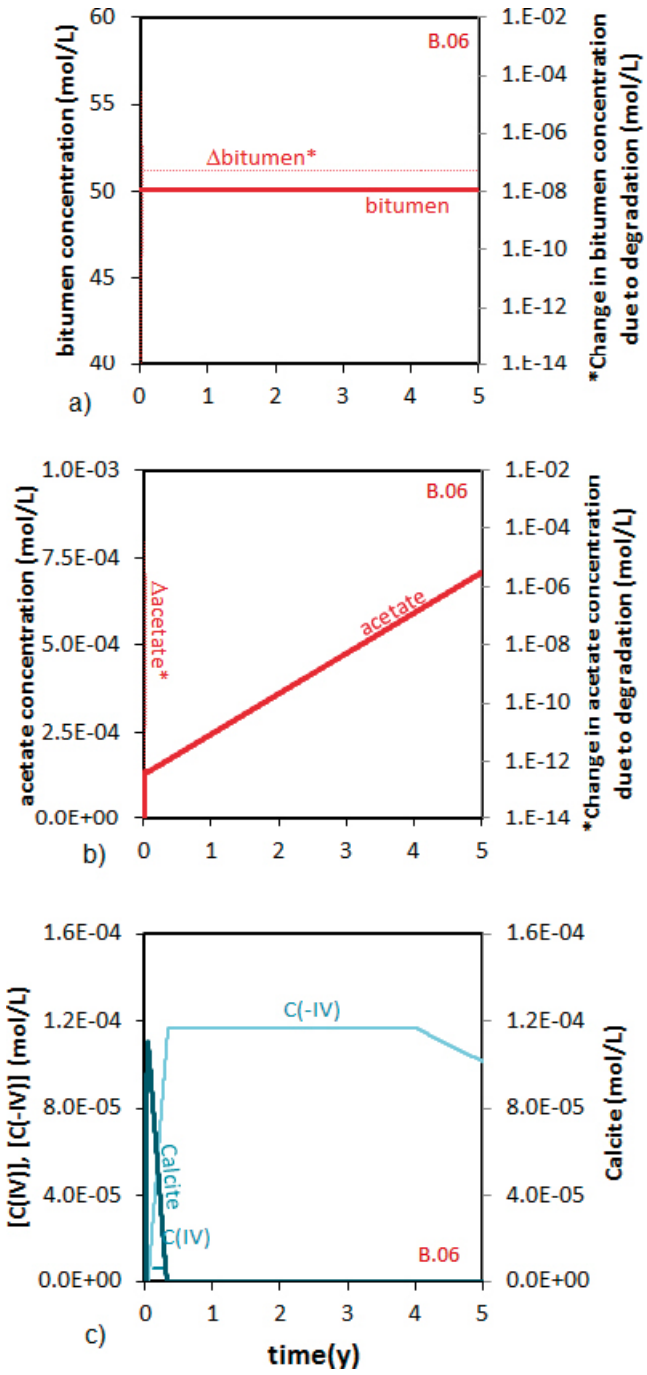

Figure A5-36. *Short term results for B.06. Temporal evolution of a) organic matter concentration and of organic matter degraded in each time step; b) acetate concentration and of acetate degraded in each time step; c) calcite, and aqueous carbonate and methane concentration.*

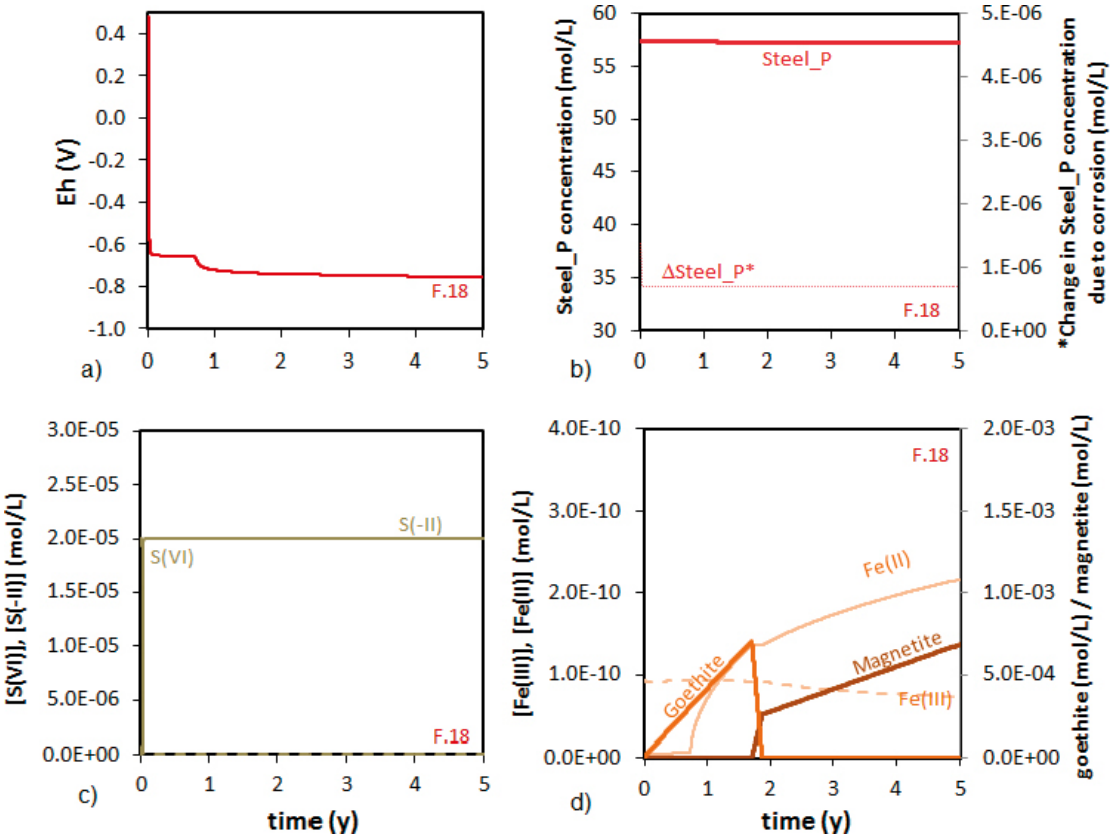

Figure A5-37. *Short term results for F.18. Temporal evolution of a) Eh; b) concentration of C-Steel and of the C-steel corroded in each time step; c) S(-II) and S(VI) total aqueous concentration; d) goethite, magnetite, Fe(II) and Fe(III) aqueous concentration.*

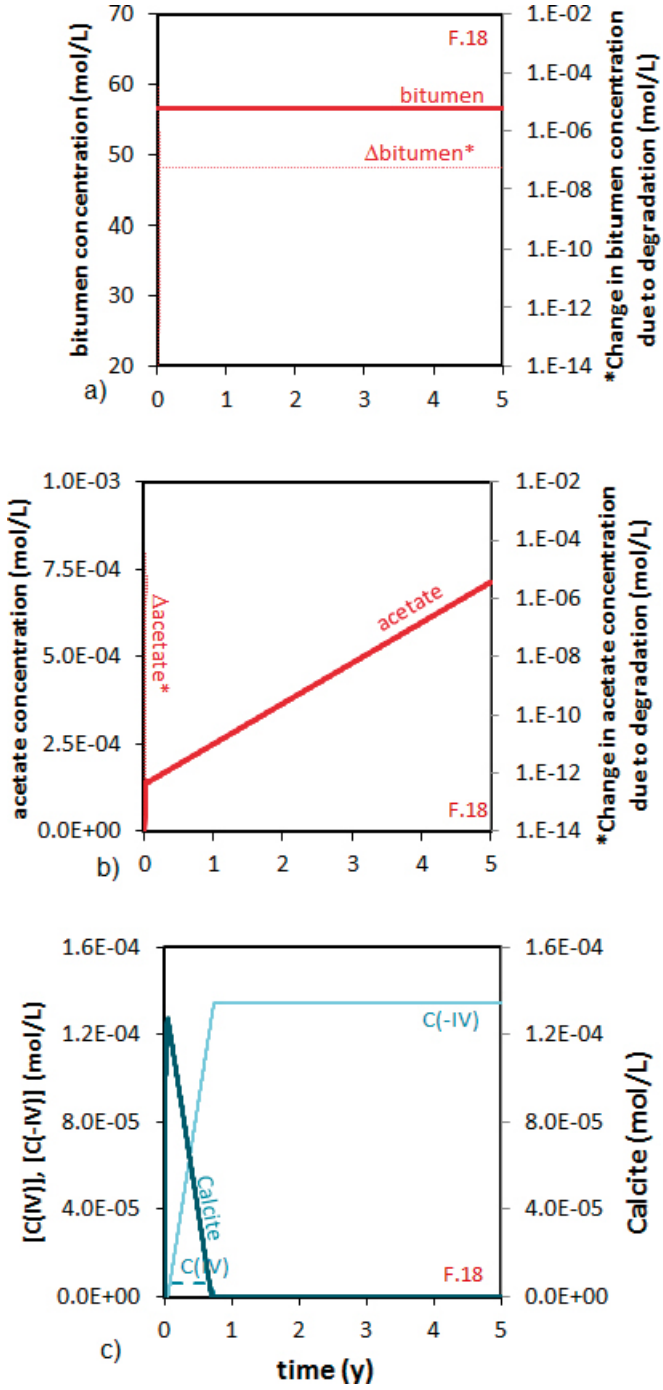

Figure A5-38. *Short term results for F.18. Temporal evolution of a) organic matter concentration and of organic matter degraded in each time step; b) acetate concentration and of acetate degraded in each time step; c) calcite, and aqueous carbonate and methane concentration.*

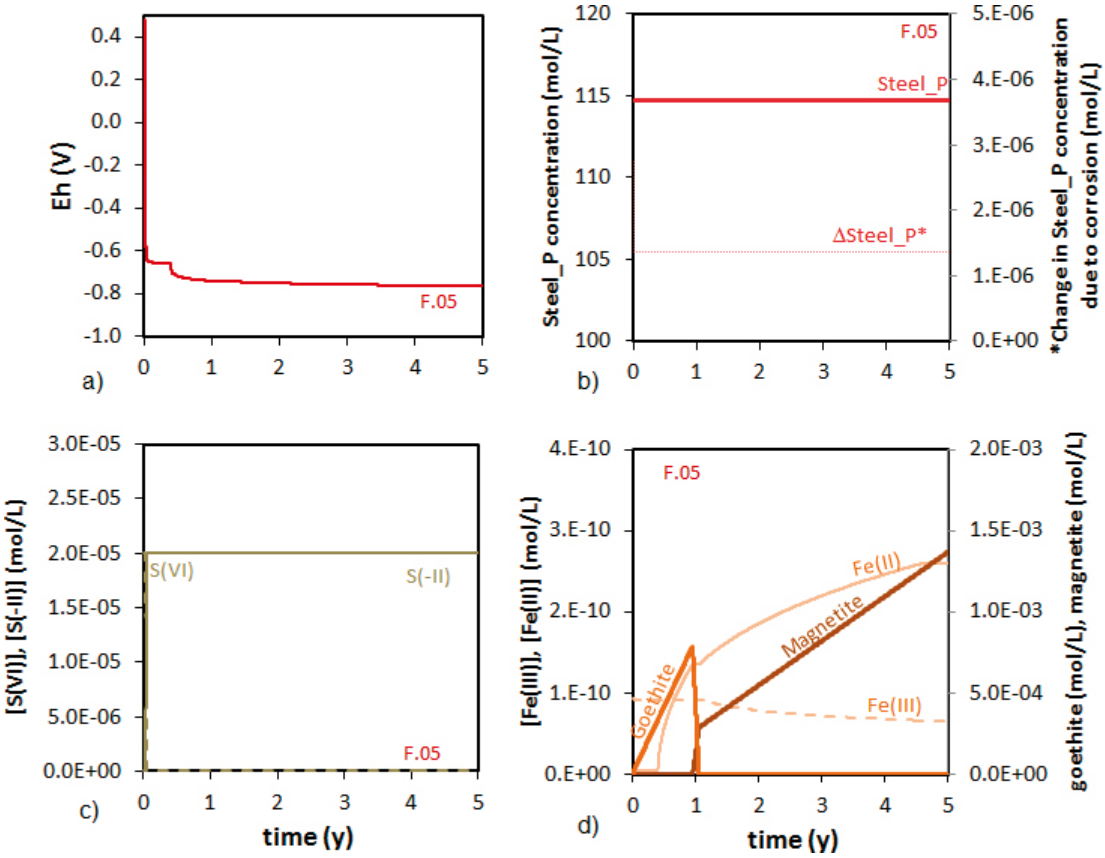

Figure A5-39. *Short term results for F.05. Temporal evolution of a) Eh; b) concentration of C-Steel and of the C-steel corroded in each time step; c) S(-II) and S(VI) total aqueous concentration d) goethite, magnetite, Fe(II) and Fe(III) aqueous concentration.*

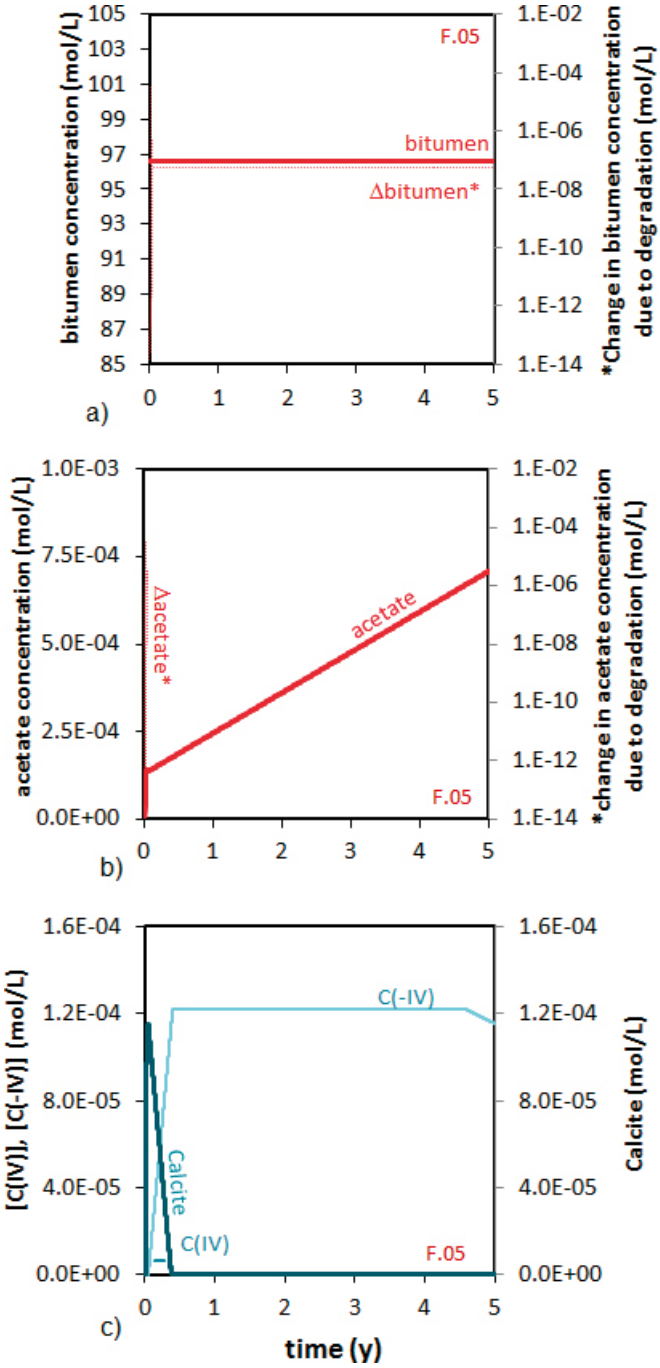

Figure A5-40. *Short term results for F.05. Temporal evolution of a) organic matter concentration and of organic matter degraded in each time step; b) acetate concentration and of acetate degraded in each time step; c) calcite, and aqueous carbonate and methane concentration.*

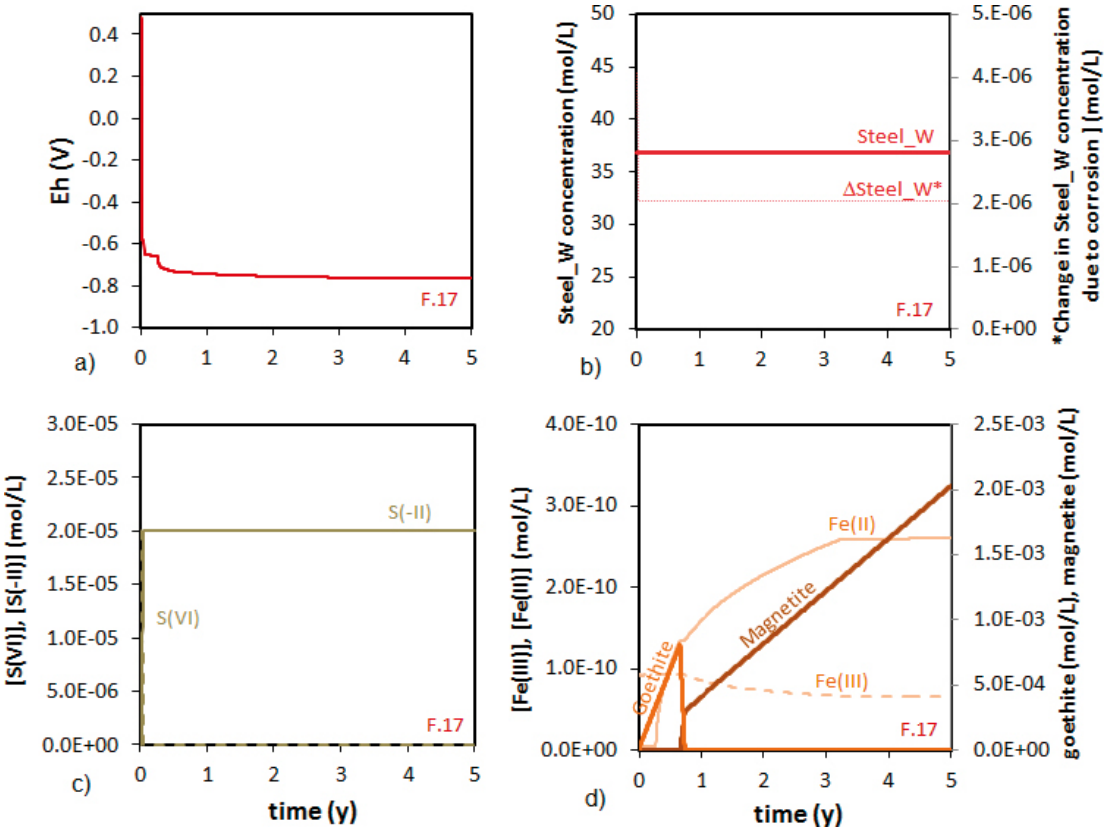

Figure A5-41. *Short term results for F.17. Temporal evolution of a) Eh; b) concentration of C-Steel and of the C-steel corroded in each time step; c) S(-II) and S(VI) total aqueous concentration; d) goethite, magnetite, Fe(II) and Fe(III) aqueous concentration.*

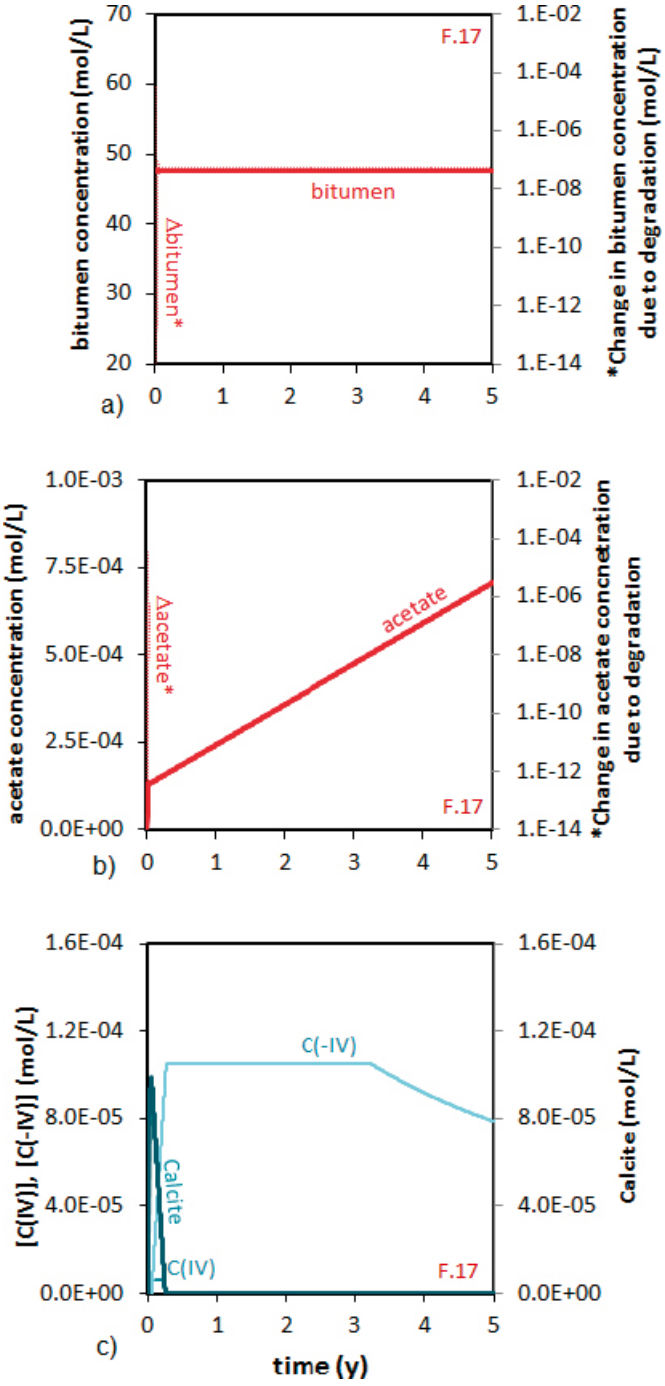

Figure A5-42. *Short term results for F.17. Temporal evolution of a) organic matter concentration and of organic matter degraded in each time step; b) acetate concentration and of acetate degraded in each time step; c) calcite, and aqueous carbonate and methane concentration.*

A5-8 Short term results. Steel and cellulose cases with bitumen or organic matter. O.23, F.23, B.05 and O.12 waste package types.

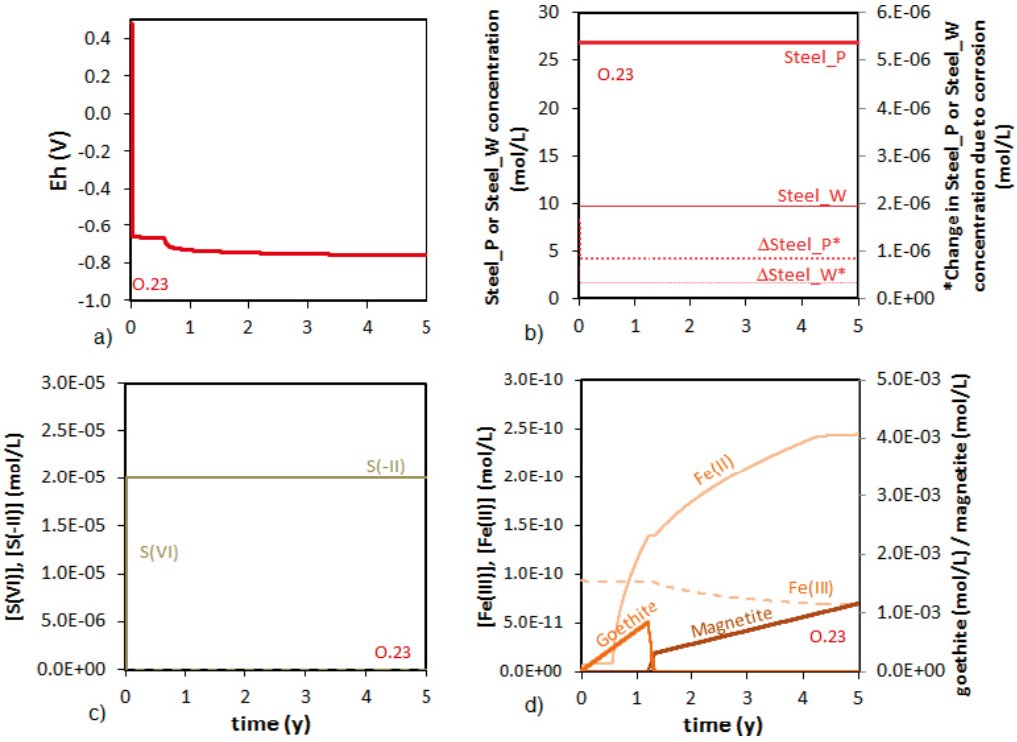

Figure A5-43. Short term results for O.23. Temporal evolution of a) Eh; b) concentration of C-Steel and of the C-steel corroded in each time step; c) S(-II) and S(VI) total aqueous concentration; d) goethite, magnetite Fe(II) and Fe(III) aqueous concentration.

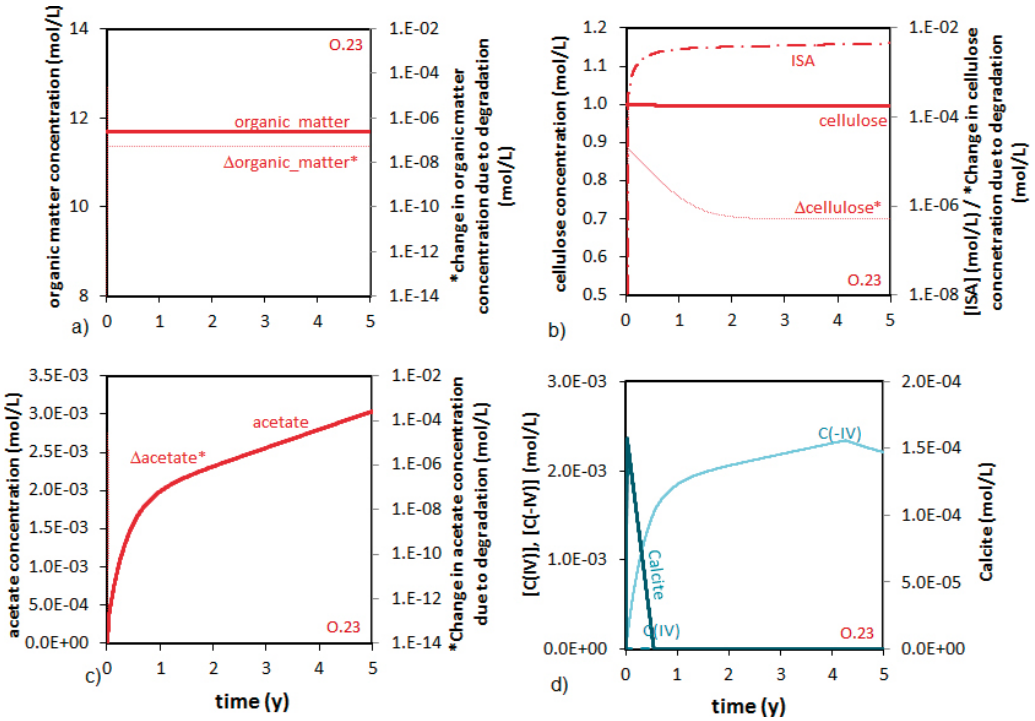

Figure A5-44. Short term results for O.23. Temporal evolution of a) organic matter concentration and of organic matter degraded in each time step; b) cellulose and ISA aqueous concentration and cellulose degraded in each time step; c) acetate concentration and of acetate degraded in each time step; d) calcite, and aqueous carbonate and methane concentration.

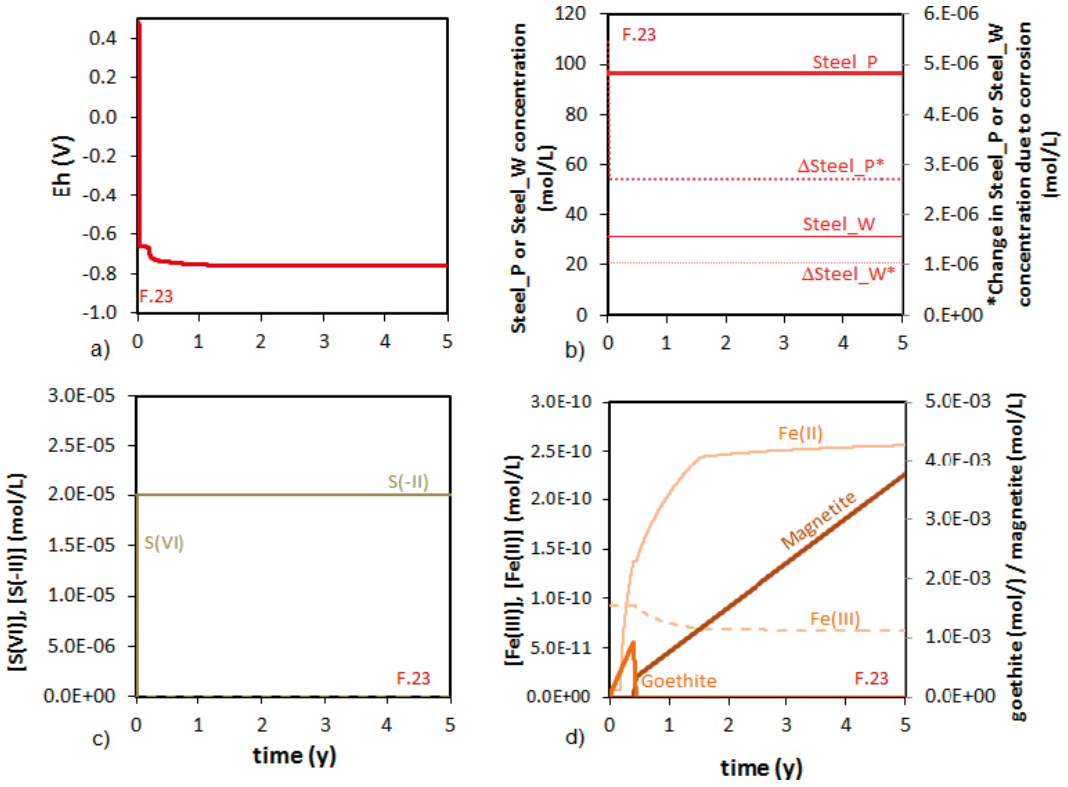

Figure A5-45. *Short term results for F.23. Temporal evolution of a) Eh; b) concentration of C-Steel and of the C-steel corroded in each time step; c) S(-II) and S(VI) total aqueous concentration; d) goethite, magnetite Fe(II) and Fe(III) aqueous concentration.*

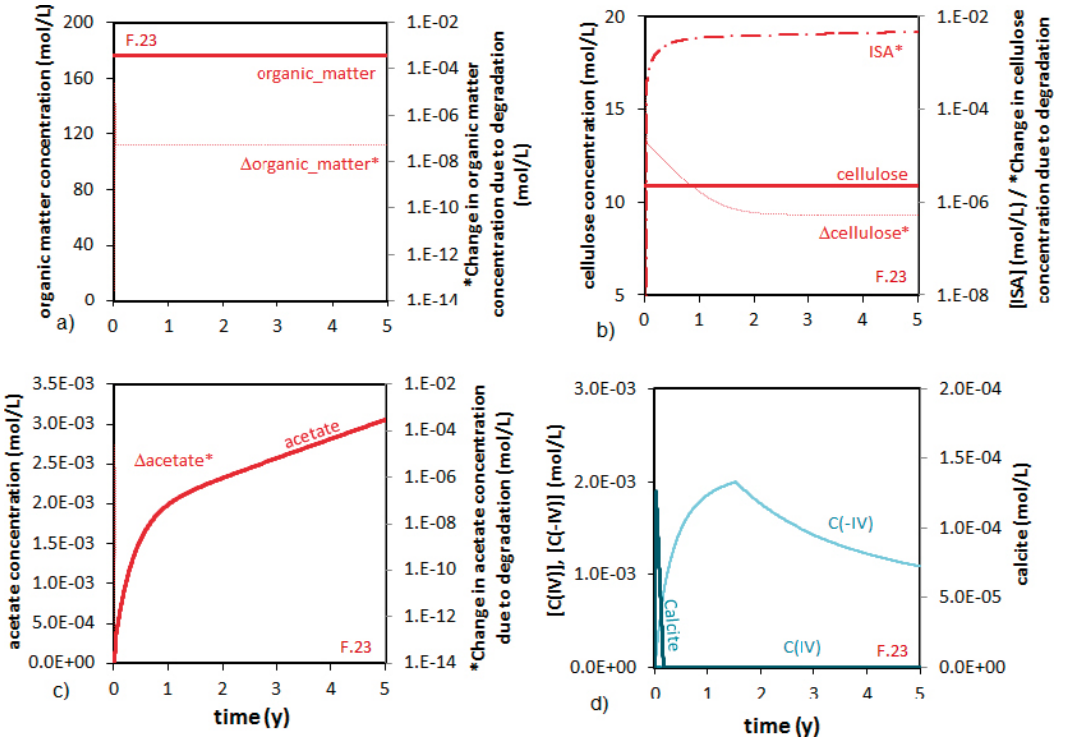

Figure A5-46. *Short term results for F.23. Temporal evolution of a) organic matter concentration and of organic matter degraded in each time step; b) cellulose and ISA aqueous concentration and cellulose degraded in each time step; c) acetate concentration and of acetate degraded in each time step; d) calcite, and aqueous carbonate and methane concentration.*

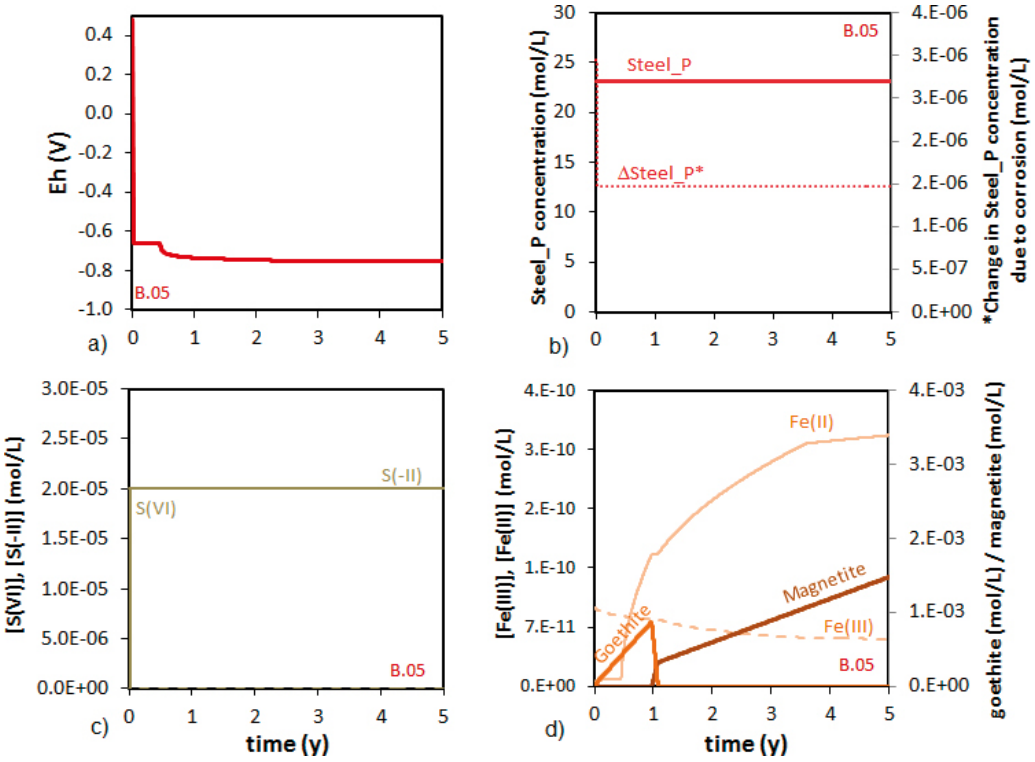

Figure A5-47. *Short term results for B.05. Temporal evolution of a) Eh; b) concentration of C-Steel and of the C-steel corroded in each time step; c) S(-II) and S(VI) total aqueous concentration; d) goethite, magnetite Fe(II) and Fe(III) aqueous concentration.*

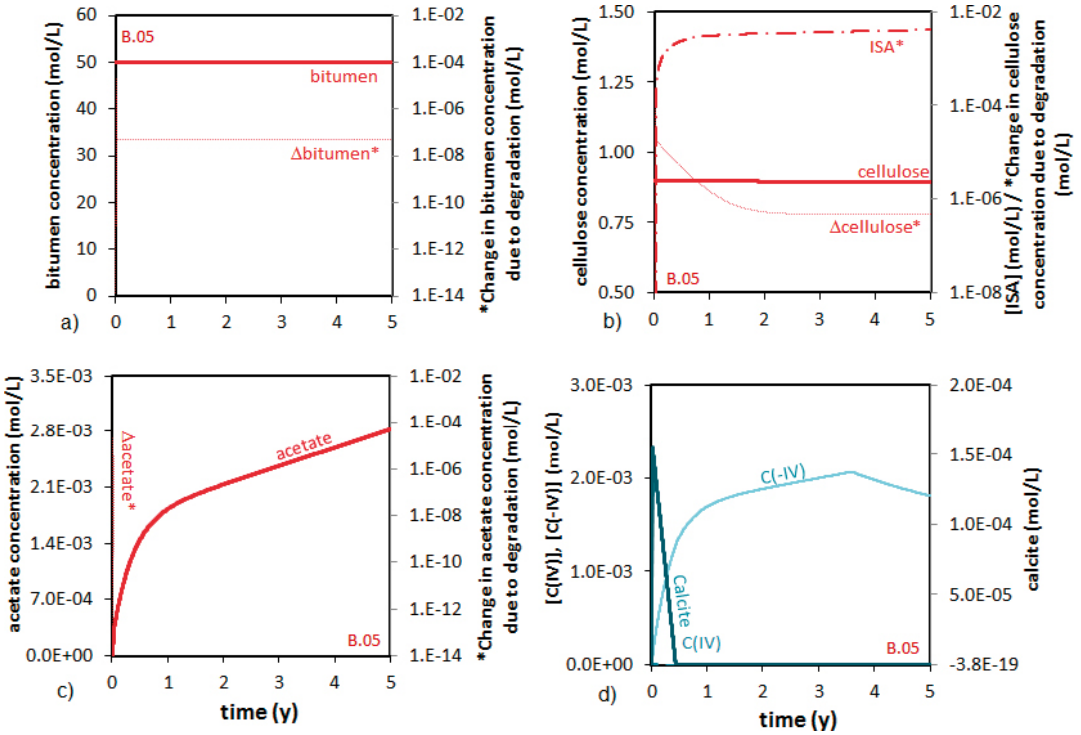

Figure A5-48. *Short term results for B.05. Temporal evolution of a) organic matter concentration and of organic matter degraded in each time step; b) cellulose and ISA aqueous concentration and cellulose degraded in each time step; c) acetate concentration and of acetate degraded in each time step; d) calcite, and aqueous carbonate and methane concentration.*

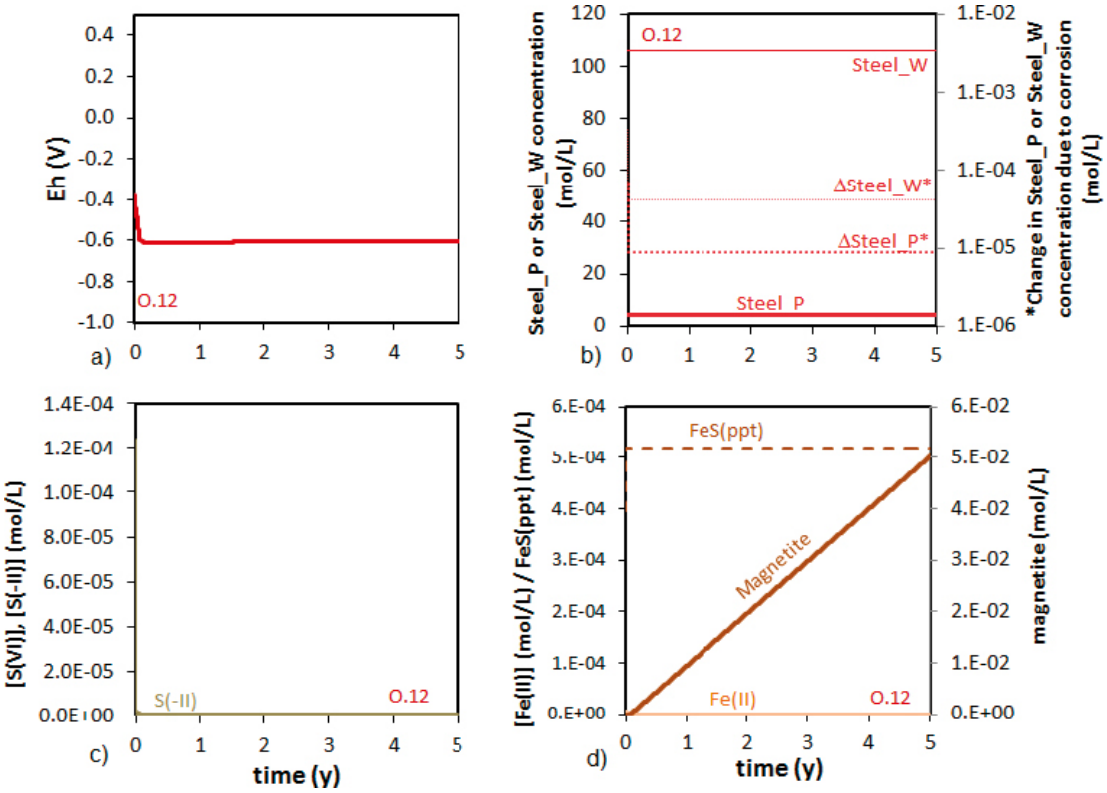

Figure A5-49. *Short term results for O.12 (methane not considered). Temporal evolution of a) Eh; b) concentration of C-Steel and of the C-steel corroded in each time step; c) FeS(ppt), S(-II) and S(VI) total aqueous concentration; d) goethite, magnetite, Fe(II) and Fe(III) aqueous concentration.*

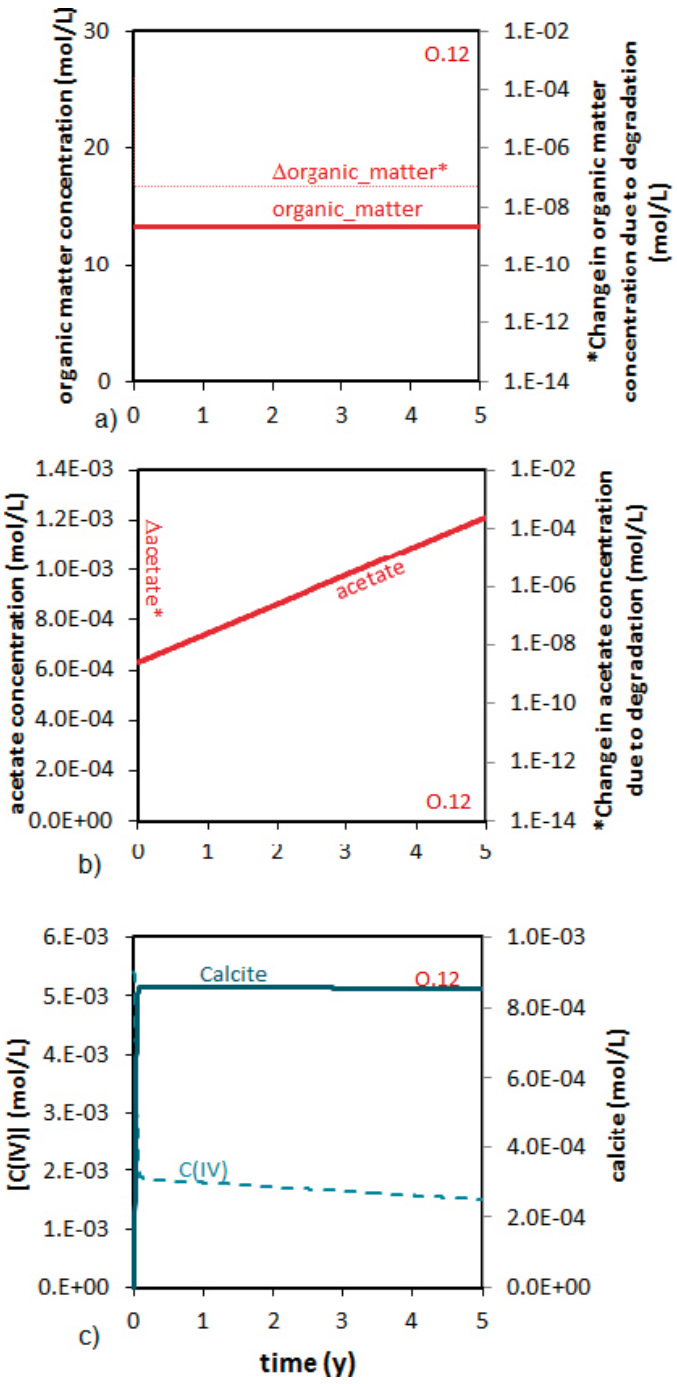

Figure A5-50. *Short term results for O.12 (methane not considered). Temporal evolution of a) organic matter concentration and of organic matter degraded in each time step; b) acetate concentration and of acetate degraded in each time step; c) calcite, and aqueous carbonate concentration.*

A5-9 Long term results. Steel cases. R.15, R.16 and S.13 waste package types.

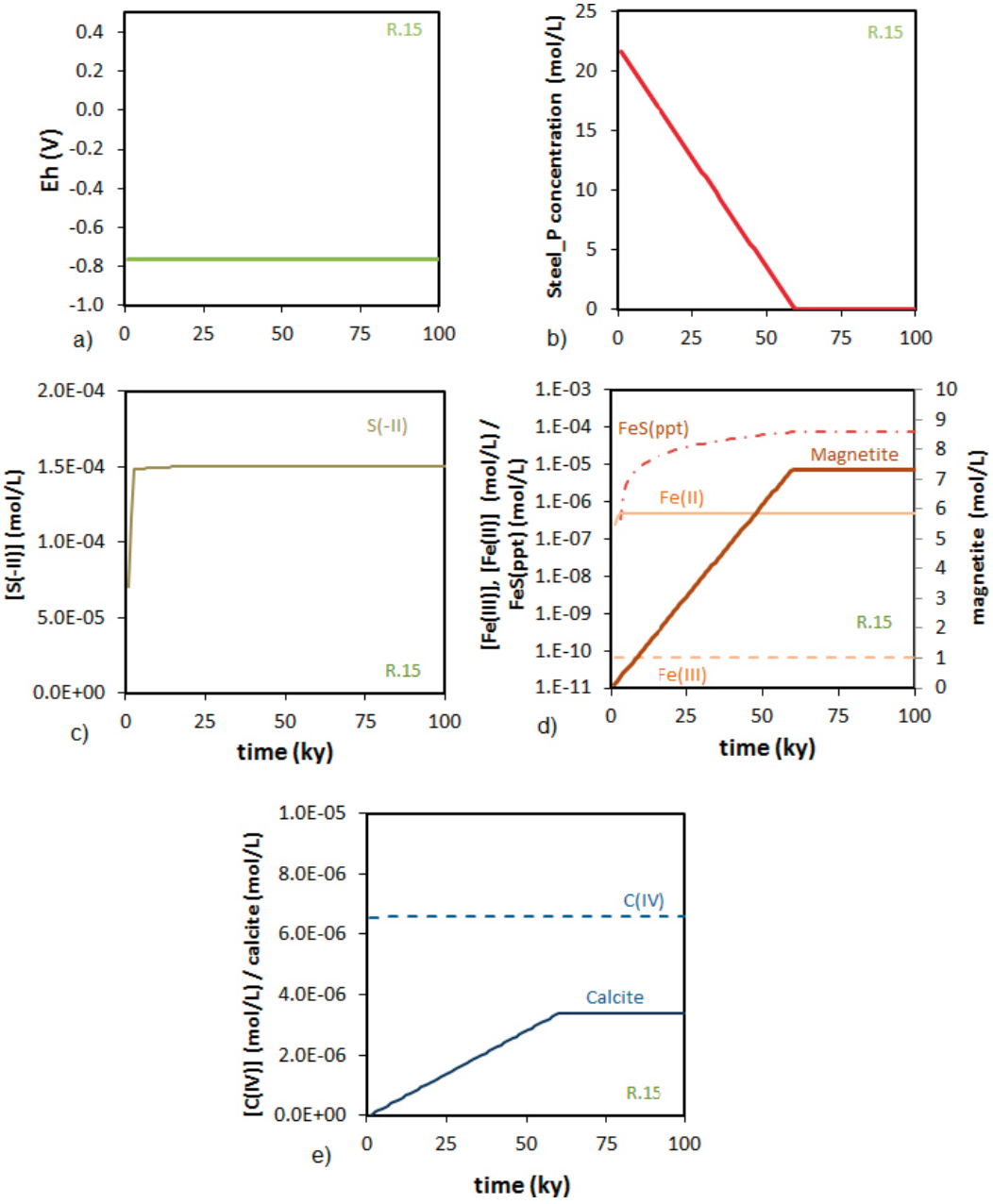

Figure A5-51. *Long term results for R.15. Temporal evolution of a) Eh; b) concentration of C-Steel; c) S(-II) total aqueous concentration; d) magnetite, FeS(ppt), Fe(II) and Fe(III) aqueous concentration; e) calcite and C(IV) total aqueous concentration.*

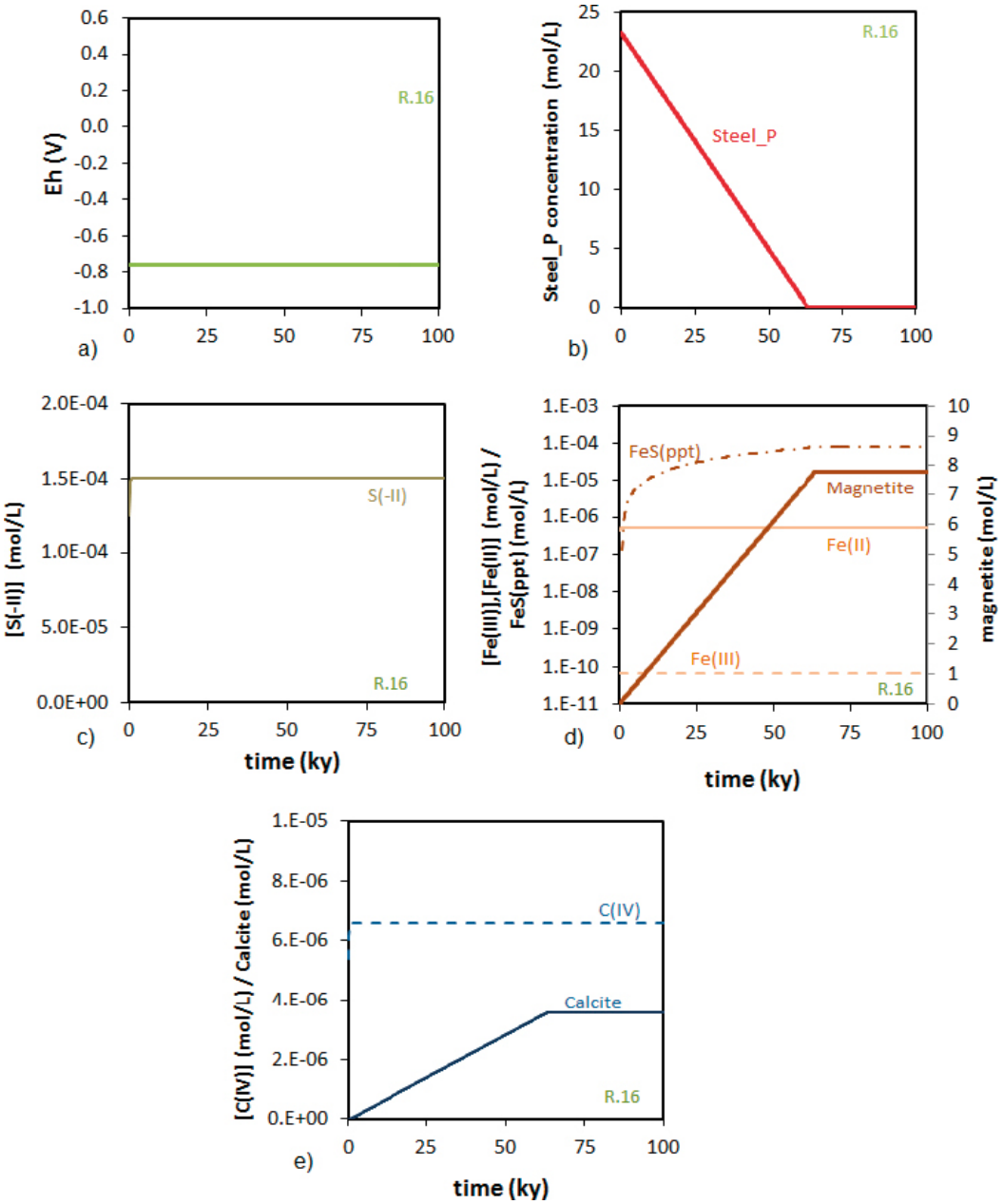

Figure A5-52. *Long term results for R.16. Temporal evolution of a) Eh; b) concentration of C-Steel; c) S(-II) total aqueous concentration; d) magnetite, FeS(ppt), Fe(II) and Fe(III) aqueous concentration; e) calcite and C(IV) total aqueous concentration.*

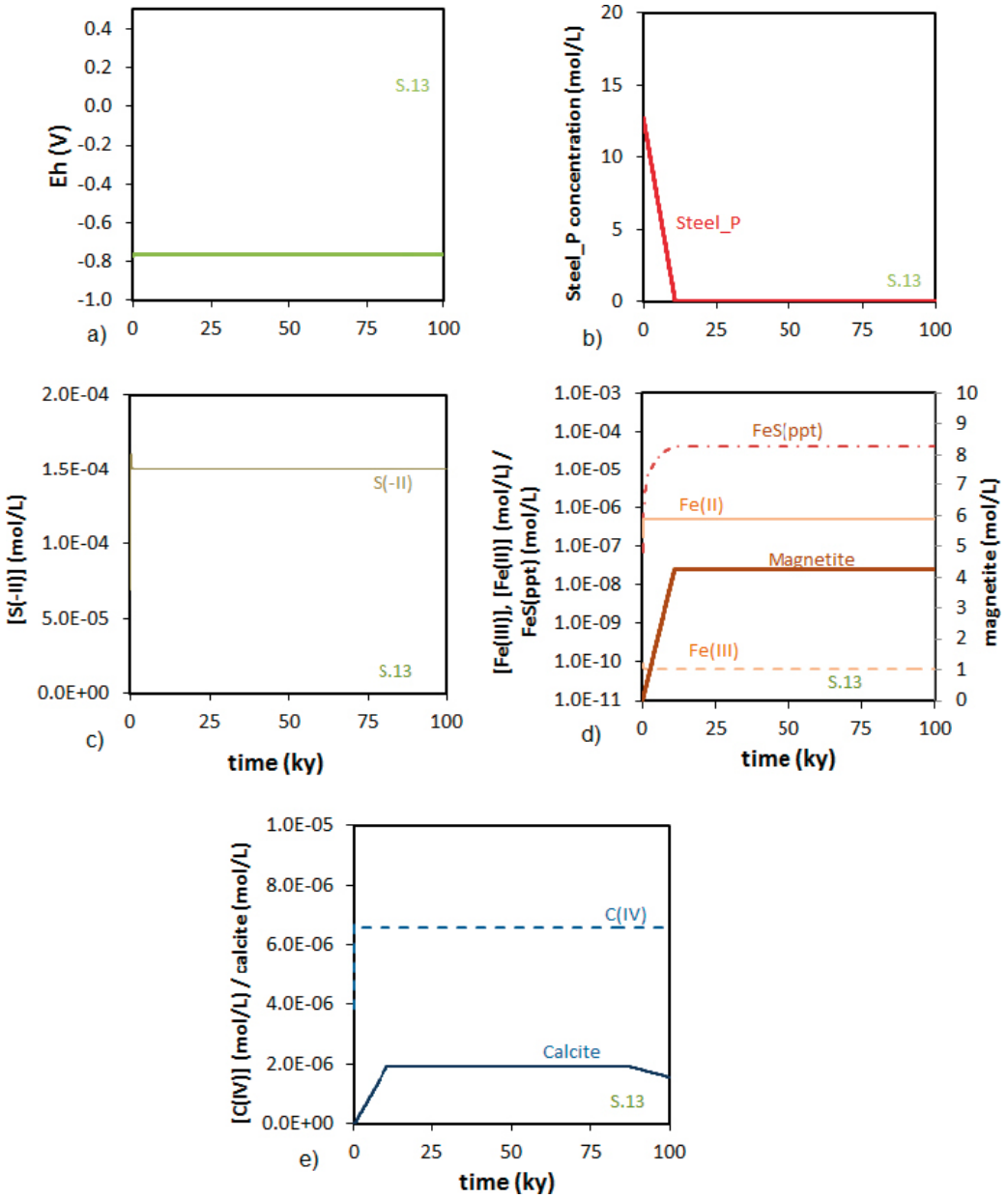

Figure A5-53. *Long term results for S.13. Temporal evolution of a) Eh; b) concentration of C-Steel; c) S(-II) total aqueous concentration; d) magnetite, FeS(ppt), Fe(II) and Fe(III) aqueous concentration; e) calcite and C(IV) total aqueous concentration.*

A5-10 Long term results. Steel and organic matter cases. O.02, R.01 and B.07_O.07 waste package types.

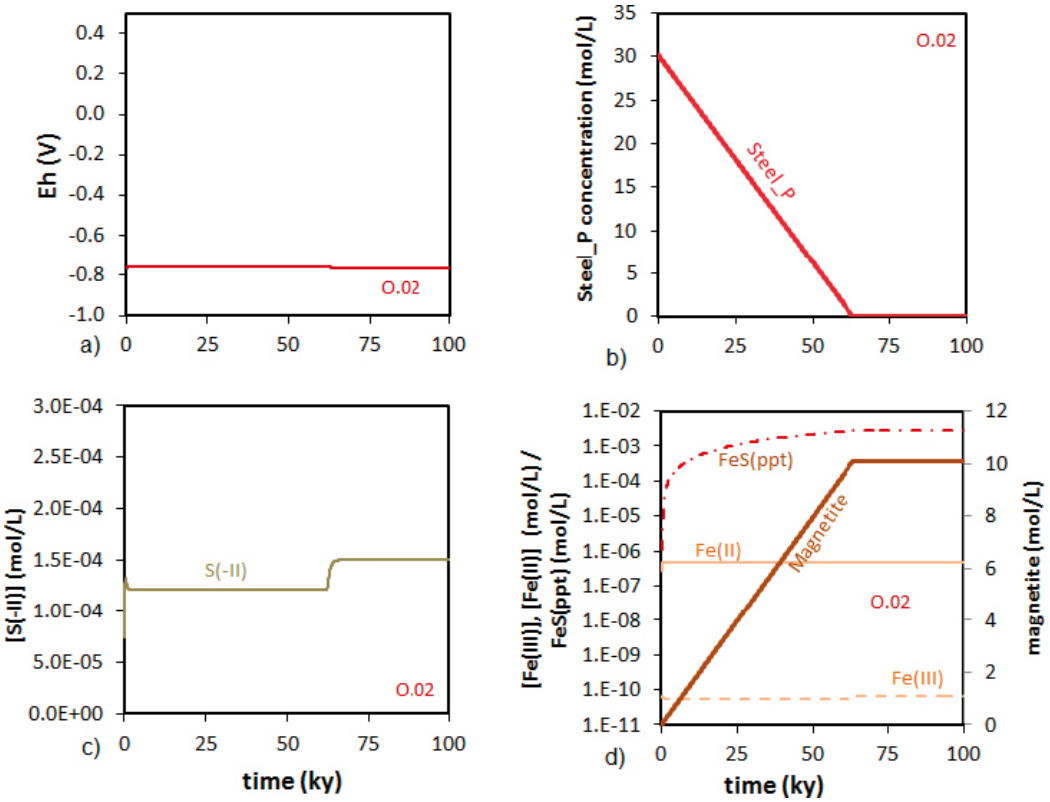

Figure A5-54. Long term results for O.02. Temporal evolution of a) Eh; b) concentration of C-Steel; c) S(-II) total aqueous concentration; d) magnetite, FeS(ppt), Fe(II) and Fe(III) aqueous concentration.

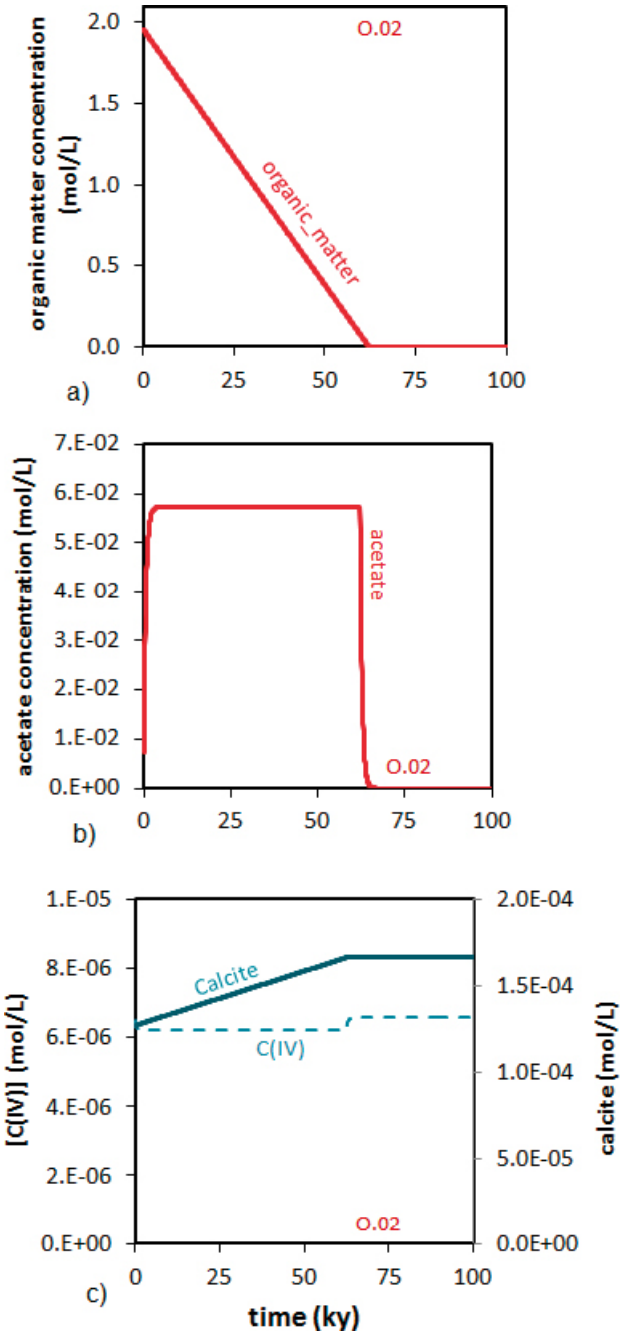

Figure A5-55. *Long term results for O.02. Temporal evolution of a) organic matter concentration; b) acetate concentration; c) calcite, and aqueous carbonate concentration.*

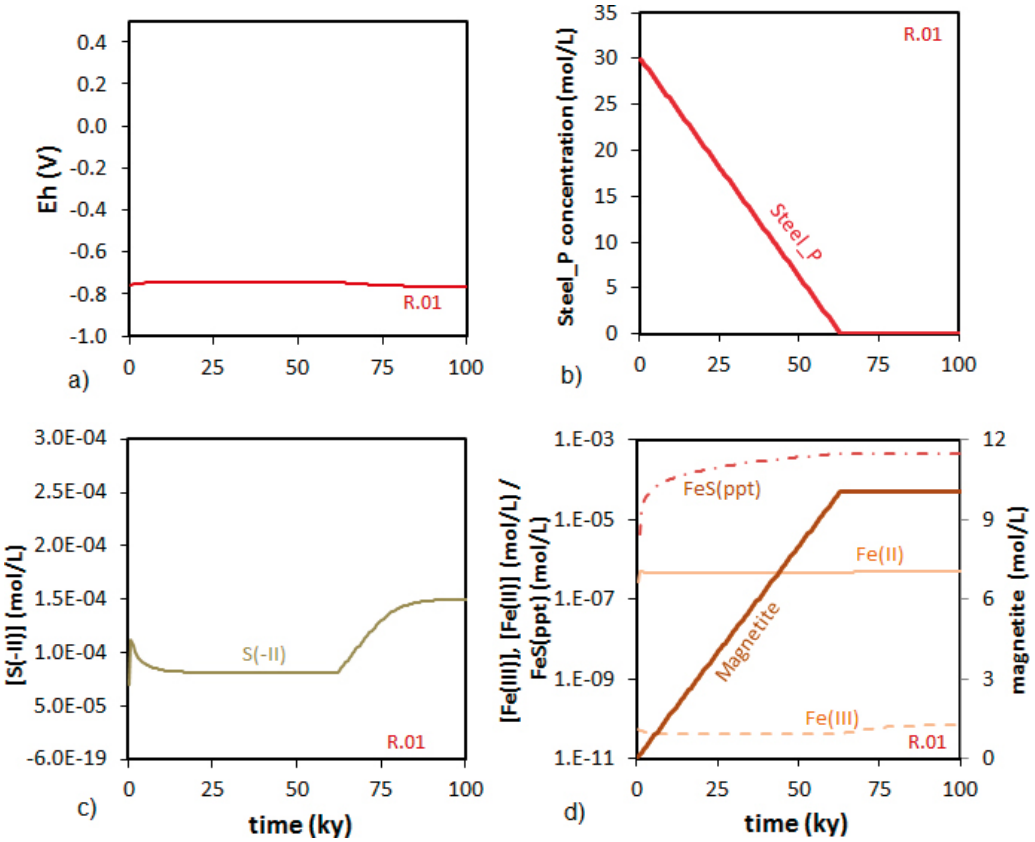

Figure A5-56. *Long term results for R.01. Temporal evolution of a) Eh; b) concentration of C-Steel; c) S(-II) total aqueous concentration; d) magnetite, FeS(ppt), Fe(II) and Fe(III) aqueous concentration.*

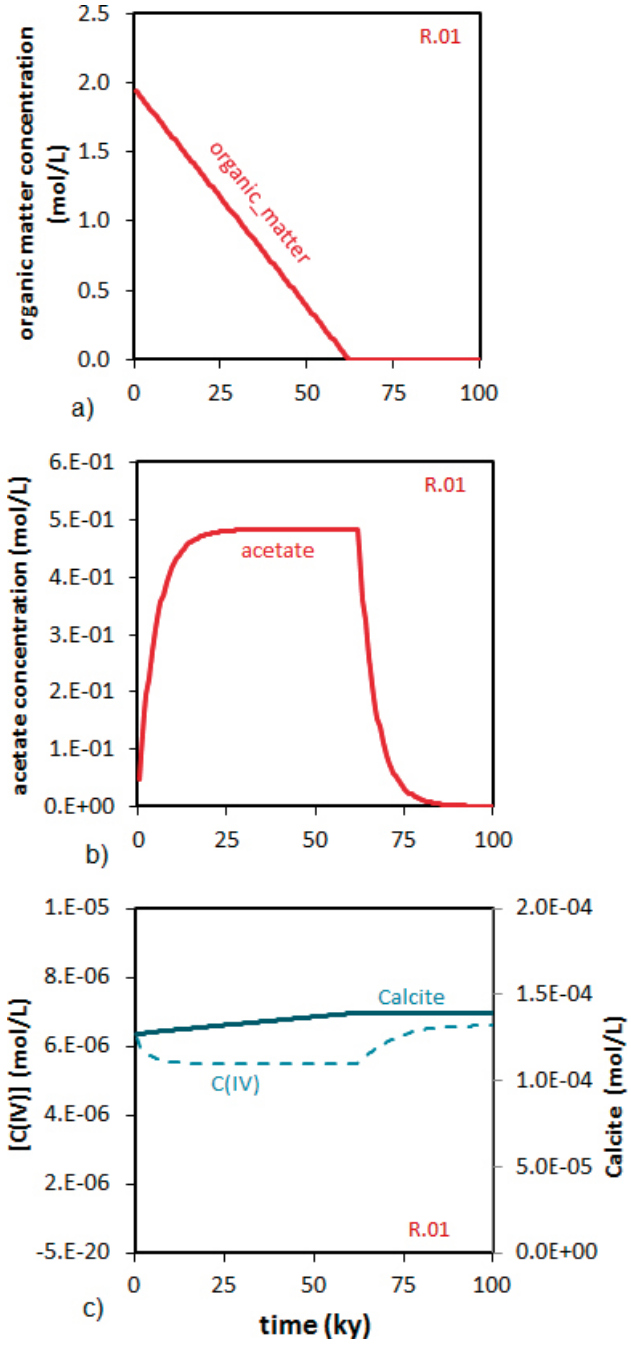

Figure A5-57. *Long term results for R.01. Temporal evolution of a) organic matter concentration; b) acetate concentration; c) calcite, and aqueous carbonate concentration.*

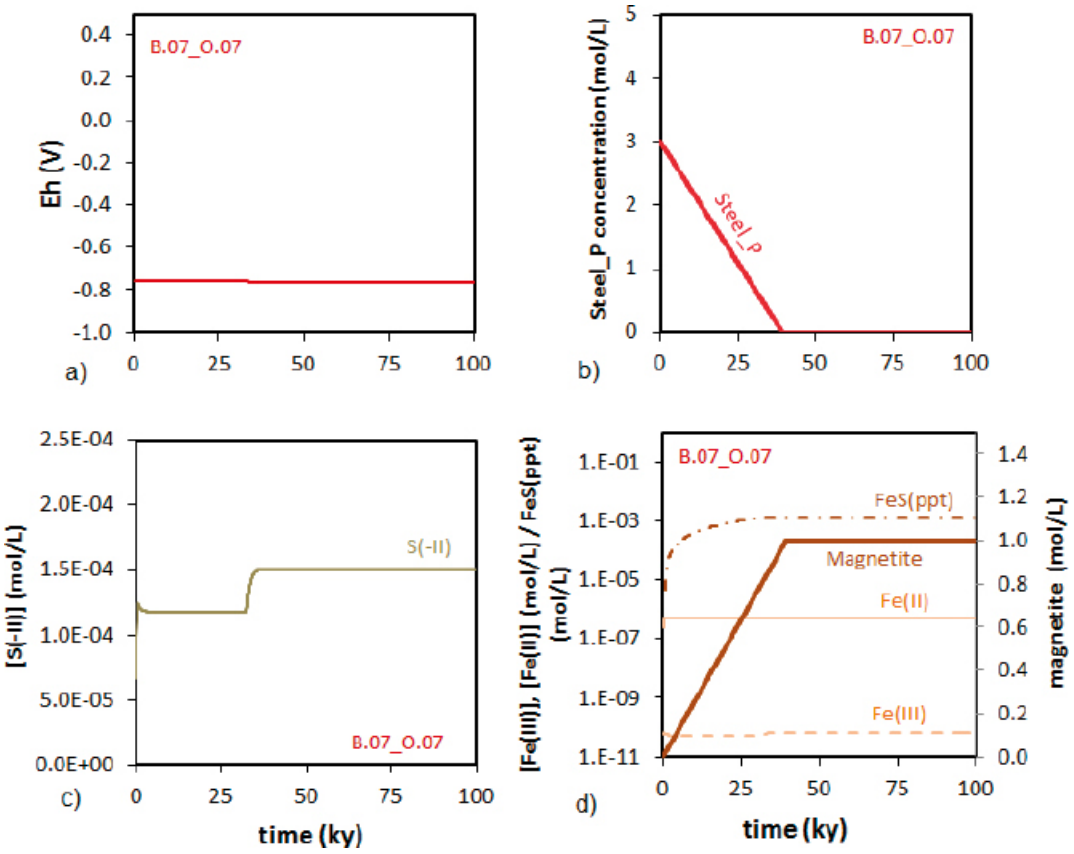

Figure A5-58. *Long term results for B.07_O.07. Temporal evolution of a) Eh; b) concentration of C-Steel; c) S(-II) total aqueous concentration; d) magnetite, FeS(ppt), Fe(II) and Fe(III) aqueous concentration.*

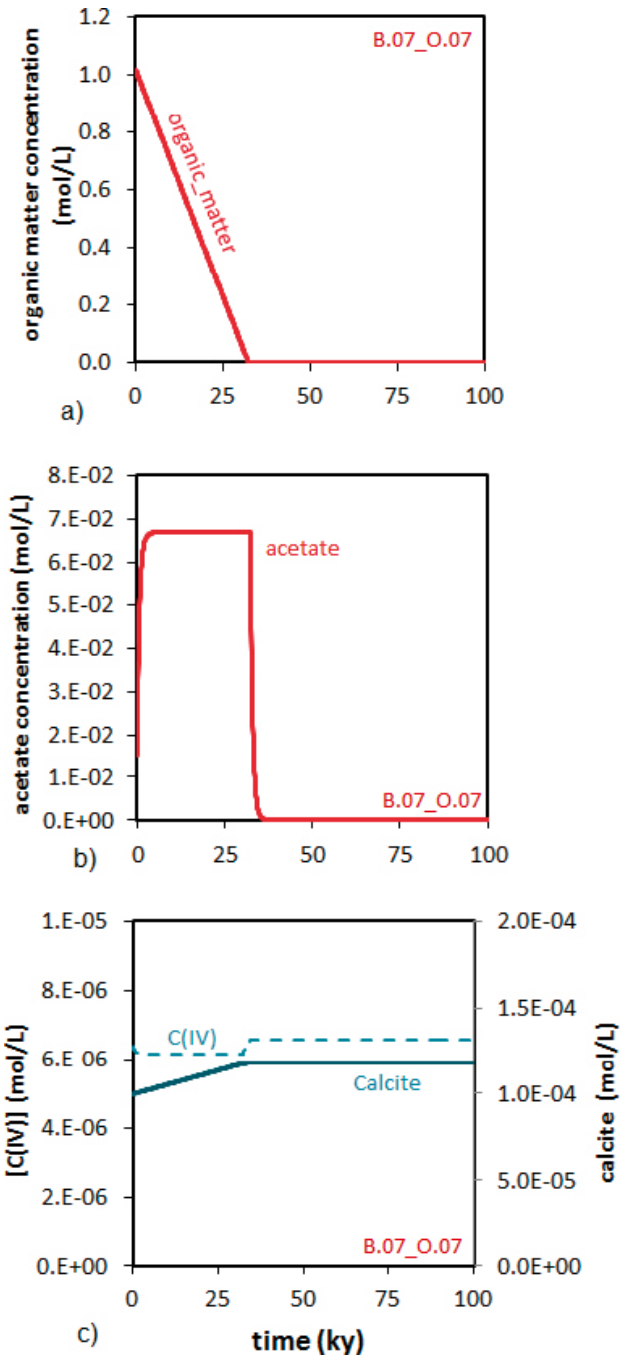

Figure A5-59. *Long term results for B.07_O.07. Temporal evolution of a) organic matter concentration; b) acetate concentration; c) calcite, and aqueous carbonate concentration.*

A5-11 Long term results. Steel and bitumen cases. B.06, F.18. F.05 and F.17 waste package types.

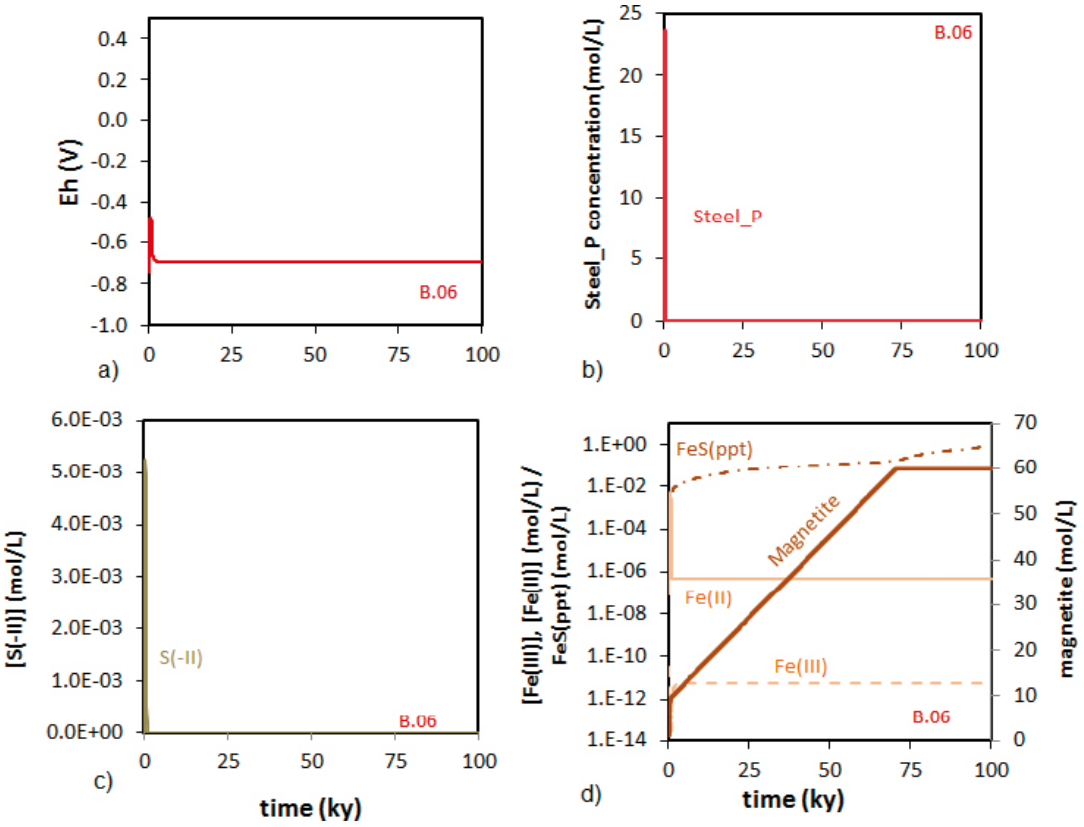

Figure A5-60. *Long term results for B.06. Temporal evolution of a) Eh; b) concentration of C-Steel; c) S(-II) total aqueous concentration; d) magnetite, FeS(ppt), Fe(II) and Fe(III) aqueous concentration.*

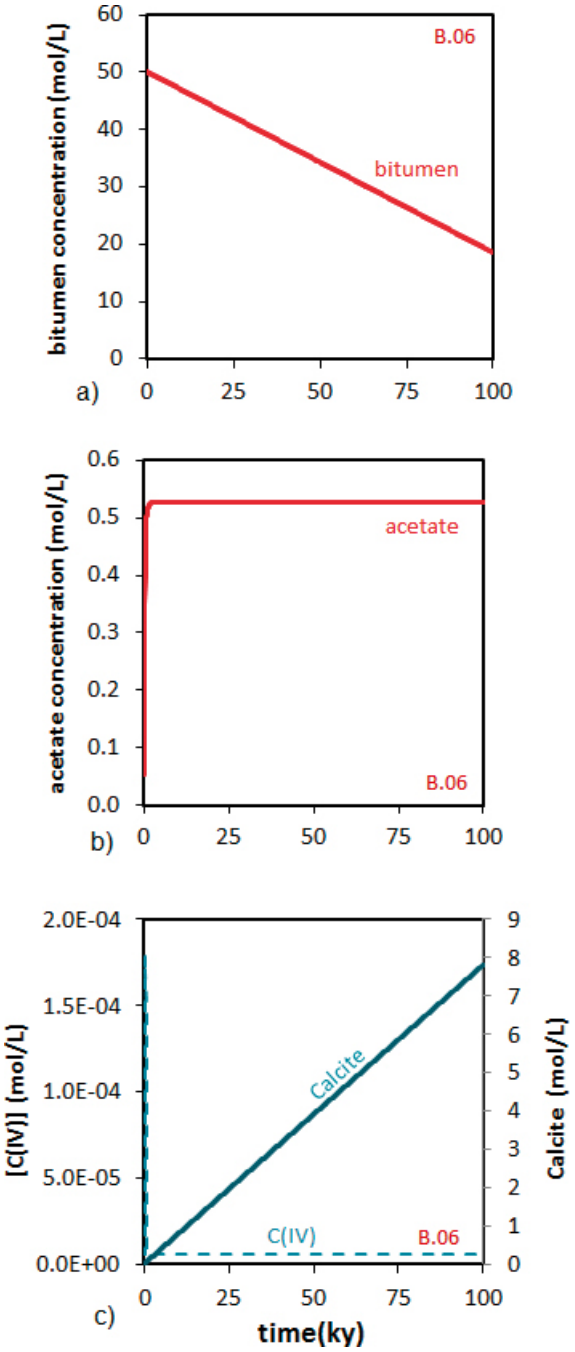

Figure A5-61. *Long term results for B.06. Temporal evolution of a) organic matter concentration; b) acetate concentration; c) calcite, and aqueous carbonate concentration.*

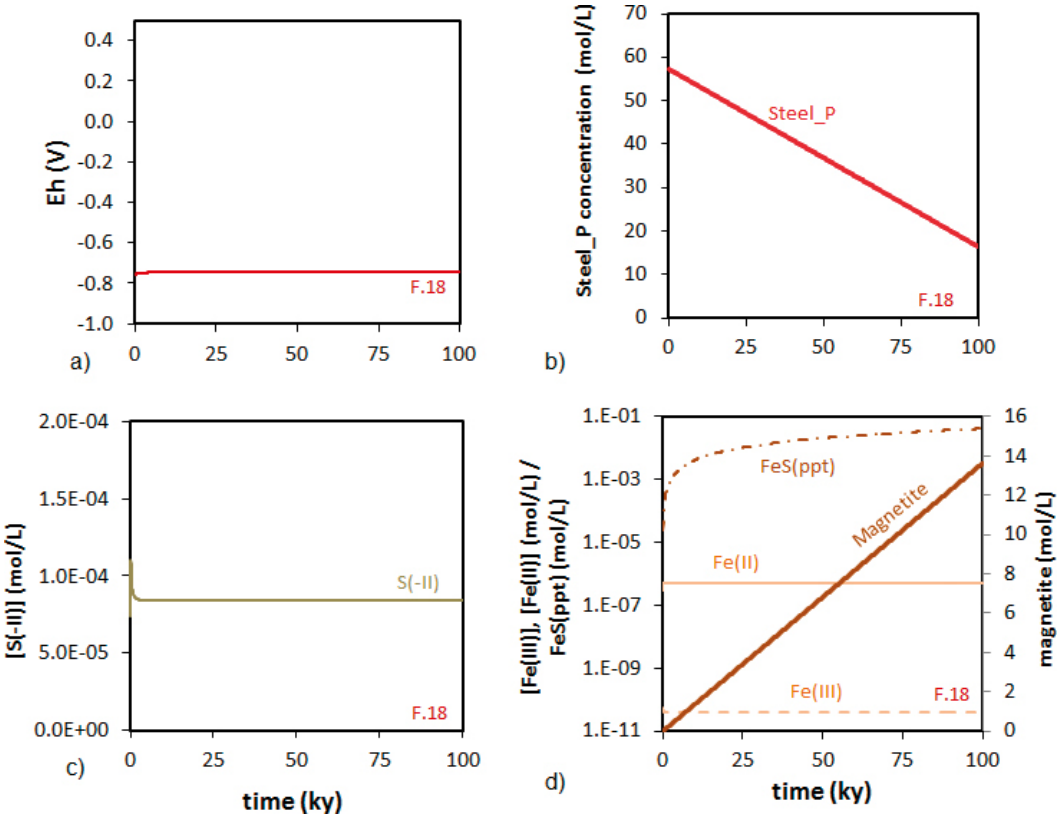

Figure A5-62. *Long term results for F.18. Temporal evolution of a) Eh; b) concentration of C-Steel; c) S(-II) total aqueous concentration; d) magnetite, FeS(ppt), Fe(II) and Fe(III) aqueous concentration.*

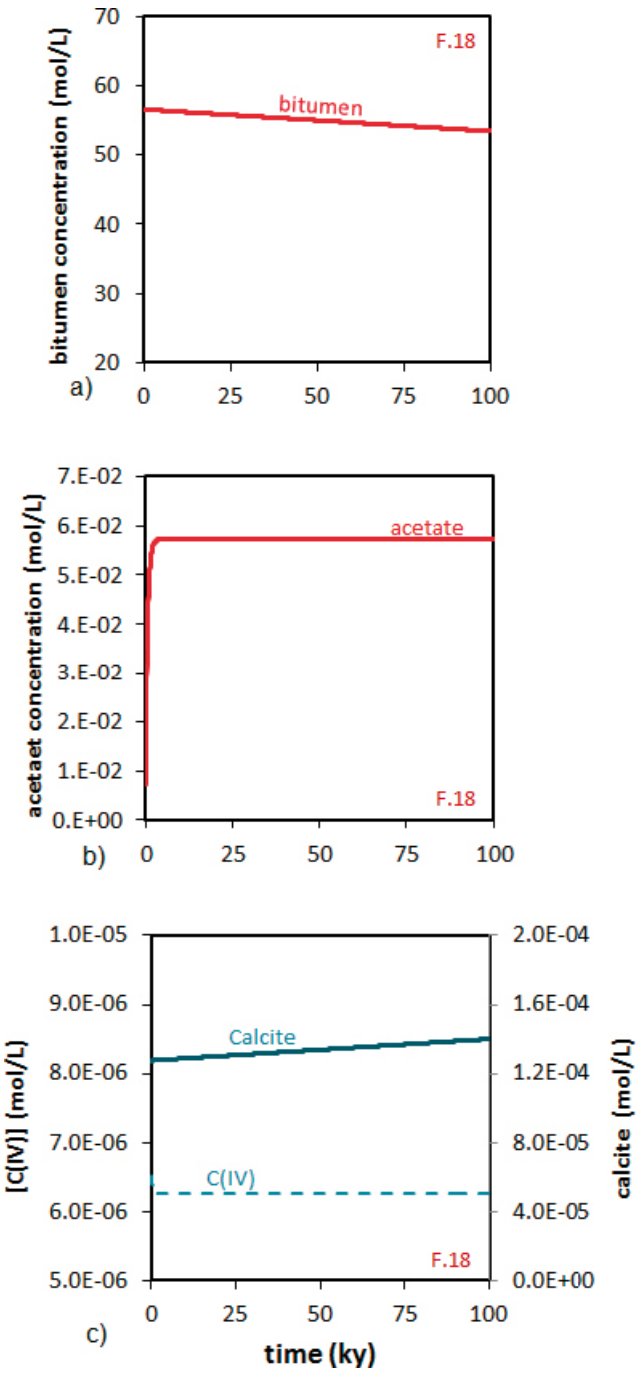

Figure A5-63. *Long term results for F.18. Temporal evolution of a) organic matter concentration; b) acetate concentration; c) calcite, and aqueous carbonate concentration.*

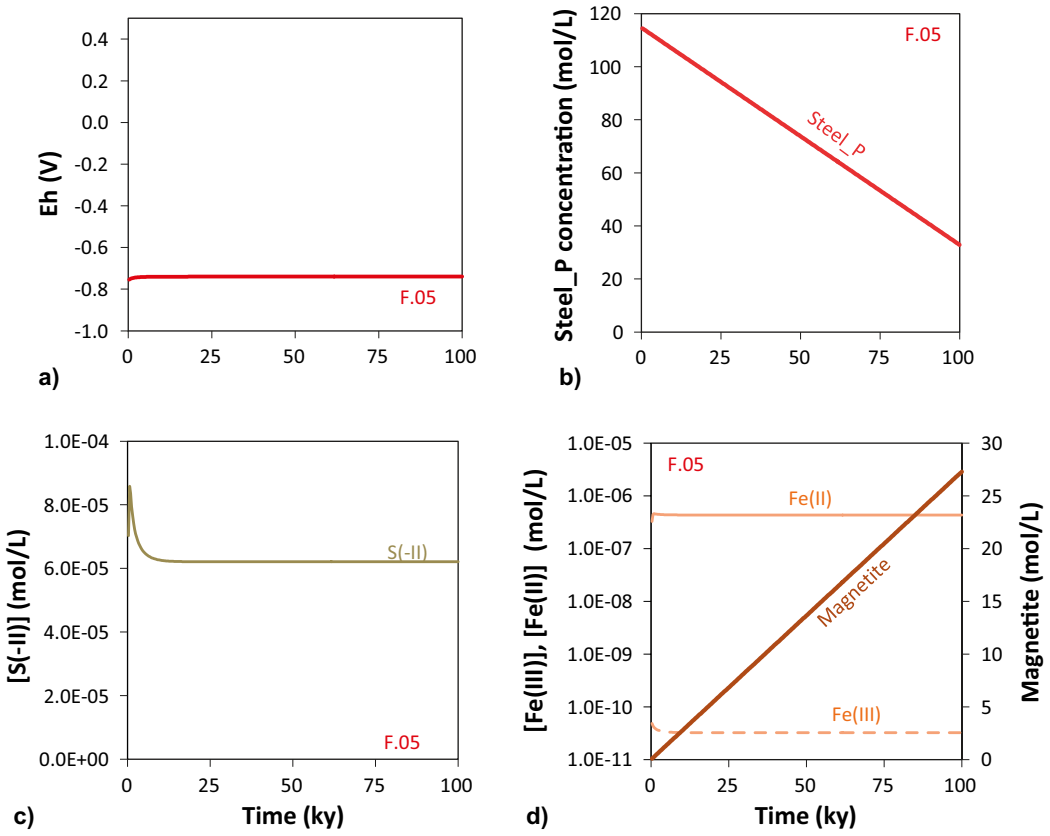

Figure A5-64. *Long term results for F.05. Temporal evolution of a) Eh; b) concentration of C-Steel; c) S(-II) total aqueous concentration; d) magnetite, FeS(ppt), Fe(II) and Fe(III) aqueous concentration.*

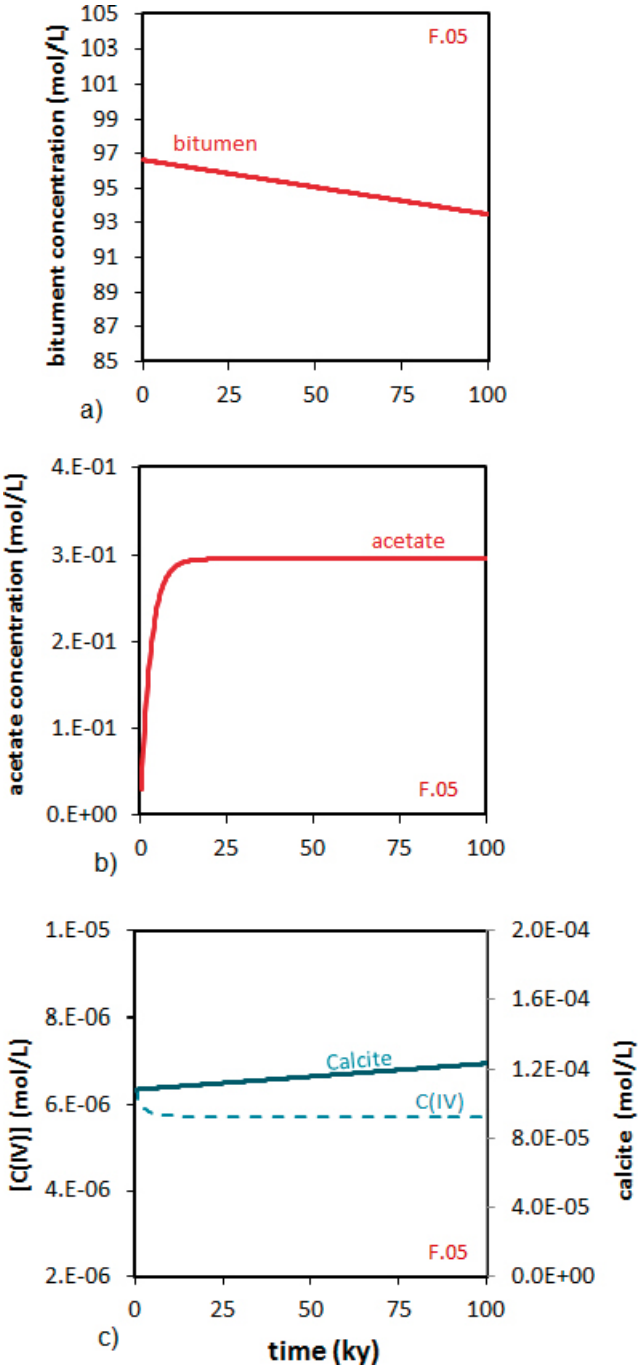

Figure A5-65. *Long term results for F.05. Temporal evolution of a) organic matter concentration; b) acetate concentration; c) calcite, and aqueous carbonate concentration.*

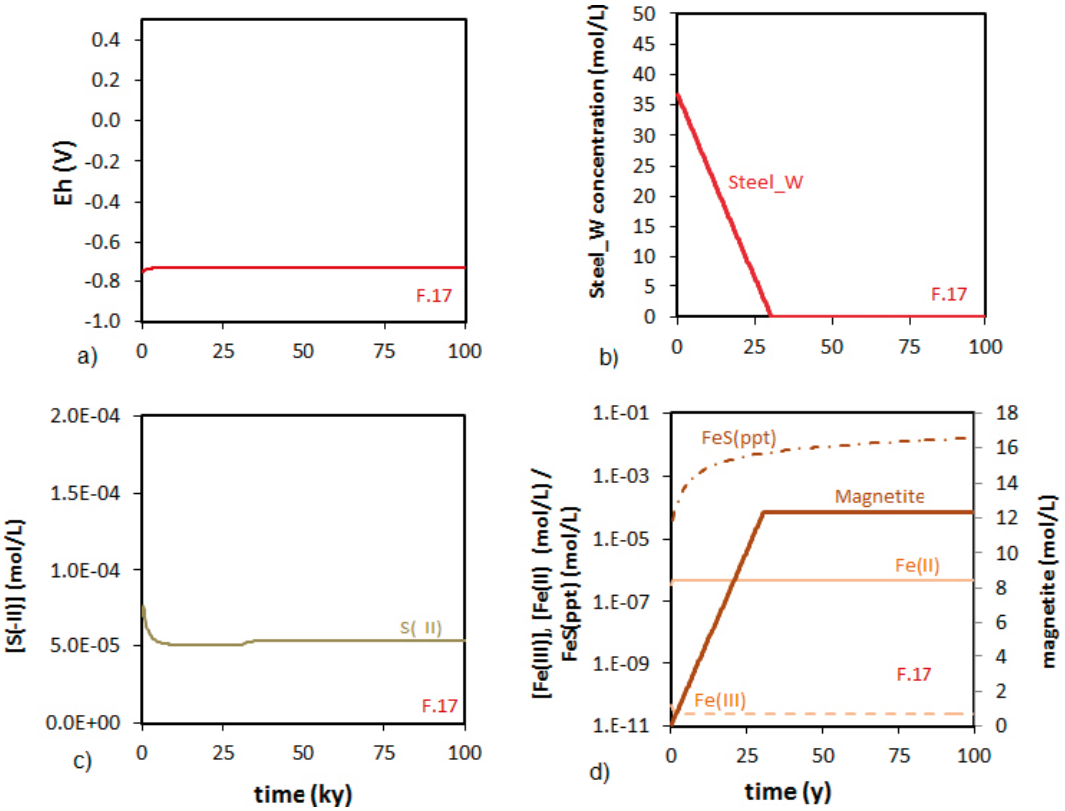

Figure A5-66. *Long term results for F.17. Temporal evolution of a) Eh; b) concentration of C-Steel; c) S(-II) total aqueous concentration; d) magnetite, FeS(ppt), Fe(II) and Fe(III) aqueous concentration.*

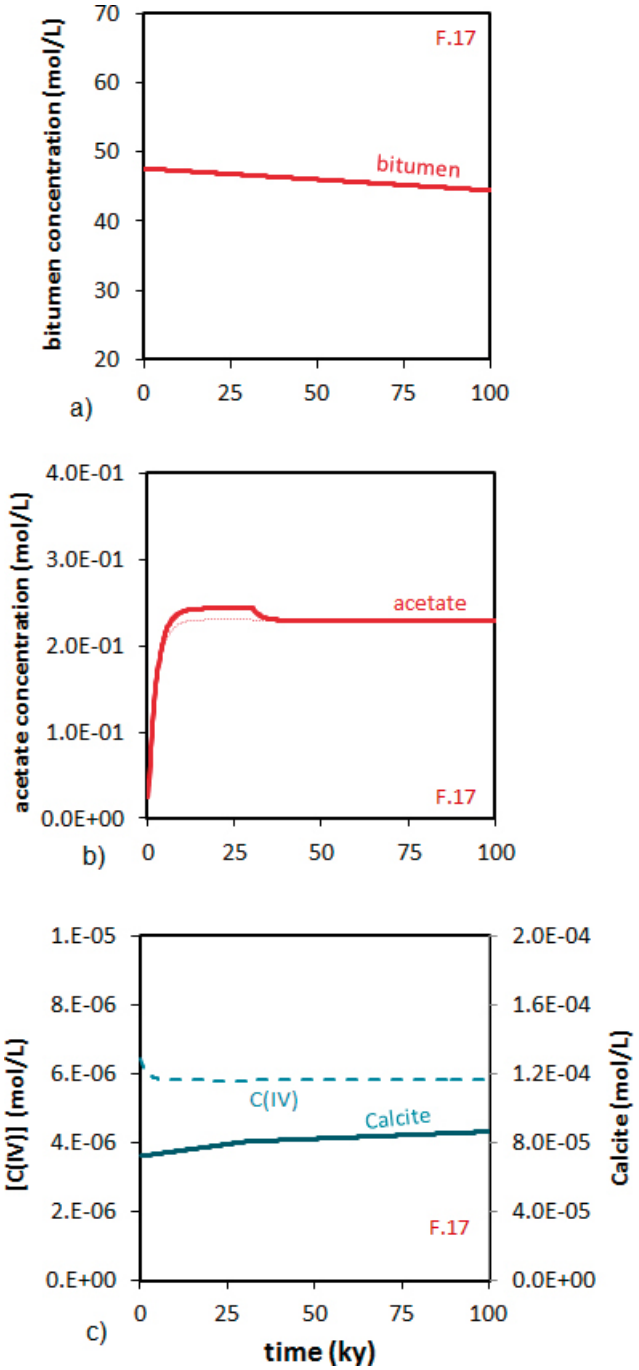

Figure A5-67. *Long term results for F.17. Temporal evolution of a) organic matter concentration; b) acetate concentration; c) calcite, and aqueous carbonate concentration.*

A5.12 Long term results. Steel and cellulose cases with bitumen or organic matter. O.23, F.23, B.05 and O.12 waste package types.

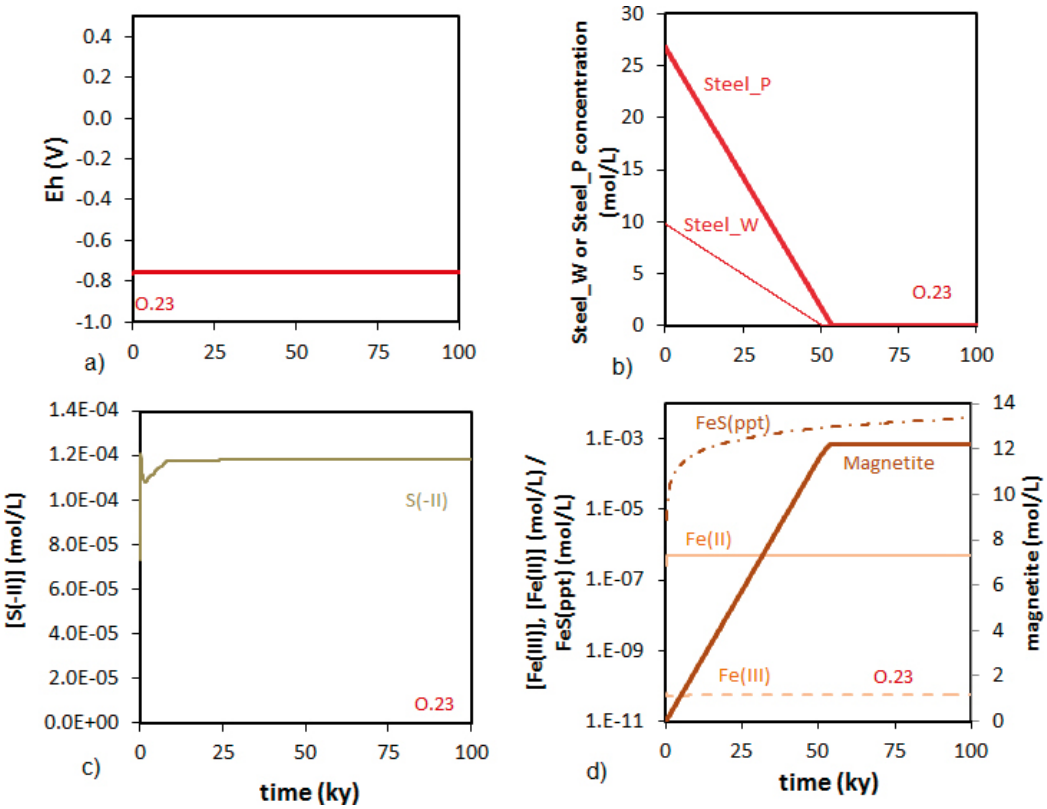

Figure A5-68. *Long term results for O.23. Temporal evolution of a) Eh; b) concentration of C-Steel; c) S(-II) total aqueous concentration; d) magnetite, FeS(ppt), Fe(II) and Fe(III) aqueous concentration.*

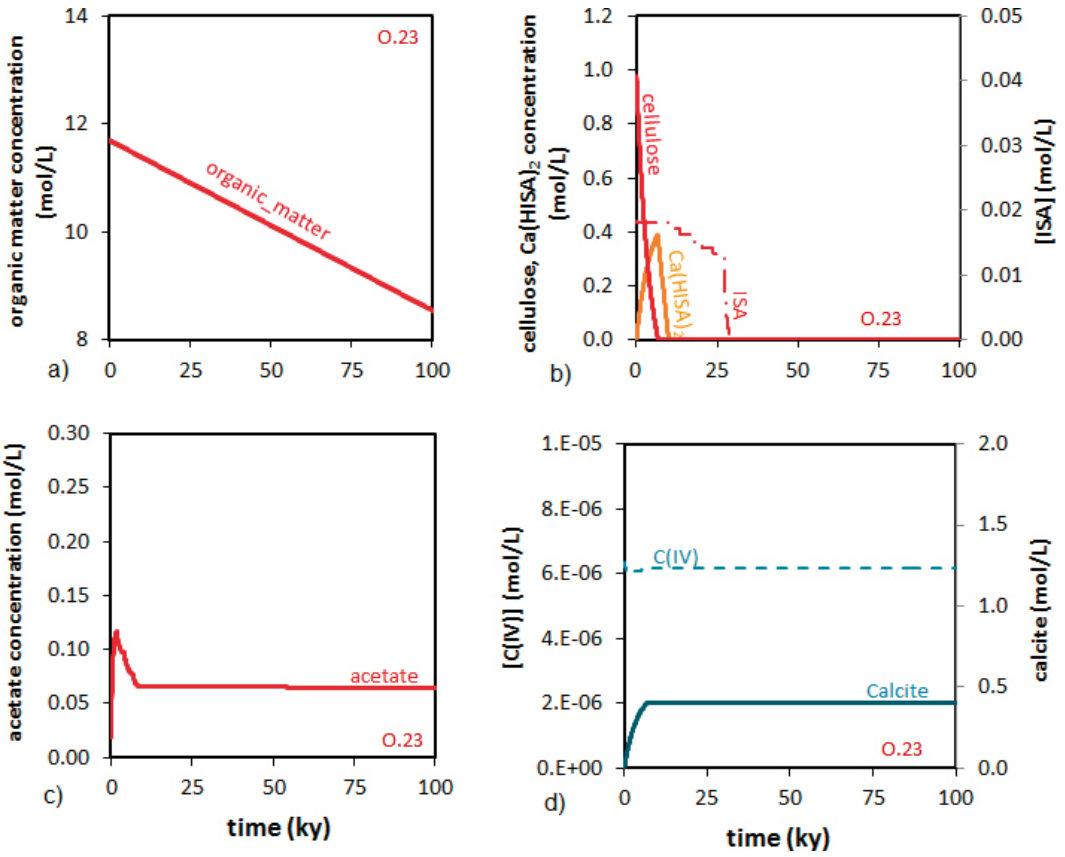

Figure A5-69. *Long term results for O.23. Temporal evolution of a) organic matter concentration; b) cellulose, $Ca(HISA)_2$(cr) and ISA aqueous concentration; c) acetate concentration; d) calcite, and aqueous carbonate concentration.*

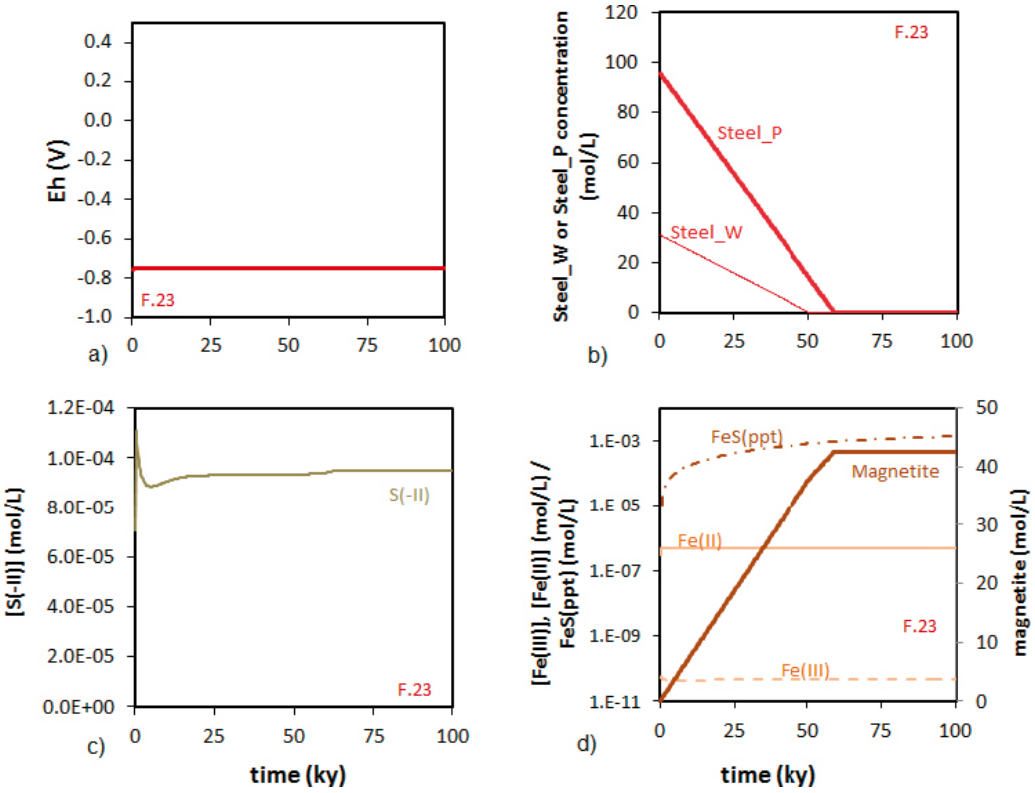

Figure A5-70. *Long term results for F.23. Temporal evolution of a) Eh; b) concentration of C-Steel; c) S(-II) total aqueous concentration; d) magnetite, FeS(ppt), Fe(II) and Fe(III) aqueous concentration.*

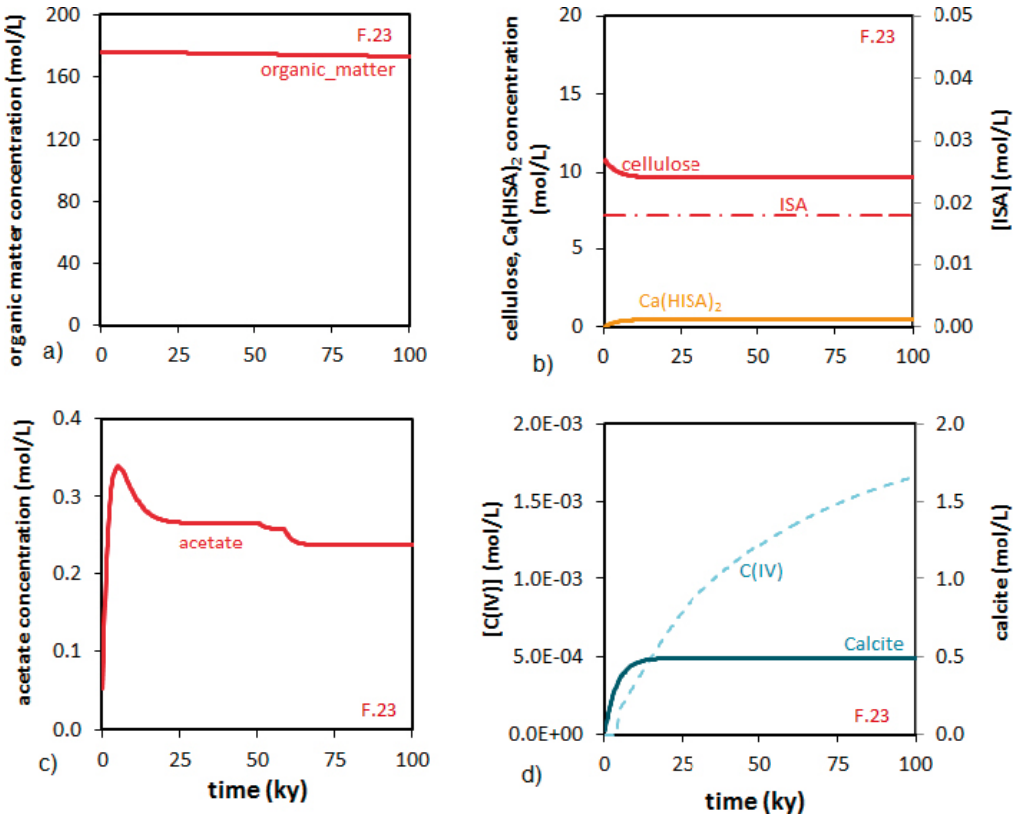

Figure A5-71. *Long term results for F.23. Temporal evolution of a) organic matter concentration; b) cellulose, $Ca(HISA)_2$(cr) and ISA aqueous concentration; c) acetate concentration; d) calcite, and aqueous carbonate concentration.*

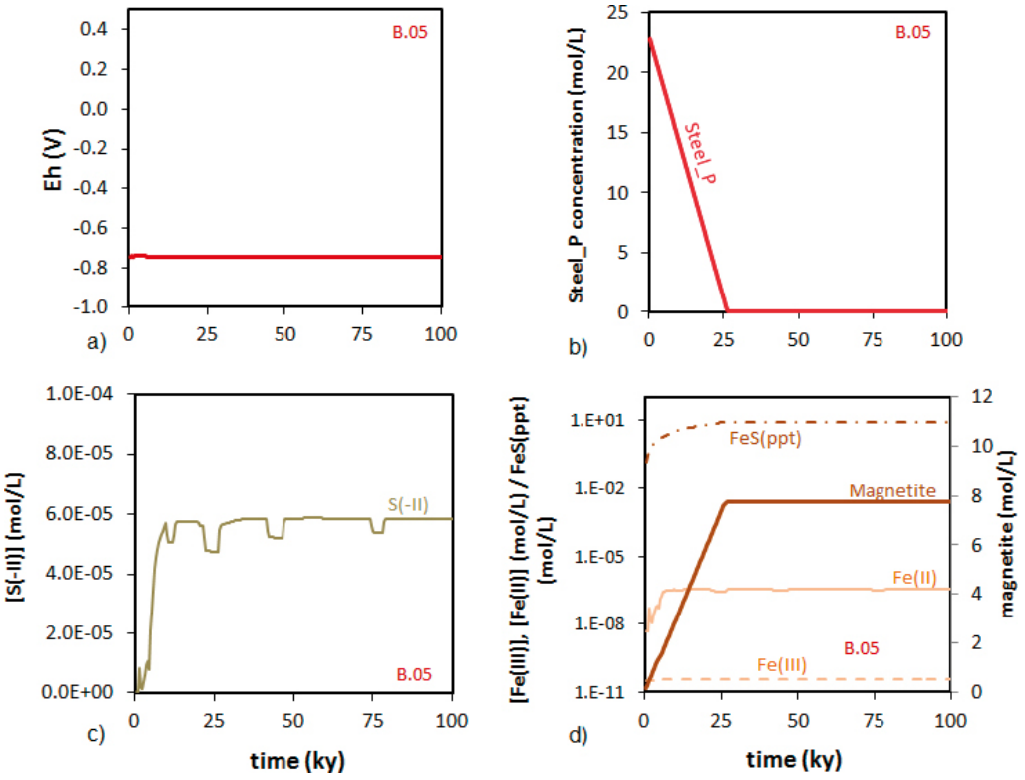

Figure A5-72. *Long term results for B.05. Temporal evolution of a) Eh; b) concentration of C-Steel; c) S(-II) total aqueous concentration; d) magnetite, FeS(ppt), Fe(II) and Fe(III) aqueous concentration.*

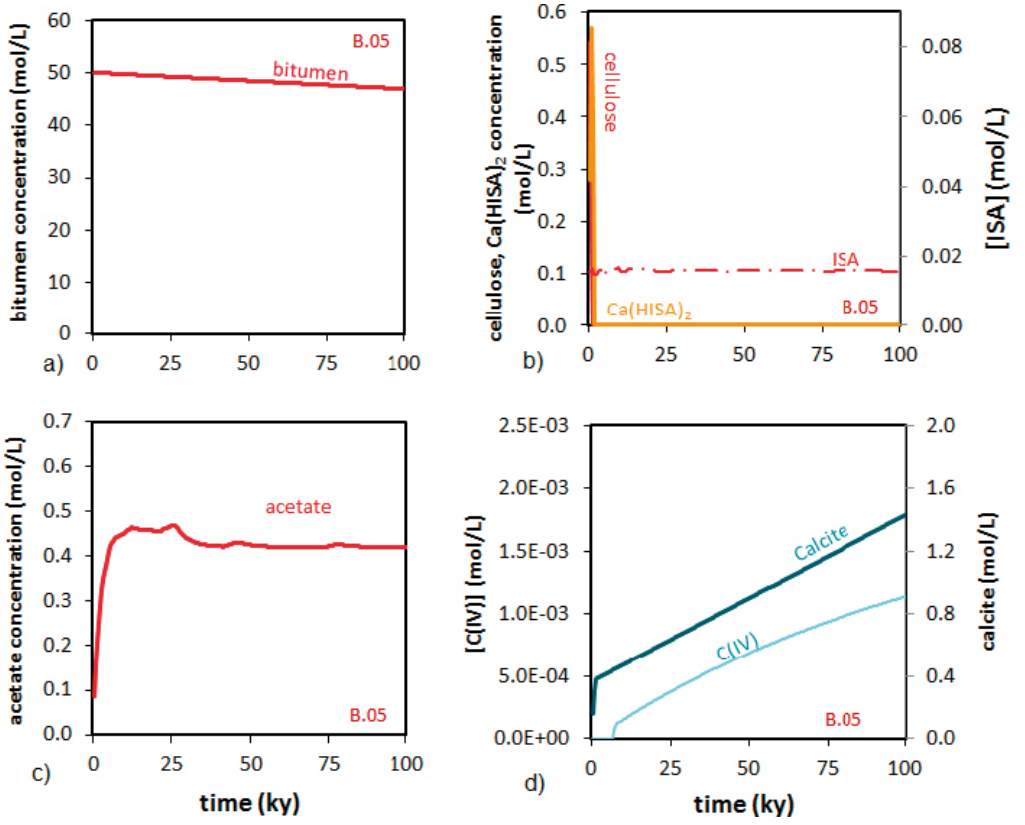

Figure A5-73. *Long term results for B.05. Temporal evolution of a) organic matter concentration; b) cellulose, $Ca(HISA)_2(cr)$ and ISA aqueous concentration; c) acetate concentration; d) calcite, and aqueous carbonate concentration.*

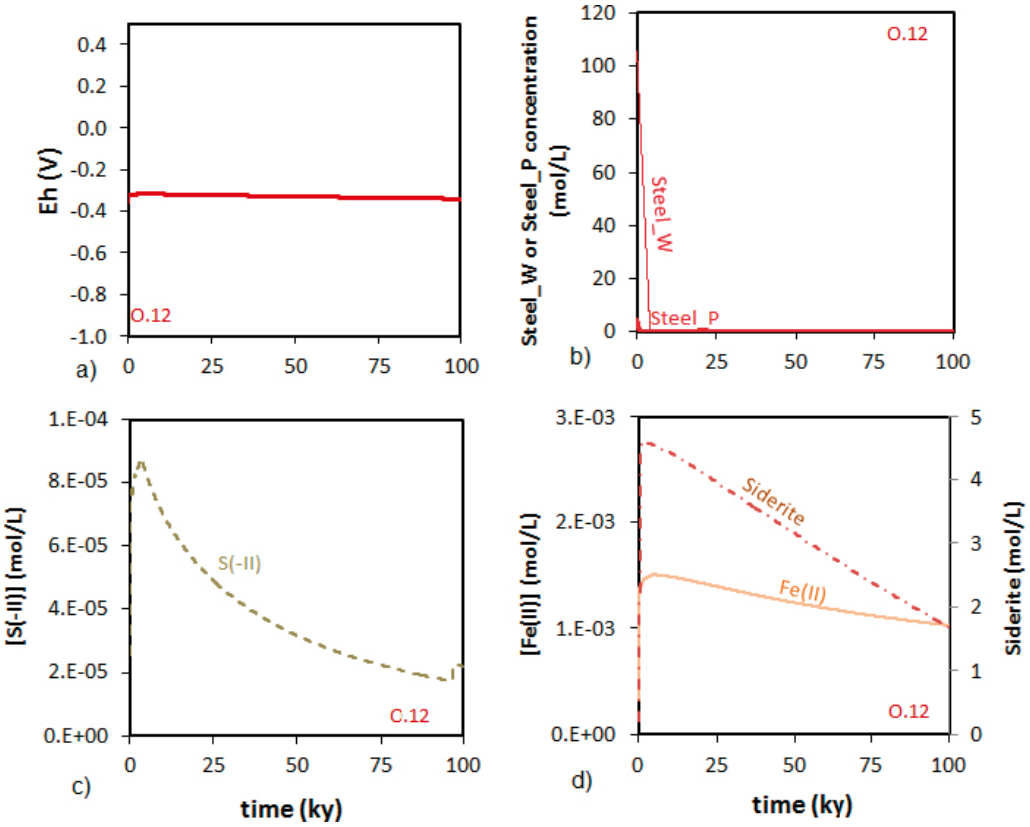

Figure A5-74. *Long term results for O.12. Temporal evolution of a) Eh; b) concentration of C-Steel; c) S(-II) total aqueous concentration; d) siderite and Fe(II) aqueous concentration.*

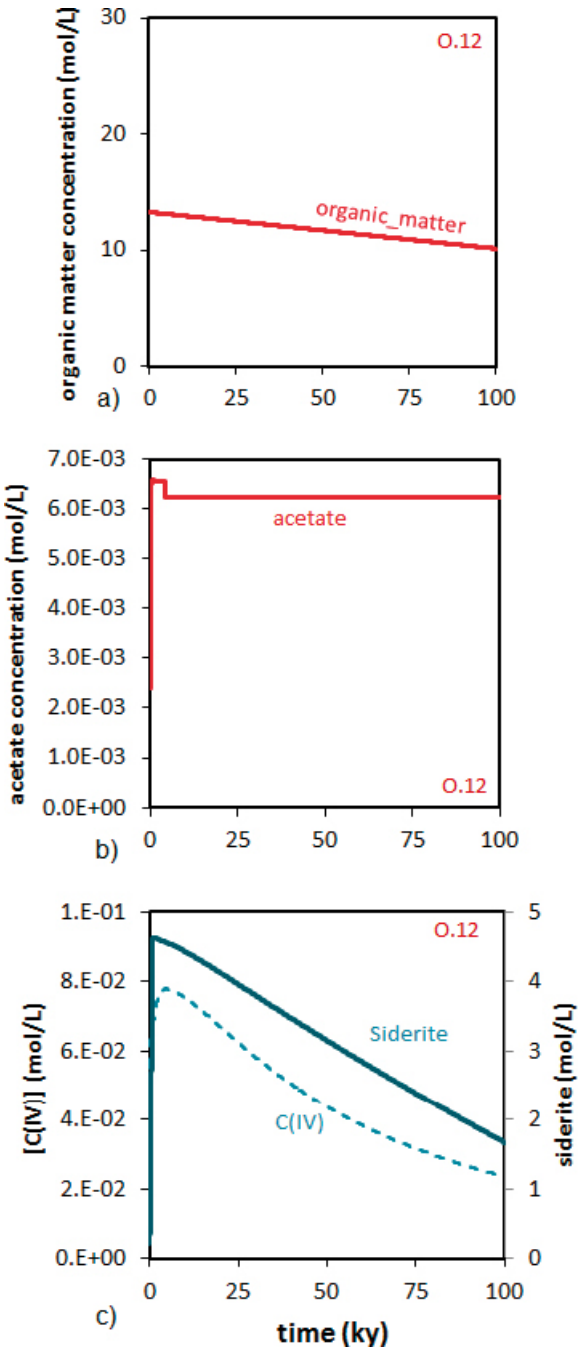

Figure A5-75. *Long term results for O.12. Temporal evolution of a) organic matter concentration; b) acetate concentration; d) siderite and aqueous carbonate concentration.*

Visualisation of the results

The evolution of the RDC in the vaults can also be spatially visualised by considering the distribution of the waste package types within the vault. In Zazzi (2011) an approximated distribution of the selected waste package types are proposed for the Silo, the BMA, the BTF and BLA vaults.

We have represented the geometry of the vaults with the COMSOL code and the evolution of the RDC in each one of the waste package types has been fed into the code so that the evolution of the overall RDC can be visualised.

In the case of the Silo we have considered that the central area (A zone in Figure A6-1a) consists of 9 shafts of type 55, containing 320 B.06 and 12 O.02 waste packages. Zone B in the same figure contains a general type shaft, with 24 O.02 and 28 R.16 waste packages. Given the lack of information on the vertical distribution of the waste package types in the shafts a homogeneous configuration has been considered (Figure A6-1b).

This waste package type distribution has been implemented in a 3D representation of the Silo (Figure A6-2, and the RDC temporal evolution has been represented. Two horizontal and vertical sections of Silo showing the RDC at different times (Figure A6-2), can be shown in Figure A6-3 and A6-4.

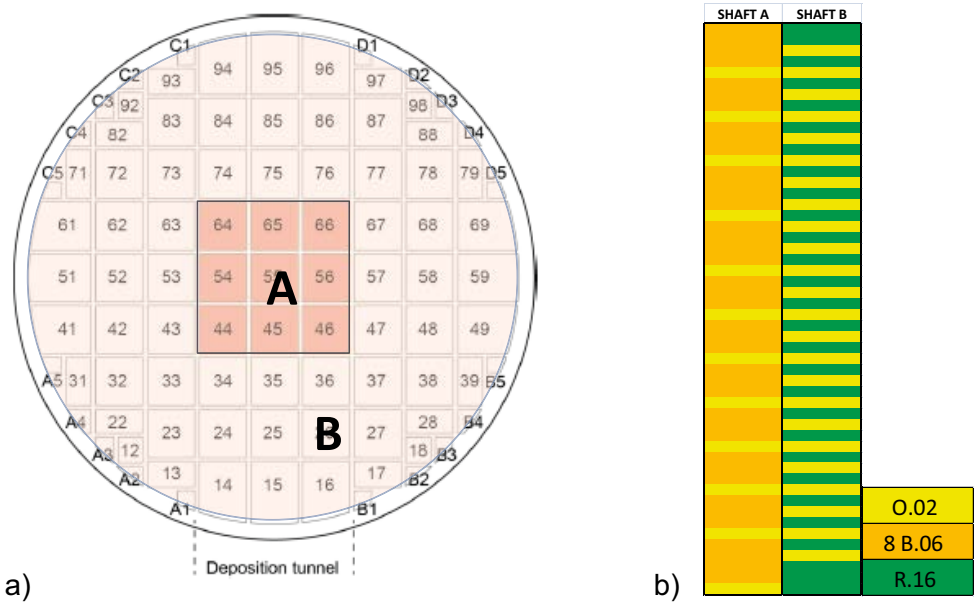

Figure A6-1. *a) Scheme showing a horizontal section of Silo and the horizontal distribution of the two different shafts considered A, and B. b) Vertical distribution of waste packages O.02, B.06 and R.16 in shafts A and B.*

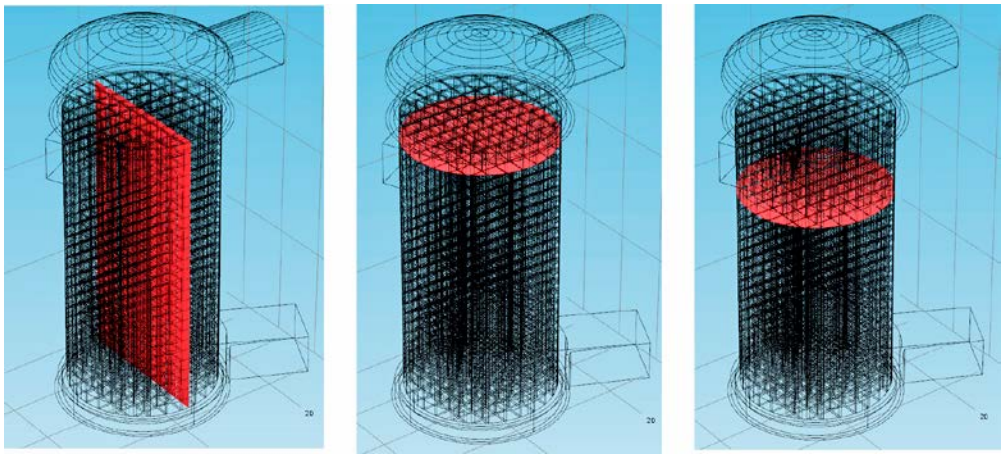

Figure A6-2. *3D scheme of the Silo, showing the vertical section (a) and the two horizontal sections (b and c) for which the temporal evolution of the RDC is shown.*

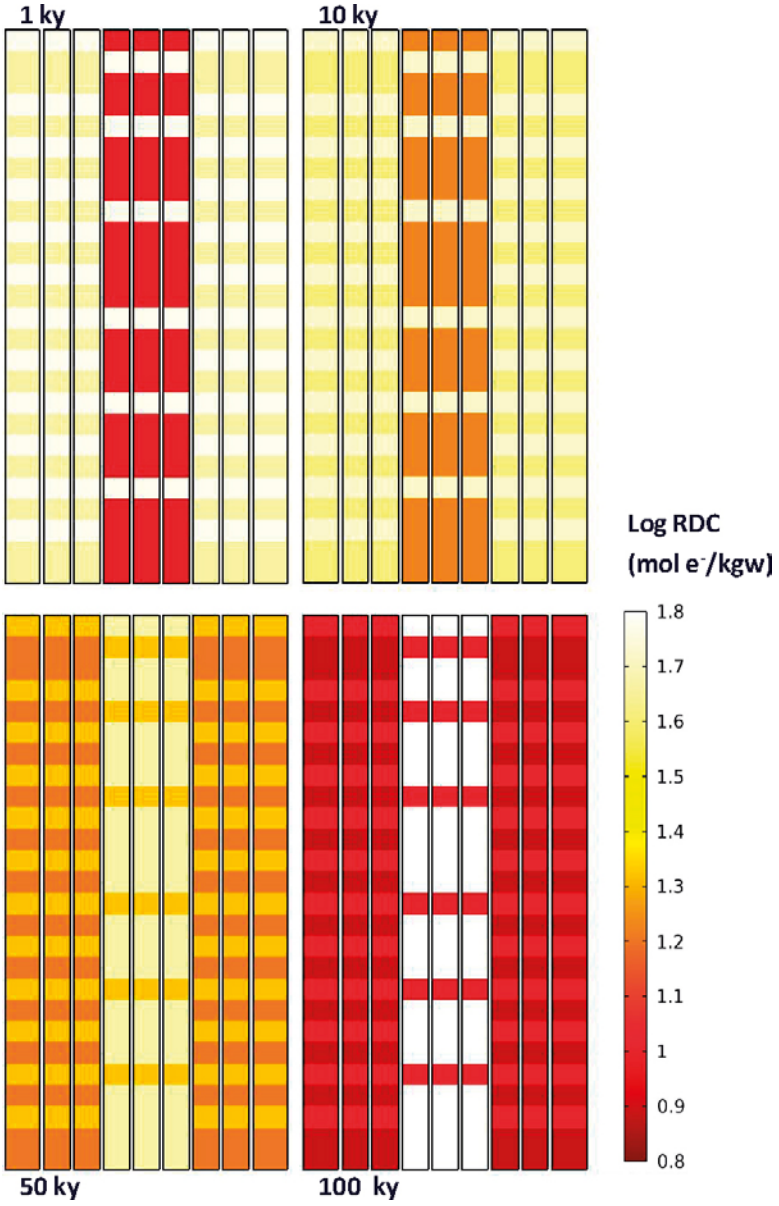

Figure A6-3. *RDC temporal evolution of the Silo for the vertical section shown in Figure A6-2.*

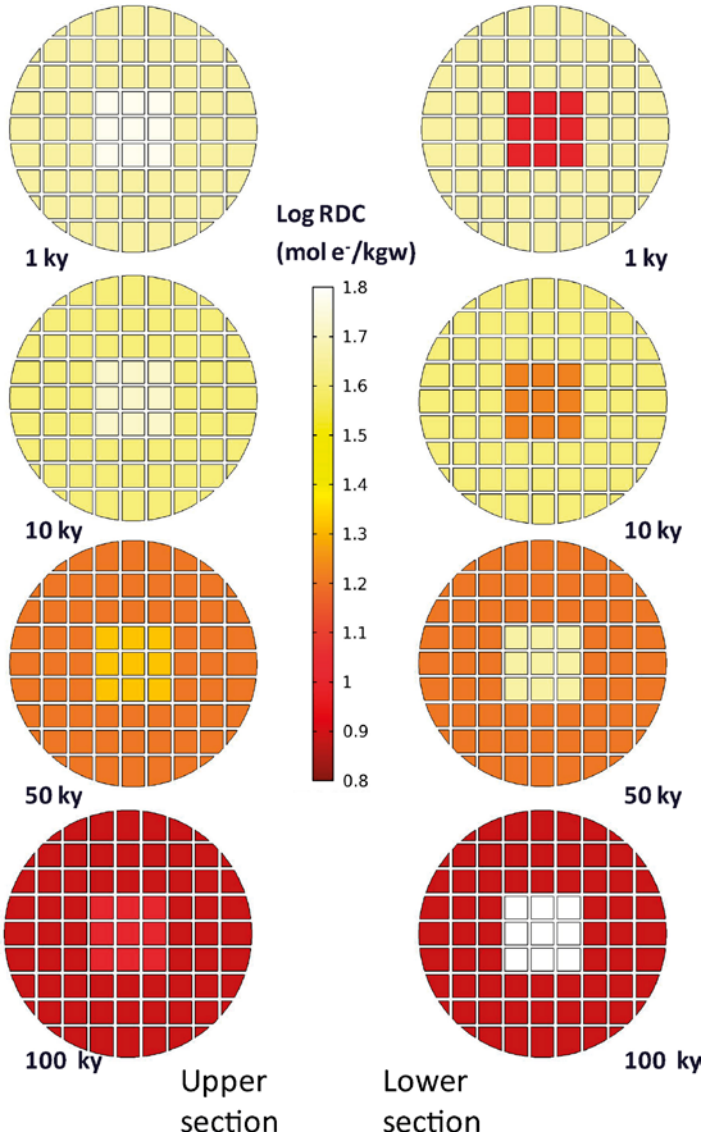

Figure A6-4. *RDC temporal evolution of the Silo for the two horizontal sections (upper and lower) shown in Figure A6-2*

The RDC evolution shown in Figure A6-3 and A6-4 indicates that in zone B, the RDC decreases with time, following the evolution of the O.02 and R.16 waste package types. The evolution of the central area, rich in bituminised waste package types, is slightly different. In general, it is seen that the global RDC increases but this is because in this area the main waste package type is B.06. In this waste package type, magnetite is the phase controlling the reductive capacity of the system, although with time the precipitation of FeS(ppt) has an important role. The contribution of this phase to the RDC is higher than the contribution of magnetite because it contains S(-II) and does not contain Fe(III). Because of this, RDC of this central area increases with time. Nevertheless, if focus is centered to the O.02 level it can be seen that RDC decreases with time (Figure A6-4, upper section).

Zazzi (2011) also selected shaft 54 as representative of area A of the Silo. This shaft is composed of 78 F.18 type and 12 O.02 type waste packages. If this shaft has been plotted in this 3D representation, the RDC evolution in the central area will have followed the same trend despite the level studied. RDC will decrease anywhere, although its value in F.18 will be higher than in the O.02 level.

Detailed information on the waste package distribution in BMA vault is only provided for compartments 1 to 4 (Zazzi, 2011) (Figure A6-5).

The 3D distribution we have implemented in each of the four first compartments is shown in Figure A6-6 and schematised in Figure A6-7.

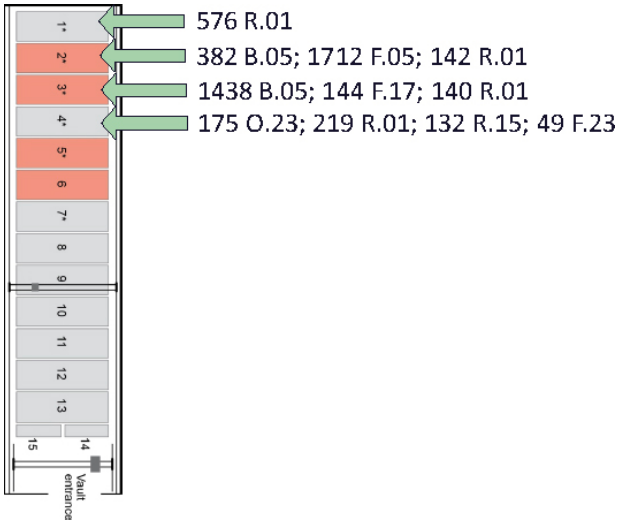

Figure A6-5. *Scheme showing an upperview of BMA vault indicating the number and type of waste packages for the first 4 compartments.*

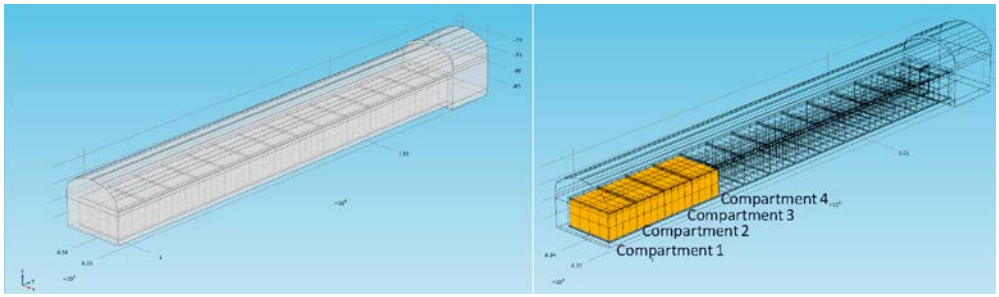

Figure A6-6. Scheme showing the BMA structure and the situation of the four compartments studied.

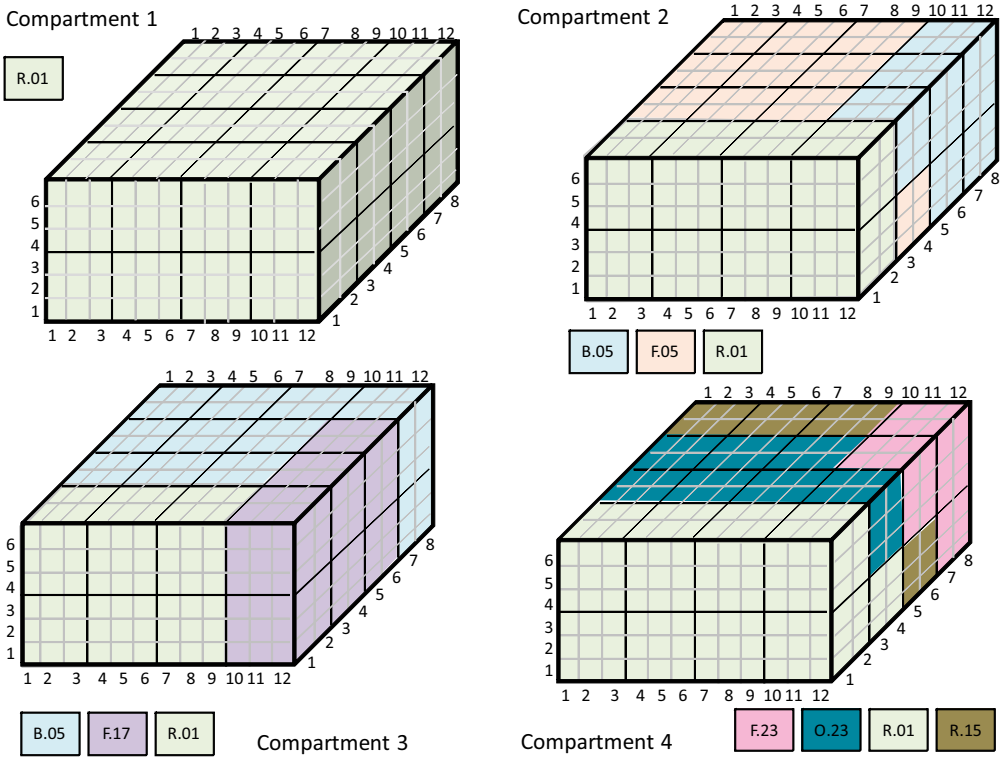

Figure A6-7. 3D distribution of waste package types in each of the four compartments of BMA vault.

Results are plotted in Figure A6-8 at four different times. As it can be seen, RDC is globally decreased with time, being the external zone the area where the RDC is in general lower. Compartments 2 and 3 are those presenting a higher RDC.

Vaults 1&2 BTF and BLA are simpler because of the lower amount of different type of waste packages present in these vaults. Therefore, 3D distribution is less complicated. In fact, only one waste package type has been selected for BLA and 2 BTF vaults. Therefore their RDC temporal evolution will not differ from that of the waste package itself.

The 1 BTF vault only contains two waste package types, S.13 and B.07_O.07. We have considered a homogeneous vertical and horizontal distribution of these two packages, as shown in Figure A6-9. The temporal evolution of RDC is shown in Figure A6-10. The RDC of both waste package types decreases fast to small values, and as can be seen in Figure A6-10, it achieves near constant values before 50 ky.

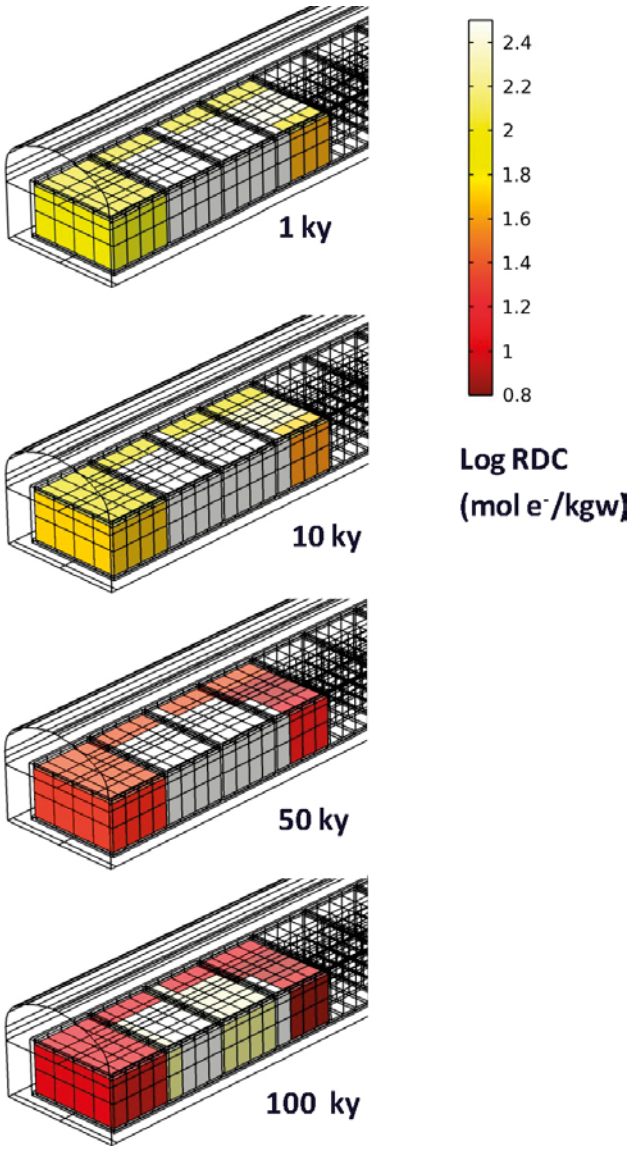

Figure A6-8. RDC temporal evolution of the BMA vault.

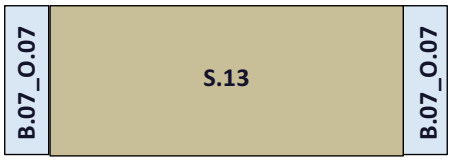

Figure A6-9. 2D distribution of waste package types in 1 BTF vault.

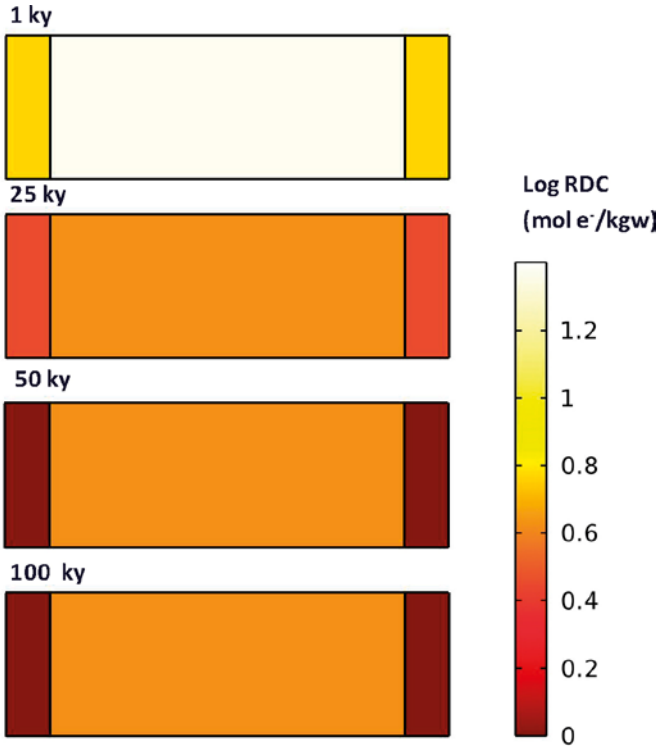

Figure A6-10. RDC temporal evolution of the 1 BTF. Vertical section.

Appendix 7

Glossary

[aq]	Aqueous concentration (mol dm^{-3})
Biotic	In this report, the "biotic" term is applied to those processes microbially driven ot to conditions where the presence of microbes is considered, while the abiotic term is applied to those conditions in which chemical reactions are not microbially driven.
b_{O_z}	Decay coefficient of O_2-consumers bacteria (s^{-1})
$b_{Fe(III)}$	Decay coefficient of Fe(III)-consumers bacteria (s^{-1})
$b_{S(VI)}$	Decay coefficient of S(VI)-consumers bacteria (s^{-1})
C-Steel	Carbon steel
$(celdeg)_t$	Fraction of cellulose degraded as a function of time
$(G_r)_0$	number of end reducing groups (estimated as the reciprocal of the initial degree of polymerisation)
k_h	normalized first-order reaction rate constant of the midchain scission in cellulose degradation (h^{-1})
k_1	reaction rate constants related to the peeling-off process in cellulose degradation (h^{-1})
k_t	reaction rate constants related to the peeling-off process in cellulose degradation (h^{-1})
$K_{acetate}^{O_2}$	Maximum acetate degradation rate by O_2-consumers bacteria ($mol_{acetate}\ mol^{-1}_{BiomassO}\ s^{-1}$)
$K_{acetate}^{Fe(III)}$	Maximum acetate degradation rate by Fe(III)-consumers bacteria ($mol_{acetate}\ mol^{-1}_{BiomassFe}\ s^{-1}$)
$K_{acetate}^{S(VI)}$	Maximum acetate degradation rate by S(VI)-consumers bacteria ($mol_{acetate}\ mol^{-1}_{BiomassS}\ s^{-1}$)
$K_{bitumen}^{O_2}$	Maximum bitumen degradation rate by O_2-consumers bacteria ($mol_{bitumen}\ mol^{-1}_{BiomassO}\ s^{-1}$)
$K_{bitumen}^{Fe(III)}$	Maximum bitumen degradation rate by Fe(III)-consumers bacteria ($mol_{bitumen} mol^{-1}_{BiomassFe}\ s^{-1}$)
$K_{bitumen}^{S(VI)}$	Maximum bitumen degradation rate by S(VI)-consumers bacteria ($mol_{bitumen}\ mol^{-1}_{BiomassS}\ s^{-1}$)
$K_{cellulose}^{O_2}$	Maximum cellulose degradation rate by O_2-consumers bacteria ($mol_{cellulose}\ mol^{-1}_{BiomassO}\ s^{-1}$)
$K_{cellulose}^{Fe(III)}$	Maximum cellulose degradation rate by Fe(III)-consumers bacteria ($mol_{cellulose}\ mol^{-1}_{BiomassFe}\ s^{-1}$)
$K_{cellulose}^{S(VI)}$	Maximum cellulose degradation rate by S(VI)-consumers bacteria ($mol_{cellulose}\ mol^{-1}_{BiomassS}\ s^{-1}$)
$k_{1/2}^{acetate,O_2}$	Half-constant for acetate degradation due to O_2-consumers bacteria (mol dm^{-3})
$k_{1/2}^{acetate,Fe(III)}$	Half-constant for acetate degradation due to Fe(III)-consumers bacteria (mol dm^{-3})
$k_{1/2}^{acetate,S(VI)}$	Half-constant for acetate degradation due to S(VI)-consumers bacteria (mol dm^{-3})
$k_{1/2}^{bitumen,O_2}$	Half-constant for bitumen degradation due to O_2-consumers bacteria (mol dm^{-3})
$k_{1/2}^{bitumen,Fe(III)}$	Half-constant for bitumen degradation due to Fe(III)-consumers bacteria (mol dm^{-3})
$k_{1/2}^{bitumen,S(VI)}$	Half-constant for bitumen degradation due to S(VI)-consumers bacteria (mol dm^{-3})
$k_{1/2}^{cellulose,O_2}$	Half-constant for cellulose degradation due to O_2-consumers bacteria (mol dm^{-3})
$k_{1/2}^{cellulose,Fe(III)}$	Half-constant for cellulose degradation due to Fe(III)-consumers bacteria (mol dm^{-3})
$k_{1/2}^{cellulose,S(VI)}$	Half-constant for cellulose degradation due to S(VI)-consumers bacteria (mol dm^{-3})
Oxic	In this report, the term "oxic" refers to conditions where dissolved oxygen concentration is above 10^{-6} moles/L, and "anoxic" to those cases when the oxygen dissolved is below this threshold.
$rate_{acetate}^{biotic,O_2}$	Biotic acetate degradation rate by O_2-consumers bacteria (mol $dm^{-3}\ s^{-1}$)

$rate_{acetate}^{biotic,Fe(III)}$	Biotic acetate degradation rate by Fe(III) -consumers bacteria (mol dm^{-3} s^{-1})
$rate_{acetate}^{biotic,S(VI)}$	Biotic acetate degradation rate by S(VI)-consumers bacteria (mol dm^{-3} s^{-1})
$rate_{bitumen}^{biotic,O_2}$	Biotic bitumen degradation rate by O_2-consumers bacteria (mol dm^{-3} s^{-1})
$rate_{bitumen}^{biotic,Fe(III)}$	Biotic bitumen degradation rate by Fe(III) -consumers bacteria (mol dm^{-3} s^{-1})
$rate_{bitumen}^{biotic,S(VI)}$	Biotic bitumen degradation rate by S(VI)-consumers bacteria (mol dm^{-3} s^{-1})
$rate_{cellulose}^{biotic,O_2}$	Biotic cellulose degradation rate by O_2-consumers bacteria (mol dm^{-3} s^{-1})
$rate_{cellulose}^{biotic,Fe(III)}$	Biotic cellulose degradation rate by Fe(III) -consumers bacteria (mol dm^{-3} s^{-1})
$rate_{celluloe}^{biotic,S(VI)}$	Biotic cellulose degradation rate by S(VI)-consumers bacteria (mol dm^{-3} s^{-1})
$rate_{bitumen}^{abiotic}$	Abiotic bitumen degradation rate (mol dm^{-3} s^{-1})
$rate_{O_2-consumer}$	Growth rate of O_2-consumer bacteria (mol dm^{-3} s^{-1})
$rate_{Fe(III)-consume}$	Growth rate of Fe(III)-consumer bacteria (mol dm^{-3} s^{-1})
$rate_{S(VI)-consumer}$	Growth rate of S(VI)-consumer bacteria (mol dm^{-3} s^{-1})
$Y_{acetate}^{O_2}$	Specific yield coefficient of O_2-consumer bacteria degrading acetate (mol biomass$_O$/mol acetate)
$Y_{bitumen}^{O_2}$	Specific yield coefficient of O_2-consumer bacteria degrading bitumen (mol biomass$_O$/mol bitumen)
$Y_{cellulose}^{O_2}$	Specific yield coefficient of O_2-consumer bacteria degrading cellulose (mol biomass$_O$/mol cellulose)
$Y_{acetate}^{Fe(III)}$	Specific yield coefficient of Fe(III)-consumer bacteria degrading acetate (mol biomass$_{Fe}$/mol acetate)